A major purpose of the Technical Information Center is to provide the broadest dissemination possible of information contained in DOE's Research and Development Reports to business, industry, the academic community, and federal, state and local governments.

Although a small portion of this report is not reproducible, it is being made available to expedite the availability of information on the research discussed herein.

JASON

JSR--79-04

DE85 005065

Technical Report

JSR-79-04

June 1980

THE LONG TERM IMPACTS OF INCREASING ATMOSPHERIC CARBON DIOXIDE LEVELS

By: G. MacDonald, Chairman
H. Abarbanel
J. Chamberlain
F. Dyson
H. Foley
N. Fortson
W. Happer
W. Munk
W. Nierenberg
O. Rothaus
M. Ruderman
S. Treiman
J. Vesecky
F. Zachariasen

Prepared For:

U. S. Department of Energy
Washington, D.C. 20545

JASON

Technical Report

JSR-79-04

June 1980

THE LONG TERM IMPACTS OF INCREASING ATMOSPHERIC CARBON DIOXIDE LEVELS

By: G. MacDonald, Chairman
H. Abarbanel
J. Chamberlain
F. Dyson
H. Foley
N. Fortson
W. Happer
W. Munk
W. Nierenberg
O. Rothaus
M. Ruderman
S. Treiman
J. Vesecky
F. Zachariasen

Prepared For:

U. S. Department of Energy
Washington, D.C. 20545

ABSTRACT

If the current growth rate in the use of fossil fuels continues at 4.3% per year, then the CO_2 concentration in the atmosphere can be expected to double by about 2035 provided the current partition of CO_2 between the atmosphere, biosphere and oceans is maintained as well as the current mix of fuels. Alternative assumptions with respect to rates of increase of the world's use of carbon based fuels, and the nature of atmosphere-ocean-biosphere interactions lead to a range of doubling dates of 2020 to 2085 with more "reasonable" models yielding dates from 2030 to 2040.

This report addresses the question of the sources of atmospheric carbon dioxide, considers the distribution of the present carbon dioxide among the atmospheric, oceanic and biospheric reservoirs, and assesses the impact of significant increases in atmospheric carbon dioxide as reflected by the change in average ground temperature at each latitude. Possible direct impacts of increased atmospheric carbon dioxide levels on the biosphere are also considered.

The oceans and biosphere, including the soils and methane hydrates, store very large amounts of carbon compared with that in the atmosphere. Small changes in these large reservoirs can have a major effect on the atmosphere. Neither the ocean-atmosphere nor the atmosphere-biosphere interfaces are well understood. In regard to the former, we propose a new model for the mixing of carbon dioxide in the oceans. The

proposed model takes explicit account of the flow of colder and/or saltier water to greater depths, carrying with it CO_2 from the surface layers. This approach differs from the conventional box model governed by vertical diffusion at some arbitrary rate. Our calculations are, however, subject to considerable uncertainty concerning the formation of deep water masses. The atmosphere-biosphere interface is significantly more complex. It is clear, however, that data on several key questions are needed: (1) clear and detailed information on long term changes of oxygen concentration in the atmosphere and oceans; (2) information on the possibility that downward transport of reduced carbon, by rainout of biological debris from the ocean surface into deeper layers, may substantially increase the net flow of CO_2 from the atmosphere into the ocean; (3) information on the interactions of soil carbon with the atmosphere and the size of the soil carbon reservoir.

Increasing CO_2 in the atmosphere perturbs climate by altering the radiative properties of the atmosphere. The resulting climate change has been calculated through highly parameterized analytic heat budget models of the ocean-atmosphere system and by large computer models. We have adopted the first approach, starting with an atmosphere locally in radiative equilibrium and then allowing meridional transport of heat. We have constructed two models for the case of radiative equilibrium: one treating the atmosphere as quasi-grey, and the other dividing the infrared emission region into nine bands. The quasi-grey atmosphere model predicts an increase of average surface temperature of $2.8^{o}K$ for a doubling of CO_2, a result in agreement with the nine band model. Both models are sensitive to

assumptions with respect to the variation in humidity and cloud formation as a result of atmospheric warming. In the models, the principal effect of increasing CO_2 is to enhance the absorption by weak CO_2 bands in 8-12 micron region. Trace gases, CH_4, N_2C, NH_3, freons and hydrocarbons can also darken the atmospheric window.

An analytic model of the atmosphere has been constructed (JASON Climate Model). Calculation with this zonally averaged model shows an increase of average surface temperature of 2.4° for a doubling of CO_2. The equatorial temperature increases by 0.7°K while the poles warm up by 10 to 12°K. These values refer to an equilibrium state where the ice caps have completely melted. In time dependent heat budget models, the increase in temperature during the summer is greater than during the winter.

The JASON Climate Model (JCM) suffers from a number of fundamental weaknesses. The role of clouds in determining the albedo is not adequately taken into account, nor is the hydrological cycle. We expect, however, that models intermediate between the large GCMs and the primitive analytic models can yield insights into the nature of climate change. A better understanding of the influence of carbon dioxide on climate will depend on the development of models that yield information on the statistical properties of a warmer atmosphere.

The formation of sea ice during winter in the high latitudes results in a downflow of ocean water in restricted geographical regions. This downflow is balanced by a slow ocean wide upwelling. The enhanced

warming at high latitudes could disturb this circulation. The high latitude warming will tend to melt ice sheets, particularly those grounded below sea level. The time scale for the disintegration of the ice sheets may be as short as a few hundred years or as long as many thousand years. This estimate is uncertain since the mechanisms for ice sheet disintegration are poorly understood.

TABLE OF CONTENTS

LIST OF FIGURES

LIST OF TABLES

1.0 THE IMPACTS OF INCREASING CARBON DIOXIDE: AN OVERVIEW

Steady, hot summer winds in 1979, accompanied by low precipitation over the grain growing areas of European Russia reduced Soviet wheat crops by about 15% below the planned goal. The Soviets had anticipated making up this shortfall by major purchases from the United States, Canada and Australia. The Soviet invasion of Afghanistan led to curtailment of further U.S. grain shipments. The Soviet livestock herd, built over twenty years, was endangered and tensions between East and West were exacerbated.

What happened in 1979 was not unique for the decade of the seventies. In January, 1972 the wheat crop in European Russia suffered from inadequate snow cover, followed by prolonged heat and drought in spring and summer. In the late fall the ripened crop was covered by snow. As a result, the Soviet Union rapidly entered the world grain markets already strained by the poor monsoon in India in the same year. The Soviet shortfall of about 12% was mitigated largely by purchases from the West with major repercussions on world trade and the Soviet hard currency position.

The events of the last years of the 1970's illustrate that relatively small changes in climatic conditions can exert a profound influence on world events.

The Soviet Union and India were not the only countries affected by abnormal climatic conditions in the early 1970's. In the same time

interval the six West African countries south of the Sahel--Mauretania, Senegal, Mali, Upper Volta, Niger and Chad--were driven to the edge of political and economic ruin by a drought that began in 1968. The Sahelian drought and the Soviet and Indian grain failures received world-wide attention. The Equadorian rice failure of 1974, the Chinese droughts and floods of the same year, and the 1973 droughts in Central America attracted less attention. All of these examples illustrate the fragility of the world's crop producing capacity, particularly in those marginal areas where small alterations in temperature and precipitation can bring about major changes in total productivity.

The examples of the impact of climatic stress on the course of world events in the 1970s are representative of similar incidents throughout history. The distribution of population in the United States was greatly altered as a result of the 1933-36 drought of the Dust Bowl when total United States production of wheat was only three-quarters of that in preceeding and subsequent years. Lamb attributes the great Irish Potato Famine of the years 1845-48 to a series of wet and warm summers suitable for the rapid growth of the potato blight fungus which had been imported from North America in diseased tubers.[1] The famine halved the population of Ireland with emigration to the United States and Britain, and left a legacy of bitterness against England which has lasted to present times as a result of famine-associated misfortunes.

The effects of climate on man are usually considered only in terms of agriculture, but climate changes can profoundly influence many of man's

other less vital activities. Melting of glaciers and ice sheets will bring about changes in sea level which, even if small, are of importance to people living in areas subjected to sea floods (i.e., Netherlands and Venice). Large shifts in sea level could bring about major population shifts. The infrastructure of the energy and power industries are based on average climatic conditions in various parts of the world. The insurance industry policies are influenced by the average incidence of drought, floods and severe storms. Planning of dams for the provision of hydroelectric power and the management of water resources relies heavily on climatic data. The tourist industry, particularly that dependent on winter sports, is heavily influenced by changing climate (as illustrated by the collapse of the New England skiing industry in the abnormally dry winter of 1979-80). The list of activities that man has been forced to adjust because of prevailing weather conditions is almost endless. How and over what time scale such activities could respond to major changes in climate is not known.

The adverse effects of long term shifts in weather are due to the variance of climate about a mean. Considerations of the impact of man-made changes in climate on man may require an assessment of the impact of slow changes in the mean and possible shifts in the variance.

The fluctuation in climate in the last thousand years is small compared with those taking place over longer periods. A warming comparable to the "altithermal" period of 4000 to 8000 years ago would bring about not only major shifts in agriculture, but would have significant demographic

effects both from the direct climate changes and from shifts in sea level resulting from the melting of the Antarctic and Greenland ice sheets.

The burning of carbon-based fuels with current technology, releases carbon dioxide into the atmosphere. Carbon dioxide is a relatively minor constituent of the atmosphere having in 1979 a concentration of 334 parts per million (ppm). This concentration corresponds to 708.5 Gigatons (Gtons) of carbon in the form of carbon dioxide, an increase of 2.6 Gtons from the previous year. Despite its small concentration, carbon dioxide exerts a major influence on the thermal structure of the atmosphere since the carbon dioxide molecule absorbs infrared radiation emitted by the earth's surface that otherwise would escape into space. Because of carbon dioxide's radiative properties, changes in the concentration of carbon dioxide alter the atmosphere's thermal properties. In this way changes in carbon dioxide concentration will produce changes in climate. There is general agreement among atmospheric scientists about the warming influence of increased carbon dioxide levels. Much less certain are the details of world-wide climate at various levels of atmospheric carbon dioxide or when these levels will be reached.

Plants in photosynthesis fix carbon from the carbon dioxide in the atmosphere. Changes in carbon dioxide concentrations can be expected to alter productivity of both natural and agricultural systems. For those plants for which carbon is a limiting nutrient, increased carbon dioxide will lead to an enhanced productivity. Increased carbon dioxide levels can

also increase the water retaining capacity of some plants, so that higher productivity in drier areas might be expected with higher carbon dioxide levels. The acidity of rainwater and of the buffered oceans depend in part on atmospheric carbon dioxide concentrations so that change in this concentration could alter growth of soil bacteria, rates of weathering, and influence marine life. These few examples illustrate the thesis that increased levels of carbon dioxide can bring about changes other than those directly or indirectly influenced by climate. The non-climate related changes have been little studied in comparison to climate and are much less well understood. However, it may turn out that the changes other than climate are of equal or even greater significance to man than climatic changes.

1.1 Climate and Carbon Dioxide in Historical Perspective

Tyndale[2] in 1861 first suggested that slight changes in atmospheric composition could bring about climatic variation. Tyndale's work was based on early experiments measuring the absorption of light as a function of gas density. Arrehnius[3] first calculated the influence of changes in carbon dioxide concentration on the surface temperature noting that enhanced absorption in the infrared should yield a higher surface temperature. For a three-fold increase in the atmospheric concentration of carbon dioxide, Arrehnius in 1896 calculated a surface temperature rise of 9°C—a remarkable result considering the paucity of data. Today's estimate for a threefold increase is 6 to 16°C. Arrehnius[4] and Chamberlain[5] speculated that the large variation in the earth's climate, and in particular the glacial epochs, could be due to changing carbon dioxide concentrations

of the atmosphere resulting from geologic processes. The work of Arrehnius and Chamberlain greatly influenced the thinking (during the first half of the 20th Century) about geologic changes in climate. The critical role of the oceans in the global distribution of carbon dioxide was first demonstrated and explored by Tolman[6] in 1899.

Calendar in 1938 recognized that man, through the burning of carbon based fuels, was changing the composition of the atmosphere.[7] The geophysical significance of the rise in atmospheric carbon dioxide was dramatically emphasized by Revelle and Suess[8]; "Human beings are now carrying out a large-scale geophysical experiment of a kind that could not have happened in the past nor be repeated in the future. Within a few centuries, we are returning to the atmospheres and oceans the concentrated organic carbon stored in the sedimentary rocks over hundreds of millions of years. This experiment, if adequately documented, may yield a far-reaching insight into processes determining weather and climate."

Revelle was instrumental in incorporating into the program of the International Geophysical Year, accurate and regular measurements of the concentration of carbon dioxide. Keeling[9,10] has led a number of investigators in maintaining, over the past 20 years, continuous monitoring programs of atmospheric carbon dioxide at Mauna Loa, Hawaii, and the South Pole.

The impact of rising carbon dioxide levels on man were alluded to by Revelle and Suess and explicitly discussed in a report of the President's Science Advisory Committee[11] in 1965. The Arab Oil Embargo,

President Nixon's Project Independence, the world-wide increased emphasis on the use of coal and oil shale as major energy resources, and the renewed interest in synthetic fuels derived from coal have focused renewed attention on the possible consequences of increased levels of carbon dioxide in the atmosphere.

1.2 Measured Changes in Atmospheric Carbon Dioxide

Figure 1.2.1 shows the record of a secular increase of atmospheric carbon dioxide obtained from a nearly continuous monitoring at Mauna Loa, a site at 3,400m altitude and well within the trade wind belt. The current content of carbon as carbon dioxide in the atmosphere is about 708 x 10^9 metric tons (Gtons). Between about 90 and 145 Gtons of carbon have been added to the atmosphere since 1850. The uncertainty arises from the unknown level of carbon dioxide in the pre-industrial atmosphere (see, for example, Calendar[7]).

A similar secular increase has been observed at the South Pole with the values lagging Mauna Loa by a few ppm in any given year. This lag is consistent with the interpretation that more than 90% of the carbon dioxide is introduced in the industrialized Northern Hemisphere, and that there is a time lag in the mixing of the atmosphere between the hemispheres.

Shorter records from Point Barrow, Alaska,[12] and from Scandinavian airplane flights[13] show similar secular trends. Superimposed on the secular trend is a regular annual change with a peak to peak variation of

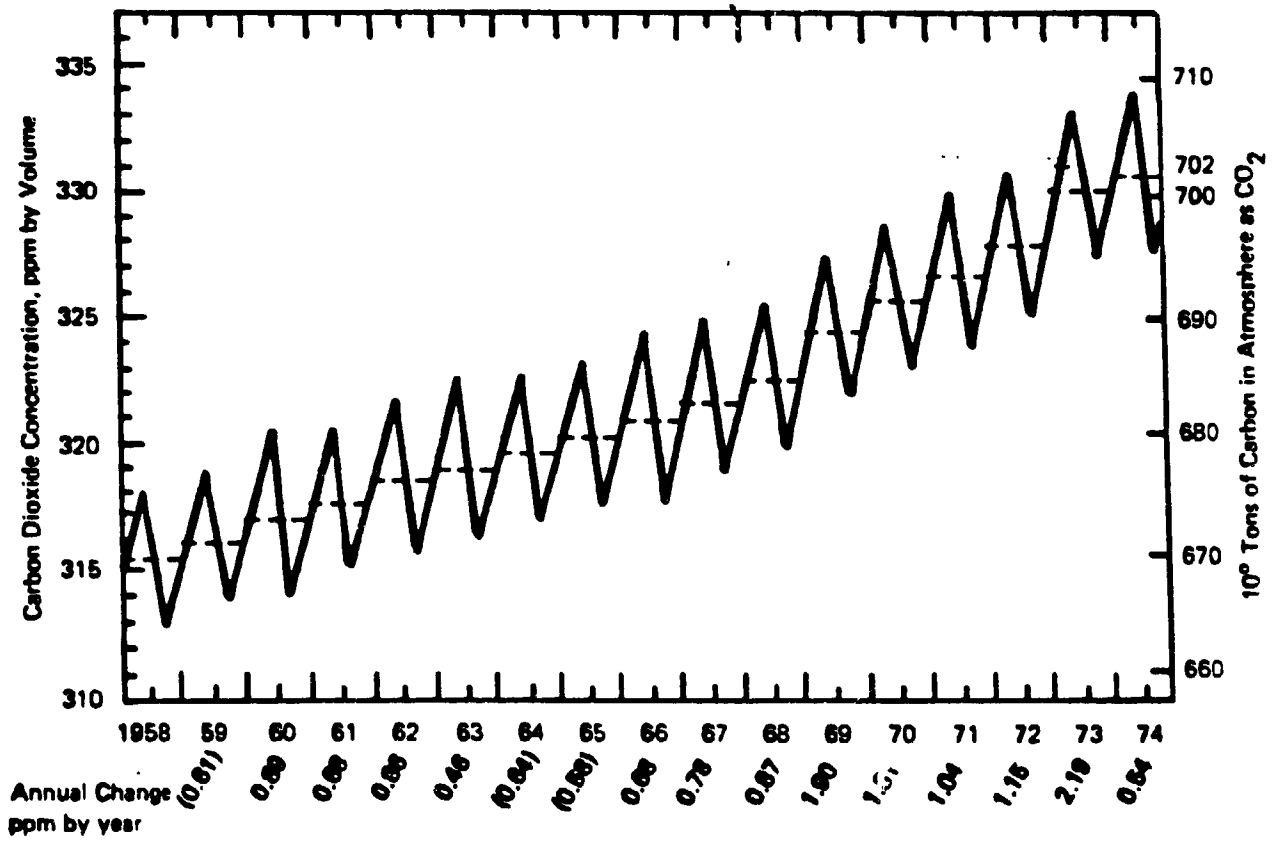

Figure 1.2.1 ATMOSPHERIC CARBON DIOXIDE CONCENTRATION AT MAUNA LOA OBSERVATORY (after Keeling, et al[9, 10])

approximately 6 ppm at Mauna Loa, 1.6 ppm at the South Pole, and as high as 15 ppm at Point Barrow. In the Northern Hemisphere, the maximum in the annual variation is in spring and the minimum in late summer. The seasonal variation is usually attributed to seasonal changes in net photosynthesis and respiration of the biosphere[14] though variations in sea surface temperature may be a minor contributor since the dissolved carbon dioxide content of the oceans is temperature dependent.

Even with the limited number of observation stations, it is clear that the carbon dioxide content of the atmosphere has been rising and that the rate of increase has accelerated over the 20 years of accurate measurements. In the late 1950's, carbon in the form of carbon dioxide was being added at a rate of about 1 Gton per year, while in 1978 the rate was approximately 2.6 Gtons per year.

1.3 Fuel Sources of Carbon

The rate at which carbon dioxide is added to the atmosphere depends both on the quantity of carbon based fuels burned and the mix of these fuels. In 1978, 5.62 Gtons of carbon were added to the atmosphere continuing a trend in which the exponential growth rate of fuels use has been 4.3% per year.[15] Per unit of heat energy delivered, the amount of carbon placed in the atmosphere depends on the fuel. Of the natural fuels, the burning of natural gas releases about one-half as much carbon per unit of delivered energy as does coal while burning oil releases an intermediate amount (see Table 2.1.2). Since the conversion of coal to synthetic fuels requires an input of energy, synthetics release substantially more carbon

dioxide per unit of delivered energy than do the natural fuels (see Table 2.1.12).

The cumulative contribution by fuel burning to the short term carbon cycle for the period 1800 through 1978 is about 160 Gtons or about one-quarter of the estimated pre-industrial atmospheric content. However, only about half of the carbon introduced into the atmosphere has remained there. In 1978, the carbon content of the atmosphere increased by 2.6 Gtons even though 5.62 Gtons of carbon were introduced into the atmosphere. A similar ratio of airborne carbon dioxide to carbon dioxide introduced by fuel burning has maintained over the twenty years of direct measurements of the concentration of carbon dioxide in the atmosphere.

1.4 The Carbon Cycle Mystery

The fact that only half the fuel based carbon introduced into the atmosphere remains there is conventionally explained through ocean absorption though the potential importance of biospheric interactions has been recognized.[16] Recently, the possibility has been advanced that current land clearing with the subsequent oxidation of plant material and the removal of carbon dioxide breathing plants may be adding to the carbon content of the atmosphere in a significant way. An understanding of the distribution of carbon between the oceans, biosphere, sediments and atmosphere is of critical importance to the forecasting of future carbon levels in the atmosphere.

The atmosphere is in fact the smallest of the major reservoirs of carbon (see Table 2.5.1). Further, the fluxes between the reservoirs are

large. For example, the biosphere puts into the atmosphere approximately 160 Gtons of carbon a year through respiration and decomposition of terrestrial and oceanic biota. The atmosphere returns an equal quantity through photosynthesis if equilibrium conditions are maintained. Small changes in the large reservoirs or in the rates of exchange between the reservoirs could bring about significant changes in atmospheric composition that would overwhelm the effects of burning carbon based fuels. Indeed, the older climate change hypothesis put forward by Arrehnius and Chamberlain were based on changes in the carbon content of the various reservoirs on geologic time scale.

The uncertainty in how much of the man-derived carbon goes rapidly into the oceans derives from the poorly understood mixing processes within the ocean. Numerous models of ocean-wide diffusive and convective exchange processes between adjoining vertical layers have been constructed to study the movement of carbon dioxide. The models and their supporting data on the movement of radioactive isotopes are not accurate enough to determine what fraction of the carbon released through fuel burning enters the ocean or whether additional carbon derived from land clearing and deforestation is also sequestered in the oceans (see Section 2.4).

The question as to whether the biosphere is a source or sink for carbon is similarly uncertain. The rates of land clearing, the resulting changes in biological productivity, the removal of organic material by sedimentation in the shallow oceans, the rates of exchange of carbon in soils, the response of the biosphere to higher carbon dioxide levels, are

all poorly known. Recent estimates suggest that the biosphere has been a moderate source of carbon in recent years, 1 to 3 Gtons/year,[17] but much higher figures have been proposed as well as suggestions that the biosphere is a sink for carbon.

A solution to the carbon mystery will require, among other things, a better understanding of the Riley-Williams pump mechanism and the world oxygen cycle. In the Riley-Williams pump, carbon is fixed by organisms in the near surface euphotic layer of the oceans. Unoxidized carbon in the form of dead organisms or fecal matter falls into the deeper parts of the ocean which mix with the rest of the ocean with a time scale of about a thousand years. In the deep ocean the carbon oxidizes removing free oxygen. The net effect of the pump is to move carbon from the atmosphere to the deep ocean, deplete oxygen levels of the deep ocean, and release oxygen to the atmosphere (see Section 2.2.4).

The burning of carbon based fuels not only produces carbon dioxide, but decreases the atmospheric concentration of oxygen. Systematic monitoring of oxygen levels in the atmosphere and oceans to a precision of one part in a thousand would provide a better description of the coupled carbon-oxygen cycle and aid in deciphering the carbon mystery (see Section 2.3).

1.5 Future Carbon Levels in the Atmosphere

Given the uncertainties in the future rate of carbon based fuels, fuel mix, biosphere-ocean-atmosphere interactions, it is hazardous to

predict future levels of carbon dioxide in the atmosphere. A common set of assumptions is that the historical exponential growth rate of 4.3% per year is maintained as is the current fuel mix and that half the carbon released remains in the atmosphere. With these assumptions the carbon content of the atmosphere would be expected to double in the year 2035.

All three assumptions can be challenged. The rapidly increasing price of carbon based fuels should decrease energy demand in both the developed and developing world. However, this growth of population, particularly in the developing world, will place heavy pressure for increased use of energy. The mix of carbon based fuels can also be expected to change from conditions in 1979 where about half of the fuel was oil, one-third coal, and one-fifth natural gas. For example, the Soviet Union plans to increase their fraction of natural gas produced energy from the 1978 value of 22% to 40% in 1985.[18] This will tend to reduce the input of carbon into the atmosphere which will, however, be offset by increased coal useage in countries such as the United States. The world reserves of carbon based fuels (see Tables 2.1.17 and 2.1.18) are probably capable of sustaining a 4.3% rate of growth through the 21st Century, but the cost of recovery and the availability of alternate sources of energy make it highly unlikely that the 4.3% rate will be maintained for very many years. The assumption that half of the fuel generated carbon dioxide remains in the atmosphere requires that the biospheric and oceanic response that is observed while the changes in concentration of carbon dioxide were small, persists during periods of large concentration changes; again, this is unlikely.

A further uncertainty in future carbon dioxide levels arises because of the unknown response of large reservoirs of carbon to increased temperatures. The feedback from the oceans where the equilibrium concentration of carbon dioxide decreases with an increase in temperature is probably small. However, the magnitude of the feedback from two large reservoirs, soils and methane hydrates, are unknown but could be significant (see Section 2.5.3). Similarly, the biosphere could provide a major negative feedback by absorbing carbon dioxide through carbon dioxide-induced increased productivity. Data are not available to estimate the magnitude of this feedback.

In Section 2.5, we consider a number of models of biospheric-oceanic interactions as well as different growth rates of carbon based fuels use but not taking into account possible positive feedbacks from the soil and methane hydrate reservoirs. The dates in these models at which the concentration of carbon dioxide doubles relative to the 1978 concentration range from 2020 to 2085 with the more "reasonable" models doubling between 2030 and 2040. The range of 65 years, 2020 to 2085, provides an estimate of the uncertainties in predicting future atmospheric carbon levels.

1.6 Climate Changes Due to Increased Levels of Carbon Dioxide

Attempts to calculate the effects of carbon dioxide on climate have focused on determining the change in the average surface temperature of the earth. Climate is much too complicated to be described by a single parameter. Amounts, geographical and temporal distribution of precipitation, onset of freezing conditions, strength and patterns of wind are all

parameters critical for understanding the impact of climatic change on man. However, present knowledge is such that surface temperature is universally used as a surrogate for climate in calculations on climatic change.

Three principal classes of models have been employed to calculate the effects of carbon dioxide on surface temperature.

1) Assume the atmosphere is everywhere in radiative equilibrium with outgoing infrared radiation balancing incoming solar radiation at each point on the earth's surface. (Zeroth order model)

2) Assume that in addition to radiative processes, heat is transported meridionally from equator to pole in the oceans and atmosphere by eddy-diffusion. (First order model)

3) Assume that the basic hydrodynamical equations describing atmospheric motion can be solved numerically. (General circulation models, GCM)

1.6.1 Zeroth Order Calculations

The earth's thermal radiation is mainly confined to the 5 to 30 μm region. The water molecule is a strong absorber over much of this region, except for the important 8 to 18 μm interval where the earth's infrared emission peaks (for a surface temperature of 290°K, the peak is at a wavelength of 10 μm). Water is a principal contributor to the greenhouse effect, even though it is not everywhere optically thick. Climate

calculation usually assumes that the water vapor concentration remains constant even though carbon dioxide and temperature vary.

Current carbon dioxide abundances are enough to make the 15 μm region optically thick so that changes in carbon dioxide concentration will alter the greenhouse heating primarily by carbon dioxide absorption in the 10 μm band and in the wings of the 15 μm band. The situation is further complicated in that a number of minor constituents such as nitrous oxide, methane, and a wide array of hydrocarbons are potentially important in enhancing the effect of carbon dioxide in closing off the 8 to 15 μm region.

If radiative transfer in the atmosphere is modeled as a partially absorbing blanket in which the detailed absorption spectrum is averaged to mimic a grey atmosphere, a doubling of the carbon dioxide content leads to an average world-wide increase in temperature of 2.8°K (see 3.1.2). A model taking into account the band structure of the absorbing molecule yields similar results. In the band model a doubling of carbon dioxide with a constant relative humidity of 50% results in a temperature increase of 3°K. Water vapor absorption strongly influences the calculated temperature change. If, as carbon dioxide doubles, the relative humidity increases to 60%, the temperature increase is 3.9°K. Alternatively, if the relative humidity decreases to 40% the temperature increase drops to 1.9°K (See Sections 3.1.2 and 3.1.3).

1.6.2 First Order Models

In the first order models, the surface temperature is permitted to vary with latitude. Heat transport is modeled as an eddy-diffusive process and the oceans and atmosphere are considered to be a coupled system. The resulting equations are non-linear since the albedo is assumed to be a function of temperature. In the simplest case, the albedo is high where the temperature is low because of ice or snow cover. Carbon dioxide will affect the radiative components in the equation and thus influence both the average temperature and the temperature distribution with latitude.

Calculations based on heat budget models show that a doubling of the carbon dioxide content raises the average temperature by 2.4°C. The temperature rise is much more marked in the polar regions with a temperature increase of 10°C at high latitudes, while in the equatorial regions it is less than the average (see Section 3.2.2).

Time dependent heat budget can be used to estimate the influence of heightened carbon dioxide levels on the seasonal variation of temperature. Results of the model calculations show that the warming takes place mainly in the summertime. For the latitude of Washington, the August temperature, after a doubling of the carbon dioxide content, is 9°C warmer than at present while the February temperature is only 2°C warmer (See Section 3.2.4).

1.6.3 Global Circulation Models

Manabe and Wetherald[19] have carried out the most detailed numerical simulations of the atmosphere but of necessity approximating very

roughly cloud formation, air-sea interaction, and albedo change. They found that a doubling of the carbon dioxide content raises the average temperature 2.9°C and the calculations indicate a warming of 8 to 12°C in the high latitude regions with smaller than average increases in the equatorial regions.

All climate models suffer from deficiencies. The heat budget models depend on a very few variables while the Global Circulation Models involve tens of thousands of meteorological variables. The heat budget models are certainly oversimplified while the Global Circulation Models require that the coupling of small scale effects to the large scale features be parameterized and in these models, potential numerical instabilities pose problems. It is likely that all models and particularly the heat budget models more accurately represent the effects of carbon dioxide on the heat budget of the atmosphere than on the detailed surface temperature. The latter will be sensitive to local and detailed dynamics which the models ignore or oversimplify (See Section 4.1).

1.7 Impacts of Changing Concentrations of Carbon Dioxide

If the world continues its heavy reliance on carbon based fuels, then we should expect during the middle of the 21st Century a warming of 2 to 3°C accentuated by a factor of three or four at high latitude regions. These average temperature changes are greater by at least a factor of three to four than those observed during abnormal historical weather conditions that prevailed for example during the "Little Ice Age" of the 16th and 17th Centuries. The changes, however, are smaller by about a factor of two than

those experienced during the past million years in the glacial and interglacial periods.

The anticipated man-made changes by the year 1990 or even 2000 are likely to be small compared with historical variations though carbon dioxide, together with minor constituent pollutants, could either amplify a natural warming trend or dampen a natural cooling episode. At the present state of knowledge, we cannot predict whether the natural variation will be in the direction of warming or cooling.

Actual observations of the predicted changes are made difficult by the large year-to-year fluctuations in weather and the incomplete geographical coverage of instrumentation that will allow the detection of a trend in the background noise of natural variations. Estimates of variation of carbon dioxide levels and associated climatic changes indicate that the world wide average increase in temperature in the 1990's will be at most a few tenths of a degree. Empirical observation of such a change will require improved world wide temperature measurements including the use of satellite-borne infrared sensors. (See section 5.5).

The amplification of the warming in the polar regions presents special problems. Generally, it is assumed that the polar ice sheets would respond to a warming trend over a time scale of thousands of years since the melting would proceed slowly at the surface exposed to the atmosphere. Mercer,[20] however, has pointed out that the characteristics of the West Antarctic ice sheet are such that melting could proceed rapidly. The

ice sheet is grounded below sea level with present summer surface temperature of -4 to -5°C. The grounded portion is fringed by ice shelves which serve to buttress the grounded part of the ice sheet. The shelves are vulnerable to both oceanic and atmospheric warming. An increase in summer temperature of 0 to 1°C could lead to rapid melting of the shelves and disintegration of the main ice sheet. The time scale for such a process is not known, but observed surges raise the possibility that the West Antarctica ice sheet could discharge one-third to one-half of its volume in 100 years. Calculations given in Section 4.3 suggest time scales of several hundred years for ice sheet melting. However, bottom melting and calving are not well enough understood to predict confidently what will happen to the ice sheets after warming. The complete melting of the ice sheet would raise world-wide sea levels by 5m with consequent major disruptions of the world's coastal region. A warming of 5°C in Antarctica could take place in 30 to 75 years, depending on rates and kinds of carbon fuels burned.

A warming amplified at high latitude regions could affect major features of the oceanic circulation. Cold, salty, dense waters are formed in wintertime by the freezing of sea ice. These dense waters plunge to the deep ocean primarily in the Norwegian and Labrador seas in the Northern Hemisphere & the Weddell sea in the Southern Hemisphere. This high velocity downflow in relatively restricted geographic regions is balanced by a general ocean-wide slow velocity upwelling. Warming in the winter will tend to decrease the volume of sea ice that is formed, decrease the flux of downward moving cold water and most importantly decrease the ocean-wide,

nutrient-carrying upwelling. The models considered in Section 3.2.4 indicate a lesser warming in winter than in summer so the effects of the warming on ocean circulation would be less than if the opposite were true. Calculations described in Section 4.3 suggest that even with a dampened wintertime warming, there could be a significant impact on the circulation originating in the Norwegian Sea.

The impact of climatic changes on agriculture are poorly understood. Existing climate models provide little guidance as to what changes in precipitation to anticipate as a result of the general warming. The productivity of any given crop will be influenced both by precipitation and temperature, as well as the length of the growing season. For example, warmer temperatures would favor wheat production in the northern part of the Canadian prairies provided the precipitation patterns were not altered since Canadian wheat yields are cut by cold summers and early frost. On the other hand, warmer temperatures might be expected to result in lower yields in the southern part of the United States wheat belt. (See Section 4.4).

The increased level of carbon dioxide can increase biological productivity for those species and those areas where carbon is a limiting nutrient through "carbon fertilization". For many species nutrients such as phosphorous and nitrogen and trace elements are limiting. Limited experimental data suggest that for some species the effects may be large with a doubling of carbon dioxide resulting in a 50 to 100% increase in yield. Further increased carbon dioxide reduces the water demands of some

species that live in arid conditions. The relative magnitudes of the changes brought about in the biosphere by shifts in climate and carbon dioxide concentration cannot be estimated on the basis of the data currently available.

1.8 Conclusions

Despite the many uncertainties about the nature of the carbon cycle and of the effect of carbon dioxide on climate, it seems highly probable that continued increases in the world-wide use of carbon based fuels will lead to significant climatic shifts in the 21st Century. The warming will be amplified in high latitude regions and in these regions man-made changes may be larger than natural variations in the 1990's or the early years of the 21st Century. Changes in climate, favorable or unfavorable in various localities, may take place on a time scale which is short, a few decades, compared to the time scale for society to change the infrastructure constructed over many decades in response to prevailing climatic conditions. The change in composition of the atmosphere could also have a profound impact principally by increasing biological productivity, particularly in arid regions. The net impact of the projected changes on man is unknown.

There exists a number of means by which the rate of increase of atmospheric carbon dioxide can be slowed if this becomes a desirable goal. All, however, only postpone the time at which large changes in atmospheric composition and climate take place. Conservation measures designed to reduce the use of carbon based fuels are in the short term most

likely to be effective. The increased use of natural gas, if available, would lengthen the time available for a shift to non-carbon based fuels. Clearly a significant shift to a nuclear or solar energy economy would postpone carbon-induced climate shifts. Increasing the standing crop through massive reforestation could provide temporary storage for carbon, but land and water availability limit this measure. In principle, carbon dioxide can be removed from stack gas for deep ocean disposal or deposited in old oil and gas fields (see Section 2.1.9). However, elementary consididerations suggest that neither of the latter suggestions are economical in comparison with alternative, nuclear or solar, energy systems.

The potential changes to the world posed by altering the composition of the atmosphere appear substantial enough to justify a comprehensive research effort designed to reduce the many uncertainties discussed above. Even though anticipated alteration would appear to be at least 50 years in the future, the world-wide nature of the changes and their possible effects on mankind warrant the continued attention of policy-makers to the carbon dioxide climate question. Since the changes are world-wide, their analysis and consequent actions should be undertaken on an international basis.

REFERENCES FOR SECTION 1.0

1. Lamb, H., "Climate: Present, Past and Future," 2, Methuen, London, 1977, 681-682.

2. Tyndall, J., Philadelphia Magazine, Journal of Science, 22, 169-194, 273-285, 1861.

3. Arrehnius, S., Phil Magazine, Journal of Science, 41, 237-276, 1896

4. Arrehnius, S., Worlds in the Making, Harper and Row, New York, 1908.

5. Chamberlain, T. C., "An attempt to frame a working hypothesis of the cause of glacial periods on an atmospheric basis," Journal of Geology, 7, 545-584, 667-685, 751-787, 1899.

6. Tolman, C. F., "The carbon dioxide of the ocean and its relation to the carbon dioxide of the atmosphere," Journal of Geology, 7, 585-618, 1899.

7. Callendar, G., Quarterly Journal of Royal Meteorological Society, 64, 223-237, 1938.

8. Revelle, R. and H. Suess, "Carbon dioxide exchange between atmosphere and ocean and the question of an increase of atmospheric CO_2 during the past decades", Tellus, 9, No. 1, 18-27, 1957.

9. Keeling, C. D., et al, "Atmospheric carbon dioxide variations at Mauna Loa Observatory, Hawaii", Tellus, 28, No. 6, 538-551, 1976.

10. Keeling, C.D., et al., "Atmospheric carbon dioxide variations at the South Pole", Tellus, 28, No. 6, pp. 552-564, 1976.

11. President's Science Advisory Committee (PSAC), Restoring the Quality of Our Environment, The White House, Washington, 1965.

12. Kelley, J. J., Jr., "Observation of carbon dioxide in the atmosphere over the Western United States," Journal Geophysical Research, 74, No. 6, 1688-1693, March 15, 1969.

13. Bolin, B. and W. Bischof, "Variations of the Carbon Dioxide Content of the Atmosphere in the Northern Hemisphere", Tellus, 22, No. 4, 431-442, 1970.

14. Bolin, B. and C. D. Keeling, "Large-scale atmospheric mixing as deduced from the seasonal and meridional variations of carbon dioxide," Journal of Geophysical Research, 68, No. 13, 3899-3920, July 1, 1963.

15. Keeling, C. D., "Industrial Production of Carbon Dioxide from Fossil Fuels and Limestone," Tellus, 2, 174-198, 1973.

16. Keeling, C. D., in Chemistry of the Lower Atmosphere, S. Rasool (ed.), Plenum Press, New York, 251-329, 1973.

17. Olson, J., H. Pfuderer, and Y. Chan, Changes in the Global Carbon Cycle and the Biosphere, Oak Ridge National Laboratory, ORNL/EIS-109, 1978.

18. Central Intelligence Agency, U.S.S.R.: Development of the Gas Industry, 1978.

19. Manabe, S. and R. Wetherald, "The effects of doubling the CO_2 concentration on the climate of a general circulation model," Journal of Atmospheric Sciences, 32, No. 1, 3-15, 1975.

20. Mercer, J.H., "West Antarctic Ice Sheet and CO_2 greenhouse effect: A theat of disaster," Nature, 271, 321-325, 1/26/78.

(This page left blank intentionally)

2.0 SOURCES AND SINKS FOR CARBON DIOXIDE

Man, through a variety of activities, burning fuels, flaring natural gas, making cement and plastics, cultivating crops, clearing land for agriculture, planting trees and adding nutrients to the lakes and oceans through fertilizer and sewage runoff, alters the carbon dioxide content of the atmosphere. Nature adjusts, but the response is such that the amount of carbon dioxide in the atmosphere is increasing at an exponential rate.

In this Section we discuss the various sources and possible sinks. In Section 2.1 we consider the contribution to atmospheric carbon dioxide made by the burning of fuels. We estimate future fuel use and possible mixes of fuels in order to provide a base for estimating future atmospheric levels of carbon dioxide. The terrestrial and marine biosphere can act both as a source and sink for carbon dioxide. These matters are taken up in Section 2.2. The carbon cycle in nature is closely coupled to the oxygen cycle since oxidation of fuels and plant materials is the key chemical reaction affecting the atmospheric carbon dioxide concentration. We present our understanding of the fundamental elements of the oxygen cycle in Section 2.3. In an appendix to this section we present an experimental method which has the promise of measuring the atmospheric concentration with the precision required to untangle the oceanic and biospheric components of the carbon cycle. The rate at which the ocean can absorb carbon dioxide by physical-chemical means depends on how the surface layers of the ocean mix with the deeper parts. We discuss one model for

hydrodynamic mixing in Section 2.4. Estimating the future levels of carbon dioxide requires a modeling of the atmospheric-biospheric-oceanic interactions. A model of these interactions is described in Section 2.5.

The principal impact of man on the chemical composition of the atmosphere is the change in concentration of carbon dioxide. In addition, man's activities add trace gases such as methane and Freon to the atmosphere. These compounds can, as does carbon dioxide, alter the radiative properties of the atmosphere and thus perturb the atmosphere's heat budget. In fact, any molecule that absorbs energy in the infrared "window" of the atmosphere enhances the warming due to the carbon dioxide. Estimates given in Section 3.1 of the magnitude of the warming due to the trace gases indicate that their effects are small compared to carbon dioxide, though not negligible. In this section we do not consider the sources or sinks of these trace components.

2.1 Carbon Dioxide From Burning of Fuels

2.1.1 Introduction

Calendar[1] first suggested that the burning of carbon-based fuels provided a major source for increasing the carbon dioxide content of the atmosphere. The burning of calcium carbonate to make quick lime in cement manufacture also adds carbon dioxide but there is only a fractional net addition of carbon dioxide to the atmosphere since carbon dioxide is partially fixed in the mortar or cement.

Using United Nations fuel production Keeling[2] and Roty[3] have estimated the historical releases of carbon through the burning of carbon-based fuels and have added carbon dioxide generated through the cement-making. The United Nations' data base is such that it is uncertain whether the use of carbon-based fuels for chemical industry feedstocks have been adequately taken into account (see Table 2.1.4). The remarkable feature of the historical data is that the use of carbon-based fuels has increased at an exponential growth rate of 4.3% per year from 1860 to the present except for three periods: the two world wars and the depression of the 1930's. Table 2.1.1 illustrates this trend.

TABLE 2.1.1

Estimated Carbon Added to the Atmosphere by the Burning of Fuels in Gtons/Year

Year	Carbon added
1950	1.63
1960	2.61
1970	3.96
1975	4.87
1978	5.62

The great increase in fuel price since 1974 might have been expected to slow the trend down but as of 1979 no significant reduction has occurred. Between 1973 and 1975 the energy consumption in the United States decreased by about three quads (1 quad = 10^{15} Btu) before again

increasing. However, the world consumption of fuels continued to increase even in the 1973-75 period. Currently the rate of growth of energy in the industrialized nations, the OECD countries, and the Soviet Bloc is less than 4.3%, but the rate of increase of energy usage in the third world countries including China has been appreciably greater than 4.3% per year.

The cumulative contribution by burning of carbon based fuels to the short term carbon cycle for the period 1800 through 1978 is about 154.4 Gtons or about one-quarter of the carbon present in the atmosphere in pre-industrial times. However, as will be described, less than half the carbon introduced into the atmosphere by the burning of carbon-based fuels remains there. Of the 154.4 Gtons added since the advent of the industrial revolution, 27% or 42.5 Gtons have been introduced in the period 1970-78.

2.1.2 Carbon Dioxide From Conventional Fuels

The amount of carbon added to the world atmosphere in any year through fuel burning depends greatly on the mix of fuels. Table 2.1.2 lists the amount of carbon emitted through combustion per unit (10^6 Btu) of thermal energy generated. Complete combustion is assumed since carbon monoxide and hydrocarbons will eventually be oxidized to carbon dioxide in the atmosphere. Per unit of thermal energy delivered, the burning of diesel oil produces 46% more carbon dioxide than the burning of natural gas, methane. The burning of sub-bituminous coal produces 87% more carbon dioxide than the burning of methane.

TABLE 2.1.2

Carbon Dioxide Produced from
Direct Combustion of Various Fuels

Fuel	Carbon dioxide generated (in kg of carbon per 10^6 Btu's of thermal energy)
Methane	14.2
Ethane	16.3
Propane	17.2
Butane	17.7
Gasoline	19.9
Diesel Oil	20.7
No. 6 Fuel Oil	21.0
Bituminous coal*	25.0
Sub-bituminous coal*	26.6
Lignite*	26.6
Biomass*	18.3

*Average values. The range can be at least ±10%.

The variation in carbon dioxide released with fuel type is dependent on the hydrogen to carbon ratio in the fuels. The higher the hydrogen to carbon ratio the greater will be the energy released per unit of carbon added to the atmosphere. In methane the hydrogen to carbon ratio is 4, in gasoline it is 2, and the ratio varies greatly in coals around an average value of 0.8.

Using the values listed in Table 2.1.2, we compute the relative contributions from burning of conventional fuels to the carbon content of

the atmosphere. Table 2.1.3 gives the estimates for the world for 1978. Coal provides only 29% of the world's use of thermal energy but is responsible for 36% of the carbon added to the atmosphere.

TABLE 2.1.3

Estimated World Generation of Carbon Dioxide (1978)

Fuel	Energy (quads)	Percent of (used)	CO_2 Generated (in metric gigatons of carbon)	Percent of CO_2 generated
Oil	128	47%	2.65	47%
Natural Gas	55	20%	0.78	14%
Natural Gas Flared	10	5%	0.14	2%
Coal	79	29%	2.05	36%
Total	272		5.62	

Table 2.1.4 provides a detailed budget for carbon-based fuels used in the United States in 1978. The use of natural gas, petroleum, and to a small extent coal as feedstocks for the petrochemical industry has been taken into account in constructing this table. Eventually the petrochemical products such as plastics will oxidize and add carbon to the atmosphere but for the time scale we are most interested in, the next 50 years, we assume that this carbon does not enter the atmosphere. The United States' contribution to the carbon content of the atmosphere in 1978 was 24% of the world's, down from about 27% in 1974. In 1978, coal

provided 20% of the thermal energy used in the United States but produced 7% of the carbon entering the atmosphere.

TABLE 2.1.4

Generation of Carbon Dioxide in the United States (1978)*

Fuel	Use (in quads)	CO_2 generation (in 10^6 metric tons of carbon)
Natural Gas		276.9
Domestic	19.3	
Imported	0.9	
Non-energy	0.7	
Petroleum and natural gas liquids		705.9
Domestic	21.2	
Imported	17.4	
Exports	0.7	
Non-energy	3.8	
Coal		364.0
Domestic	15.1	
Exports	1.0	
Non-energy	0.1	
Hydroelectric	1.0	0.0
Nuclear	3.0	0.0
Total U.S. Energy Use	72.6	1,346.8
Total	77.9	

*Data derived from statistics provided by the Energy Information Administration

The mining, cleaning and transportation of coal generates about 35 kg of carbon per metric ton of coal used.* This corresponds to about 1.6 kg/10^6 Btu so that the total carbon loading of the atmosphere from obtaining 10^6 Btu's of thermal energy from sub-bituminous coal is 28.2 kg or almost exactly twice the amount of carbon delivered to the atmosphere by burning natural gas to obtain the same thermal energy.

*In comparing the relative merits of various fuels with respect to generation of carbon dioxide not only the carbon dioxide generated in burning must be taken into account but also the carbon dioxide released by the use of energy in the extraction and transportation of the fuel.

For natural gas and oil these additional contributions tend to be small compared to the carbon dioxide generated by burning, but for coal they can become significant.

For coal, energy is expended in mining (strip or underground), in beneficiation (crushing and cleaning), in transportation, as well as in final utilization. The energy used in extraction varies with location and type of mining; a representative average value is 10^6 Btu/metric ton.[4] If half this energy is derived from coal burning and half from diesel fuel, then about 23.6 kg of carbon are added to the atmosphere per metric ton of coal mined.

Coal beneficiation refers to the process by which undesirable materials are removed from the coal. The crushing and screening processes generate minor amounts of carbon dioxide, the major source is thermal drying. Thermally dried coals represent only 13% of all U.S. coal with about 10^6 Btu's required to thermally dry a ton of coal. If coal provides the drying energy then the U.S. average coal cleaning adds about 3.5 kg of carbon per metric ton of coal.

The energy required to transport coal ranges from 410 Btu/ton mile for rail to 1500 Btu/ton mile by truck. If the coal is transported an average distance of 500 miles and the fuel used for transportation is diesel then between 4 and 15 kg of carbon are added to the atmosphere for the transportation of a metric ton of coal.

2.1.3 Carbon Dioxide from Production of Electricity

In 1978, 21.6 quads of energy were used to deliver 6.5 quads of electricity in the United States. Table 2.1.5 lists the sources of energy used in generating electricity and the resulting contributions of carbon to the atmosphere. In 1978 the average conversion efficiency for coal, petroleum, nuclear and the natural gas to electricity was 32% and the average total loss from turbine to end use was 14%.

TABLE 2.1.5

Carbon Dioxide Released in
Delivering 6.5 Quads of Electricity

Fuel	Energy used in generation (quads)	Carbon Dioxide released (in 10^6 metric tons of carbon)
Coal	10.4	280.5
Petroleum	3.9	81.9
Natural Gas	3.3	46.9
Nuclear	3.0	0.0
Hydrothermal	1.0	0.0
Total	21.6	409.3

In order to deliver one quad of electrical energy 63 million metric tons of carbon are introduced into the atmosphere given the current U.S. fuel mix. This figure can be contrasted with the delivery of one quad of natural gas which on burning releases 14.2 million metric tons of carbon or 22% that derived from electricity. Electricity and natural gas have

different end use efficiencies so that a more realistic comparison between the carbon dioxide generated through the use of electricity and natural gas would take into account these differences. In the residential sector the average electrical appliance efficiency is about 94% while the average residential gas end use efficiency is about 64%. Electricity in residential end use generates 67 million metric tons of carbon per quad while natural gas in the same end use generates 22 million metric tons. In residential applications electricity derived from the fuel sources listed in Table 2.1.5 generates three times the carbon dioxide than does natural gas in the same end use.

2.1.4 Carbon Dioxide from Synthetic Fuels

2.1.4.1 Introduction

Because of the very large coal reserves of the world, the United States and other countries have mounted significant research efforts into converting coal into fuels such as oil and methane that can be used more widely than coal. In fiscal 1979 the United States planned to spend $206 million on converting coal to a liquid fuel and $160 million on coal gasification. In 1979, the U.S. Congress and Executive Branch put forward proposals involving investments of tens of billions of dollars a year in synthetic plants. The basic chemistry in producing synthetic fuels requires an enrichment of the hydrogen poor coal into a product with a higher hydrogen-to-carbon ratio. The hydrogen is generally obtained from water. The conversion of coal to synthetic oil or gas requires energy. In considering the carbon budget of the total synthetic fuel process, the

carbon dioxide generated during the production of the synthetic fuel must be added to the carbon dioxide emitted in the burning of the synthetic fuel in order to obtain the total carbon dioxide released in the burning of synthetic fuels. Because of the energy requirements in the production of synthetic fuels, the use of these fuels adds substantially more carbon dioxide to the atmosphere than does the direct combustion of natural gas, oil or coal.

2.1.4.2 Coal Liquification

Coal liquification refers to a variety of chemical processes by which coal is converted from its natural solid state to a more flexible liquid product. In essence, coal liquification is a fuel pretreatment process that transforms a high-ash, high-sulfur coal into an ash-free, low-sulfur fuel thus reducing the conventional environmental problems at the cost of lower overall energy efficiency and higher total carbon dioxide emissions.

The major types of liquification are direct hydrogenation, pyrolysis, indirect liquification and solvent extraction. The carbon dioxide emission varies somewhat among the processes and their variants. We examine in detail the direct hydrogenation process[5] to illustrate the carbon dioxide emissions associated with liquification.

Direct hydrogenation involves processes in which hydrogen is catalytically added to coal in a reactor under high pressure and temperature. The coal is converted to liquids and vapors which are further

refined to remove by-products. In 1979, the H-Coal project was the most advanced hydrogenation process with a 600 short ton per day pilot plant under construction in Catlettsburg, Kentucky.

In an operational sized plant, 2600 metric tons per day of coal would be converted to fuel gas to power the auxiliaries. The use of the fuel gas would release 1935 metric tons of carbon as carbon dioxide. The coal fed into the process itself would contain 14,550 metric tons of carbon and in the processing an additional 4200 metric tons of carbon would be released as carbon dioxide. The products would be 15,000 barrels a day of naptha and 55,000 barrels a day of heavy oil. Table 2.1.6 summarizes the carbon dioxide-energy balance for a H-Coal plant. In the overall H-Coal process, neglecting extraction and transportation uses of energy, 39.2 kg

TABLE 2.1.6

Carbon Dioxide and Energy Balance
for a H-Coal Plant

	Carbon dioxide released (in metric tons of carbon/day)	Thermal energy delivered (in 10^9 Btu's)
Inputs		
Fuel Gas	1,835	
Process	4,200	
Products		
Naptha (15,000 bbl/day)	1,727	83.2
Heavy Oil (55,000 bbl/day)	8,363	328.0
Total	16,125	411.2

of carbon are produced for each 10^6 Btu's of thermal energy. Liquid products from the H-Coal process produce 2.8 times as much carbon dioxide as does the burning of natural gas to obtain the same amount of thermal energy and 1.5 times as much as burning coal directly.

2.1.4.3 Coal Gasification

Producing gas from coal is not a new technology. In the late 19th and early 20th centuries there were some 11,000 "gasifiers" in the United States producing low Btu gas. These were replaced as natural gas, kept inexpensive by governmental regulation, came on the market.

Chemically, coal gasification involves exposing crushed coal to a hot gaseous stream of steam and oxygen. The resulting combustible gas contains methane, carbon monoxide, water vapor and hydrogen in proportions depending on the process. When a steam-air mixture is used low-Btu gas is produced, less than 200 Btu/cubic foot. This gas can be used under boilers. Replacing air with oxygen yields medium Btu gas (300-500 Btu/cf) which can be used in energy intensive industries. High Btu gas (900-1100 Btu/cf) would be required for commercial and residential uses and for many industrial applications. High-Btu gas requires either direct hydrogenation or further processing of medium Btu gas.

As an example of coal gasification, we examine the HYGAS process[6] for high-Btu gas which in 1979 was in the pilot plant stage with a demonstration plant under design. The relevent data for the process in an operational plant are given in Table 2.1.7. In the overall HYGAS process,

42.3 kg of carbon are produced for every 10^6 Btu's of energy contained in the product methane. Synthetic gas from this process yields about 3 times as much carbon dioxide as obtaining the same unit of energy from natural gas and 60% more carbon dioxide than obtaining the energy directly from coal.

TABLE 2.1.7

Carbon Dioxide and Energy Production in HYGAS Process

	Carbon dioxide released (in metric tons of carbon)	Energy produced (in 10^9 Btu)
Inputs		
Auxiliaries (dry coal feed)	2325	
Gasifier (dry coal feed)	8000	
Outputs		
CO and CO_2	400	
Methane	3470	244
Net Totals	10,325	244

2.1.5. Carbon Dioxide from Oil Shale

Oil shale is a sedimentary rock containing a waxy organic material known as "kerogen" embedded in a matrix of clay minerals, carbonates and sand grains. When the shale is heated to temperatures of 450 to 540°C the kerogen undergoes a chemical change (pyrolysis) in which about 65% of the kerogen is converted to hydrocarbon liquids, about 10% to a low Btu gas

product and leaving a 25% carbonaceous residue. In the heating (or retorting) three barrels of water are used in recovering one barrel of liquid product. Typically, 25 to 30 gallons of liquid product can be obtained from a metric ton of shale. The liquid product can then be turned into a high quality crude oil.

In 1979, three retorting processes were under consideration. In surface retorting, the oil shale is mined, crushed and then heated in a retort vessel. In "in situ retorting" the rock is heated in place and the products from the kerogen are brought to the surface through fractures in the rock. In the "modified in situ" process, part of the shale is mined and brought to surface and retorted while the rest is fractured and retorted in place.

The use of shale oil has a long history; for example, shale oil was used for decades in the Scottish low lands only to be replaced by inexpensive Middle Eastern oil. In 1979, three processes were ready either for advanced demonstration or early commercialization: Paraho, TOSCO II and Union B. All three are surface retorting processes with differing designs.

Table 2.1.8 summarizes the energy and carbon dioxide budget for a generalized surface retort of oil shale that yields 27.5 gallons of useful liquid product suitable for further refining. The energy expended in mining and crushing is taken from experience in the coal industry at 1×10^6 Btu/metric ton. The heat required to retort at 500°C is calculated

TABLE 2.1.8

Carbon Dioxide and Energy Balance
for Oil Shale Production

Process	Energy Used per Metric Ton of Shale (in 10^6 Btu's)	Energy Delivered per Metric Ton of Shale (in 10^6 Btu's)	Carbon Dioxide Emitted per ton of Shale (in kg of carbon)
Mining and Crushing	1.00		23.6
Retorting at 500°C	0.59		11.5
Inorganic CO_2 (20% $CaCO_3$ of which 5% dissociated)			1.5
Burning 27.5 gallons liquid product		4.0	84.0
Total	3.50	4.0	120.6

using a heat capacity for the shale of 1.25 joules/g°K. This value is almost certainly low because the heat capacity refers to dry rock and does not include the heat required for drying the shale, for pyrolysis and for dissociating either calcite ($CaCO_3$) or dolomite [$MgCa(CO_3)_2$]. Three-fourths of the heat required for retorting is assumed to be derived from the burning of heavy shale liquid product and one-fourth from the relatively low Btu gas derived in retorting. The shale is assumed to contain 20% calcium carbonate by weight; natural oil shales vary from 15 to 30%. Five percent of the calcium or magnesium carbonate present is assumed to

dissociate. This, again, is probably a low estimate for retorting at 500°C. The 27.5 gallons of liquid product are assumed to have a density of 0.9 g/cm^3 and a heating value of 40,700 Btu/kg. Shale oil in production and burning will deposit at least 30 kg of carbon in the atmosphere for generation of 10^6 Btu's of energy. This is 20% more than the direct burning of coal and 2.1 times the carbon generated in burning methane.

In the "in situ retorting" less energy is required in mining and crushing, but the efficiency of the recovery of the liquid product is less. Since the figure of 30 kgC/10^6 Btu used conservative numbers for calculating CO_2 emissions in retorting and carbonate dissociation, it is unlikely that shale oil can be produced and used without emitting at least 30 kgC/10^6 Btu.

2.1.6 Advanced Coal Power Cycles for Electricity

A number of improved coal conversion processes have been proposed to increase the overall efficiency of the conversion of coal to electricity. In the atmospheric fluidized-bed combustion process, the coal is crushed to fine grains and the combustion takes place while the coal particles are suspended by an upward moving gas stream. Calcium carbonate is injected to remove the sulfur in the coal by forming calcium sulfate releasing carbon dioxide. A magnetohydrodynamic generator is an expansion engine in which hot, partially ionized gases flow down a duct lined with electrodes and surrounded by coils that produce a magnetic field across the duct. The expanding gas propels only itself and there are no turbines involved. The movement of the electric conducting gas through the magnetic field generates a current which the electrodes collect.

The principle problems in employing the fluidized bed combustion and magnetohydrodynamic processes to generate electricity are associated with materials that can withstand the high temperatures and corrosive gases involved in the processes. Additionally, both processes, but particularly the magnetohydrodynamic process generate large quantities of oxides of nitrogen.

Table 2.1.9 lists the carbon dioxide output from advanced electrical power systems in terms of kg of carbon per 10^6 Btu's (290 kwh) of electrical energy produced at the power plant. In all cases, the coal is

TABLE 2.1.9

Carbon Dioxide Generated in
Advanced Electric Power Plant

Plant	Average Power (in MWe)	Coal Feed (in Metric Tons per Day)	Efficiency in Converting Thermal to Electrical Energy (percent)	Carbon Dioxide Released (in kgC/10^6 Btu electric)
Modern Conventional Coal Powered Plant with Scrubbers	1000	6000	33	72
Atmospheric Fluidized-Bed Combustion	814	4750	35	72
Magneto-hydro-dynamic Open Cycle	1930	7900	57	50

assumed to contain 70% carbon with a heating value of 24860 Btu/kg, typical of treated coals from Southern Appalachia or the Green River in the Western states. The atmospheric fluidized bed combustion yields the same carbon dioxide per unit of electrical energy produced as does a modern power plant equipped with scrubbers in part because of the carbon dioxide released in the sulfur removal through introduction of calcium carbonate.

2.1.7 Energy from Biomass

The biosphere, including the carbon in soils, is a large reservoir for carbon containing approximately 2400 Gtons of carbon as compared with the atmospheric reservoir of about 700 Gtons. Further, the rates of interchange of carbon between the atmosphere and the biosphere is large compared with the rate of release of carbon by the burning of fuels. The biosphere can act as a source and sink for carbon, a problem discussed in Section 2.2. Changes in the carbon concentration of the atmosphere can bring about changes in the biosphere which is treated in Sections 2.5 and 4.5. In the present Section, we consider the biosphere as a source of fuel.

Wood was the principle fuel source prior to the widespread use of coal at the beginning of the industrial revolution. The current energy problems have prompted a renewed interest in biomass either as a direct source of thermal energy by cultivating, harvesting and burning large forests for thermal energy, or by converting the biomass into a more flexible fuel such as ethanol or methanol.

Table 2.2.10 lists the productivity, standing biomass and thermal energy fixed by photosynthesis for various ecosystems[7]. In constructing this table, forests are assumed to have a carbon concentration of 50% by weight while other systems are assumed to be 45% carbon. While Whitaker's and Liken's estimates are generally assumed to be the best current values, the uncertainties can be as large as a factor of two, particularly for the tropical forests.

Table 2.1.10 illustrates that most (98%) of the standing biomass is terrestrial, but that the total productivity of the marine biosphere is half that of the terrestrial biosphere. The energy fixed by the biosphere through photosynthesis is an order of magnitude greater than the current yearly world consumption of energy. The heat value of the aboveground growth in world's forests is almost three times current annual energy consumption.

The carbon dioxide-energy balance for biomass is illustrated by considering a cultivated crop, corn, used both as a direct fuel and as a feedstock for methanol. The energy input for transportation and fertilizer to produce a metric ton of corn is about 1.2×10^6 Btu[8]. If this energy is provided half by natural gas and half by diesel fuel, then the production of the corn generates carbon dioxide at a rate of 1.2 kgC/10^6 Btu. The direct burning of the corn generates an additional 22.3 kgC/10^6 Btu so that the generation of a million Btu's of thermal energy releases a total of 23.5 kg of carbon. If corn is used as a renewable resource, the net carbon release is 1.2 kgC/10^6 Btu as contrasted to 14.2 kg of carbon for a million Btu derived from methane.

TABLE 2.1.10

Productivity and Standing Biomass for Various Ecosystems

Vegetation Unit	Area Size 10^6 km^2	Net Primary Productivity (tons/km^2/year)	Total Productivity (Gtons/year)	Total Heat Value (quads/year)	Total Fixed Carbon (Gtons/year)	Standing Biomass (Gigatons of carbon)
Tropical Rain Forest	17.0	2200	37.4	609	18.7	383
Tropical Seasonal Forest	7.5	1600	12.0	200	6.0	130
Temperate Evergreen	5.0	1300	6.5	119	3.2	87
Temperate Deciduous	7.0	1200	8.4	153	4.2	105
Boreal Forest	12.0	800	9.6	183	4.8	120
Total Forest	48.5		73.9	1264	36.9	824
Total Stem (above ground)			44.3	758	22.1	618
Woodland & shrub	8.5	700	6.0	110	2.7	23
Cultivated Land	14.0	650	9.1	148	4.1	6.3
Other Terrestrial	78.0	608	29.0	530	12.9	54.9
Total Terrestrial	149.		118.	2052	56.6	908.2
Total Marine	361.	160	56.	1024	25.2	1.8
Total Biosphere	510.		174.	3076	81.8	910.

Corn can be converted into methanol (CH_3OH) through a variety of processes. One kilogram of corn yields 0.53 kg of methanol. Table 2.1.11 gives the carbon dioxide-energy balance in using corn as a feedstock for methanol. Since corn is a renewable resource, only the carbon dioxide related to growing is a net addition, but the inefficiencies associated with the corn to methanol increases the land requirements for producing a unit of thermal energy. The generation of 10^6 Btu's of thermal energy requires 85.3 kg of biomass in the form of corn. A cornfield with a primary productivity of 2400 metric tons/km^2 yields 2.8 X 10^{10} Btu's of thermal energy as methanol as compared with 4.3 X 10^{10} Btu's if the corn were burned directly. For a crop having very high primary productivity (see Table 2.1.10), a quad per year of thermal energy derived from burning biomass requires 23,000 km^2 or 36,000 km^2, if the biomass is converted to methanol.

TABLE 2.1.11

Carbon Dioxide Generated in Corn-Methanol Process

Process	Carbon Dioxide Generated in $kgC/10^6$ Btu
Growing Corn	1.8
Conversion of Corn to Methanol	17.1
Burning Methanol	17.3
Total CO_2 Generated	36.2

2.1.8 Summary of Carbon Dioxide Released by Various Fuels and Advanced Fuel Systems

Table 2.1.12 summarizes the relative average carbon dioxide emissions from a wide range of natural and synthetic fuels in terms of carbon added to the atmosphere per unit (10^6 Btu's) of thermal energy generated. The values listed must be used with caution in any comparative evaluation. For example, end use efficiency should be taken into

TABLE 2.1.12

Comparison of Carbon Dioxide Release from Production of Thermal (or Electrical) Energy by Various Fuels (Average Values)

Fuel	Carbon Dioxide Released (in kgC/10^6 Btu)	Ratio of Carbon Released by Fuel to that Released by Methane
Natural Fuels		
Natural Gas (methane)	14.2	1.00
Oil	21.0	1.48
Coal	26.0	1.83
Shale Oil*	30.0	2.11
Biomass (renewable)	1.2	0.08
Synthetic Fuels		
Gas	42.3	2.98
Oil	39.2	2.76
Methanol from Biomass (renewable)	1.8	0.13
Electrical Power (kgC/10^6 Btu electric)		
1978 Mix of Fuels (coal, nuclear, etc.)	63.0	4.44
Conventional Coal Fired	72.0	5.07
Fluidized Bed	72.0	5.07
Magnetohydrodynamics	50.0	3.52

*Minimum Value

account. If the end use is the residential sector (gas = 64% efficient, electricity = 94% efficient) then synthetic gas generates 66.1 kg of carbon, electricity with a 1978 mix of fuels 67.0 kg of carbon and electricity from a coal fired plant 76.6 kg of carbon per 10^6 Btu's of end use energy. Non-carbon-based fuel sources such as solar or nuclear will generate no carbon dioxide. Combination processes will generate intermediate amounts. A few candidate systems are listed in Table 2.1.13.

TABLE 2.1.13

Carbon Dioxide Generated From Advanced Systems

Fuel System	Carbon Dioxide Generated (kgC/ 10^6 Btu)
Solar-direct or electric	0.
Nuclear including breeders	0.
Nuclear electrolytic for hydrogen	0.
Solar electrolytic for hydrogen	0.
Synthetic Gas from coal and nuclear hydrogen	14.2
Hydrogen from natural gas reforming	14.2
Hydrogen from coal gasification	34.8

2.1.9 Carbon Dioxide Control

The prospect of rapid increases in carbon dioxide raises questions as to possible means of controlling the rate of increase, either by taking measures now or planning for such steps if the increase in carbon dioxide

does lead to detectable detrimental effects. A decrease in the rate of increase of the use of carbon-based fuels, currently 4.3% per year, will slow the atmospheric build-up of carbon dioxide (see Section 2.1.10). Conservation measures adopted worldwide could postpone or ameliorate any harmful impacts of increasing carbon dioxide. A worldwide shift from carbon-based fuels to nuclear or solar-based fuels would bring about a halt to increased atmospheric CO_2 loadings from the burning of fuels. However, the worldwide infrastructure supporting any fuel economy prevents a rapid shift from one fuel type to another. The shift from a major dependence on coal to one on petroleum products took about 60 to 100 years. In 1920 coal was the world's major fuel source providing about 70% of the world's energy. In 1980, oil will be the major fuel supplying 45% of the world's needs. A switch away from carbon-based fuels on a worldwide basis can be expected to have a similar time scale. However, the use of carbon-based fuels may produce adverse effects for society in fifty years, yet these might not be recognized for another ten to twenty years. These time scales, accentuated by the delays in developing an international consensus for action, argue for the analysis of means to control carbon dioxide now. As will be discussed in Section 2.1.10, energy conservation appears to be the most effective near-term method of controlling carbon dioxide, though alternate fuel sources could become significant in the fifty year time span.

A variety of ways of controlling carbon dioxide have been proposed[9]. Carbon dioxide can, in principle, be removed from stack gas effluent and then disposed by land or sea burial. Technology for carbon

dioxide removal from gases has been developed in the natural gas industry since carbon dioxide is often a constituent of natural gas that reduces the heat value of that fuel. Alternatively, the biosphere could be managed in such a way as to remove carbon dioxide from the atmosphere either by terrestrial or marine organisms.

Recent proposals to use carbon dioxide, pumped from deep wells in enhanced oil recovery operations[10] have focused attention on disposing of CO_2 in abandoned gas fields. Preliminary estimates indicate that 5-10 billion barrels of oil could eventually be produced by enhanced oil recovery by CO_2 flooding. These operations would require about 50 trillion cubic feet of carbon dioxide which corresponds to 7.58×10^8 metric tons of carbon. If all the CO_2 that could be used for enhanced oil recovery were derived from stack effluents, about one-half of a year of the U.S.'s generation of carbon dioxide could be employed or disposed of in this way.

The control of carbon dioxide emissions at the source is made difficult since about half (51%) of the U.S. emissions are from distributed sources (see Table 2.1.14). The problems of controlling CO_2 from automobile emissions and residences are far different from controlling CO_2 from power plants, industrial sources or synthetic fuel plants. On a worldwide basis, the CO_2 emitted from transportation sources is lower and the fraction from point sources is higher so that the technical control of carbon dioxide on a worldwide basis may be a simpler problem than for the U.S.

TABLE 2.1.14

Energy Use and Carbon Dioxide Production in the United States by Sector for 1978

Sector	Energy Derived from Carbon Based Fuels (quads)	Percent Energy Derived from Carbon Based Fuels	Carbon Dioxide Emitted (in 10^6 metric tons of carbon)	Percent of Carbon Dioxide Emitted
Utility Electricity Generation	17.6	26%	396	29%
Residential and Commercial	15.1	22%	264	20%
Industrial	14.6	22%	266	20%
Transportation	20.5	30%	421	31%
Total	67.8	100%	1347	100%

Recovery and disposal of carbon dioxide from power plants and industrial stacks is complicated by the relatively low concentration of CO_2 in the effluent (see Table 2.1.15) and the presence of sulfur oxides. Analysis of carbon dioxide removal from stack gases assume that scrubbers are used[10]. Because of the relatively low concentration of carbon dioxide in the stack gases, transportation costs from the plant to the disposal field are high enough to examine the economics of purification of the carbon dioxide prior to transportation.

TABLE 2.1.15

Composition of Typical Flue Gas of a
Coal Fired Power Plant After Sulfur Oxide Removal

Component	Mole Percent	Weight Percent
Carbon Dioxide	16	25
Nitrogen	65	61
Oxygen	6	6
Water	13	8
Total	100	100

A number of processes are available to recover CO_2 from flue gases[11]. These include chemically reactive systems, physical absorbent systems, dry bed combustion systems, and cryogenic systems. The low concentration of CO_2 and the high volume of gases emitted by power plants and industrial facilities suggest that only the chemically reactive systems are economically viable. In particular, cryogenic [illegible]ification has costs that are at least an order of magnitude greater than the chemically reactive systems. A contrary claim appears unfounded[12].

Of the chemically reactive processes, alkanolamine-monoethanolamine (MEA) is particularly well suited for carbon dioxide removal when the gas is at low pressure as it is when emerging from a stack. In the process, CO_2 is chemically removed in solution. The MEA is regenerated and the CO_2 product obtained by heating is stripped out of the product with steam. Hare, et al[10] estimates a cost of about one dollar per thousand

cubic feet a day for CO_2 removal for a 1000 MWe plant burning 6000 tons of 70% carbon coal. This cost corresponds to about 1.3 cents per kilowatt hour. These costs do not include MEA recovery system, cooling water circulation pumps or disposal of the condensed process water.

The most economical method of transport of carbon dioxide is by pipeline with the gas at a supercritical pressure, 73.9 bars[10]. The pipeline cost will depend on the length and the type of terrain over which the pipeline passes. For transportation over 800 km of average terrain of 300 million cubic feet per day, output of a 1000 MWe plant, the cost including operation and capital investment are about one dollar per thousand cubic feet, which would correspond to an additional cost of about 1.3 cents per kwh of electricity.

In addition to the purification and transportation cost, there is the cost of injecting the carbon dioxide into old gas or oil fields. These costs will vary greatly depending on the depth of the depleted porous zone, the status of the drill holes, etc. An order of magnitude estimate of an average cost is again one dollar per thousand cubic feet. If the field was still producing, then the operating cost of injecting CO_2 would be 5 cents per thousand cubic feet. In an abandoned field the casing of every well would have to be checked and repaired, the integrity of dry holes examined, compressors installed, and distribution pipeline put down. These capital costs could raise the total costs well above one dollar per thousand cubic feet.

Old petroleum field disposal is also limited by the availability of depleted fields. For example, the cumulative production of natural gas in the United States through 1978 was about 500 trillion cubic feet. If all these reservoirs were used for the disposal of carbon dioxide, then 7.6 Gtons of carbon could be sequestered in these reservoirs. Since, in 1978, about 0.4 Gtons of carbon, or 26% of the total were emitted into the atmosphere by electrical generating plants in the U.S. (see Table 2.1.14), gas reservoirs could be used to bury about 20 years of carbon produced by electrical generation at the 1978 rate.

The pumping of carbon dioxide into the deep ocean provides a very large sink (see Section 2.3). Since the continental shelf drops sharply off the Pacific Coast, ocean disposal on the West Coast would be [illegible] costly than land disposal. The wide Atlantic shelf and the shallow Gulf of Mexico implies high transportation costs for deep ocean disposal over much of the country.

In economic terms a mixed strategy of land and ocean disposal could be used to minimize the cost of physical removal of carbon dioxide. Technology for carbon dioxide scrubbing and disposal exists, and in an industrialized country such as the U.S., could be applied. However, the economic costs are considerable. Even when account is taken of the very considerable uncertainties in cost estimates, such disposal would approximately double the cost of electricity generated by the use of carbon-based fuels and a higher cost would be expected for products whose manufacture requires the use of carbon-based fuels. As noted above, such

measures would control only that half of the carbon dioxide generated by point sources.

An alternative disposal mechanism is to transfer the carbon dioxide into a biospheric bank of carbon[9]. The transfer to a terrestrial bank could be accomplished by growing long-lived trees which are left unharvested, or by growing short-lived plants which are converted to humus or allowed to accumulate in artificial peat bogs. Each year 56 Gtons of carbon are transferred from the atmosphere to the terrestrial biosphere through net photosynthesis (see Table 2.1.10). This is ten times the amount of carbon put into the atmosphere in 1978 by the burning of fuels so that a 10 percent increase in primary productivity would equal the fuel input. The increase in productivity could be achieved by increasing the area for growing either long-lived trees or short-lived humus forming plants, or by increasing primary productivity in existing plant communities. However, projected future rates of use of carbon-based fuels (see Section 2.1.10) indicate that the rate of carbon release into the atmosphere, 10-20 Gtons/year in the year 2000, will become a much larger fraction of the primary productivity.

The principal limitation on developing a terrestrial biospheric carbon bank is one of land availability as is indicated in Table 2.1.10, 38% of the available land is covered with trees having a net primary productivity greater than 700 tons/km^2/year. Nine and a half percent of the land is under cultivation, and this fraction will increase in the future under pressure from increased population. Low productivity lands

comprise 52% of the total area. The relative percentage of area coverage of lands in this category is shown in Table 2.1.16. If all the land in savanna and grasslands were converted into forest with a standing crop averaging a biomass of 15,000 tons C/km^2, an average value of tropical and temperate forest, then 360 Gtons of carbon could be stored in the living forest and additional carbon in the soil. This is equivalent to the cumulative total of carbon released over the next 30 to 40 years depending on assumptions of the growth of use of carbon-based fuels (Section 2.1.10).

TABLE 2.1.16

Land Area Coverage of Lower Primary Productivity Ecosystems

Ecosystems	Area (in 10^6 km^2)	Percentage of Total Land Area
Savanna	15	10.1
Temperate Grasslands	9	6.0
Tundra and Alpine	8	5.4
Desert	18	12.1
Rock, sand and ice	24	16.1
Lake and Stream	2	1.3

A massive forestation program involving 16% of the earth's surface could ameliorate any adverse carbon dioxide effects. The area required might be significantly less if only a fraction of the fuel generated carbon remains in the atmosphere. In Sections 2.2 and 2.5 we explore the possibility that only 20% of the fuel generated carbon remains in the

atmosphere. In this case, the land area to be forested in order to remove the CO_2 is 5 million km^2, still a vast undertaking.

A principal technical limitation for a rapid forced growth of trees would be availability of appropriate fertilizer. However, it would appear that the institutional, political, social and economical deterrents to massive forestation limit the availability of the biospheric option for carbon storage. Savanna and grasslands play a critical role in maintaining diversity of the biosphere. They serve as pasture land and hunting grounds for many societies. They are governed by large numbers of political institutions, not all of which have consistent goals.

In summary, it seems likely that there are technical means of slowing the growth of carbon dioxide in the atmosphere, while still continuing the use of increasing amounts of carbon-based fuels. Our preliminary assessment indicates, however, that significant non-technical barriers, both economical and social, to the implementation of these options must be surmounted if they are to be employed in a significant scale.

2.1.10 Future Inputs of Carbon into the Atmosphere from the Use of Carbon-Based Fuels

Predictions of the future impacts of carbon dioxide on the environment and on man depend critically on forecasting future levels of carbon dioxide in the atmosphere. Such a prediction requires an understanding of the essential elements of the carbon cycle. The burning of

carbon-based fuels adds carbon to the atmosphere as does deforestation and soil erosion. The oceans can absorb carbon and the biosphere may be a source or sink of carbon. Some of the complexities and uncertainties in understanding the carbon cycle are discussed in Sections 2.2 and 2.5. In this subsection we consider only estimates of the future contribution of fuel use to the world's carbon balance.

Estimates of future fuel inputs of carbon depend most sensitively on the world wide rate of increase in the use of carbon-based fuels. The carbon input will also depend on the mix of fuels used to provide the demanded energy (Table 2.1.12). Both the role of increase of fuel usage and the mix of fuels employed is changing in varying ways in different parts of the world. In the industrialized world the rate of increase of use of carbon-based fuels is decreasing while in the developing world the reverse is true. In 1974, the United States used 27% of the carbon-based fuels; in 1978 this figure was down to 24%. In terms of fuel mix the U.S. plans in the 1980's to increase the use of coal and lessen the use of oil while the Soviet Union plans to raise the fraction of its total energy derived from natural gas from 22% in 1978 to 40% in 1985. Such shifts in fuel mix and rate of usage make uncertain any forecast of future fuel inputs of carbon to the atmosphere.

In 1978, the industrialized world, the OECD countries, the USSR and Eastern Europe used about 74% of the world's carbon-based fuels. The estimated rate of growth in 1978 of carbon-based fuels in these countries was 3.7% per year while the use in developing countries was about 6% per

year. In the future, the trend towards decreasing rates of growth in the industrialized world can be expected, particularly as prices rise and the rate of growth of population (now about 0.8% per year) decreases; the future pattern in developing countries is much less certain. In a country with abundant energy supplies, the USSR, industrialization during the 1930 to 1955 period, except for the war years, was accompanied with annual increases in energy consumption of 10 to 20% per year. As industrialization was achieved, energy growth rates in the 1960's and 1970's were close to those of Western Europe and the U.S., the Soviets became more careful in their energy usage. In the current developing world, a few countries, for example Mexico and China, have abundant energy resources and industrialization in these countries may be accompanied by very high rates of increased energy usage. Other developing countries will feel strong pressures for industrialization since they face population growth rates of 2% per year and will face even higher growth rates in the working age population in the 1980's and 1990's. The pressures for industrialization, however, may be dampened by ever-increasing energy costs.

In view of these uncertainties, we examine two models for future world consumption of carbon-based fuels. In the first model the growth rate is maintained at the historical rate of 4.3% per year. In this projection the world's annual carbon-based fuel consumption is 700 quads in the year 2000 and grows to 2550 quads in 2030 (see Figure 2.1.1). In the second model, the historical growth rate is maintained to 1990 and then the rate of growth decreases linearly to zero over the fifty year period 1990-2040. With the tapered growth, the world would consume 660 quads in the year 2000 and the consumption becomes constant at 1225 quads/year in 2040.

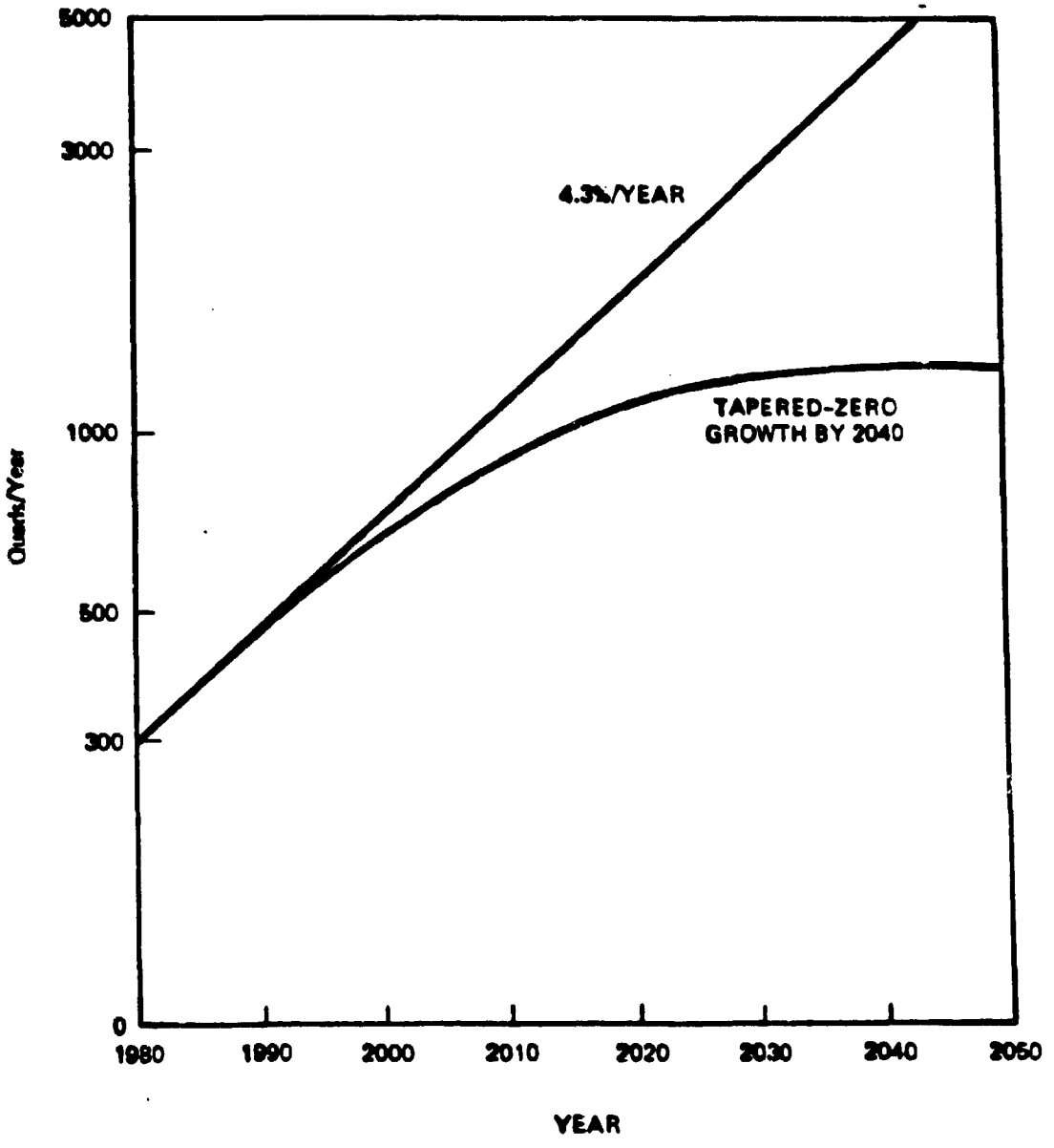

Figure 2.1.1 TWO MODELS OF FUTURE WORLD CONSUMPTION OF CARBON BASED FUEL

Estimates of proved reserves* of the world's carbon-based fuels (1978) are shown in Table 2.1.17[13]. If the world continued to use carbon-based fuels at 4.3% per year, then the cumulative use would exhaust the proved reserves by the year 2010-2015. For the tapered growth scenario, exhaustion is postponed by five to ten years. This rapid depletion of proved reserves suggest that both models over-estimate future use of carbon-based fuels. However, estimates of recoverable resources, Table 2.1.18., indicate that the world's supply of carbon-based fuels could be used over longer periods of time.

TABLE 2.1.17

Estimates of the World's Proved Reserves
Carbon-Based Fuels

Fuel	Recoverable Reserves (Quads)	Carbon Release (Gtons)
Oil	3,200-3,700	64-74
Gas	1,700-2,600	24-37
Coal	15,000	381
Total	19,900-21,300	469-492

*Proved reserves are identified resources which are economically and technologically recoverable at the time the estimate is made.

TABLE 2.1.18

Estimate of Recoverable Resources

Fuel	Recoverable Resources (Quads)	Carbon Release (Gtons)
Oil	8,700- 11,000	174- 220
Gas	9,100- 9,800	131- 141
Coal	86,000-160,000	2,184-4,064
Sub-Total	103,800-180,000	2,489-4,425
Oil Shales and Tar Sand	14,000-100,000	280-2,000
Non-Conventional Gas (U.S. Only)	20,000- 60,000	288- 864
Total	137,800-340,800	3,057-7,289

Continuing the historical rate of growth through 2050 would exhaust recoverable resources if the lowest estimate were appropriate, while in the tapered growth model, the resources could be sufficient to carry the world into the 2400's. Clearly these extrapolations, designed to provide minimum times of exhaustion, are vastly oversimplified since actual use will follow a logistics curve rather than a simple exponential or a tapered exponential growth.

The comparison of energy demand and resource availability indicates that the historical extrapolation represents the worst case scenario and that even the tapered growth model probably overestimates the contributions of fuels to the world's carbon cycle.

The cumulative amount of carbon placed into the atmosphere by the burning of fuels will depend on the mix of fuels. Figure 2.1.2 shows the cumulative carbon deposited in the atmosphere for the 4.3% per year model if the present fuel mix is maintained. In addition, three extreme cases are shown in which all the energy is derived from natural gas, or coal or synthetic fuels. For synthetic fuels, the carbon to energy ratio is taken as 40 kgC/10^6 Btu (see Table 2.1.12). In addition, the time at which the carbon content of the atmosphere is doubled is noted. This time is calculated on the assumption that the ratio of carbon released by fuel burning to the carbon increase in the atmosphere is one-half. This ratio has been empirically determined by observations over the past twenty years. However, this interpretation neglects possible biospheric and oceanic interactions which could substantially lower the fraction of fuel carbon that remains in the atmosphere (see Section 2.5).

Figure 2.1.3 presents similar projections of fuel carbon assuming a tapering of the growth rate to zero in 2040. The comparison of Figures 2.1.2 and 2.1.3 illustrates the sensitivity of estimates of future atmospheric carbon levels to growth rate assumptions. With the present fuel mix, 1400 Gtons of carbon will be added to the atmosphere by the year 2035 if the historical growth rate is maintained; with a tapered growth rate the date is pushed forward 20 years. Because of the nature of exponential growth small shifts in the direction of reducing use of carbon-based fuels through conservation can bring about significant reductions in the cumulative amount of carbon added to the atmosphere over a fixed period.

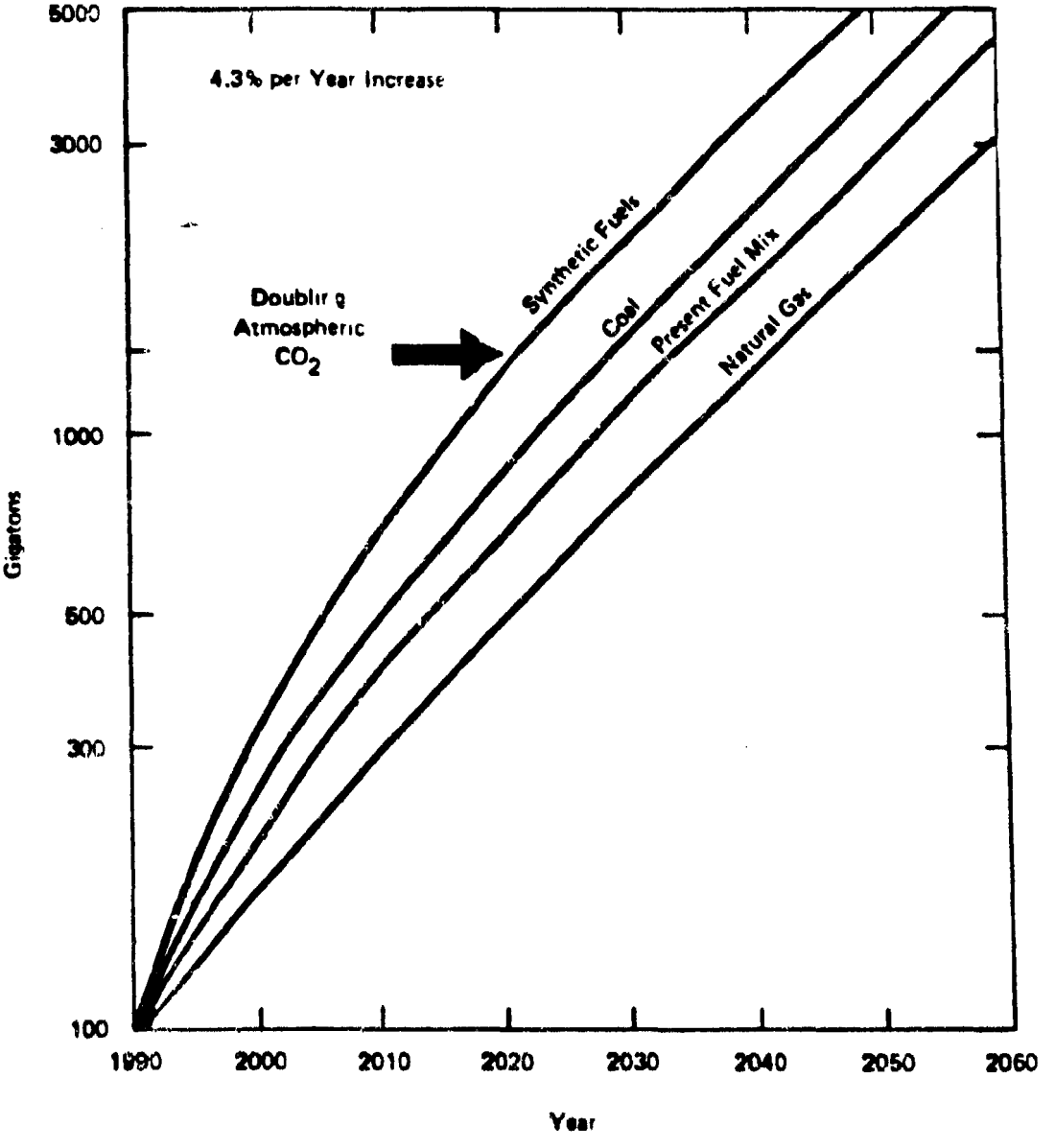

Figure 2.1.2 CUMULATIVE CARBON EMITTED INTO ATMOSPHERE SINCE 1978

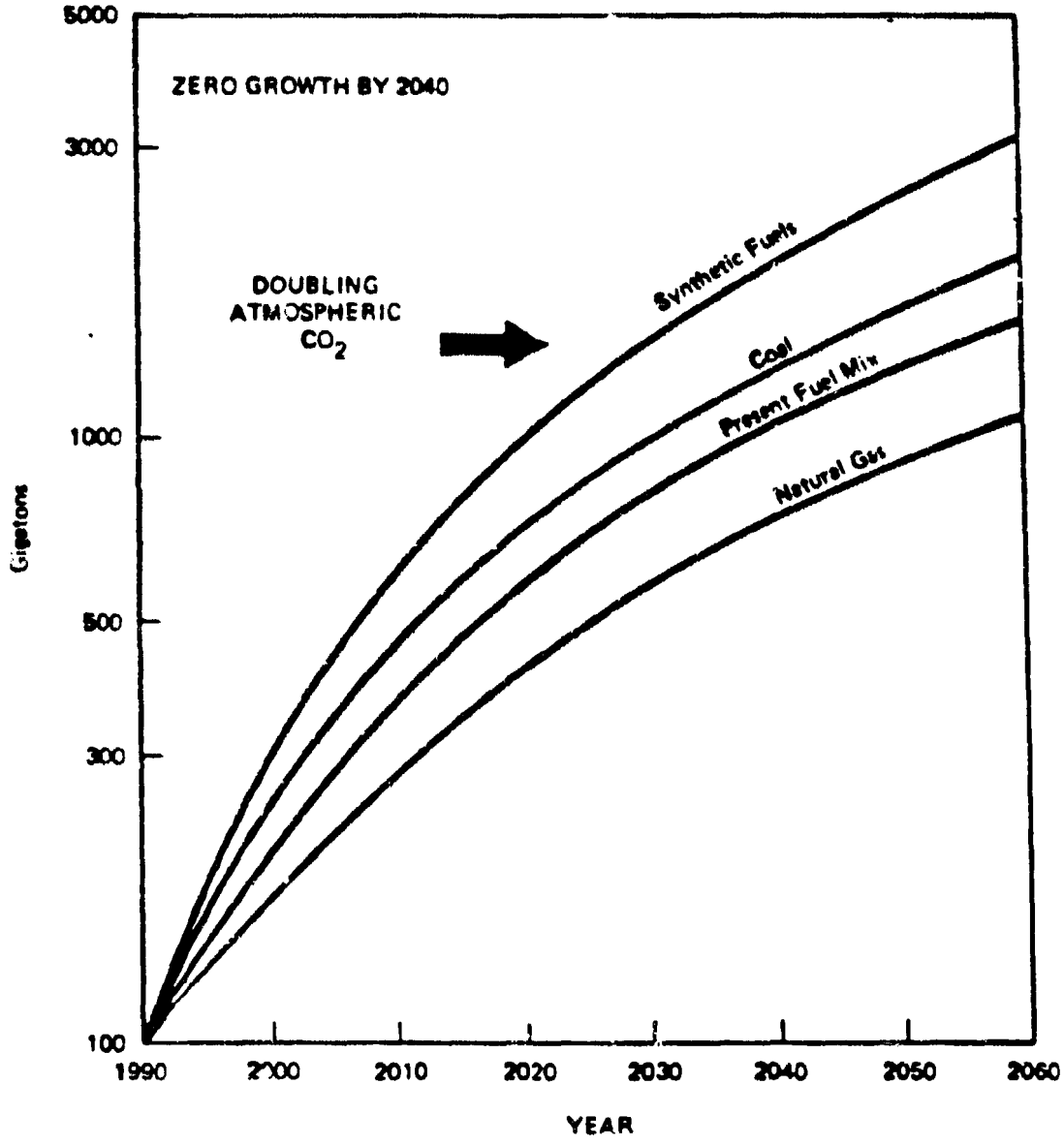

Figure 2.1.3 CUMULATIVE CARBON EMITTED INTO ATMOSPHERE SINCE 1978

The mix of fuels used also influences the rate at which carbon is added to the atmosphere. If all energy were derived from synthetic fuels, then in the tapered model, 1400 Gtons of carbon would be placed in the atmosphere by the year 2030 as contrasted with the date 2055 if the present mix of fuels were maintained. Clearly the world will not depend solely on synthetic fuels in the foreseeable future. However, the existence of abundant coal reserves in the United States, the Soviet Union, Great Britain, and Australia (for possible use by Japan) suggests that countries may select a coal and/or synthetic fuels option. Steps in that direction will accelerate the addition of carbon to the atmosphere.

In summary, estimates of the fuel input to the carbon cycle are uncertain primarily because of the unknown rate of energy usage and the fuel mix of the future. In 1978, the contribution to energy demand by non-carbon producing sources--hydropower, solar and nuclear--was small compared with carbon-based sources. These will grow in the future displacing oil, coal and natural gas. While the hydropower potential of certain regions is near exhaustion, further contributions, particularly in low-head hydropower can be anticipated. Passive solar is economical in 1979 in many parts of the world and active solar could become important two to three decades hence. The industrialized world is pursuing the nuclear option, and nuclear energy will very probably make a significant contribution to energy usage. However, the vast investment in the infrastructure of industrialized societies in carbon-based fuels makes it unlikely that these fuels will not be a major source of energy in the coming decades. In view of these considerations, we will use the present fuel mix and a tapered growth

rate in the base case model projections. In this model the enhanced use of synthetic fuels and coals with increased carbon production is assumed to be offset by the increased use of nuclear, hydroelectric, solar and possibly fusion sources of energy. In this model, the cumulative total of carbon put into the atmosphere by burning fuels will be 1400 Gtons in 2055.

REFERENCES FOR SECTION 2.0-2.1

1. Callendar, C., Quarterly Journal of Royal Meteorological Society, 64, 223-237, 1938.

2. Keeling, C. D., Tellus, 25, 174-198, 1973.

3. Rotty R. M., in The Fate of Fossil Fuel CO_2 in the Oceans, N. Anderson and A. Melahoff (eds), Plenum Press, New York, 1977.

4. U.S. Department of Interior, Environmental Impact Statement: Federal Coal Management Program, 1978.

5. Flour Engineers and Constructors, Inc., H-Coal Commercial Evaluation, Los Angeles, California, 1976.

6. Jahnig, C., HYGAS Process, EPA 650/2-74-009-h, NTIS-PB 247-275, Springfield, Virginia, 1975.

7. Whittaker R., in Primary Productivity of the Biosphere, H. Lieth and R. Whittaker (Eds). Springer-Verlag, 305-328, 1975.

8. Pimentel, D., et al., "Food production and the energy crisis", Science, 182, 443-448, Nov. 2, 1973.

9. Dyson, F. and Morland, G., in Workshop on the Global Effects of Carbon Dioxide from Fossil Fuels, ed. W. Elliot and L. Machta, Department of Energy, Conf - 770385, 1979.

10. Hare, M., et al., Sources and Delivery of Carbon Dioxide for Enhanced Oil Recovery, Department of Energy, FE-2515-24, 1978.

11. Pappano, A., et al., Availability and Economics of CO_2 for Enhanced Oil Recovery in Appalachia, ERDA Grant No. G0155014, 1976.

12. Marchetti, C., On Geoengineering and the CO_2 Problem, RM-76-17, International Institute for Applied Systems Analysis, Laxenburg, Austria, 1976.

13. MacDonald, G., Long-Term Availability of Natural Resources in Alternatives for Growth, ed. H. McHains and L. Wilcox, Ballinger, Cambridge, 1978.

2.2 Influence of the Biosphere on the Carbon Cycle

2.2.1 Balance-Sheet of the Carbon Cycle

We may crudely represent the balance-sheet of the carbon cycle by an equation

$$A = F - B + D - S \quad . \qquad (2.2.1)$$

A is the annual increase in atmospheric CO_2, F is the annual release of CO_2 in fossil-fuel burning and cement manufacture, B is the net increase of biomass and soil carbon produced in response to the increase of atmospheric CO_2, D is the decrease in biomass and soil carbon produced by deforestation and erosion, and S is the net annual flow of CO_2 into the oceans. All these quantities are conveniently expressed in Gtons of carbon per year. The 1978 values of A and F are accurately known and are $A = 2.6$, $F = 5.6$ in these units. The values of B , D , and S are highly uncertain. In trying to predict the future carbon content of the atmosphere in response to the burning of carbon-based fuels, it is essential to determine the magnitude and probable trend of each of the quantities F , B , D , and S separately. As has been discussed in Section 2.1, the projections of F are uncertain, those of B , D and S are even more so.

In recent years the problem of the "missing carbon" has received attention. Estimates of B and D by terrestrial ecologists (for

example, Woodwell, et al[1]) and of S by oceanographers (for example, Broecker, et al[2]) were in glaring disagreement with Equation (2.2.1). Typical estimates were B ~ 1, D ~ 6, S ~ 2, leaving a discrepancy of 6 gigatons of "missing carbon" between the left and right sides of the equation. At least one of these estimates must be seriously wrong. Either B or S was underestimated or D was overestimated. To pin down the source of the discrepancy an understanding of biospheric processes is essential. The following three subsections consider B , D , and S in turn.

2.2.2 Response of Natural Vegetation to Increasing Atmospheric CO_2

There are two distinct ways in which atmospheric CO_2 increase may contribute to the quantity B . We define B_1 and B_2

$$B = B_1 + B_2 \quad , \tag{2.2.2}$$

where B_1 is the annual increase in biomass above-ground and B_2 is the increase in biomass and soil carbon below-ground. The mechanisms giving rise to B_1 and B_2 are different. B_1 is the effect of increased growth in long-lived vegetation, principally trees. B_2 is the effect of increased root-to-shoot ratios, not only in trees but also in short-lived plants, grassland and swamps. The importance of root-to-shoot ratios lies in the fact that shoots and leaves decay more rapidly than roots. An increased root-to-shoot ratio means that a larger fraction of net primary production of biomass is being transferred to the long-lived reservoir underground (for details of the underground reservoir see Schlesinger[5,6]).

It is quite possible that B_1 is zero, if it happens that biospheric growth is not CO_2-limited. To estimate an upper limit to B we may assume that the entire net primary production (NPP) of the terrestrial biosphere (about 57 Gtons of carbon per year, see Table 2.1.10) response to CO_2 increases as indicated by the growth-chamber experiments discussed in Section 4.5. These experiments suggest that approximately

$$\frac{\delta NPP}{NPP} = \beta \frac{A}{C} \qquad (2.2.3)$$

where δNPP is the increased net primary productivity in one year associated with an increase A in the carbon content of the atmosphere and is a constant whose value is probably between 0 and 1 and C is the current concentration of CO_2 in the atmosphere. The 57 Gtons of NPP was in balance with decay processes before fossil-fuel burning began. If we assume that the 7% increase (over the last 20 years) in atmospheric CO_2 produced a $3\frac{1}{2}$ % increase in NPP while the decay processes remained unchanged, then the resulting excess of NPP over decay gives our upper limit for B_1

$$B_1 < 1.75 \qquad (2.2.4)$$

A similar argument is more difficult to apply to B_2 because we lack evidence for response of root-to-shoot ratios to CO_2 in ecologically important species. According to Strain[3] reporting an experiment of Knecht[4], root-to-shoot ratio of radishes increases by more than a factor of 2 when CO_2 concentration is increased by a factor of 3. This evidence, for what it is worth, indicates that root-to-shoot ratios may increase roughly

in proportion to the concentration of CO_2. If y is the aggregate root-to-shoot ratio of NPP in the terrestrial biosphere, and if f is the fractional change in y produced by CO_2 increase, then the increase in underground growth due to the change in y is

$$U = fy(1 + y)^{-2} \times NPP \quad . \tag{2.2.5}$$

Since (2.2.5) is a maximum for $y = 1$,

$$U < f/4 \times NPP \quad . \tag{2.2.6}$$

We assume, as we did in estimating B_1 , that the underground growth was in equilibrium with decay before the rise in atmospheric CO_2 began, and that the increase U in underground growth is uncompensated by increased decay. Equation (2.2.6) therefore gives an upper limit for B_2 . The NPP of terrestrial plants including short-lived species is about 57 Gtons, and f may be as large as 0.07% if radishes are representative of the biosphere. Therefore, Equation (2.2.6) gives the estimate

$$0 < B_2 < 1 \quad . \tag{2.2.7}$$

Putting together the estimates for B_1 and B_2 and adding a little extra for errors and omissions, we obtain our estimate for B ,

$$0 < B < 3 \quad . \tag{2.2.8}$$

The important conclusion of this analysis is that B cannot be large enough to cover the "missing carbon" deficit. Even with our generous estimates of the responses in NPP and root-to-shoot ratios to atmospheric CO_2 increase, the present contribution of B to the carbon cycle is insufficient.

We are led to conclude that the terrestrial biosphere is a net source of atmospheric CO_2 and that the "missing carbon" must be somehow finding its way into the oceans if indeed D is positive and of the same order as F .

It is, of course, possible that the terrestrial biospheric reservoir of carbon is increasing or decreasing in response to climatic changes that have occurred in recent centuries, quite independently of the changes in atmospheric CO_2. If this is so, we must add to our estimate (2.2.6) a contribution from CO_2-unrelated growth. Increases in temperature may have a negative effect on the rate of photosynthesis about equal to the gain in photosynthesis (see Section 4.5). We do not attempt a numerical estimate of the CO_2-unrelated contribution to B . The rate of growth of the biosphere is a measurable quantity, and we hope that within a few years we may be determining its value by measurement rather than by speculative guesswork.

2.2.3 Deforestation and Erosion

Bolin[7], Stuiver[8], Tans[9], Woodwell, et al[1] and Schlesinger[6] have recently analyzed the impact of deforestation and soil erosion on the

terrestrial carbon balance. Our analysis follows closely along the lines of this earlier work.

We divide D into two parts

$$D = D_1 + D_2 \qquad (2.2.9)$$

representing loss of carbon from plants D_1 (mainly trees) and from soil, D_2. We place primary reliance of the estimates of Schlesinger

$$D_2 = 0.8 \quad , \qquad (2.2.10)$$

and of Woodwell, et al[1]

$$D_1 = 5.8 \quad , \quad D_2 = 2 \quad , \qquad (2.2.11)$$

obtained by looking in detail at the selected areas of the world in which soil is being eroded and forests destroyed. Woodwell (personal communication, June 1979) revised the published estimate (2.2.11) downward to $D_1 = 3.9$, but Woodwell maintains that D_1 is large mainly because of the destruction of tropical forests. Bolin's[7] estimates are much lower

$$D_1 = 0.7 \quad , \quad D_2 = 0.3 \quad . \qquad (2.2.12)$$

Stuiver and Tans derive their estimates of D from a study of the ratios of the isotopes Carbon 12, Carbon 13, and Carbon 14 in trees. These

ratios give information about the net annual decrease of biomass $(D - B)$ rather than about D separately. According to Stuiver, the ratios indicate

$$D - B = 0 \quad , \tag{2.2.13}$$

and according to Tans

$$D - B = -1 \quad , \tag{2.2.14}$$

in sharp disagreement with Woodwell. Tans (personal communication, June 1979) argued that the tree-ring data are affected by large fluctuations of unknown origin. Tans does not regard C^{12}/C^{13} ratios as providing a reliable estimate of biospheric decrease. Review of the C^{12}/C^{13} literature[10] indicate that different substances in plant tissue show considerable differences in relative concentrations of C^{12} and C^{13}. Such differences are also shown in trees growing a few hundred meters apart. In view of these uncertainties, we have not used the isotope data to estimate $D - B$. Broecker, et al[13] rely on tree ring data to reach the conclusion that $D - B$ is small.

The estimates of D_1 and D_2 regarded as most probable by Schlesinger and Woodwell are

$$3 < D_1 < 7 \quad , \quad 1 < D_2 < 2 \quad , \tag{2.2.15}$$

giving the total annual biospheric loss

$$4 < D < 9 \qquad (2.2.16)$$

If Bolin's[7] estimates are included then the range for annual biospheric loss becomes

$$1 < D < 9 \qquad (2.2.17)$$

2.2.4 Eutrophication of the Ocean

The annual net flow of CO_2 into the oceans is composed of two parts

$$S = S_1 + S_2 \quad , \qquad (2.2.18)$$

the first being the effect of mechanical transport and mixing of surface water saturated with CO_2 into the deep ocean, the second being the effect of biological activity in the ocean. The physical-chemical mixing processes are discussed in Section 2.3. Although the uncertainties are large, the consensus among oceanographers agrees with the estimate of Broecker, et al.[2]

$$S_1 = 2 \quad . \qquad (2.2.19)$$

Here we discuss the biological contribution S_2 arising from eutrophication of the ocean.

The basic reactions contributing to S_2 are:

(1) Photosynthesis

$$CO_2 \rightarrow C + O_2$$

in the surface layer of the ocean. Carbon is not a limiting nutrient in the surface layer.

(2) Descent of particulate carbon, either as intact organisms, as fecal pellets or as organic molecules adsorbed onto inorganic dust, into deeper layers.

(3) Bacterial oxidation of particles

$$C + O_2 \rightarrow CO_2$$

in the deeper layers.

The net effect of these reactions is to pump CO_2 from the atmosphere down into the deep ocean, and to transfer O_2 from the deep ocean into the surface ocean layer where it becomes super-saturated and is released to the atmosphere.

Williams (personal communication, June 1979) has measured the particulate carbon descent and oxidation in the North Pacific. He finds that between 10% and 16% of the net primary production in the surface layer descends to depths greater than 300 meters before being oxidized. Since the net primary production of the ocean surface layer is about 25 Gtons per year (Table 2.1.11), extrapolation of the results of Williams to the entire

ocean gives S_2 between 2.5 and 4. Riley (personal communication, March 1979) had made earlier determinations of particulate carbon in the North Atlantic. The extrapolation of his observations gives $S_2 = 6$. Eppley and Peterson[14] conclude that global new production in the euphotic zone of the ocean approximates the sinking flux of particulate organic matter to the deep ocean. Their estimate of the new production is 3.4 to 4.7, consistent with the estimates of Riley and Williams. We conclude that S_2 lies in the range

$$2 < S_2 < 6 \quad . \tag{2.2.20}$$

For a description of the experimental difficulties which complicate the monitoring of particulate carbon in the oceans see Riley[11] and Eppley and Peterson[14]. If we accept (2.2.20), then we obtain for the current total flux of CO_2 into the ocean

$$4 < S < 8 \quad . \tag{2.2.21}$$

Our inclination to trust the estimates of Williams and Riley is strengthened by the fact that (2.2.21) gives a large enough carbon sink to bring Equation (2.2.1) into balance and solve the "missing carbon" mystery. Equation (2.2.1) requires that

$$S + B - D = F - A = 3 \tag{2.2.22}$$

Since D is probably greater than 1 (see Equation 2.2.17), B less than 1.5, then S must be greater than 3.5. A consistent set of numbers is

$$A = 2.6 \ , \quad F = 5.6 \ , \quad D = 4 \ , \quad S = 6 \ , \quad B = 1 \qquad (2.2.23)$$

which would require that $S_2 = 4$, near the center of the limits indicated by Equation (2.2.20), and D is at the lower limit of the Woodwell-Schlesinger estimates, Equation (2.2.16). An alternative set of numbers consistent with Bolin's interpretation of the biospheric situation would be

$$A = 2.6 \ , \quad F = 5.6 \ , \quad D = 1 \ , \quad S = 3 \ , \quad B = 1 \qquad (2.2.24)$$

which would put $S_2 = 1$ at the lower range of the Riley-Williams estimates and below the Eppley-Peterson estimates. Clearly, the numerical values of D and S are very uncertain, but we consider it probable that D and S are both large and approximately equal at present.

2.2.5 Summary and Conclusions

If the numbers (2.2.23) happened to be correct, it would mean that the total man-made production of CO_2 would be 8.6 Gtons of carbon per year, 65% from fossil-fuel burning and 35% from deforestation and erosion. Of these 8.6 Gtons, 30% would remain in the atmosphere, and the remainder would go into the ocean. The increase in terrestrial biosphere is at present smaller than the other terms in Equation (2.2.1). Alternatively, if the numbers (2.2.24) are adopted, then 40% of the man-made CO_2 remains airborne.

We have reached, subject to the usual uncertainties, the conclusion that only about one-fourth to two-fifths of our production of man-made CO_2 remains in the atmosphere. The atmosphere is currently saved from a far more rapid build-up of CO_2 by the operation of the Williams-Riley oceanic pump. Unfortunately, as often happens in ecological situations, a problem is mitigated at one point of a cycle at the cost of intensifying another problem somewhere else. In this case, the mitigation of CO_2 build-up in the atmosphere is achieved at the cost of intensifying the eutrophication of the ocean. If our estimate (2.2.20) of the throughput of the Williams-Riley pump is correct, it means that 13 Gtons of molecular oxygen per year are pumped out of the deep ocean into the atmosphere. The ocean contains at present a total of about 8400 Gtons of dissolved oxygen[12]. The oxygen deficit (difference between the quantity of O_2 in a saturated ocean and the quantity actually present) is already about 3000 Gtons. We therefore raise the question whether the depletion of oxygen in the ocean may not be as critical an environmental problem as the increase of CO_2 in the atmosphere. The oxygen cycle will be discussed in detail in the following section.

REFERENCES FOR SECTION 2.2

1. Woodwell, G. M., R. H. Whittaker, W. A. Reiners, G. E. Likens, C. Delwiche, and D. B. Botkin, "The Biota and the World Carbon Budget", Science, 199, 141-146, Jan. 13, 1978.

2. Broecker, W.S., T. Takahashi, H. J. Simpson, and T. H. Peng, "The Fate of Fossil Fuel CO_2: Can the Global Carbon Budget be Balanced?" Lamont-Doherty Geological Observatory, Palisades, N.Y., Preprint, 1976.

3. Strain, B.R., "Report of the Workshop on Anticipated Plant Responses to Global Carbon Dioxide Enrichment", Duke University, Durham, North Carolina, 1978.

4. Knecht, G. N., "Response of Radishes to High Carbon Dioxide", Hortscience, 10, 274-275 (1975).

5. Schlesinger, W. H., "Carbon Balance in Terrestrial Detritus", Ann. Rev. Ecological Systems, 8, 51-81 (1977).

6. Schlesinger, W. H., "The World Carbon Pool in Soil Organic Matter: A Source of Atmospheric CO_2?" in The Role of Terrestrial Vegetation in the Global Carbon Cycle, Woodwell, G. M., Eds. (Wiley, New York, N.Y. 1979).

7. Bolin, B., "Changes of Land Biota and Their Importance for the Carbon Cycle", Science, 196, 613-615 (May 6, 1977).

8. Stuiver, M., "Atmospheric Carbon Dioxide and Carbon Reservoir Changes", Science, 199, 253-258 (Jan. 20, 1978).

9. Tans, P. P., "Carbon 13 and Carbon 14 in Trees and the Atmospheric CO_2 Increase", University of Groningen Thesis, Veenstra, Groningen (1978).

10. Bell, P. R., Carbon-13 from Tree Rings as a Tracer in the Carbon Dioxide Problem, Institute of Energy Analysis, Oak Ridge, ORAO/IEA-79-10, 1979.

11. Broecker, W., T. Takahashi, H. Simpson, and T. Peng, "Fate of Fossil Carbon Dioxide and the Global Carbon Dioxide Budget", Science, 206, 409-418, 1979.

12. Eppley, R., and B. Peterson, "Particulate Organic Matter Flux and Planktonic New Production in the Deep Ocean", Nature, 282, No. 5740, 677-680, 1979.

13. Riley, G. A., "Particulate and Dissolved Carbon Dioxide in the Oceans", Proc. 24th Brookhaven Symposium in Biology, Ed. G. M. Woodwell and E. V. Pecan, USAEC Tech. Inf. Center, 204-220 (1973).

14. Kester, D. R. "Dissolved Gases Other Than CO_2, "Chemical Oceanography, Ed. J. P. Riley and G. Skirrow, 2nd Ed., Chapter 8, 1, 530-541 (Academic Press), London, 1975.

2.3 Oxygen Cycle

The burning of carbon-based fuels and deforestation and erosion remove oxygen from the atmosphere through the formation of carbon dioxide. Since the rate of addition of carbon dioxide from the burning of fuels is known, an understanding of the oxygen cycle could aid in determining the net contribution of the biosphere to the carbon cycle[1].

2.3.1 Balance-Sheet of the Oxygen Cycle

The oxygen balance-sheet can be summarized in the equation

$$P + Q - R = \frac{8}{3}(A + S) + 8H \quad . \qquad (2.3.1)$$

Here P is the annual decrease of oxygen in the atmosphere, Q is the annual decrease of dissolved molecular oxygen in the ocean, and R is the annual net increase of combined oxygen resulting from chemical reactions of nitrogen, sulfur and iron, etc., all expressed in Gtons of oxygen per year. H is the number of Gtons of hydrogen burned per year in fossil fuel, and A, S are the numbers of Gtons of carbon in CO_2 added to the atmosphere and the ocean respectively (see Equation 2.2.1). The quantity H can be determined from the mix of fuels burned (see Table 2.3.1)

$$H = 0.89 \qquad (2.3.2)$$

TABLE 2.3.1

Estimated World Generation of Water
Through Burning Carbon-Based Fuels (1978)

Fuel	Assumed H/C Ratio	Water Generated in Gtons of Hydrogen
Oil	2	0.44
Natural Gas	4	0.26
Natural Gas Flared	4	0.05
Coal	0.8	0.14
Total		0.89

The estimation of R will be considered in Section 2.3.2. It turns out that R is small compared with the other quantities in Equation (2.3.1) and is approximately equal to 1 Gton per year. When the numerical values of R , A and H are inserted, Equation (2.3.1) becomes

$$P + Q - \frac{8}{3}S = 15 \quad . \qquad (2.3.3)$$

If we could independently measure P and Q , the annual fluxes of oxygen out of the atmosphere and ocean, Equation (2.3.3) would provide an independent determination of the crucial quantity S , the flux of CO_2 into the ocean.

Machta and Hughes[2] determined the oxygen content of the atmosphere in 1968-70 to an accuracy of about three parts in 10^5. Comparison with

measurements made in 1911 indicates that in the 59-year period the oxygen concentration changed by less than 0.01% from the present value of 20.946% by volume. The total mass of oxygen in the atmosphere is about 1.2×10^6 Gtons. If the oxygen-nitrogen ratio in the atmosphere could be measured with an accuracy of 1 part per million, P would be determined within 1 Gton. Happer describes in Section 2.3A a method of measuring oxygen-nitrogen ratios which would provide the required accuracy.

A measurement of P will be immensely valuable, just as the measurements of atmospheric CO_2 by Keeling[3] have been invaluable, because the atmosphere is a well-mixed reservoir both for oxygen and for CO_2 with a mixing-time on the order of a year or two. We expect that the local fluctuations in space and time of O_2 and CO_2 concentrations in the atmosphere will be of comparable magnitude, if both concentrations are measured in parts per million of the total atmosphere. The fact that the atmosphere contains a thousand times as much O_2 as CO_2 does not imply that the measurement of O_2 will be inherently noisier than the measurement of CO_2. Both for O_2 and CO_2, the local noise and annual fluctuations will give valuable information about the distribution of sources and sinks. The mean trend of P at any one site over a series of years will give an accurate determination of the rate of change of the world inventory of oxygen in the atmosphere. P ought to be measured at several places, but there will be no need to sample the atmosphere at a large number of sites.

The determination of the changes in oxygen concentration in the ocean presents a more formidable problem. The ocean is not well-mixed even

on a time-scale of centuries. A direct measurement of the fluxes Q and S of oxygen and CO_2 into the ocean necessarily requires a massive sampling program. But there are two differences between oxygen and CO_2. The total reservoir of oxygen in the ocean is much smaller than the reservoir of CO_2. The measurement of oxygen concentration is not complicated by the chemical intricacies of carbonate and bicarbonate and buffering with other species which influence the behavior of CO_2 in solution. For both reasons, a direct measurement of Q is likely to be easier than a direct measurement of S. As a practical matter, it makes sense to concentrate on measuring the oxygen fluxes P and Q and to use Equation (2.3.3) to derive the CO_2 flux S.

2.3.2 Minor Reactions Contributing to the Oxygen Cycle

The annual net increase of combined oxygen due to minor reactions may be expressed as

$$R = R_1 + R_2 - R_3 \quad , \qquad (2.3.4)$$

where R_1 is the effect of oxidation of nitrogen, R_2 is the effect of oxidation of sulfur, and R_3 is the effect of the reduction of iron ores in steel-making. Other processes of oxidation and reduction give smaller contributions to R and are here ignored.

The main reaction contributing to R_1 is the oxidation of atmospheric N_2 to nitrate. There are many intermediate reactions involving biospheric nitrogen, ammonia and the various nitrogen oxides.

Industrial production of fertilizer is only 0.04 Gtons of nitrogen per year. Biological nitrogen fixation contributes to R_1 about ten times as much, but is uncertain by at least a factor of two. Stewart[4] estimates total nitrogen fixation at about 0.2, while the NRC report on Nitrogen Oxides[5] estimates 0.5 Gtons of nitrogen. We adopt the estimate 0.4 Gtons of nitrogen, which is converted to nitrate with the removal of

$$R_1 = 1.1 \qquad (2.3.5)$$

Gtons of oxygen.

Oxidation of sulfur, mainly associated with the burning of fossil fuel, is estimated by Stewart at 0.065 Gtons per year. This is converted to sulphate by combination with

$$R_2 = 0.1 \qquad (2.3.6)$$

Gtons of oxygen.

Present world production of steel is about 0.7 Gtons, which releases from the ore about

$$R_3 = 0.3 \qquad (2.3.7)$$

Gtons of oxygen. Putting together Equation (2.3.4-7) we estimate

$$R = 1 \quad . \qquad (2.3.8)$$

The uncertainty in Equation (2.3.8) is about a factor of two, mainly due to the uncertainty in the nitrogen contribution R_1 . But we can say with assurance that R makes only a minor contribution to the oxygen balance-sheet Equation (2.3.1).

2.3.3 Oxygen in the Oceans

Kester[6] gives detailed information about the distribution of dissolved oxygen in the oceans. The distribution of oxygen in the oceans can be estimated from Kester's diagrams to be as follows.

	Pacific	Indian	Atlantic	Total
Oxygen capacity	6000	3000	2600	11600
Oxygen content	3600	2400	2400	8400
Oxygen deficit	2400	600	200	3200

"Oxygen capacity" is the amount (in Gtons) of O_2 which the ocean would contain if it were everywhere saturated. The oxygen deficits occur in a thick layer of water extending from 100m below the surface to several kilometers in depth. The deficits are distributed unevenly over the oceans and are strongly correlated with regions of high biological productivity at the ocean surface.

The crucial question which has to be answered is whether the oxygen deficit of the oceans is increasing or not. In other words, is the

net flow Q of oxygen in or out of the ocean. If the oceans were in a state of natural equilibrium, Q would be zero on the average and would only fluctuate above and below zero in response to natural fluctuations in ocean dynamics and in biological activity. The time-scale of such natural fluctuations would be related to the turn-over time of the deep ocean (500-1000 years) but the magnitude of such natural fluctuation is not known. Nevertheless, if it should happen that Q is measured and found to be large and positive, that would be prima facie evidence indicating that the oxygen deficit may not be in equilibrium and may be increasing as a result of human actions.

We present a very preliminary analysis of the processes contributing to Q. Let

$$Q = -Q_1 + Q_2 \quad , \tag{2.3.9}$$

where $(-Q_1)$ is the effect of physical transport and diffusion in the ocean and Q_2 is the effect of biological activity. This division of Q is analogous to the division of the CO_2 flux S into two parts in Equation (2.2.17). In the physical transport, oxygen and CO_2 move together, while in the biological processes of the Williams-Riley pump oxygen and CO_2 move in opposite directions.

For the physical part of Q and S we write

$$Q_1 = M\left(f_{os} - f_{od}\right) \quad , \tag{2.3.10}$$

$$S_1 = M\left(f_{cs} - f_{cd}\right) \quad . \tag{2.3.11}$$

Here

$$M = 10^6 \qquad (2.3.12)$$

is the mass-flow of the physical transport processes in Gtons of water per year. The numerical value Equation (2.3.12) is estimated from the pipe-model of ocean transport described in Section 2.4 of this report. The ratio f_{os} is the mass-fraction of dissolved oxygen in the water entering the transport cycle at the ocean surface, while f_{od} is the mass-fraction of dissolved oxygen in the flow returning to the surface from below. Similarly, f_{cs} and f_{cd} are the mass-fractions of carbon in the form of dissolved CO_2. Since the surface water is saturated with both oxygen and CO_2, we have roughly

$$f_{os} = 300 \text{ micromole/kg} = 9.6.10^{-6} \quad , \qquad (2.3.13)$$

$$f_{cs} = 2500 \text{ micromole/kg} = 3.10^{-5} \quad . \qquad (2.3.14)$$

The value of f_{od} differs from ocean to ocean. An accurate estimate of Q_1 would require a detailed account of flow-volumes and oxygen deficits in the various oceans. For a preliminary estimate, we assume that f_{od} is equal to the mean oxygen-fraction of the entire ocean, namely

$$f_{od} = 7.0.10^{-6} \quad . \qquad (2.3.15)$$

Then Equations (2.3.10) and (2.3.12) give

$$Q_1 = 2.6 \quad . \qquad (2.3.16)$$

The estimation of f_{cd} is much more difficult since the CO_2 is close to saturation throughout the ocean. In Section 2.2 [Equation (2.2.18)] we used Broecker's estimate

$$S_i = 2 \quad , \tag{2.3.17}$$

which is equivalent to assuming

$$f_{cs} - f_{cd} = 2.10^{-6} \quad . \tag{2.3.18}$$

The near-equality of Q_1 and S_1 appears to be a numerical accident without causal implications.

The relation between the biological fluxes Q_2 and S_2 is much more direct, since the Williams-Riley process releases 1 mole of CO_2 for every mole of O_2 consumed in the deep ocean. Therefore

$$Q_2 = \frac{8}{3} S_2 \quad . \tag{2.3.19}$$

If the estimate Equation (2.2.2) for S_2 is valid, then Equation (2.3.19) gives

$$5 < Q_2 < 16 \quad , \tag{2.3.20}$$

and Equation (2.3.9) with Equation (2.3.20) implies

$$2 < Q < 14 \quad . \tag{2.3.21}$$

The conclusion Equation (2.3.21) is not strong enough to prove that the oceanic oxygen deficit is not in equilibrium. The value $Q = 0$ is not significantly outside our limits of error. But if we believe that the numerical values Equation (2.2.23) of D and S are near to the truth, then Equation (2.3.19) gives

$$S_2 = 5 \quad , \quad Q_2 = 13 \quad , \quad S = 7 \quad , \quad Q = 10 \quad . \qquad (2.3.22)$$

and the ocean is losing oxygen at a rapid rate.

From Equation (2.3.3) we have that the oxygen content of the atmosphere is presently decreasing at a rate

$$P = 15 + \frac{8}{3} S - Q \qquad (2.3.23)$$

For a large biospheric carbon contribution the values of Equation (2.3.22) yield

$$P = 23 \qquad (2.3.24)$$

and because of the dependence of Q on S_2 a lower biospheric source gives a similar value. The observation of Machta and Hughes provide an upper limit to the average value of P over the period 1911-1970 of about 10 Gtons/year based on the limit on the change in oxygen concentration of 0.01% or less over this period[2]. Because of the exponential growth of fuel usage and industry, the calculated value of P for 1978 in Equation (2.3.24) is not inconsistent with the Machta-Hughes limits.

The current removal of oxygen from the ocean is probably not due to natural phenomena. With Q in the range of 2 to 10 Gtons/year, then all the oxygen in the ocean would be removed in a period 1000 to 4000 years, periods short compared with geologic changes, though of the same order as the overturn time of the deep ocean, about 500 to 1000 years. The turnover would not resaturate the deep waters with oxygen unless Q_1 were of the same magnitude as Q_2 .

The conclusions of this preliminary analysis of oxygen in the oceans are as follows:

(1) In the natural state of the oceans before human activities became important, a large oxygen deficit of the order of 3000 Gtons of O_2 existed.

(2) We do not have enough evidence to establish with certainty that the oceanic oxygen deficit is increasing.

(3) Rough estimates indicate that the deficit may be increasing at a rate of the order of 10 Gtons of O_2 per year.

(4) The flow of oxygen out of the ocean, if it is real, cannot be attributed to the effects of atmospheric CO_2 increase. The oceans are almost everywhere almost saturated with CO_2 and the biological productivity of the ocean is never CO_2-limited.

(5) The flow of sewage and of runoff from agricultural land will fertilize the ocean and cause an increase in the oxygen deficit. But these direct effects of human activity seem to

be quantitatively insufficient to explain an increase as large as 10 Gtons per year[6].

(6) Indirect effects of human activity, for example the increase of atmospheric dust falling into the ocean and providing nuclei for the adsorption of dissolved organic carbon, may be increasing the efficiency of transport of organic carbon from the ocean surface to deeper levels. Such indirect effects, when added to the direct effects of nitrogen and phosphorus in human effluents, may be sufficient to account for 10 Gtons per year increase in oxygen deficit[7,8].

(7) It is essential to study the causes of oxygen depletion in detail, using a consistent model of oceanic circulation which also accounts for the transport of CO_2, salinity, temperature and other oceanographic observables.

(8) Above all, copious and long-continued observations are required to eliminate the many uncertainties of the oxygen balance-sheet. In particular, we strongly recommend a program of systematic measurement of the rate P of decrease of oxygen in the atmosphere, either following the suggestion of Happer described in the Appendix to this Section, or otherwise.

REFERENCES FOR SECTION 2.3

1. Machta, L., Personal Communication, May, 1979.

2. Machta, L., and. E. Hughes, "Atmospheric Oxygen in 1967 to 1970", Science, 168, No. 3939, 1582-1584, 1970.

3. Keeling, C. D., et al, Tellus, 28, No. 6, 1976, 538-551, "Atmospheric carbon dioxide variations at Mauna Loa Observatory, Hawaii, Tellus, 28, No. 6, 1976, 552-564, "Atmospheric carbon dioxide variations at the South Pole."

4. Stewart, R. W., S. Hameed, and J. Pinto, "The Natural and Perturbed Troposphere", Man's Impact on the Troposphere, Ed. J. S. Levine and D. R. Schryer, (NASA Reference Publication 1022, 1978).

5. National Research Council Report, "Nitrogen Oxides", ISBN-0-309-02615-6, U.S. National Academy of Sciences, Washington, D.C. (1977).

6. Kester, D. R., "Dissolved Gases Other Than CO_2", Chemical Oceanography, Ed. J. P. Riley and G. Skirrow, 2nd Ed., 1, Chapter 8, 530-541 (Academic Press, London, 1975).

7. Ellsaesser, H. W., "The Upward Trend in Airborne Particulates that Isn't", The Changing Global Environment, S. F. Singer, ed. 235-269, (Reidel, Dordrecht, 1975).

8. Mitchell, J. M., "A Reassessment of Atmospheric Pollution as a Cause of Long-Term Changes of Global Temperature", The Changing Global Environment", S. F. Singer, ed., 149-173 (Reidel, Dordrecht, 1975).

2.3-A APPENDIX

2.3-A. Raman Scattering: A Possible High-Precision Measurement of the Oxygen-Nitrogen Ratio in Air

Raman scattering is the inelastic scattering of light by atoms and molecules. Raman scattering is routinely used for high sensitivity spectroscopic work. Here we consider whether Raman scattering can be used to measure the ratio of oxygen to nitrogen in ordinary air to a precision of one part per million. Schwiesow and Dero[1] first suggested in 1970 the use of Raman scattering to determing the oxygen concentration of the atmosphere. Here we review some of the key considerations for successful application of Raman scattering.

The ground states of the O_2 and N_2 molecules are sketched in Fig. 2.3-A.1.

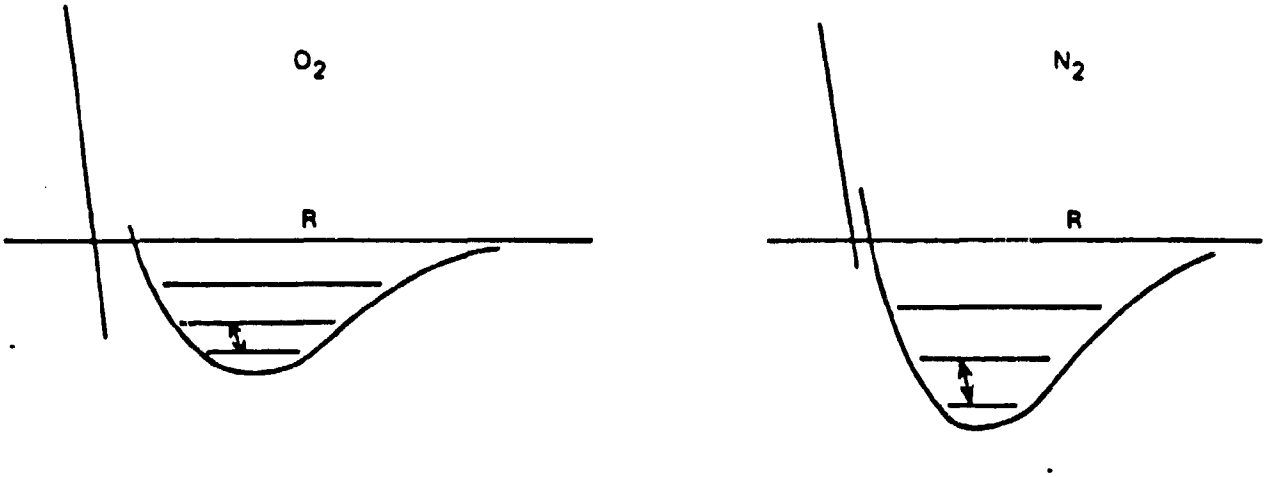

Figure 2.3-A.1 GROUND STATES OF O_2 AND N_2 MOLECULES

Here R is the internuclear separation and the vibrational energies of the ground state are

$$\omega(O_2) = 1554.7 \text{ cm}^{-1}$$
$$\omega(N_2) = 2330.7 \text{ cm}^{-1}$$

Note that at room temperature, 20° C, thermal energy is

$$kT = 203 \text{ cm}^{-1}$$

Thus both N_2 and O_2 will be mainly in the lowest vibrational state at room temperature and below. Raman scattering on a molecule works as shown in Fig. 2.3-A.2.

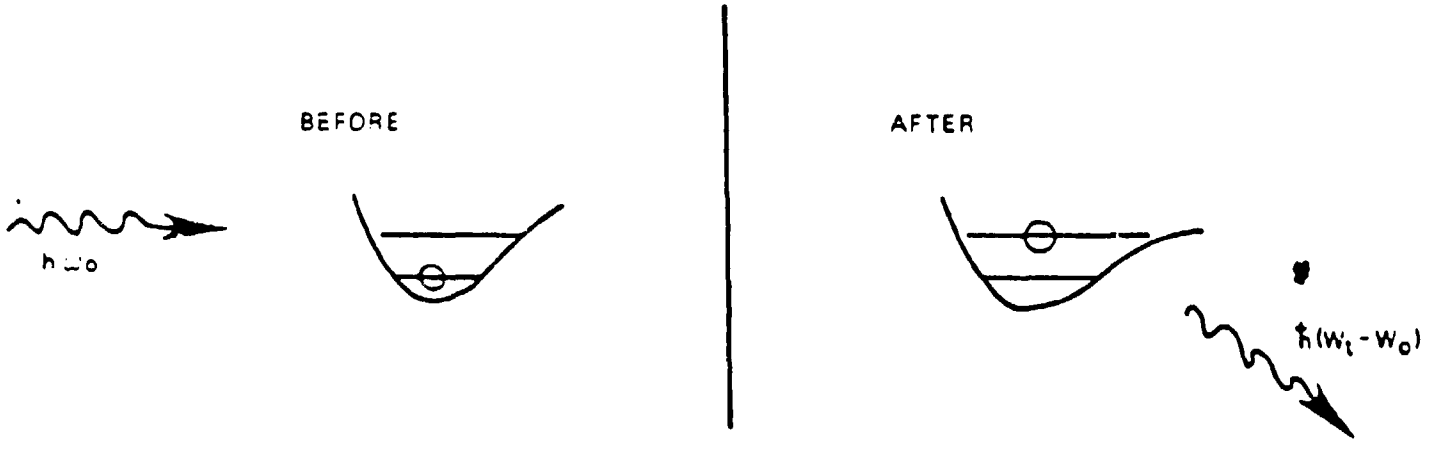

Figure 2.3-A.2 RAMAN SCATTERING

Thus if an intense laser beam is incident on a sample of air the scattered light will contain the initial laser frequency and downshifted or Stokes lines as shown in Fig. 2.3-A.3.

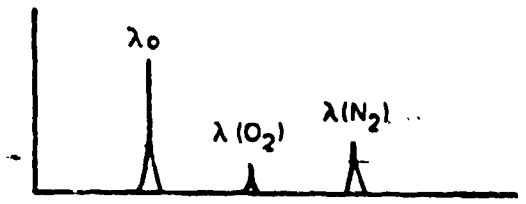

Figure 2.3-A3

We see an extremely intense line at the laser wavelength λ_o due to instrumental scattering and Raleigh scattering by O_2 and N_2. In addition we see a pair of weaker lines at larger wavelengths due to Raman scattering from O_2 and N_2. By energy conservation these lines are located at the wavelengths

$$\frac{1}{\lambda(O_2)} - \frac{1}{\lambda_o} = 1554.7 \text{ cm}^{-1}$$

$$\frac{1}{\lambda(N_2)} - \frac{1}{\lambda_o} = 2330.7 \text{ cm}^{-1}$$

If we assume that $\lambda_o = 5145$ Å, a common line of the Ar^+ laser, we find

$$\lambda(O_2) = 5592.3 \text{ Å}$$

$$\lambda(N_2) = 5846.0 \text{ Å}$$

Thus, both Stokes lines are separated from the laser line by several hundred angstroms and they are separated from each other by 254 Å . This is excellent resolution and it allows the use of very efficient spectrometers to collect the light.

We now calculate the magnitude of the signal for the somewhat oversimplified apparatus depicted in Fig. 2.3-A.4. The number of photons per second in the incident laser beam is Φ_o . The Raman scattering cross section for O_2 and N_2 at 5145 Å are[2]

$$\frac{\partial \sigma}{\partial \Omega} (O_2) = 4.8 \times 10^{-31} \text{ cm}^2 \text{ steradian}^{-1}$$

$$\frac{\partial \sigma}{\partial \Omega} (N_2) = 4.0 \times 10^{-31} \text{ cm}^2 \text{ steradian}^{-1}$$

The acceptance solid angle of the spectrometer is

$$\Delta\Omega = \frac{A}{x^2} \qquad (2.3\text{-A.1})$$

where A is the grating area and s is the distance between the grating and the slit. The grating efficiency can be very high for appropriate blazing and for simplicity we assume it is 50%. The photomultiplier quantum efficiency can also be very high and we will also assume it is 50%. Then the overall efficiency of the grating and the photodetector is

$$\eta = 0.25$$

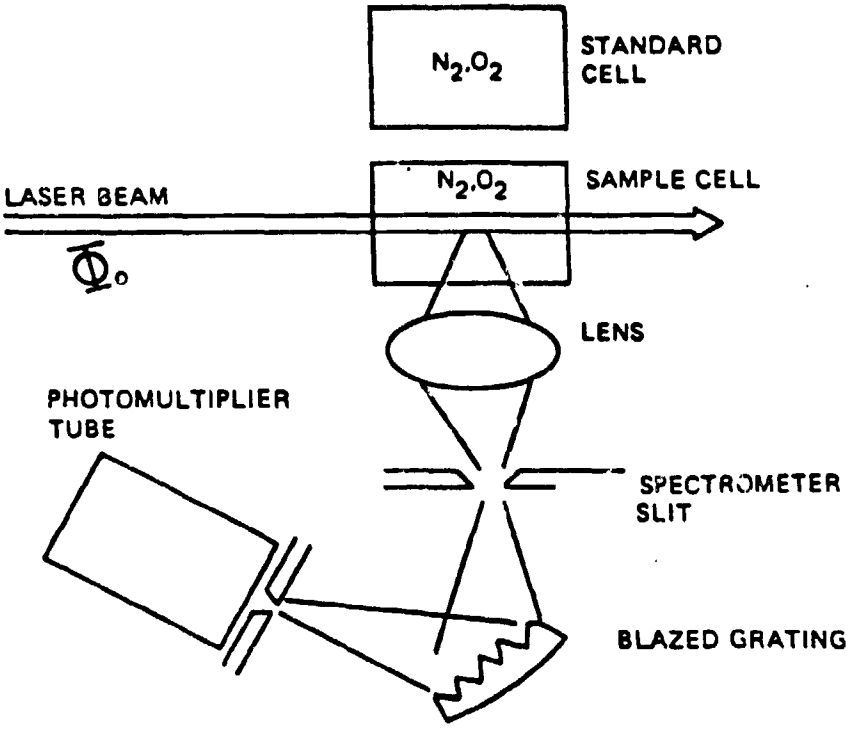

Figure 2.3-A.4 SIMPLIFIED EXPERIMENTAL APPARATUS

The photon count rate is thus

$$\Phi = \Phi_o[x] \frac{\partial \sigma}{\partial \Omega} \Delta\Omega \, \eta \, \ell \qquad (2.3\text{-A}.2)$$

where $[x]$ is the number density of molecules per unit volume of the scattering species, ℓ is the cell length and the other factors were defined earlier. In a well-designed experiment we may approach the shot-noise limit and we may therefore define the signal S as the number of counts in an integration time t, i.e.

$$S = \Phi t$$

The noise is simply the statistical fluctuation is S or

$$N = \sqrt{S}$$

Hence the signal-to-noise ratio is

$$\frac{S}{N} = \sqrt{S} = \sqrt{\Phi t} \qquad (2.3\text{-A.3})$$

If we demand sensitivity of a part per million we must have

$$\frac{S}{N} = 10^6 = \sqrt{\Phi t}$$

or the integration time is

$$t = \frac{10^{12}}{\Phi} \quad . \qquad (2.3\text{-A.4})$$

We now use the formula (2.3-A.2) to calculate the integration time t for detecting O_2 concentration at the part per million level. Suppose that

$$\dot{+}_o = 100 \text{ watts} = 2.59 \times 10^{20} \text{ photons/sec at } 5145 \text{ Å} \quad .$$

This is a reasonable intra-cavity flux for an Ar^+ ion laser. At standard temperature and pressure we have

$$[O_2] = 5.63 \times 10^{18}\ cm^{-3} \qquad 20.9\%\ O_2$$

$$[N_2] = 2.10 \times 10^{19}\ cm^{-3} \qquad 70.08\%\ N_2$$

Further assume that

$$\Delta\Omega = 0.04$$

a reasonable value for a monochrometer, and

$$\eta = 0.25$$

and

$$\ell = 1\ cm$$

Then

$$t(O_2) = 1.49 \times 10^{6}\ sec = 40\ hours$$

$$t(N_2) = 4.60 \times 0^{4}\ sec = 12.8\ hours$$

Both numbers are far too long to be of practical interest!

The basic difficulty is the small Raman scattering cross section $\sigma = 10^{-30}\ cm^2\ steradian^{-1}$ and the relatively small number density of molecules in a gas at atmospheric pressure. We may improve the experimental outlook by increasing the scattered flux Φ. Let us examine the factors which enter into Φ .

ϕ_o the incident laser flux could be increased by a factor of 10 from 100 watts to 1000 watts intra-cavity with a very large Ar^+ laser.

$[x]$ the number density could be increased by a factor of 10 to 100 by compressing the gas. Even better, $[x]$ could be increased by about 1000 by using <u>liquid</u> air.

$\frac{\partial\sigma}{\partial\Omega}$ the Raman cross section could be increased by using shorter wavelength light. The Raman cross section scales as $(\omega_o)^4$ or faster in the neighborhood of resonance.[3] Hence, by using 3500 Å light where another strong line of the Ar^+ laser exists one could gain at least a factor of 5 in increased cross section.

$\Delta\Omega$ the spectrometer solid angle could be increased somewhat by using narrow band interference filters. A factor of 10 or 20 is feasible.

η the spectrometer and photodetector efficiency might be increased by a factor of less than 2.

ℓ the interaction length might be increased by a factor of 2 or 3.

Thus there is ample room for improvement and the most dramatic results can be achieved by using liquid air. We may estimate the density of O_2 and N_2 molecules in liquid air very roughly as follows. The specific gravities of liquid oxygen and nitrogen are respectively

$$\rho(O_2) = 1.14 \text{ gram cm}^{-3}$$

$$\rho(N_2) = 0.808 \text{ grams cm}^{-3}$$

Assuming for simplicity that negligible change of volume occurs when O_2 and N_2 are mixed in the liquid state we find that the liquid-state number densities are

$$[O_2] = \frac{f}{f + \frac{\rho(O_2)M(N_2)}{\rho(N_2)M(O_2)}} \cdot \frac{\rho(O_2)}{M(O_x)} N_A$$

$$[N_2] = \frac{\frac{\rho(O_2)M(N_2)}{\rho(N_2)M(O_2)}}{f + \frac{\rho(O_2)M(N_2)}{\rho(N_2)M(O_2)}} \cdot \frac{\rho(N_2)}{M(N_2)} N_A$$

Here Avogadro's number is

$$N_A = 6.02 \times 10^{23}$$

The mole fraction of O_2 to N_2 in air is

$$f = \frac{20.946}{78.084} = 0.2682$$

and the gram molecular weights of O_2 and N_2 are

$$M(O_2) = 31.9988$$

$$M(N_2) = 28.0134$$

Substituting into the density formulas we find

$$[O_2] = 3.82 \times 10^{21} cm^{-3}$$

$$[N_2] = 1.43 \times 10^{22}\ cm^{-3}$$

The integration times for detection at the part per million level are now

$$t(O_2) = 2.20 \times 10^{3}\ sec = 3.51\ minutes$$

$$t(N_2) = 67.5\ sec = 1.13\ minutes$$

These integration times are not out of the question and they can be further reduced by perhaps a factor of 10 by optimization of other experimental parameters.

We note that the vibrational Raman lines are split by rotational fine structure for gaseous samples but this fine structure is absent for the condensed phase. However, the condensed phase spectra are modified in the case of O_2 by scattering from O_4 polymers.

In practice, experimental measurements should be done with a standard cell and a sample cell which are placed one after another in the laser

beam at an appropriate period. This will allow one to compare the difference in scattering by the two cells and to compensate for the slight systematic differences between the standard and the sample. Very clever experimental work will be required to design an apparatus free of systematic errors and we hesitate to introduce much detail here. One concept, not necessarily the best, is sketched in Fig. 2.3-A.5. Such an instrument could be calibrated by tuning onto the N_2 peak and adjusting the attenuator until the signals from A and B were equal. One could then tune onto the O_2 line and read the difference between A and B .

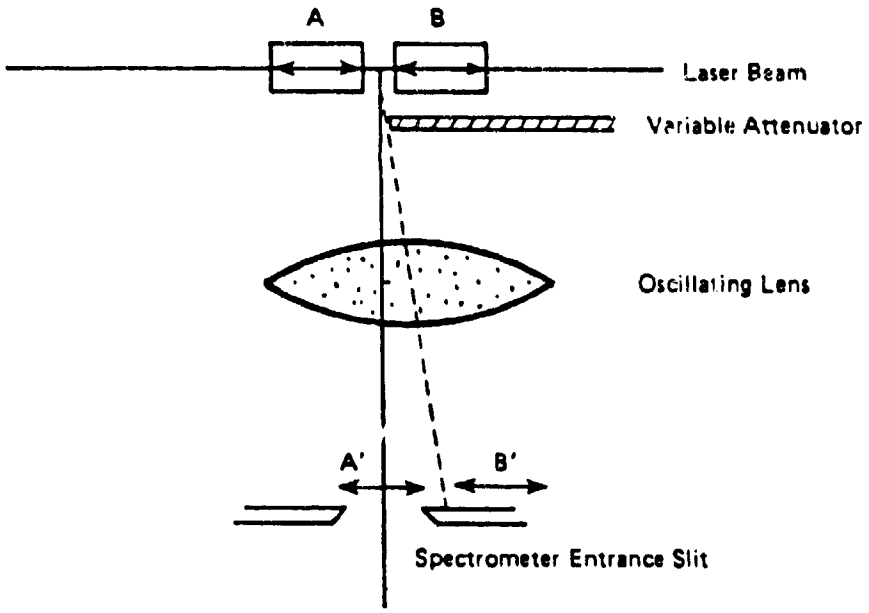

Figure 2.3-A.5 EXPERIMENTAL CONCEPT FOR DETERMINING OXYGEN CONCENTRATION

Of course the attenuator and other system components would have to be wavelength independent to a high degree, but not to one part per million if little attenuation is required. In operation one would spend about 3% of the time measuring the N_2 peak to provide continuous adjustment of the attenuator balancing, and the bulk of the time would be spent measuring on the O_2 peak.

Additional difficulties are possible fractional distillation in the condensation of the air sample, possible contamination from the walls by adsorption or evolution of O_2 and N_2, possible photochemical reactions of O_2 with the container walls, and heating of the cryogenic sample. Nevertheless, there is a real chance that Raman spectroscopy can be used to make part-per-million measurements of the O_2/N_2 ratio of air.

REFERENCES TO SECTION 2.3A

1. Schwiesow, R. and V. Derv, "A Raman Scattering Method for Precise Measurement of Atmospheric Oxygen Balance," Journ. Geophys. Res., 75, 1629-1632, 1970.

2. Hertzberg, G., Molecular Spectra and Molecular Structure: Spectra of Diatomic Molecules, 1, 2nd Ed., Van Nostrand Reinhold Co., 1950.

3. Cherlow, J. M., and S.P.S. Porto, "Laser Raman Spectroscopy of Gases," Topics of Applied Physics Series, Laser Spectroscopy of Atoms and Molecules, 2, 253-282, Walther, H., (Springer Verlag, Berlin, 1976).

2.4 The Oceans as a Sink for Carbon Dioxide

It is a sad commentary on the state of oceanography that we do not know of the applicability (if any) of two extreme models:

(i) oceanwide diffusive and convective exchange processes between adjoining vertical layers, and

(ii) processes at the ocean boundaries which alter the temperature and salinity (and hence density), with the newly formed water masses spreading into the ocean interior along surfaces of constant density.

It is possible (though not necessary) that the two models predict very different time histories for the amount of atmospheric CO_2 which can be deposited in the oceans. In the past, most estimates of oceanic carbon have been based on model (i); it is our intent here also to explore the consequences of model (ii). We first consider the general issue of cold ocean sinks, then we develop a "pipe" model of the oceans.

2.4.1 Maximum Effect of Cold Ocean Sinks on Atmospheric CO_2

The air-sea interface at which CO_2 is exchanged between the atmosphere and the oceans is adjoined to a well-mixed sea surface layer whose average thickness is conventionally taken as about 75 m. The total carbon in the layer (about 580 Gtons) is very comparable to that present as CO_2 in the atmosphere (702 Gtons); but only 1% of the mixed layer carbon is in the form of dissolved CO_2--10% is in the carbonate ion $CO_3^=$ and almost

all of the rest is HCO_3^- . The relatively small mixed layer volume thus contains about 10^2 times the carbon density of the adjacent atmosphere by storing almost all the excess in carbonate and bicarbonate ions. But the layer is, at present, about 85% saturated and it is, consequently, difficult for it to absorb much more; almost all additional absorbed CO_2 must be accompanied by the disappearance of a carbonate ion, effectively through the reaction $CO_3^= + CO_2 + H_2O \rightarrow 2HCO_3^-$. Because of the large amount of CO_2 already absorbed, there is little $CO_3^=$ still available and further increases in atmospheric CO_2 would be accompanied by very much smaller increases in the carbon content of a mixed ocean layer with which it remained in equilibrium.

For small departures from equilibrium

$$\zeta \frac{\Delta[C]_A}{[C]_A} = \frac{\Delta[C]_{ML}}{[C]_{ML}}$$

where $[C]_A$ is the carbon density in the atmosphere, $[C]_{ML}$ that in the mixed layer, and $\zeta^{-1} \approx 8\text{-}15$; ζ^{-1} , the so called "Revelle factor", reaches the larger value at 0^oC and the lower value at 30^oC . The time needed to establish approximate CO_2 equilibrium between the atmosphere and the mixed ocean layer is then a factor ζ less than the seven years needed to attain equilibrium between C^{14} contents; the latter essentially requires an exchange of the entire carbon reservoir of the mixed layer with that of the atmosphere. This time, 7ζ yrs $\approx$ 8 months is not short enough to maintain atmosphere-mixed layer CO_2 equilibrium at all latitudes because horizontal surface motion exchanges water between hotter and colder regions in less

than this time. However, it is short enough so that when averaged over the whole ocean mixed layer, CO_2 equilibrium with the atmosphere is re-established after an atmospheric perturbation in less than a year. This is so very much less than the time for doubling the atmospheric CO_2 burden from fossil fuel burning or the residence time for a carbon atom in the mixed layer that we shall henceforth assume atmosphere-mixed layer CO_2 equilibrium is always achieved.

The ocean can absorb more than the fraction $\zeta \approx 10^{-1}$ of any additional CO_2 injected into the atmosphere only because the rapidly responding mixed ocean layer is slowly replaced by fresher water which has not yet absorbed the added CO_2 burden. Models for this replacement involve either or both of two mechanisms:

(i) The mixed layer exchanges water with layers directly below it, probably by the exchange of eddies--a process represented phenomenologically by a diffusion equation (box models). The time scale depends sensitively on the spatial separation between the mixed layer and the depth of the most relevant fresher layers.

(ii) Cold water from the mixed layer can, in certain regions, drop relatively rapidly to much lower depths then spread horizontally and be replaced by a continued upwelling in the rest of the ocean. The largest such removal of surface water appears to occur in the Antarctic region--a downflow of about $20 \times 10^6\ m^3 s^{-1}$. This would be balanced by

an average upwelling of 1 cm/day in the rest of the oceans. In the Atlantic a similar upwelling might be expected from a downflow of order 10×10^6 $m^3 s^{-1}$ in the Norwegian Sea. The time scale for replacing a mixed layer of thickness $H = 75$ m by this mechanism is

$$\tau_{ML} = \frac{75 \text{ m}}{4.4 \text{ m/yr}} = 17 \text{ yrs} \qquad (2.4.1)$$

We consider first only an estimate of the maximum consequences of mechanism (ii) for ventilating the mixer layer.

We define the total carbon contents of the atmosphere, mixed layer, and the deeper rest of the ocean by $[C]_A$, $[C]_{ML}$, and $[C]_D$, respectively. Then, if CO_2 is injected into the atmosphere-ocean at the rate $f(t)$

$$f(t) = [\dot{C}]_A + [\dot{C}]_{ML} + [\dot{C}]_D \qquad (2.4.2)$$

At present

$$\frac{[\dot{C}]_{ML}}{[C]_{ML}} = \zeta \frac{[\dot{C}]_A}{[C]_A} \qquad (2.4.3)$$

with ζ^{-1} as the Revelle factor. The factor ζ will decrease if very much more CO_2 enters the system because of the near saturation of the mixed layer and the ratio $[C]_{ML}/[C]_A$ will decrease as $[C]_A$ increases. We shall approximate the product

$$\zeta[C]_{ML}/[C]_A \equiv \zeta' \qquad (2.4.4)$$

by a constant equal to the present value $= 0.7\zeta = 10^{-1}$. The direct coupling between $[\dot{C}]_{ML}$ and $[\dot{C}]_D$ is model dependent because $[C]_D$ can vary throughout the deeper layers. Therefore, the negative contribution to $[\dot{C}]_D$ carried by the general upwelling accompanying the local downflow into it from the mixed layer is not simply related to $[C]_D$. We maximize the effect of the upwelling from the cold water sinks by assuming

$$[\dot{C}]_D = \frac{[C]_{ML} - [C]_{ML}(-\infty)}{\tau_{ML}} \qquad (2.4.5)$$

The reference time $t = -\infty$ refers to the steady state which existed before fossil fuel burning significantly changed $[C]_A$ and thus $[C]_{ML}$, when $[\dot{C}]_D(-\infty) = 0$. This assumption that the upwelling water into the mixed layer is so old that its carbon content is independent of recent increases from terrestrial surface activity during the past 150 years will, of course, exaggerate the [illegible] this mechanism in supplying surface water capable of maximally absorbing increasing atmospheric CO_2. Because $\left[[C]_{ML} - [C]_{ML}(-\infty)\right]\left[[C]_{ML}^{-1}\right]$ is very small, we can use Eqs. (2.4.3) and (2.4.4) in Eqs. (2.4.2) and (2.4.5) to obtain

$$[\dot{C}]_D = \frac{[C]_A - [C]_A(-\infty)}{\tau_{ML}}\ \zeta' \qquad (2.4.6)$$

and

$$f(t) = (1 + \zeta')[\dot{C}]_A + \frac{[C]_A - [C]_A(-\infty)}{\tau_{ML}}\zeta' \qquad (2.4.7)$$

For the present exponentially increasing CO_2 injection

$$f = f_o \exp(t/\tau_f) \qquad (2.4.8)$$

and the solution of Eq. (2.4.7) is

$$[C]_A - [C]_A(\infty) = \frac{\tau_f f_o \exp(t/\tau_f)}{1 + \zeta'}\left[1 + \frac{\zeta'\tau_f}{(1 + \zeta')\tau_{ML}}\right]^{-1} . \qquad (2.4.9)$$

The terms before the bracket on the RHS of this equation describe the reduction of atmospheric CO_2 by an unventilated mixed layer. For a 10^2m mixed layer and $\zeta' = 10^{-1}$ it alone would leave 90% of newly injected CO_2 in the atmosphere. (This would be reduced to 80% for a doubled mixed layer thickness.) The bracket describes the effect of ventilating the layer. It is insensitive to the assumed mixed layer thickness; a thicker layer takes longer to ventilate. It does depend upon the presumed 1 cm day^{-1} average upwelling rate. With this value and $\tau_f = 23$ years corresponding to a 4.3% increase per year in CO_2 injection into the ocean-atmosphere reservoir, it gives an additional 10% of this injected CO_2 stored in the deep oceans. Thus with $\tau_{ML} = 17$ yrs , and $\zeta' = 0.1$, Eq. (2.4.9) gives 0.8 for the total fraction of injected CO_2 which should still reside in the atmosphere. Because of the small ζ' , a τ_{ML} very much less than τ_f is needed before $[C]_A - [C]_A(-\infty)$ would depart greatly from the value it

would have when in equilibrium with a non-ventilated mixed layer, represented by the first term on the RHS of Eq. (2.4.9). This is particularly true in that the use of Eq. (2.4.5) makes the whole discussion an overestimate of the cold water sinks. Thus, it is very unlikely that cold water sinks of presently estimated magnitude could by themselves account for the observations which show only about half of the CO_2 from fossil fuel burning still airborne. When, however, the continually accelerated rate of fossil fuel burning begins to diminish, τ_f will grow and the corrective factor $[1 + \zeta' \tau_f (1 + \zeta')^{-1} \tau_{ML}^{-1}]^{-1}$ can be important; but, if atmospheric CO_2 has increased greatly by that time, the accompanying decrease in ζ' may no longer be small. This decrease is no longer negligible in the discussion that follows.

2.4.2 A Pipe Model of the Oceans

The ocean is modeled as a series of horizontally uniform layers, from $i = 1$ representing the mixed layer at the top, to $i = N + 1$ at the bottom. Because of the horizontal uniformity, we can discuss everything per unit surface area, and we effectively have a one dimensional picture.

One-d models are rightfully in disrepute and we do not need to join the chorus of disclaimers (all of whom use such models). In fact, one of us (WM) is the originator of a particularly naive one-d model, but in limiting this model to Antarctic bottom water and the resulting constant rate of upwelling by 1 cm day^{-1}, and ignoring the large intermediate sources, he now suspects that he has thrown out the baby with the bottom water.[7]

What we are trying to model are some of the following processes:

(a) The Norwegian Sea is filled with shallow Atlantic water, in winter the surface water is cooled by contact with the atmosphere, eventually the water column turns over forming a fairly homogeneous cold and moderately salty water mass which flows over a sill into a depth appropriate to its density; presumably this is the origin of North Atlantic Deep Water.

(b) In the process of freezing at high latitudes, the newly formed sea ice is fresh, and the residual water is salty and cold. Some form of this process in the Weddell Sea is probably responsible for the formation of Antarctic Bottom Water.

(c) Extensive evaporation from the Mediterranean Sea results in increased salinity that leads to the formation of dense water. Suppose that on the average Q m^3/sec of Mediterranean water flows through Gibralter and down the continental slope into the Atlantic. In the process it mixes with the local water with the consequence that by the time it arrives at equilibrium depth, the flow consists of Q' m^3/sec of diluted Mediterranean water, with $Q' > Q$. We will want, somehow, to include this dilution as part of the processes of water mass formation.

The layers are connected by pipes, which transport water at known rates Q_i and inject the water at the bottom of each layer, thus creating

an upwelling of velocity W_i in the layer. Evidently

$$Q_i = (W_i - W_{i+1}) \cdot A$$

where $A = 3 \times 10^{14}$ m^2 is the surface area of the oceans.

We take the view that the water is drawn from the upper layer and injected into the lower layers. All biology is ignored in this model (see Section 2.1). Application of the pipe-model to oxygen as well as to CO_2 might provide a way of joining ocean biology with physical oceanography. The pipes thus transport temperature T, salinity S, density ρ and carbon concentration $[C]$ from the surface to the deep ocean. Carbon concentration is transported unchanged, but the transport mechanism must change the density to match that at the injection depth--otherwise, the inflowing water would be too heavy or too light and would sink or rise to the appropriate depth in a few Vaisala periods. The transport also changes temperature and salinity, though not to values matching the ambient temperature and salinity at the injection depths.

Mathematically, the model described above may be set up as follows: we consider a single quantity, such as carbon concentration, $[C](z,t)$, which we take to be horizontally uniform and a function only of depth and time. At the surface, z_s, we take $[C](z_s,t) = [C]_s(t)$, as a given carbon concentration in the mixed layer. At the bottom, z_B, we take $[C](z_B,t) = [C]_B$, a constant. In between the surface and the bottom are N sources of CO_2, at depths $z_1 \cdots z_N$, injecting carbon with

concentrations $[C]_i(t)$ at rates ΔW_i . ΔW_i has the dimensions of a velocity rather than volume per second because we normalize everything per unit horizontal area; ΔW_i is just the rate at which water is injected by the i^{th} "pipe". That is, $\Delta W_i = Q_i$/unit area. Thus between the i^{th} and $(i+1)^{st}$ "pipe" there is an upwelling of water with velocity W_{i+1} , where $\Delta W_i = W_i - W_{i+1}$. To conserve water, there must then be an outflow of water at a rate $\Delta W_o = W_1$ immediately below the surface z_s . This removes carbon with concentration $[C]_s(t)$. The geometry is illustrated in Fig. 2.4.1. Carbon is thus distributed through the water column both by diffusion and by being pumped from the surface to various depths z_i at known rates, ΔW_i . The carbon concentration then satisfies the diffusion equation

$$-\kappa \frac{\partial^2 [C]}{\partial z^2} + \frac{\partial}{\partial z}(W[C]) = -\frac{\partial [C]}{\partial t} + \sum_{i=1}^{n} \Delta W_i [\bar{C}]_i \delta(z-z_i) - W_i [C]_s \delta(z-z_s) \tag{2.4.10}$$

with the boundary condition

$$[C](z_s,t) = [C]_s(t) \tag{2.4.11a}$$

$$[C](z_B,t) = [C]_B \quad . \tag{2.4.11b}$$

For the case we are dealing with here, all the $[\bar{C}]_i = [C]_s(t)$ since the pumping mechanism simply redistributes the surface carbon concentration.

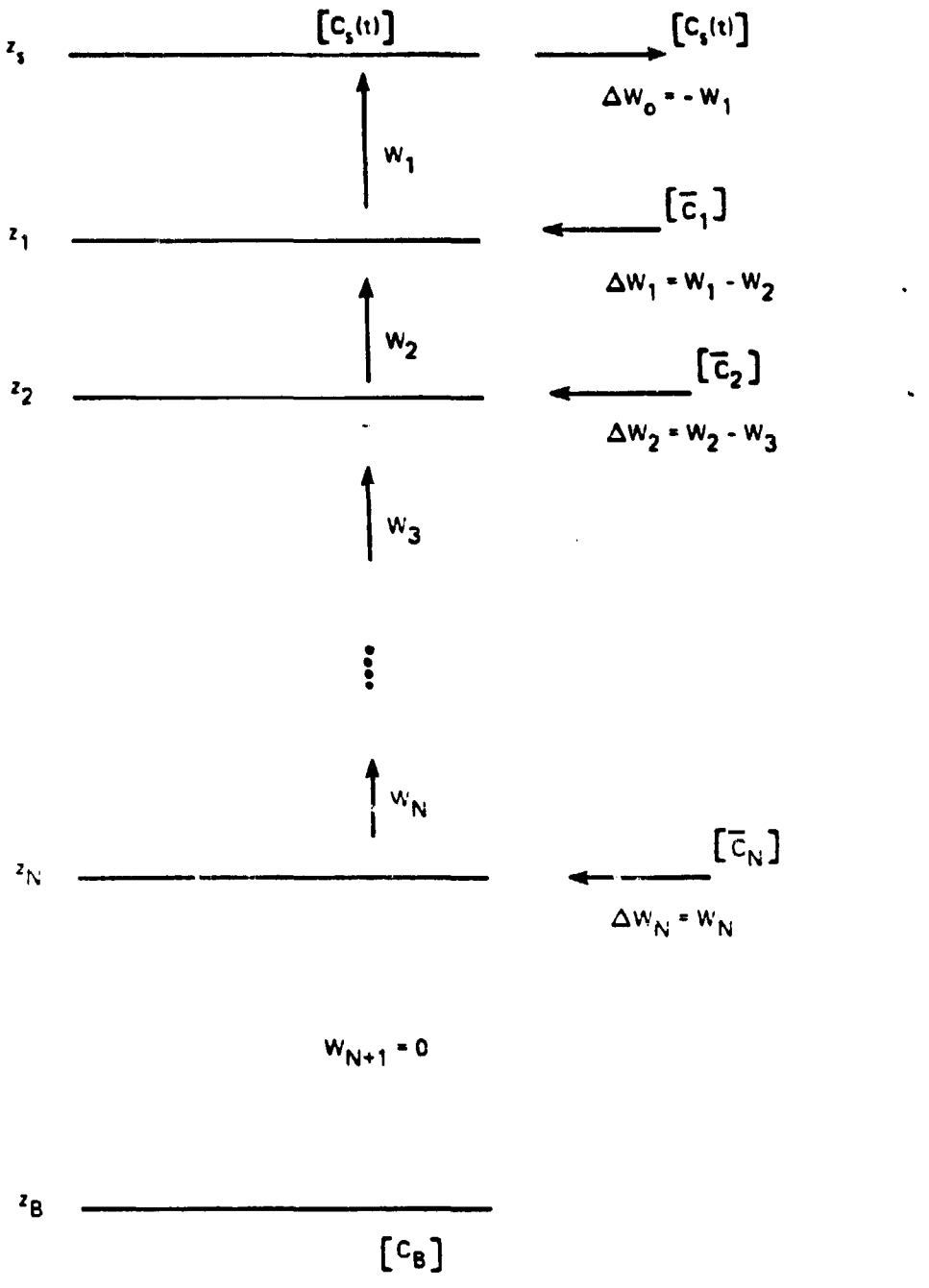

Figure 2.4.1 THE GEOMETRY ILLUSTRATING THE USE OF THE PIPE MODEL

Temperature, $T(z,t)$, and salinity, $S(z,t)$, satisfy the same equation with two modifications. First, we take the surface boundary conditions to be time independent so that $T = T(z)$ and $S = S(z)$ only; thus $\partial T/\partial t$ and $\partial S/\partial t$ disappear. Secondly, we assume that the pumping mechanism injects water of known temperature and salinity $\bar{T}_i$ and $\bar{S}_i$. Then we invoke the equation of state and require the density $\rho(\bar{T}_i,\bar{S}_i)$ of the injected water to equal the density $\rho\big(T(z_i),S(z_i)\big)$ of the ambient water. For given ΔW_i, $\bar{T}_i$ and $\bar{S}_i$ these conditions are used to determine the injection depths z_i.

In a complete study of the pipe model, we would first calculate $T(z,t)$ and $S(z,t)$, (using the injection depths from the equation of state), and then compare these with experimental temperature and salinity profiles as a check on the oceanographic consistency of the model. Then we would readjust the injection depths z_i from each pipe to match the experiments. The problem is to determine reasonable source functions that lead to acceptable distributions of $T(z)$ and $S(z)$.* We would then have confidence in the model and in the choice of parameters, so we would then feel safe in applying the model to carbon. As a matter of practice, however, we shall omit all these consistency checks, and go directly to the carbon problem using (educated?) guesses as to flow rates W_i and injection depths z_i representing the known processes mentioned earlier.

*The problem is mathematically straightforward, but oceanographically very tricky.

The mathematical treatment of the problem is described in Appendix 2.4-A.

We can construct a simple, but perhaps not totally unrealistic, model of the carbon concentration $[C]_s(t)$ in the mixed layer as a function of time. At present, the mixed layer contains about 600 Gtons of carbon. As the atmospheric CO_2 concentration grows, the amount of carbon in the mixed layer grows too, but because of the buffer mechanism of seawater (expressed through the Revelle factor) it cannot grow very much. In fact, as atmospheric CO_2 goes to infinity, the amount of carbon can increase only by about 25%, to 750 Gtons. Thus, taking the mixed layer thickness to be 75 m, the carbon concentration in the layer grows from 2.67×10^{-14} Gtons/m^3 at present to 3.33×10^{-14} Gtons/m^3. The growth rate is similar to that of the atmosphere, and we take it to be characterized by $1/\tau = 0.03/yr$. So let us take as the <u>incremental</u> carbon concentration produced by the industrial resolution the formula

$$[C]_s(t) = \frac{[C]_o[C]_\infty e^{t/\tau_f}}{[C]_\infty - [C]_o + [C]_o e^{t/\tau_f}} \qquad (2.4.12)$$

with $[C]_o = 2.22 \times 10^{-17}$ Gtons/m^3 (corresponding to .5 Gtons present at $t = 0$, which we take as 1860) and $[C]_\infty = .67 \times 10^{-14}$ Gtons/m^3 (corresponding to 150 Gtons present asymptotically). Then, in the limit where pipes dominate diffusion, Eq. (2.4-A27) states that the total incremental carbon content (per unit area) of the ocean at time t is

$$\int_{-\infty}^{z_s} [C](z,t)dz = \sum_{i=1}^{N} \tau[C]_\infty W_i \log\left(\frac{[C]_\infty - [C]_o + [C]_o e^{t/\tau_f}}{[C]_\infty - [C]_o + [C]_o e^{t/\tau_{fe}} e^{-d_i/W_i\tau_f}}\right) \quad . \tag{2.4.13}$$

Asymptomatically, when $t \gg \tau$, the total incremental carbon content becomes $[C]_\infty\left(\sum_{i=1}^{n} d_i\right) = [C]_\infty \times$ (depth of the deepest pipe), which simply reflects the statement that (in the absence of diffusion) the entire ocean above the lowest pipe is saturated with carbon. If the deepest pipe is at 5 km, this asymptotic incremental carbon content is (re-inserting the ocean area 3×10^{14} m^2) 10^4 G tons. The time history of Eq. (2.4.13), showing the approach to this asymptotic value, is shown in Fig. 2.4.2. The figure is drawn for two pipes, representing Antarctic bottom water (AABW) and North Atlantic deep water (NADW) at depths of 5 and 3 km and with injection rates (per unit area) of 2 m/yr and 3 m/yr respectively. (It must be kept in mind that we are here ignoring other sinks of atmospheric CO_2 and therefore assuming that the atmospheric CO_2 concentration remains high enough to feed the mixed layer indefinitely).

For comparison with the results just described we next outline very briefly the opposite limit, in which the pipes are turned off and mixing occurs only by diffusion.

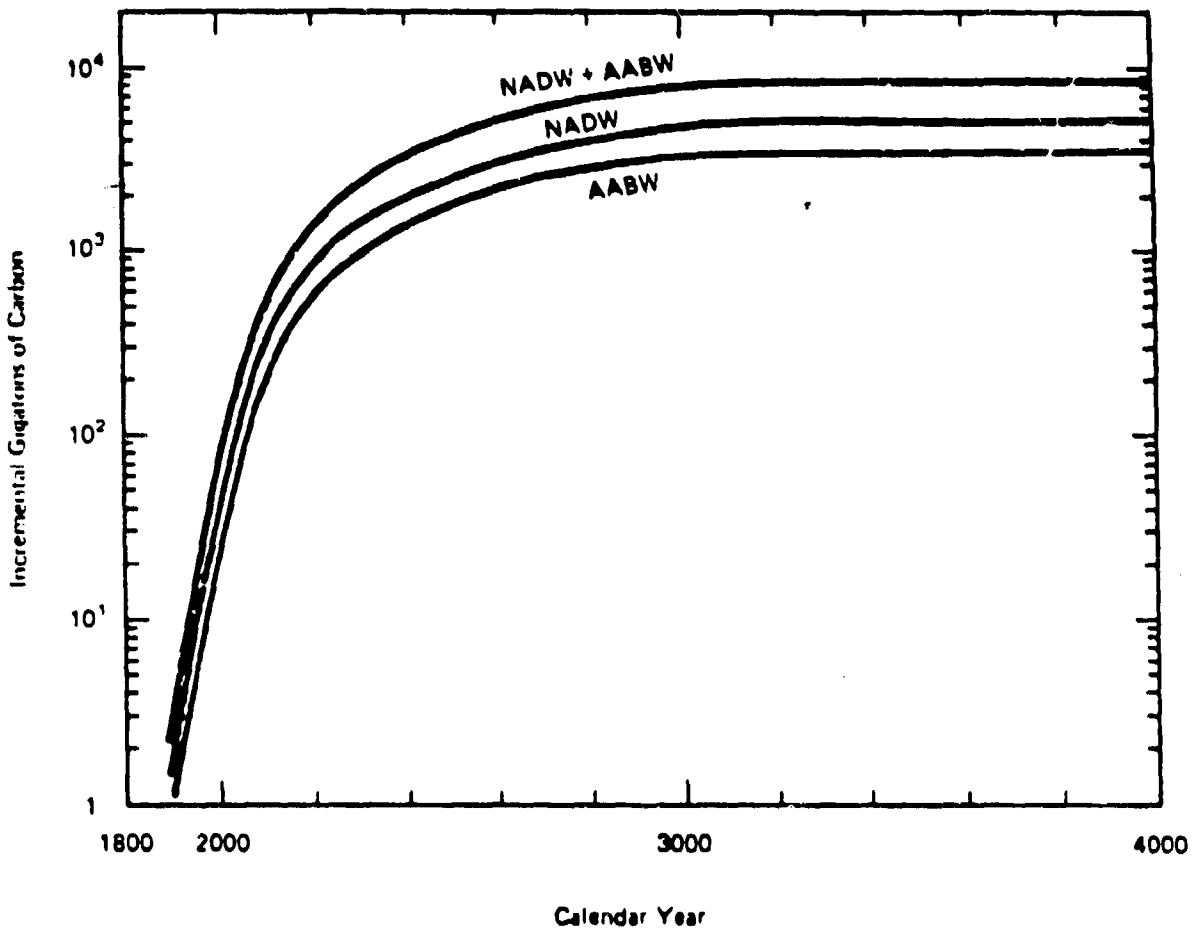

Figure 2.4.2 CHANGE IN CARBON IN THE OCEAN AS A FLUCTUATION OF TIME

In this case the solution to the basic equation (2.4.10) is

$$[C](z,t) = \frac{2}{\sqrt{\pi}} \int_0^\infty d\xi e^{-\xi^2} [C]_{ML}\left(+ \frac{z^2}{4\kappa\xi}\right) \qquad (2.4.14)$$

and therefore

$$\int_{-d}^{0} [C](z,t)dz = \sqrt{\frac{\kappa}{\pi}} \int_{-\infty}^{t} [C]_s(t')\left(1 - e^{-\frac{d^2}{4\kappa(t-t')}}\right)\frac{dt'}{\sqrt{t-t'}} \qquad (2.4.15)$$

With the same model (Eq. 2.4.12) of carbon concentration in the mixed layer, we note that for early times, when the mixed layer growth is exponential, we have

$$\int [C](z,t)dz = [C]_s(t)\sqrt{\kappa\tau_f}$$

to be compared with

$$\int [C](z,t)dz = [C]_s(t) \sum_{i=1}^{N} W_i \tau_f$$

for the pipe dominant case. For comparison we can get $K = 0.26$ cm^2/sec, so that the behavior of the pure pipe and pure diffusion cases coincide at an early time.

For very late times, however, where $[C]_s(t) \to [C]_\infty$, Eq. (2.4.14) tells us that

$$\int [C](z,t) \rightarrow [C]_{\infty} \cdot d \quad ;$$

that is, the ocean saturates. The time for this to happen with pure diffusion however, is $d^2/\kappa \sim 30{,}000$ years , to be compared with $d_i/W_i \sim 3000/3$, or $2000/2$, that is, about 1000 years. Thus at late times, the approach of the ocean to saturation is much faster with the pipe mechanism. Fig. 2.4.3 shows the time history of the pure pipe and pure diffusion cases, with $K = 0.26$ cm^2/sec .

It may be that a diffusion coefficient of 0.26 cm^2/sec is too small, however. We therefore display in Fig. 2.4.4 the pure diffusion case with $K = 1$ cm^2/sec (a more popular value). With such a large value of K , the short time growth of the pure diffusion saturation is now more rapid than with pure pipes, but the approach to the asymptotic limit remains slower.

It is apparent that the time for approach to saturation predicted by the pipe model is sensitively dependent on what is assumed for the injection rates of AABW and NADW. In this regard we should emphasize that there seems to be considerable uncertainty in the flow of NADW. Estimates as low as 3×10^6 m^3/sec , instead of the 30×10^6 m^3/sec we used, are quoted. If this much lower number is indeed correct, then the AABW is the dominant effect, and the time scale for saturation stretches out to $d/W = 5000/2 \sim 2500$ years.

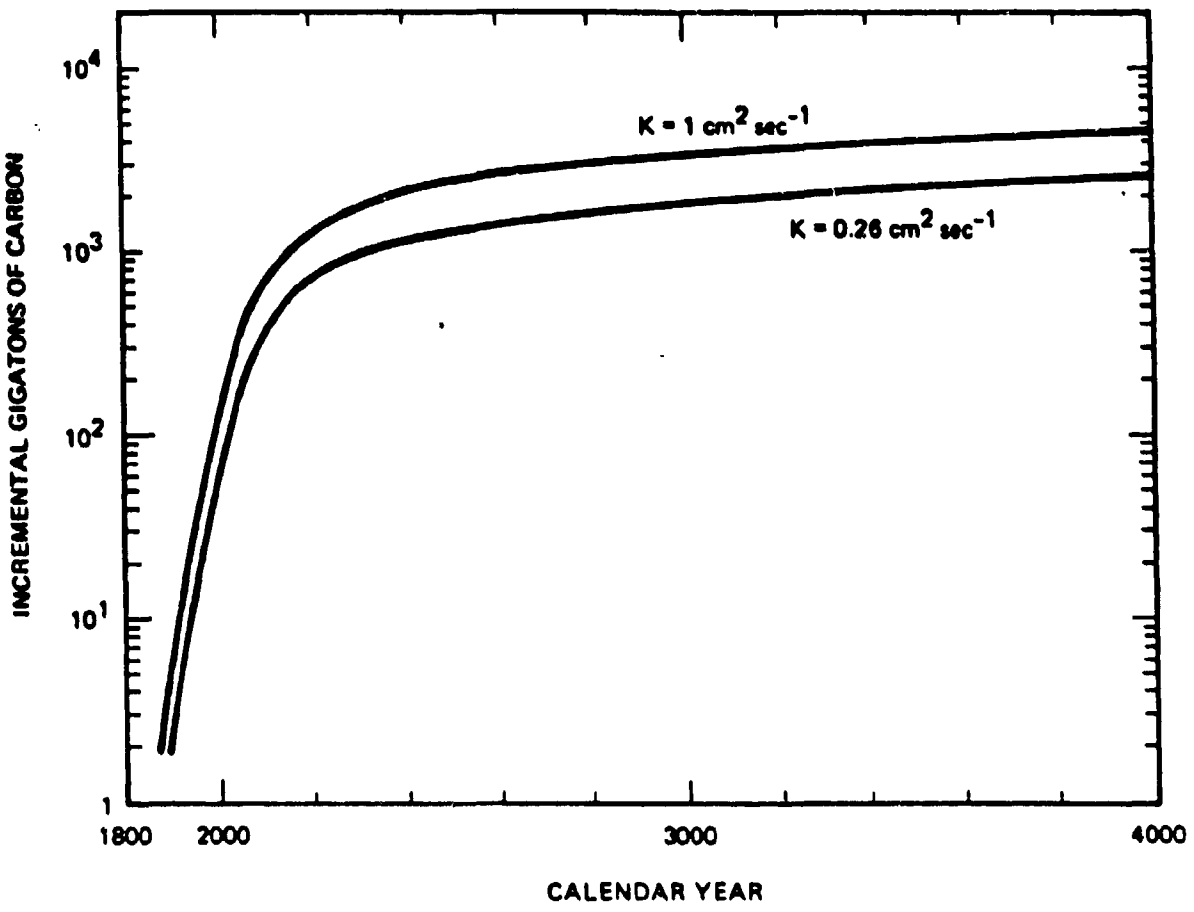

Figure 2.4.3 STORAGE OF CARBON IN THE OCEANS AS A FUNCTION OF DIFFUSSION MODELS

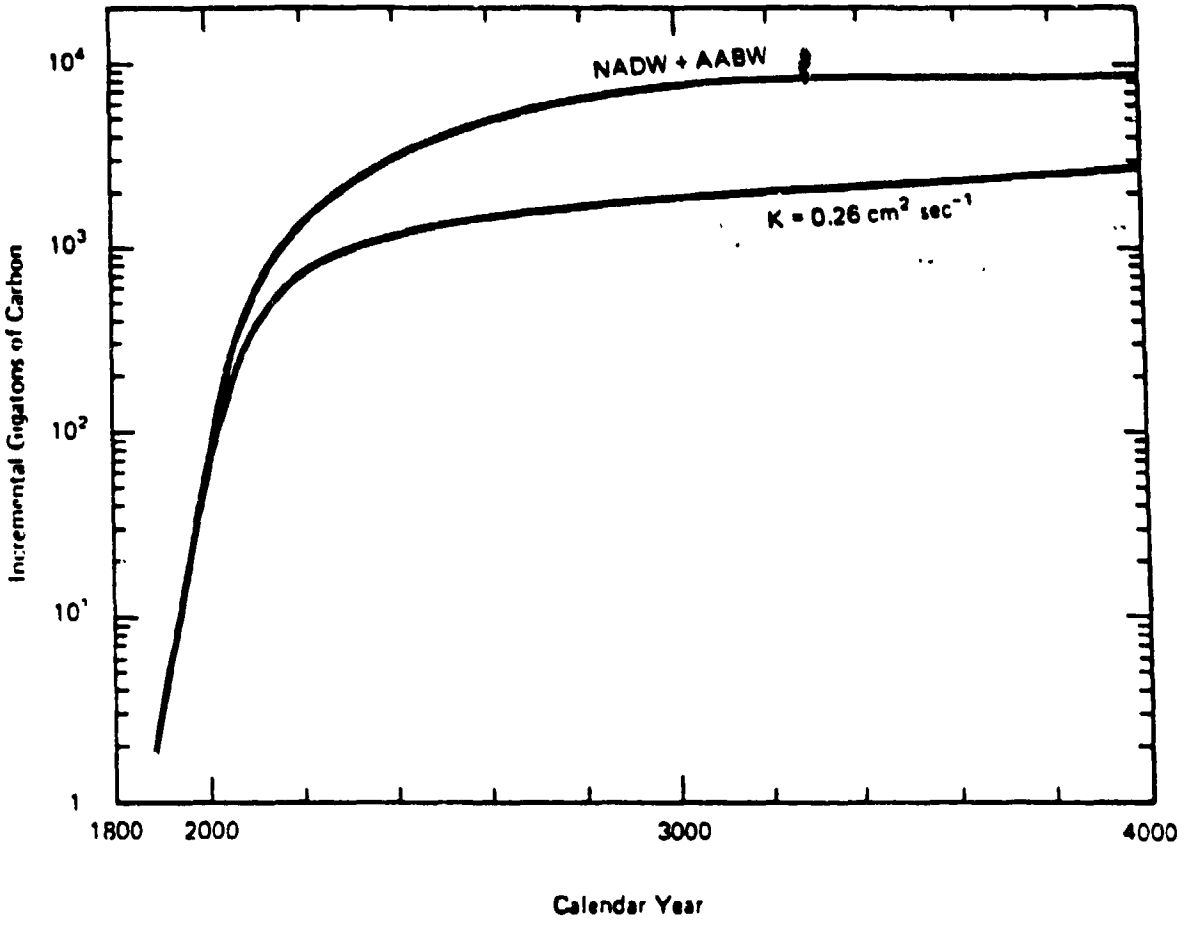

Figure 2.4.4 COMPARISON OF PURE DIFFUSION MODEL WITH PIPE MODEL

The above results for the amount of atmospherically injected CO_2 which ultimately may be buried in the ocean cannot be directly compared with Eq. 2.4.9 which limits only the amount left in the atmosphere. This is because in deriving Eq. 2.4.9 we assume a constant Revelle factor while Eq. 2.4.12 assumes this factor will approach zero in a time $t \sim \tau_f \ln([C]_\infty/[C]_o) \sim 2 \times 10^2$ years. After that time the mixed layer carbon content, and therefore that of the entire ocean in this pipe model, is not sensitive to any further increases in atmospheric CO_2.

APPENDIX 2.4-A

MATHEMATICAL TREATMENT OF THE PIPE MODEL

We wish to outline the solution to Eq. (2.4.10). First, however, we make a few general remarks.

We note that $[C](z,t)$ is continuous across the layer boundaries, and the vertical derivative $\partial[C]/\partial z$ is not. In fact, from Eq. (2.4.10) we see that

$$\lim_{\varepsilon \to 0} \kappa \left(\left. \frac{\partial [C]}{\partial z} \right|_{z=z_i+\varepsilon} - \left. \frac{\partial [C]}{\partial z} \right|_{z=z_i-\varepsilon} \right) = \left(W_i - W_{i+1} \right) \left([C](z_i,t) - [C]_i(t) \right) \quad .$$

Thus we can also formulate the problem by writing

$$[C](z,t) = [C]_i(z,t) \qquad z_{i-1} > z > z_i$$

where

$$-\kappa \frac{\partial^2 [C]_i}{\partial z^2} + W_i \frac{\partial [C]_i}{\partial z} = \frac{-\partial [C]_i}{\partial t} \tag{2.4-A1}$$

with the boundary conditions

(i) $$[C]_1(z_s,t) = [C]_s(t) \tag{2.4-A2a}$$

(ii) $$[C]_{N+1}(z_B,t) = [C]_B \tag{2.4-A2b}$$

(iii) $$[C]_i(z_i,t) = [C]_{i+1}(z_i,t) \qquad i=1\ldots N \qquad (2.4\text{-A2c})$$

(iv) $$\kappa\left(\frac{\partial[C]_i}{\partial z} - \frac{\partial[C]_{i+1}}{\partial z}\right)\Bigg|_{z=z_i} = \left(W_i - W_{i+1}\right)\left([C]_{i\ z=z_i} - [\bar{C}]_i\right) \quad i=1\ldots N$$

(2.4-A2d)

Equation (2.4.10) leads to a simple conservation law. By integrating from z_B to z_s we find

$$\frac{\partial}{\partial t}\int_{z_B}^{z_s} [C](z,t)dz = \kappa\left(\frac{\partial[C]}{\partial z}\bigg|_{z_s} - \frac{\partial[C]}{\partial z}\bigg|_{z_B}\right) + \left(-W_i[C]_s + \sum_{i=1}^{n} \Delta W_i[\bar{C}]_i\right)$$

(2.4-A3)

If we have $[\bar{C}]_i = [C]_s$, $i=1\ldots N$, then the second term on the RHS of Eq. (2.4-A3) disappears. This simply expresses the obvious fact that the rate of change of carbon in the water column equals the rate at which it diffuses in through the surface minus the rate at which it diffuses out into the bottom.

The first step in solving an equation like Eq. (2.4.10) is to Fourier transform in time. We define

$$[C](z,\omega) = \int_{-\infty}^{\infty} dt e^{i\omega t}\ [C](z,t) \qquad (2.4\text{-A4})$$

with inverse

$$[C](z,t) = \int_{-\infty}^{\infty} \frac{d\omega}{2\pi} e^{-i\omega t} [C](z,\omega) \quad . \qquad (2.4\text{-A5})$$

Corresponding definitions obtain for $[C]_s(t)$. Then Eq. (2.4.10) becomes, for the Fourier transforms,

$$-\kappa \frac{\partial^2[C]}{\partial z^2} + \frac{\partial}{\partial z}(WC) - i\omega[C] = -W_1[C]_s\delta(z-z_s) + \sum_{i=1}^{N} \Delta W_i[\bar{C}]_i\delta(z-z_1) \quad . \qquad (2.4\text{-A6})$$

Equivalently, Eq. (2.4-A1) becomes

$$-\kappa \frac{\partial^2[C]_i}{\partial z^2} + W \frac{\partial[C]_i}{\partial W} - i\omega[C]_i = 0 \qquad (2.4\text{-A7})$$

and the boundary conditions in Eq. (2.4-A2) also hold for the Fourier transforms. The solution to Eq. (2.4-A7) is

$$[C]_i(z,\omega) = A_i^+(\omega)\, e^{\alpha_+(\omega)z} + A_i^-(\omega)\, e^{\alpha_-(\omega)z} \qquad i=1\ldots N+1 \qquad (2.4\text{-A8})$$

where

$$\alpha_\mp(\omega) = \frac{W}{2\kappa} \mp \sqrt{\frac{W^2}{4\kappa^2} - i\frac{\omega}{\kappa}} \qquad (2.4\text{-A9})$$

The boundary conditions in Eq. (2.4-A2) then form a set of $2N + 2$ linear equations which determine the $A_i^{\mp}(\omega)$ in terms of $[C]_s(\omega)$ and $[C]_L$. The solution is then obtained by evaluating Eq. (2.4-A5). For a large value of N, this is in practice a messy procedure, and we shall therefore, for purposes of orientation, first look at the case of a single source.

The model is shown below in Figure 2.4-A1.

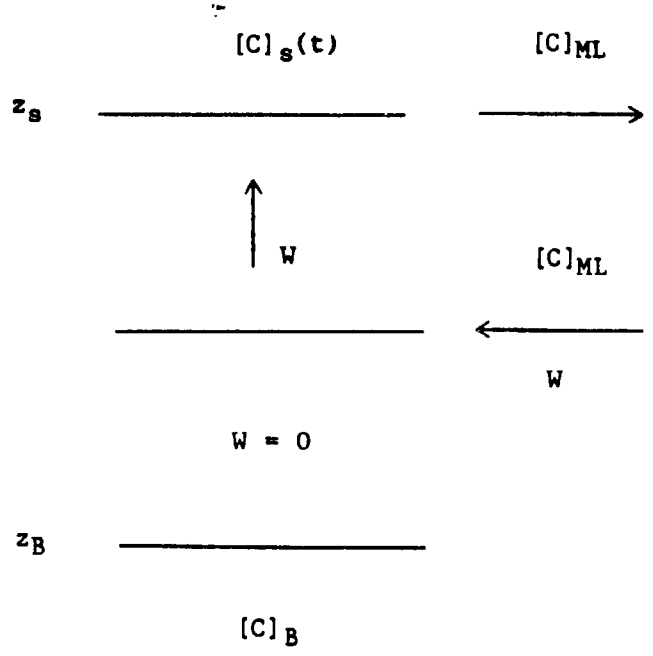

FIGURE 2.4-A1
SINGLE SOURCE MODEL

For simplicity we choose $z_B = -\infty$ and $[C]_B = 0$. We also choose $z_1 = 0$. In the two layers we then have

$$-\kappa[C]_1'' + W[C]_1' - i\omega[C]_1 = 0 \qquad (2.4\text{-A10})$$

$$-\kappa[C]_2'' \qquad - i\omega[C_2] = 0 \ . \qquad (2.4\text{-A11})$$

Thus

$$[C]_1 = \left(A_+ e^{\alpha z} + A_- e^{-\alpha z}\right) e^{\frac{W}{2\kappa} z} \qquad (2.4\text{-A12})$$

$$[C]_2 = \left(B_+ [C]^{\beta z} + B_- e^{-\beta z}\right) \qquad (2.4\text{-A13})$$

with

$$\alpha = \sqrt{\frac{W^2}{4\kappa^2} - i\frac{\omega}{\kappa}} \qquad (2.4\text{-A14})$$

$$\beta = \sqrt{-i\frac{\omega}{\kappa}} \ . \qquad (2.4\text{-A15})$$

Since $[C]_2$ must vanish as $z \to \infty$, we set $B_- = 0$. (Note that $\sqrt{-i\omega/\kappa}$ has a positive real part for ω in the upper half plane.) The remaining boundary conditions are

$$\left(A_+ e^{\alpha z_s} + A_- e^{-\alpha z_s}\right) e^{\frac{W}{2\kappa} z_s} = [C]_s(\omega,$$

(2.4-A16a)

$$A_+ + A_- = B_+ \qquad (2.4\text{-A16b})$$

$$\kappa\alpha(A_+ - A_-) = \left(\frac{W}{2} + \kappa/\beta\right)B_+ - W[C]_{ML}(\omega) \quad . \qquad (2.4\text{-A16c})$$

These equations can be solved for A_+, A_- and B_+ .

$$[C]_l(a,\omega) = e^{\frac{Wz}{2\kappa}}\,[C]_M(\omega)\,\frac{\left(W\sinh\alpha(z_s-z) + \left[\kappa\alpha\cosh\alpha z + \left(\frac{W}{2} + \kappa\beta\right)\sinh\alpha z\right]e^{-\frac{Wz_s}{2\kappa}}\right)}{\left[\left(\frac{W}{2} + \kappa\beta\right)\sinh\alpha z_s + \kappa\alpha\cosh\alpha z_s\right]} \qquad (2.4\text{-A17a})$$

$$[C]_{ML}(z,\omega) = \frac{e^{\beta z}[C]_s(\omega)}{\left[\left(\frac{W}{2} + \kappa\beta\right)\sinh\alpha z_s + \kappa\alpha\cosh\alpha z_s\right]} \quad . \qquad (2.4\text{-A17b})$$

We also write the solution for the quantity $\kappa\,\partial[C]/\partial z\big|_{z=z_s}$, which is relevant for the conservation law in Eq. (2.4-A3). (Note that $\kappa\,\partial[C]/\partial z\big|_{z=-\infty}$ vanishes.)

$$\kappa\left.\frac{\partial[C]}{\partial z}\right|_{z=z_s} = \frac{W}{2}\,[C]_{ML}(\omega) + \kappa\alpha e^{\frac{Wz_s}{2\kappa}}\,[C]_{ML}(\omega) \quad .$$

$$\frac{\left(\left[\kappa\alpha \sinh\alpha z_s + \left(\frac{W}{2} + \kappa\beta\right)\cosh\alpha z_s\right] e^{-\frac{Wz_s}{2\kappa}} - W\right)}{\left[\left(\frac{W}{2} + \kappa\beta\right)\sinh\alpha z_s + \kappa\alpha \cosh\alpha z_s\right]} \quad . \tag{2.4-A18}$$

To make those somewhat formidable looking expressions more transparent, let us choose

$$[C]_{ML}(t) = \begin{cases} [C]_{ML} e^{t/\tau} , & t < T \\ 0 , & t < T \end{cases} .$$

Then

$$[C]_{ML}(\omega) = [C]_{ML} \frac{e^{(i\omega + 1/\tau)T}}{(i\omega + 1/\tau)}$$

Since the solution $[C]_1(z,\omega)$ and $[C]_2(z,\omega)$ are proportional to $[C]_{ML}(\omega)$, they both have a pole in the upper half ω plane at $\omega = i/\tau$. This pole produces, on inverting the Fourier transforms through Eq. (2.4-A5) the "steady state" contributions to $[C]_1(z,t)$ and $[C]_2(z,t)$; that is, the part proportional to $e^{t/\tau}$ are simply residues of this pole. These residues are easy to compute, particularly in various limits.

We can identify three times in the problem: (i) τ, the growth rate of the mixed layer concentration; (ii) z_s/W, the time for transport of the water through the "pipe"; and, (iii) κ/W^2, a diffusion time.

In the limit where the diffusion time is very short--i.e., $\tau >> \kappa/W^2$ and $z_s/W >> \kappa/W^2$ --it is easy that the "steady state" solution is simply

$$[C]_1(z,t) = [C]_{ML} e^{t/\tau} \qquad (2.4\text{-A19a})$$

$$[C]_2(z,t) = [C]_{ML} e^{t/\tau} e^{z/\sqrt{\kappa\tau}} . \qquad (2.4\text{-A19b})$$

The solution is simply constant in depth down to the source, and below that dies off exponentially. This is because in the upper layer the carbon is uniformly mixed by the "pipe", while in the lower it spreads only by diffusion.

The opposite limit, in which $W \to 0$, of course yields simply

$$[C]_1(z,t) = [C]_2(z,t) = [C]_{ML} e^{t/\tau} e^{\frac{z-z_s}{\sqrt{\kappa\tau}}} ; \qquad (2.4\text{-A20})$$

now, the only spreading is by diffusion everywhere.

These steady state solutions, however, are relevant physically only if the time for water transfer through the "pipe" is short compared to the growth time τ of the mixed layer concentration; i.e., if $z_s/W << \tau$. But for the real ocean we have $z_s \sim$ kilometers, $W \sim$ a few meters per year, so $z_s/W \sim$ hundreds of years, while the characteristic time for CO_2 growth is only about 20-30 years. Thus the pumping mechanism

cannot in fact keep up with the CO_2 growth, and hence the steady state situation is irrelevant; we must look for transients. This means we cannot confine our attention only to the pole as $W = i/\tau$; we must look more widely at the ω dependence.

This is not difficult to do if we are willing to assume that the "pipe" transport dominates diffusion--that is, if κ is very small. It is easier to look directly at Eq. (2.4-A18). When $\kappa \to 0$, we find from Eq. (2.4-A18) that

$$\kappa \frac{\partial [C]}{\partial z}\bigg|_{z=z_s} + W[C]_{ML}(\omega)\left(1 - e^{i\omega z_s/W}\right) \qquad (2.4\text{-A21})$$

$$+ \text{terms which vanish with } \kappa \quad .$$

Upon inverting the Fourier transform, and invoking the conservation law (2.4-A3), we find

$$\frac{\partial}{\partial t}\int_{-\infty}^{z_s} [C](z,t)dz = W\left([C]_{ML}(t)_{ML} - [C](t-s/w)\right) \quad . \qquad (2.4\text{-A22})$$

Thus, if $S/W \ll \tau$, the right hand side is just

$$S\frac{\partial}{\partial t}[C]_{ML}(t)$$

in conformity with the steady state solution in which $[C](z,t)$ is constant in z in the upper layer of the ocean. But if $S/W \gg \tau$, then the right hand side is

$$W[C]_{ML}(t) \quad .$$

Thus, in the physically relevant case we find, if diffusion is small,

$$\frac{\partial}{\partial t}\int_{-\infty}^{z_s} [C]_{ML}(z,t)dz = W[C]_{ML}(t) \quad . \qquad (2.4\text{-A23})$$

This case has been analysed in Section 2.4.1 of this report--Eq. (2.4-A23) above is Eq. (2.4.5), so we do not need to study it further here. Numerically, for this case, the effect of the "pipe" is not large. For it to be large, one would have to be in the regime where $z_s/W \ll \tau$ instead.

The solution (2.4-A22), for the case where the "pipes" dominate diffusion, can be trivially extended to an arbitrary number of pipes. We obtain for the total amount of carbon in the ocean at time t, the expression

$$\int_{-\infty}^{z_s} [C](z,t)dz = \sum_{i=1}^{N} W_i \int_{t-d_i/W_i}^{t} [C]_{ML}(t')dt' \quad . \qquad (2.4\text{-A24})$$

Here d_i is the width of the i^{th} layer--i.e., $d_i = z_{i-1} - z_i$.

REFERENCES FOR SECTIONS 2.4 AND 2.4-A

1. Revelle, R., and Suess, H., "Carbon dioxide exchange between atmosphere and ocean and the question of an increase of atmospheric CO_2 during the past decades," Tellus, 9, No. 1, 18-27, 1957.

2. Craig, H., "The natural distribution of radiocarbon and the exchange time of carbon dioxide between atmosphere and sea," Tellus, 9, No. 1, 1-17, 1957.

3. Keeling, C., in Chemistry of the Lower Atmosphere, S. Rasoul ed., Plenum Press, 251-329, 1973.

4. Stuiver, M., "Atmospheric Carbon Dioxide and Carbon Reservoir Changes," Science 199, 253-258, Jan. 20, 1978.

5. Tans, M., Carbon 13 and Carbon 14 in Trees and the Atmospheric CO_2 Increase, Thesis, Groningen, 1978.

6. Siegenthaler U. and H. Oeschger, "Predicting Future Atmospheric Carbon Dioxide Levels", Science, 199, 388-395, Jan. 27, 1978.

7. Munk, W. H., Abyssal recipes. Deep-Sea Research, 13, 707-730, 1966

2.5 Future Carbon Dioxide Levels in the Atmosphere

Forecasting future carbon dioxide levels of the atmosphere, an essential first step in predicting the global impact of increased levels of carbon dioxide, requires an understanding of the response of five reservoirs to changing carbon dioxide concentrations and associated climatic changes. Four of the reservoirs, the atmosphere, oceans, biosphere and soils, can be considered active in the sense that they can exchange carbon with other reservoirs on a time scale on the order of a few decades. Sedimentary rocks form the largest reservoir of carbon (see Table 2.5.1) but its rate of carbon interchange with other reservoirs; for example, the rate of dissolution of calcite or dolomite with the ocean, is

TABLE 2.5.1

RESERVOIRS OF CARBON IN GTONS

Sediments	
Oxidized	5×10^7
Reduced	2×10^7
Igneous Rocks	3×10^6
Methane Hydrates	$5 \times 10^{5(?)}$
Oceans (Total)	4×10^4
Fuels	7×10^3
Soils	$1.6 \times x10^3$
Biosphere (Living)	8×10^2
Atmosphere	7×10^2

generally assumed to be very slow. However, methane hydrates may store large amounts of carbon in regions of permafrost and in ocean sediment.[1] Gas hydrates are unusual structures in which ice lattices physically trap gas molecules without the aid of direct chemical bonds. These substances form at appropriate temperature and pressure conditions when the water is saturated with methane. Increases in temperature could release this carbon to the atmosphere. Whether methane hydrates are classed as sedimentary or soil carbon is a matter of definition, but the potential reservoir is large.

2.5.1 Historical Extrapolation

The most often used method of calculating the future carbon content of the atmosphere assumes a rate of increase of world wide use of carbon based fuels and that the present ratio of the increase of the CO_2 content of the atmosphere to the CO_2 emitted into the atmosphere is maintained. This ratio has held a more or less constant value of one-half over the period 1958 to 1978. The dates at which the present concentration of CO_2 would double under the assumption that the historical pattern is maintained are listed in Table 2.5.2 (See Figs. 2.1.2, 2.1.3). We note from the discussion in Section 2.2 that this assumption neglects the atmosphere-biosphere interaction, or at least keeps the fraction of carbon in the biospheric reservoir constant.

2.5.2 Future Carbon Dioxide Level Taking Into Account Atmosphere-Biosophere-Oceanic Interactions

In order to obtain a range of dates at which carbon dioxide would double, we consider possible interactions between the atmosphere and the

TABLE 2.5.2

Doubling Dates for Carbon Dioxide Concentration
Assuming One-Half of Fuel Generated CO_2 Remains
In Atmosphere and No Net Atmosphere-Biosphere Interchange

Fuel	4.3% Exponential Growth	Tapered Growth (See Section 2.1.10)
Current Fuel Mix	2035	2055
All Coal Past 1990	2030	2045
All Synthetics Past 1990	2022	2030
All Natural Gas Past 1990	2043	2075

oceans and the biosphere. Our calculations are in principle much over-simplified in comparison with the detailed "box models" that have been analyzed in great detail by a number of investigators[2,3,4]. However, the uncertainties in the basic parameters of the models and in the basic physical process are such that sophisticated modeling is probably not warranted at this time.

In the carbon balance equation

$$A = F - B + D - S \qquad (2.5.1)$$

F rapidly becomes large (see Table 2.5.3) with respect to D for either an exponential or tapered growth in carbon based fuel usage even if the high estimates of current forest destruction hold true for the future (see Figures 2.1.2 and 2.1.3). The rate of deposition of organic carbon in the oceans, S_2, is not limited by the carbon content of the atmosphere, but

TABLE 2.5.3

Annual Additions of Carbon Dioxide to Atmosphere
With Present Mix of Fuels (GIGATONS/YEAR)

Year	Exponential Growth at 4.3% per Year	Tapered Growth to Zero Growth in 2040
1978	4.6	5.6
1990	9.4	9.4
2000	14.5	13.6
2020	34.2	22.1
2040	80.8	25.3

rather by other nutrients whose concentrations are assumed not to be affected in any major way by future activities of man. In our models we assume that

$$S_2 = D \qquad (2.5.2)$$

so that Equation (2.5.1) becomes

$$A = F - B - S_1 \quad . \qquad (2.5.3)$$

The physical-chemical absorption of CO_2 by the oceans, S_1, is assumed to depend linearly on the increase in atmospheric content of carbon dioxide

$$S_1 = \alpha A \quad . \qquad (2.5.4)$$

As discussed in 2.2 we assume that the increase in net primary productivity depends linearly on the fractional increase in atmospheric carbon dioxide

as in Eq. (2.2.3) where

$$\delta NPP/NPP = \beta \frac{A}{[C]} . \qquad (2.5.5)$$

As the concentration of carbon dioxide in the atmosphere increases, the net primary productivity increases and we assume that this increase is not balanced by an increase in decay rate.

Figure 2.5.1 shows the variation of carbon content of the atmosphere under the assumption that half of the net carbon dioxide added to the atmosphere enters the oceans. The importance of the biospheric take up of carbon is illustrated by assuming three values of β : 0 , 0.2 and 0.5 . If the ocean uptake is less, as is indicated by the analysis of Section 2.4, then the increase of carbon dioxide in the atmosphere is more rapid. Figure 2.5.2 illustrates this possibility where the ocean absorbs 20% of the net increase of the carbon content of the atmosphere. In both Figures 2.5.1 and 2.5.2 the present world mix of fuels is assumed to hold over the period of interest. The extreme case in which the world uses only synthetic fuels is illustrated in Figure 2.5.3.

Table 2.5.4 summarizes the results of the various model calculations. The date at which the carbon dioxide content doubles ranges from 2033 to 2085 depending on the assumed absorptive capacity of the oceans and biosphere and whether the carbon based fuel contribution grows at a tapered rate and the present fuel mix is maintained.

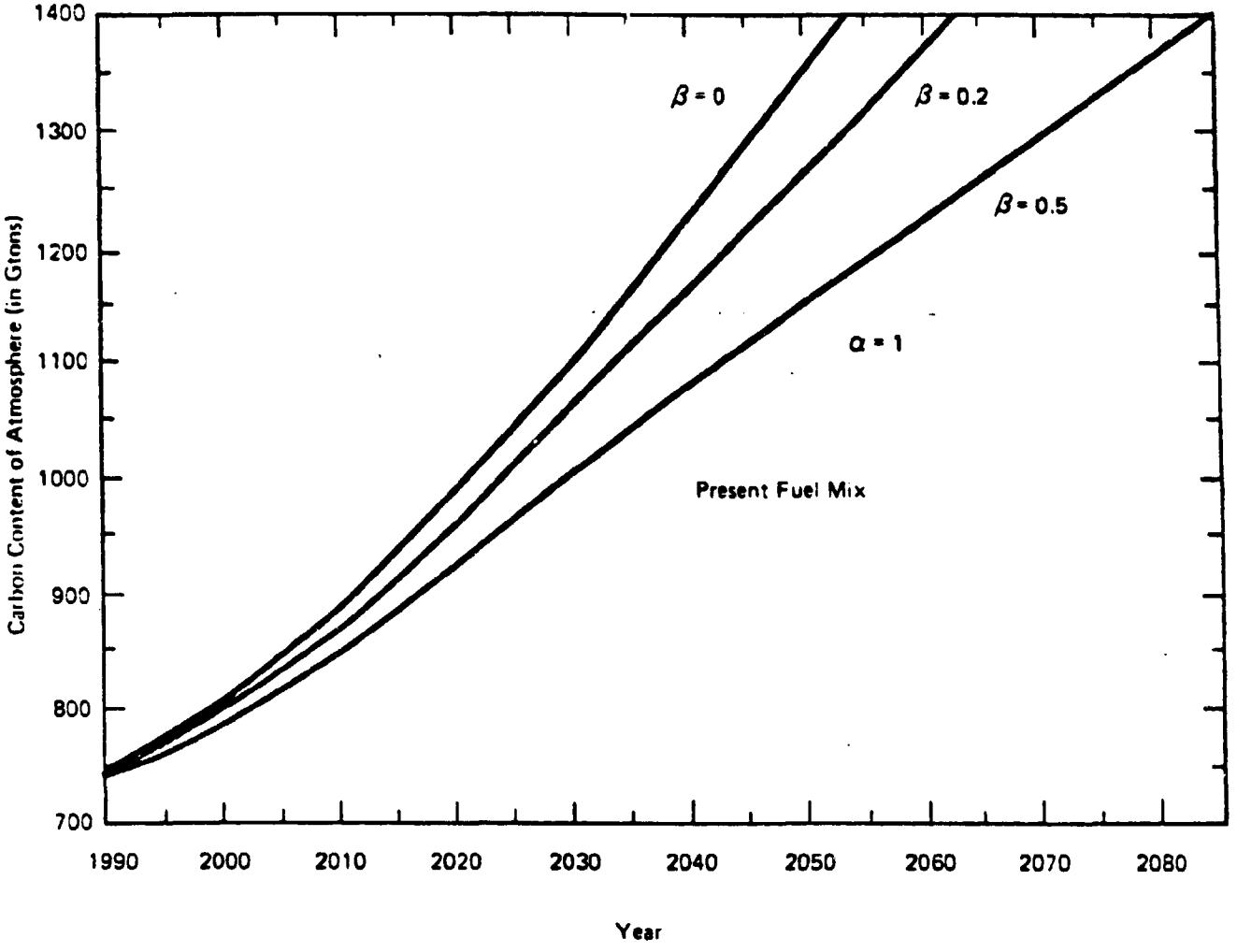

Figure 2.5.1 CHANGE IN ATMOSPHERIC CARBON CONTENT

ASSUMING $A = \frac{F - 8}{2}$

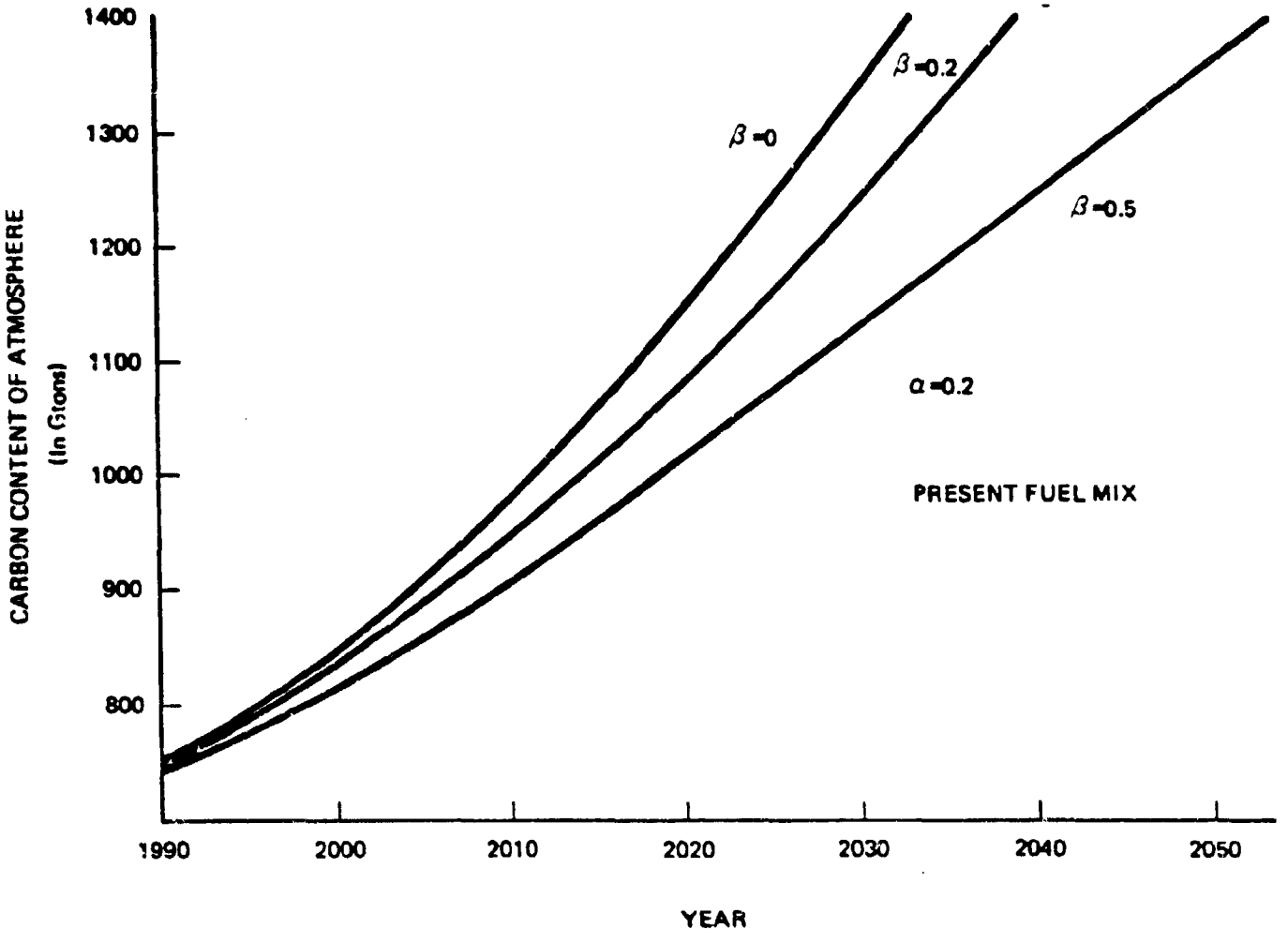

Figure 2.5.2 CHANGE IN ATMOSPHERIC CARBON CONTENT ASSUMING

$$A = \frac{F - B}{1.2}$$

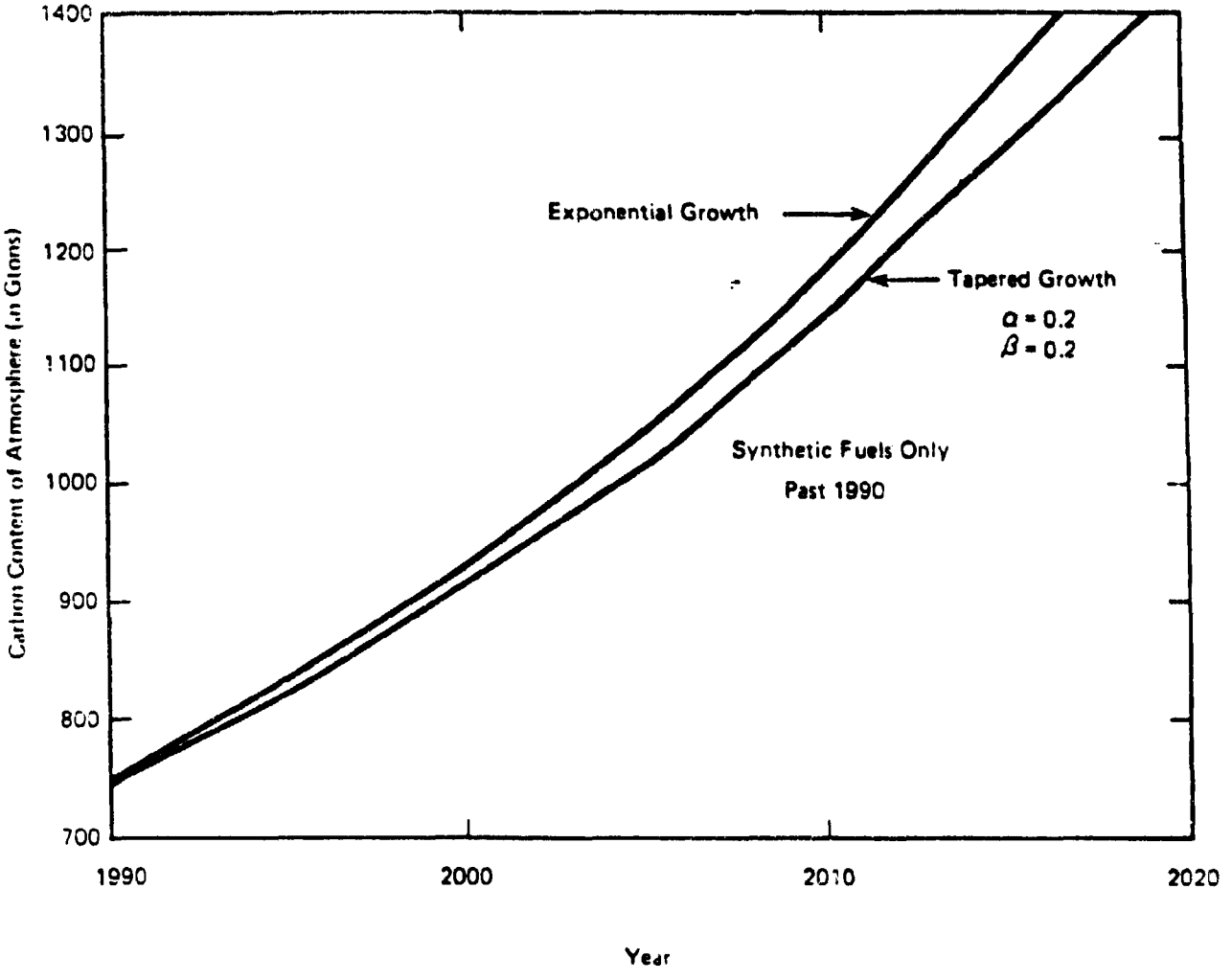

Figure 2.5.3 CARBON CONTENT OF THE ATMOSPHERE ASSUMING WORLD USES ONLY SYNTHETIC FUEL BEYOND 1990

As noted in Section 2.1.9 the lack of land availability limits biospheric growth. If the grass lands of the world, approximately 16% of the land area, were to be converted to forest, then 360 Gtons of carbon could be stored as forest on these lands.

The total capacity of these lands to store carbon is greater since forest growth would add carbon to the soils. While it is imaginable for forests to grow in a time scale comparable to fuel additions, the additions to soil carbon would take place over a longer time.

In both models with $\beta = 0.5$, the net increase of the biosphere would exceed 360 Gtons by a substantial amount (see Table 2.5.5). If this limitation of the biosphere is taken into account, then models with $\beta = 0$ or $\beta = 0.2$ seem more reasonable and the range of the doubling dates is reduced to thirty years--2033 to 2063. From the arguments presented in Section 2.4, a value of α of about 0.2 seems more probable so that a doubling date of about 2035 appears to be a reasonable estimate given the large uncertainties involved. Table 2.5.3 also shows that by about the year 2020, the increase in carbon dioxide in the atmosphere will be about one-half of the amount now present.

2.5.3 Possible Feedback from Large Carbon Reservoirs

In Section 3, we discuss the possible temperature increases in the atmosphere that result from increased carbon dioxide content of the atmosphere; a doubling of the carbon dioxide concentration leads to an average world-wide increase in temperature of about $3^{\circ}C$ with higher values at high latitudes and lower values in the tropics.

TABLE 2.5.4

Dates for Carbon Dioxide Increase

Model		Date of 50% Increase	Date of 100% Increase
Present Fuel Mix-Tapered Growth			
α	β		
1	0	2025	2054
1	0.2	2029	2063
1	0.5	2036	2085
0.2	0	2011	2033
0.2	0.2	2018	2038
0.2	0.5	2023	2055
Synthetic Fuels Only Past 1990			
Tapered Growth	α = 0.2 , β = 0.2	2007	2019
Exponential Growth	" "	2005	2017

TABLE 2.5.5

Mass Increase of Biosphere Associated With Doubling CO_2 Content of Atmosphere

Model	Date	Total Increase of Biosphere in Gton of Carbon		Net Primary Productivity (Gtons/year)
Present Fuel Mix Tapered Growth				
α	β			
1	0.2	2063	240	62
1	0.5	2085	840	73
0.2	0.2	2038	180	63
0.2	0.5	2055	560	72

The biospheric reservoir would respond to a temperature increase by an increase in net productivity, particularly if the temperature increase is accompanied by an increase in precipitation. Leith[5] argues that a 1^{o} C rise in temperature accompanied by a 6% increase in precipitation raises net primary productivity (NPP) world wide by about 5%. However, the increase of NPP as a result of temperature changes will be accompanied by an increase in decay rate for changes; the decay rate can be assumed to grow exponentially with temperature. Whether the temperature increase will lead to large enhanced storage of carbon in the biosphere is thus problematical. Further, as noted above, the biospheric storage is limited by the availability of land and nutrients other than carbon. We assume the impact of temperature on the biosphere to be less important than that from increasing carbon dioxide levels in the atmosphere.

The enormous size of the organic carbon pool in the soils implies that small changes in the rate of humus oxidation with its exponential temperature dependence can lead to large carbon exchanges in the atmosphere. Loomis[6] calculations, when adjusted for a lower total carbon content of the soils (see Section 2.2.2), suggests that a degree rise in temperature could release as much as 100 to 200 Gtons of carbon (see Table 2.5.6). The rate of soil carbon release will depend on the rate at which the temperature wave penetrates the soil, the rate at which the humus oxidizes, and the upward diffusion rate of carbon dioxide. These are poorly known, but it is probable that the time scale for the response of the soil is long compared with the time scale for fuel additions to the atmosphere.

TABLE 2.5.6

Large Temperature-Sensitive Sources or Sinks of Carbon Dioxide (in Gtons of Carbon)

Soils	
Stored Carbon	1600 Gtons
Temperature dependence	100-200 Gtons/degree
Oceans	
Mixed layer	600 Gtons
Deep oceans	4×10^4 Gtons
Temperature dependence mixed layer	21 Gtons/degree
Methane Hydrates	
Terrestrial	2000 (?)
Oceanic	4.5×10^4 (?)
Temperature dependence terrestrial	70 Gtons/degree

The impact of an increase in temperature on the chemical composition of the upper layers of the oceans is well understood[4] and a relatively small quantity of carbon is released into the atmosphere by the oceans by a temperature change, about 20 Gtons/degree. The methane hydrate reservoir is the least well understood of the large carbon reservoirs. The rate of release of carbon from methane hydrates in ocean sediments will depend on the warming of the deep ocean which has a time scale of 1000 years. The rate of release of terrestrial methane hydrates will be controlled by processes similar to those involved in the release of soil carbon. However, because the temperature increase is accentuated at the poles, the methane hydrates in the permafrost regions could release significant amounts of carbon (see Table 2.5.6).

In summary, a worldwide warming will tend to produce a positive feedback releasing carbon from the soils, methane hydrates and oceans. The rate of release is not known, though the ocean response should be rapid. Because of this we are uncertain as to whether these large carbon pools will play a significant role in leading to further warming of the earth or even how such feedbacks may compare with that from changes in the biosphere.

REFERENCES FOR SECTION 2.5

1. Makogan, Yo., Hydrates of Natural Gas, Geoexplorers, Inc., Denver, 1978.

2. Oeschger, H., H. Siegenthaler, J.,Schotterer, U. and Gugelmann, A., "A Box Diffusion Model to Study Carbon Dioxide Exchange in Nature", Tellus, 27, No. 2, 168-192, 1975.

3. Stuiver, M., "Atmospheric Carbon Dioxide and Carbon Reservoir Changes", Science, 199, 253-258, Jan. 20, 1978.

4. Keeling, C. D., and R. Bacastow, "Impact of Industrial Gases on Climate," in Energy and Climate, National Academy of Sciences, Washington, D.C., 72-95, 1977

5. Lieth, H., "Vegetation and CO_2 Changes" in Carbon Dioxide, Climate and Society, ed. by J. Williams, Pergamon Press, New York, 1978

6. Loomis, R., "CO_2 and The Biosphere," in Carbon Dioxide Effects Research and Assessment Program, ed. by W. Elliott and L. Machta, U.S. Department of Energy, CONF 770385, 1979

THIS PAGE LEFT BLANK INTENTIONALLY

3.0 MODELS OF CLIMATE CHANGE RESULTING FROM CHANGES IN THE CHEMICAL COMPOSITION OF THE ATMOSPHERE

Early attempts to calculate the effects of changes in the concentration in the atmosphere of carbon dioxide and other minor constituents centered on determining the change in the average surface temperature of the earth. Climate is much too complicated to be described by a single parameter. The geographical and temporal distributions of precipitation, onset of freezing conditions, strength and patterns of storms are all critical for understanding the impact of climatic change on man. Present models of climatic change are inadequate to provide the large number of descriptors needed to understand climatic change and its impact on man. In part, our lack of understanding flows from the complex interactions of the atmosphere with other elements of our planet.

The climate system of ocean-land-cryosphere-biosphere is governed by numerous feedback mechanisms having both positive and negative responses to changes in temperature and changes in atmospheric composition. In our studies we have isolated and discussed many of these, but have not evaluated the full effect of each (See Section 2.5). In order to give some indication of the issues, we discuss briefly various feedbacks and their signs:

A. <u>Temperature - Infrared Radiation Feedback</u>:

As the temperature rises, so does the outgoing infrared radiation. This is a negative feedback and is the primary mechanism

determining the overall magnitude of the earth's temperature. It is included in all recent models of climatic change due to increased carbon dioxide.

B. Water-Greenhouse Feedback:

As temperature rises, the amount of water vapor increases since relative humidity seems rather independent of temperature (Manabe and Wetherald[1], and Section 3.1). A rise in water vapor increases the infrared blanket of the atmosphere and thus causes a further temperature increase. So this is a positive feedback.

C. Ice and Snow Cover Albedo Feedback:

As the temperature is increased, snow cover and ice will melt back. This decreases the Earth's surface albedo and the increased absorption of sunlight further raises the temperature. This is clearly a positive feedback. This mechanism is central to the energy budget models initiated by Budyko[2] and Sellers[3], and is the main feedback feature in the climate models considered here (See Section 3.2).

D. Cloud Cover Feedback:

As cloud cover is increased, two opposing effects occur:

- o the Earth's albedo increases and this tends to lower the temperature and
- o the amount of IR trapped is increased and this tends to increase the temperature.

Analysis by Cess[4] indicates that these two effects seem largely to cancel one another. We have not considered changes in cloud cover in our deliberations. This is likely to be an important point of omission and needs to be addressed in future work (See also Section 3.3 and 4.1).

E. CO_2 Biofeedback:

Increasing the CO_2 concentration in the atmosphere will increase the growth of the biosphere (See Section 2.2 and 2.5). This new growth will fix carbon via photosynthesis and tend to reduce the atmospheric CO_2. So this is a negative feedback.

F. Iceberg Formation Feedback

If the temperature increases and begins the breakup of large ice sheets, the calving and surging mechanisms described in Section 4.3 will create vast areas of new icebergs. The area covered by these bergs is likely to be substantially larger and further equatorward than the present ice. These two effects increase the earth's albedo until the ice melts, so, for some time, this mechanism acts to decrease the temperature. Here we have another negative feedback.

G. Temperature-Convection Feedback:

As temperature is increased at the ground, convection will increase. This carries sensible heat away from the ground and cools it. Thus, we have a negative feedback.

H. Evaporation-Precipitation Feedback:

Increasing the temperature will increase the intensity of the hydrologic cycle. Increased evaporation will carry off the additional temperature rise in latent heat while increased precipitation will be working to return that same energy. In this cycle both positive and negative feedback effects are present. The hydrologic cycle is absent from the simple energy-budget models we employ here. Along with the absence of consideration of cloud, this is probably the most severe defect in our work.

I. Sea Ice-Ocean Current Feedback:

The bottom water producing currents discussed at some length in Section 4.2 of this study are driven in the Antarctic by the formation of sea ice in the Weddell Sea. An increase in temperature due to CO_2 will inhibit or stop sea ice formation and remove the pump during these currents. As a result the cold bottom waters will not be replenished and an increase in ocean temperature will occur, leading to loss of CO_2 from the oceans and a further increase in temperature. This is another positive feedback mechanism.

J. Biomass Albedo Feedback:

Cess[5] has noted that an increase in temperature will lead to a decrease in albedo because of the stimulation of new growth in the biosphere. The effect is small ($d\alpha/dT = 0.0062$) but provides yet another positive feedback.

This list exhibits some of the complexity of the climate system and gives a hint as to the remarkable stability of the system. Indeed,

although we have not done so here, one is led to contemplate the dynamics of systems with very large numbers of both positive and negative feedbacks as a model for the climate. Such systems may possess a kind of statistical stability absent in the consideration of any individual feedback mechanism. Actually, we have seen in our study of the JASON Climate Model, and in other work on more complex climate models, a severe sensitivity to changes in climate parameters. This sensitivity is so extreme as to be almost unbelievable. One has the expectation that the real Earth is far less sensitive, and that the origin of this stability may originate in the competition of numerous feedback effects.

Partial insight into the impact of changing atmospheric composition on climate can be achieved by examining simple models of the atmosphere. In Section 3.1 we consider models of the atmosphere in which radiation is the only mechanism by which e[illegible]s transferred. In Section 3.2 we consider both time independent and [illegible]me dependent models of lumped ocean-atmosphere systems.

REFERENCES

1. Manabe, S. and R. T.Wetherald, "Thermal Equilibrium of the Atmosphere With a Given Distribution of Relative Humidity," J. Atmos. Sci., 24, 241-259 (1967).

2. Budyko, M.J., "The Effect of Solar Radiation Variations on the Climate of the Earth," Tellus, 21, No. 5, 611-619, (1969).

3. Sellers, W.D., "A Global Climatic Model Based on the Energy Balance of the Earth-Atmosphere System," J. Appl. Meteorol., 8, 392-400 (1969).

4. Cess, R.D., "Climate Change: An Appraisal of Atmospheric Feedback Mechanisms Employing Zonal Climatology," J. Atmos. Sci., 33, 1831-1843 (1976).

5. Cess, R.D., "Biosphere-Albedo Feedback and Climate Modeling," J. Atmos. Sci., 35, 1765 (1978).

3.1 Radiative Limits on Climate

3.1.1 Introduction

The sun's radiation in the visible part of the spectrum, except for that fraction which is directly reflected back out into space, warms the Earth. For an Earth in radiative equilibrium, the solar radiation which interacts with the atmosphere and the Earth's surface must be balanced by an equal amount of outgoing infrared radiation. The temperature of the Earth as observed from space, the "effective temperature", is determined by the amount of energy which the Earth must lose to remain in radiative equilibrium. The effective temperature is lower than the surface temperature since all parts of the atmosphere radiate into space in addition to the land and oceans. The actual surface temperature and the temperature profile of the atmosphere are determined by the interplay of radiative processes, convective transfer of heat and the heat released in the phase transitions of water. Altering the radiative properties through changing the concentrations of infrared absorbers will change climate on a global scale.

In this section we explore two models of the atmosphere in which only the radiative processes are taken into account. These models are a first step in a hierarchy of atmospheric models of increasing complexity. The first model uses a grey atmosphere approach in which the Earth's surface is viewed as a "hot plate" at temperature T_g. The atmosphere is seen as a partially absorbing blanket through which only a portion of the radiation emitted by the hot plate is allowed to pass into space. The

amount of absorption encountered by outgoing radiation is a function of the amounts of various atmospheric constituents (CO_2, H_2O, hydrocarbons, etc.) residing in the atmosphere.

By contrast, the second model may be conveniently understood by picturing an observer in space receiving the Earth's outgoing radiation in nine infrared spectral bands. In each band one observes radiation arising from an effective radiating level somewhere in the atmosphere. This level is determined by how far down into the atmosphere the observer can see before absorption becomes too great. In opaque bands, such as the 15 μ CO_2 band, the radiating level is high, near the tropopause. In nearly transparent bands, such as the 12 μ atmospheric window, the radiating level is low in the troposphere, near the surface. Thus, in this second model, radiation is viewed as arising primarily from the atmosphere itself rather than the surface as in the first model. The second model approaches the first as a limiting case when a given spectral band is transparent or nearly so and the effective radiating level is at the surface. A primary objective of this band model is the comparison of model results with satellite spectrometer observations of the Earth's infrared radiation to space.

Our objective in pursuing these two different approaches is to make two largely independent estimates of the Earth's infrared radiation losses and thus two largely independent estimates of the increases in surface temperature caused by increases in atmospheric CO_2 (or other infrared absorbers). If the two approaches give roughly the same result,

then that result can be viewed with more confidence than a single result by either approach above. In addition, the infrared fluxes in nine spectral bands predicted by the second model are compared to Nimbus 4 satellite observations with reassuring results.

3.1.2 Changes in the Planetary Heat Balance with Chemical Changes in the Atmosphere

3.1.2.1 Introduction

What approximate analytic models lose in accuracy (compared with more elaborate computer-based analyses) they gain in clarity and adaptability. The model developed here is a case in point. It is a simple matter to change the CO_2 content of the atmosphere and find what change will occur in the global mean temperature. One can go a step further and find how the H_2O vapor content will be altered and include that feedback in the solution. This technique, of approximating the atmosphere as a quasi-grey one (with opacity versus wavelength given by a step function), improves the utility of analytic, zonally averaged models, such as North's[1,2] version of the Budyko[3] and Sellers[4] models. Other representations of opacity by a step function are due to Sagan and Mullen[5] and to Henderson-Sellers and Meadows[6].

The troposphere is not in radiative equilibrium nor is it even approximately grey (meaning that the absorption coefficient is independent of frequency). Further, it is not vertically homogeneous, since H_2O is distributed with a scale height of about 2 km, CO_2 with 8 km, and O_3

existing mainly in the stratosphere. Hence it is surprising that a quasi-grey, radiating homogeneous model has any value at all. Certainly this kind of model would not yield a very useful temperature-height profile, nor is there any reason to expect it will reproduce the absolute temperature at the ground. We may, however, consider an "equivalent radiative atmosphere" (ERA) that mimics the radiative aspects of a real atmosphere. Such a simplified model can be useful for exploring the importance of changes in the greenhouse effect caused by changes in the atmospheric composition, and of changes in the incident solar flux. The reasonably satisfactory nature of the radiative approximation is due in part to the small mean optical thickness of the atmosphere. Thus, in this model, if the emitting level characterized by an optical depth $\tau_e = 2/3$, has $T_e = 257^oK$, then at the ground $\tau_g = 0.77$ for $T_s = 288^oK$. For a purely convective model, τ_g would be 0.82.

3.1.2.2 The Quasi-Grey Model

In the grey, ERA model only two temperatures are important: The effective emission temperature, T_e, of the planet is fixed by balance between the incident solar flux and the planetary thermal emission. For a rotating planet of radius R

$$4\pi R^2 \sigma T_e^4 = (1 - A)\pi R^2 [\pi F] \quad , \qquad (3.1.2.1)$$

where A is the omnidirectional albedo and πF is the solar flux outside the atmosphere. The surface temperature, T_s, is assumed to be the immediate source of radiation as far as the atmospheric heating is concerned.

We can relate T_s to T_e through some unknown absorptivity of the atmosphere, A, such that $AT_s^4 = T_e^4$, where $A^{1/4}$ is the greenhouse factor. To evaluate the dependence of A on composition, we may mimic the real atmosphere with a highly simplified quasi-grey radiative model, which gives $A = 1 + (3/4)\ \tau_g$ or[7]

$$T_s^4 = T_e^4 \left[(1 + (3/4)\ \tau_g) \right] \quad , \qquad (3.1.2.2)$$

where τ_g is the vertical opacity of the atmosphere, which we now estimate.

With $A = 0.29$, we have $T_e = 257^{\circ}K$; then $T_s = 288^{\circ}K$ gives $A = 1.58$ or $\tau_g = 0.77$. As we shall show, this is about the mean gaseous opacity of the atmosphere, although some variation can be obtained, depending on the amount of H_2O vapor assumed. The greenhouse effect of clouds (not included here) would considerably raise T_s but convective adjustment, also neglected, lowers T_s by a comparable amount[8]. Thus, in what follows, we are not supposing that T_s is fixed by radiative equilibrium, but rather that <u>changes</u> in greenhouse heating can be estimated from <u>changes</u> in gaseous opacities of the ERA.

If the ground emits isotropically with intensity $B_\lambda(T_s)$, the flux transmission directly to cold space is

$$\sigma T_s^4 Q(\tau) = \int_0^\infty d\lambda B_\lambda(T_s) \int_0^{2\pi} d\phi \int_0^1 e^{-\tau/\mu} \mu d\mu$$

$$= \sigma T_s^4 2E_3(\tau) \approx \sigma T_s^4 e^{-\beta\tau} \qquad (3.1.2.3)$$

where $E_3(\tau)$ is the exponential integral, which we approximate with a simple exponential. Eq. (3.1.2.3) defines the extinction coefficient β. As τ varies from ∞ to 0 and the <u>transmission function</u> $Q = 2E_3(\tau)$ varies from 0 to 1, the coefficient β varies from 1.2 to 2.0. For H_2O and O_3 we choose $\beta = 1.66$, which gives the exact value of E_3 when $Q = 1/2$ or $\tau = 0.42$; for CO_2 at 15 μm, we take $\beta = \beta^* \equiv 1.2$.

For a non-grey atmosphere the same kind of considerations hold except that τ is a function of λ, and

$$Q = \sum_{i=1}^{n} p_i e^{(-\beta\tau_i)} \qquad (3.1.2.4)$$

where the summation is over narrow wavelength intervals and p_i is the fractional flux in the <u>i^{th}</u> interval,

$$p_i = \frac{\pi B_{\lambda i}(T_s)\Delta\lambda_i}{\sigma T_s^4} \qquad (3.1.2.5)$$

3.1.2.3 <u>Earth's Infrared Absorption</u>

The Earth's thermal radiation is mainly confined to the 5 to 30 μm region (See Figure 3.1.2.1). Between 0.54 and 8 μm H_2O has strong vibration-rotation bands and longward of 15 μm occur rotational lines from

the ground vibrational state. The H_2O molecule is thus a strong absorber over the thermal spectrum, except for the important 8 to 18 μm interval, where the Earth's emission peaks (at 290°K, λ_{max} = 10 μm) . The 12 to 18 μm region is dominated by the CO_2 ν_2- (bending) mode fundamental, leaving an 8 to 12 μm transparency window. A portion of this window is blocked by the 9.6 μm band of O_3. Greenhouse heating of the atmosphere is thus dependent on composition in several distinct ways as illustrated in Figure 3.1.2.1.

First, water vapor is dominant over a wide wavelength interval, although in much of this region it is not optically thick. Hence, atmospheric cooling to space is critically dependent on H_2O abundance and even the vapor in the stratosphere is significant.

Second, CO_2 fills a large part of the H_2O window, and current CO_2 abundances are enough to make the 15 μm region optically thick. Major CO_2 abundance changes will alter the greenhouse heating mainly by CO_2 absorption in the 10 μm bands and widening the 15 μm bands.

Finally, minor constituents that absorb strongly in the 8-12 μm region can be critically important. Nitrous oxide (N_2O) and a wide array of hydrocarbons are potentially important, and the grey model can be used to estimate their effects.

The abundance of water vapor typically varies from 0.2 to 2 gm/cm^2 (or cm of precipitable water). We adopt a global average of 1 gm/cm^2.

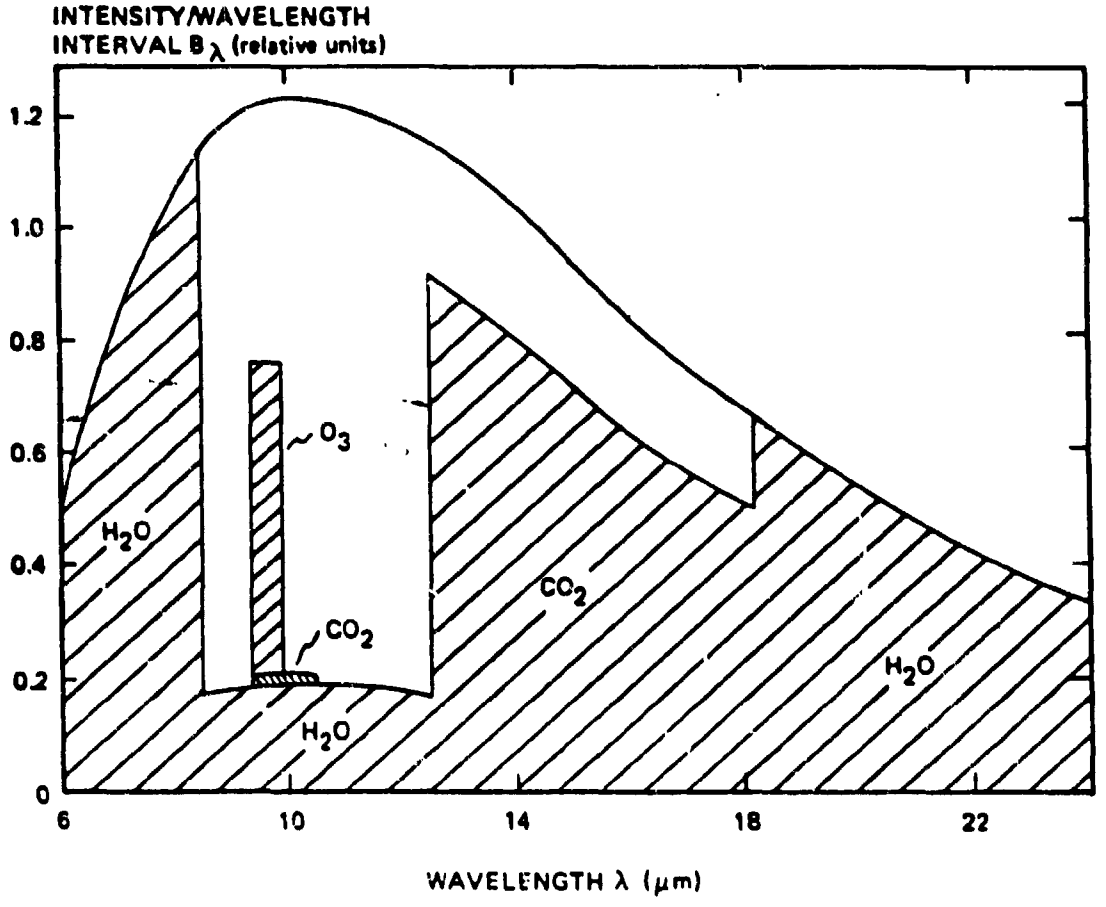

Figure 3.1.2.1 THERMAL EMISSION OF THE EARTH'S SURFACE AT T = 290°K (after KONDRATYEV [1969], p.119), WITH RELATIVE VALUES OF THE ABSORPTION, $1 - \exp(-\beta\tau)$, INDICATED BY SHADED AREAS. THE FIGURE ILLUSTRATES WHY TRACE AMOUNTS OF ABSORBERS IN THE 8.5-12.5 μm REGION CAN BE CRITICALLY IMPORTANT.

With sufficient accuracy H_2O may be regarded as completely opaque except in the near infrared and visual ($p_i = 0.03$); from 8.5 to 12.5 μm where $\tau = 0.10$ and $p = 0.29$; and 12.5 - 15 μm where $\tau < 1$ and $p = 0.14$. However, H_2O does not contribute importantly to atmospheric heating in the region where the absorption is dominated by CO_2, and the H_2O therefore can be treated as transparent from 12.5 to 18 μm with[9] $p = 0.26$. Thus, Eq. (3.1.2.4) gives the absorption function due to water alone as

$$A(H_2O) = 1 - Q(H_2O) = 0.45 \qquad (3.1.2.6)$$

As CO_2 increases, the mean opacity within a fixed wavelength interval also increases, but also, the band effectively widens as weaker absorptions become stronger. This discussion necessarily oversimplifies the complex role of the weak isotopic and hot bands near 15 μm. For a detailed treatment of CO_2 radiation, see Augustsson and Ramanathan[10].

For CO_2 a volume mixing ratio of $f = 333$ ppm corresponds to an equivalent thickness at STP conditions of

$$\xi(CO_2)' = 266 \text{ atm-cm} \qquad (3.1.2.7)$$

An empirical formula for the mean transmission in the nearly saturated 15 μm band is

$$Q(15\ \mu) = \exp\ (-\beta^* a \xi^b) \qquad (3.1.2.8)$$

where β^* is the value of β appropriate at large τ. The absorption data near $\xi = 300$ atm-cm yield $\beta^* = 1.2$, $a = 0.361$, and $b = 0.23$. Then the total absorption due to CO_2 at 15 μm (or more precisely between 12.5 and 18.2 μm) is

$$A(CO_2) = 1 - Q(CO_2) = p(15\ \mu)\ [1 - \exp(-\beta^* a \xi^b)] = 0.27(0.791) = 0.214 \qquad (3.1.2.9)$$

For the weak CO_2 band absorption we use the treatment in Section 3.1.2.4, below, for minor constituents. The properties of the two inter-combination bands at 10 μm are listed in Table 3.1.2.1 and from Eq. (3.1.2.24) we have $A(10\ \mu) = 0.025$.

For $\xi = 0.3$ atm-cm of ozone in the stratosphere we find[9], over the band (9.4 to 9.9 μm), a mean transmission of

$$\langle Q(9.6\ \mu) \rangle = \exp(-2.8\xi) \qquad (3.1.2.10)$$

or

$$A(O_3) = 1 - Q(O_3) = p(9.6\ \mu)(1 - e^{-2.8\xi}) = 0.035(.57) = 0.020 \qquad (3.1.2.11)$$

TABLE 3.1.2.1

ABSORBER IN 8 - 12 μm WINDOW*

Species	Band, λ (μm))		f(ppm)	S(cm)
N_2O Nitrous Oxide[1]	ν_1	7.8	0.28	10^{-17}
CH_4 Methane[1]	ν_4	7.66	1.6	7×10^{-18}
NH_3 Ammonia	ν_2	10.5	6×10^{-3}	(?) 10^{-20}
CF_2Cl_2 F-12	ν_1	9.1	1×10^{-4}	5×10^{-17}
	ν_6	8.7		3×10^{-17}
	ν_8	10.9		5×10^{-17}
$CFCl_3$ F-11	ν_1	9.2	1×10^{-4}	3×10^{-17}
	ν_4	11.8		6×10^{-17}
Hydrocarbons	------		4×10^{-3}	5×10^{-17}
CO_2	$2\nu_2-\nu_3$	9.4		8.6×10^{-22}
	$\nu_1-\nu_3$	10.4	333	2.7×10^{-21}

---

* For uniform mixing the integrated abundance is $N = f d_{atm}$ $= f \times 2.15 \times 10^{25}\ cm^{-2}$. Since the STP thickness is $\xi = N/N_o$ $= f N_{atm}/2.687 \times 10^{19}$, we have $f(ppm) \simeq 1.25\ \xi\ (atm\text{-}cm)$.

1 Note that N_2O and CH_4 are not optically thin and the analysis of this section does not apply.

The computation of the various A's is illustrated in Figure 3.1.2.1. If the various substances do not overlap seriously in their spectral regions of absorption, the A's can be added. Thus, from Eqs. (3.1.2.4), (3.1.2.6), (3.1.2.9), (3.1.2.11) and (3.1.2.24), we have (with $\beta = 1.66$)

$$Q_{net} = e^{-\beta\tau_g} = 1 - [A(H_2O) + A(CO_2,15\mu) + A(CO_2,10\mu) + A(O_3)] = 0.29 \qquad (3.1.2.12)$$

giving

$$\tau_g = 0.748 \qquad (3.1.2.13)$$

With an albedo $A = 29\%$, Eq. (3.1.2.1) gives $T_e = 257^oK$. Then Eqs. (3.1.2.2) and (3.1.2.13) yield

$$T_s = 287.2 \qquad (3.1.2.14)$$

which is close to the world average (288^oK).

3.1.2.4 Variation of Ground Temperature with CO_2 Abundance:

Differentiating Eq. (3.1.2.12) with Eqs. (3.1.2.9) and (3.1.2.24), below, gives

$$\beta e^{-\beta\tau} = \frac{dA(cO_2)}{d\tau} = p(15\mu)\exp(-\beta^* a\xi^b)\ \beta^* ab\xi^b \left(\frac{1}{\xi}\frac{d\xi}{d\tau}\right)$$

$$\left(+ 1.08 \times 10^{-3}\ S_\nu N_o \frac{d\xi}{d\tau}\right)$$

In terms of the mixing ratio or volume concentration

$$\frac{d\tau}{df} = [CO_2]\frac{d\tau}{d[CO_2]} = \frac{p(15\mu)\beta^* ab \exp(-\beta^* a\xi^b)\xi^b}{\beta e^{-\beta\tau}}$$

$$+ \frac{1.08 \times 10^{-3} S_\nu N_o \xi}{\beta e^{-\beta\tau}} = 4.21 \times 10^{-2} + 7.5 \times 10^{-2} = 0.117 \qquad (3.1.2.16)$$

Similarly, from Eq. (3.1.2.2), we obtain

$$\frac{dT_s}{d\tau} = \frac{3T_e}{16(1 + .75\tau_g)^{3/4}} = \frac{3T_s}{16(1 + .75\tau_g)} = 34.5 \qquad (3.1.2.17)$$

and therefore,

$$f\frac{dT_s}{df} = 4.0^0K \qquad (3.1.2.18)$$

if the CO_2 f actional concentration were changed by a small amount. If the CO_2 content were doubled, the grey model would give $\tau_g = .828$, $T_s = 290.0$ or $\Delta T_s = 2.8^oK$. This value compares nicely to values obtained from more elaborate models. In reviewing a number of recent studies, Schneider[11] concluded that a doubling of CO_2 would produce a ΔT_s of 1.5 to 3^oK. As CO_2 is increased further, the temperature will continue to rise; although the 15 μm bands are already nearly saturated, the 10 μm bands are effectively closing the 8 - 12 μm window, as illustrated in Fig. 3.1.2.2.

3.1.2.5 Radiative Effects of Minor Constituents:

The addition to the atmosphere of a minor constituent that absorbs

in the 8 to 12 μm window could be important. In this region $\pi B_\lambda / \sigma T_s^4 \approx .060 - .070/\mu$ and hence, Eq. (3.1.2.5) is

$$p_i \approx 0.065\ \Delta\lambda_\mu \qquad (3.1.2.19)$$

where $\Delta\lambda_\mu$ is the width of the absorption in microns. We will estimate the minimum amount of a trace gas that would produce a 1°K change in global temperature.

For an optically thin amount of absorber, we have simply,

$$A_i = p_i\left[1 - e^{-\beta\tau i}\right] \approx \beta p_i \langle\tau_i\rangle \quad , \qquad (3.1.2.20)$$

where $\langle\tau\rangle$ is the mean value in the band, or

$$\langle\tau\rangle \frac{N}{\Delta\lambda_\mu} \int \alpha d\lambda_\mu \qquad (3.1.2.21)$$

which gives

$$A = \beta(.065)\ N \int \alpha d\lambda_\mu = .108 N S_\lambda \qquad (3.1.2.22)$$

where N is the integrated column density (molecule/cm^2 and S_λ the integrated absorption coefficient or strength (in units of cm^2 micron). The more common units for strengths are cm (cross section in cm^2; spectrum in cm^{-1}):

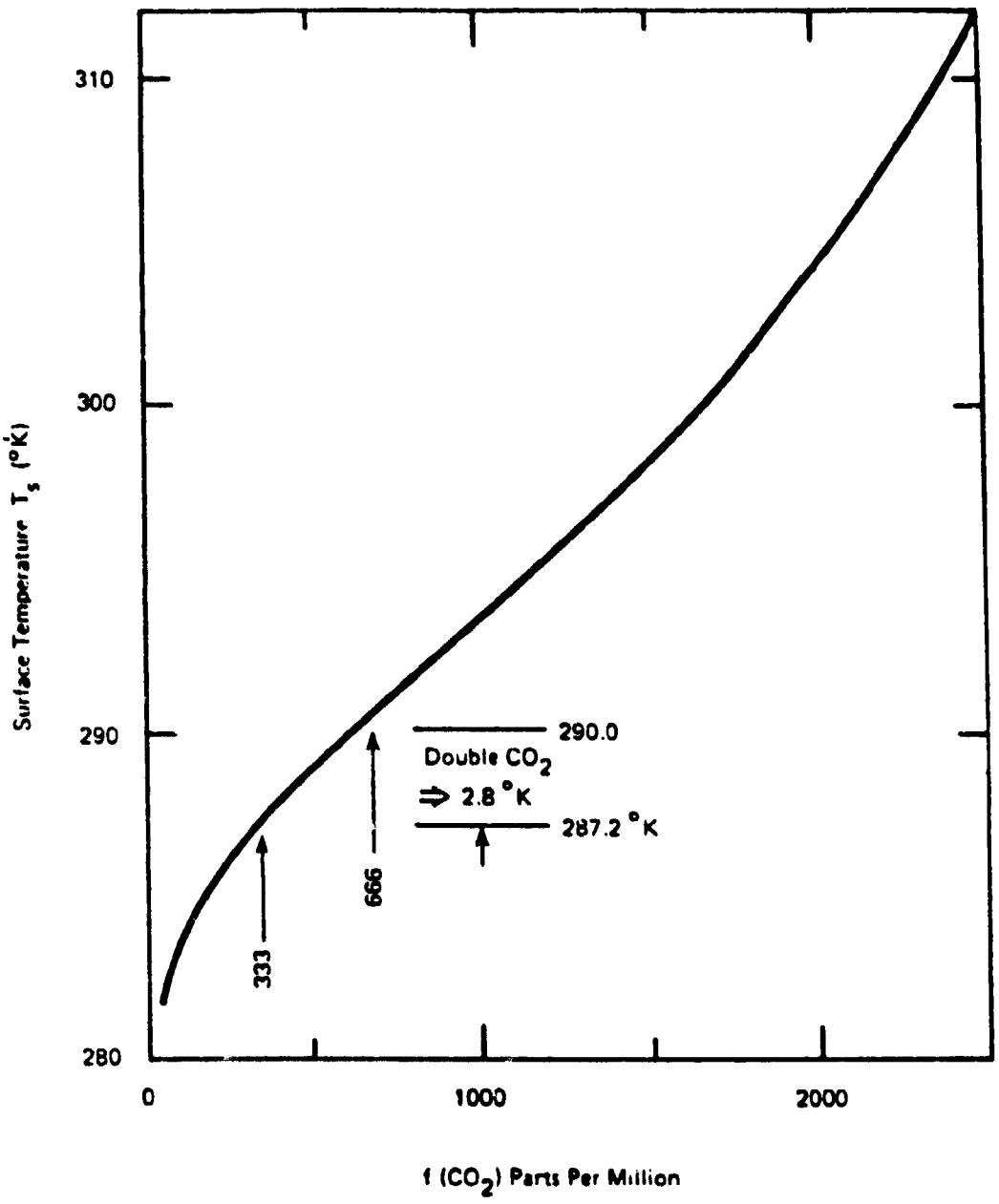

Figure 3.1.2.2 TEMPERATURE VERSUS CO_2 ABUNDANCE FOR GLOBAL RADIATIVE EQUILIBRIUM WITH THE QUASI-GREY MODEL

$$S_\nu = \int \alpha d\nu \qquad (3.1.2.23)$$

Hence, at 10 μm ,

$$A = 0.108\ N S_\nu\ \lambda_\mu^2\ 10^{-4} = 1.08 \times 10^{-3}\ N S_\nu \qquad (3.1.2.24)$$

The maximum band strengths are not likely to exceed 5×10^{-17}cm.

From Eq. (3.1.2.12) we have, for $A = 1 - Q_{net}$,

$$\frac{dA}{d\tau_g} \equiv \beta e^{-\beta\tau_g} = 1.66\ (0.25) = 0.415 \qquad (3.1.2.25)$$

and with Eq. (3.1.2.17), the $T_s - A$ relation becomes

$$\frac{dT_s}{dA} = \frac{dT_s/d\tau_g}{dA/d\tau_g} = 83 \quad . \qquad (3.1.2.26)$$

Thus, for 1^oK changes in T_s , we are searching for increments in A the order of 1×10^{-2}, or from Eq. (3.1.2.24);

$$\Delta N \gtrsim \frac{1 \times 10^{-2}}{1.08 \times 10^{-3} \times 5 \times 10^{-17}} = 2 \times 10^{17} cm^{-2} \qquad (3.1.2.27)$$

The integrated column density of the atmosphere is 2.15×10^{25} cm^{-2} so we are concerned with mixing ratios of minor constituents greater than

$$\Delta f \sim 10 \times 10^{-9} \qquad (3.1.2.28)$$

or a few parts per billion (ppb) for substances that have a single strong absorbing band in the 8 to 12 μm window.

The halogenated methanes (Freons) have been cited as a striking example of the effect we are examining here[12]. The two Freons F-11 and F-12 together have five bands with strengths $S\nu \sim 3 \times 10^{-17}$cm. The 1975 abundance was 0.1 ppb; an increase of 10^2 times would place these substances in the climate critical category.

Most substances will not have bands in the window with strengths close to the maximum. From Eq. (3.1.2.27) the pertinent quantity for bands in the window is

$$\Delta \cdot S \gtrsim 10 \text{ or } \Delta f(\text{ppm}) \cdot S \gtrsim 5 \times 10^{-19} \qquad (3.1.2.29)$$

if an absorber is to produce a 1°C change on future climate (See Table 3.1.2.1). Both N_2O and CH_4 sit in regions where there is already strong absorption and they have to be analyzed (as we did CO_2) allowing for the present near-saturation.

All of the substances in the Table except the hydrocarbons have been examined with a more elaborate radiative model and found to be marginally important, if their abundances increase.[13] For N_2O, CH_4, and NH_3, factors of two are important.

More attention needs to be directed toward the global abundance and long term growth rate of hydrocarbons, which are among the primary urban pollutants, and whose emission is largely uncontrolled. The abundance in Table 3.1.2.1 applies to the total hydrocarbon population; the strength listed is the maximum allowable and probably is much smaller. Aldehydes (a hydrocarbon family) are partly destroyed near their urban source, where they participate in the production of oxidants. Away from high concentrations of NO_x, the aldehydes disappear by photodissociation and attachment to aerosols.

Also, physical processes in the stratosphere can feed back on surface temperatures. The water abundance in the stratosphere is only several parts per million and is probably fixed by the vapor pressure at the tropical tropopause (although H_2O can be made in the stratosphere by reaction of CH_4 with OH). A change in the content of water due to a change in stratospheric temperature will affect the earth's greenhouse[14]. An alteration of the ozone abundance will change the absorption at 9.6 μm , which is the main absorber in the 8 - 12 μm window. Thus an increase in tropospheric CH_4 could affect stratospheric HO_x chemistry, the ozone abundance, and thence, the climate.

3.1.2.6 Zonal Energy Balance:

The assumption of radiative equilibrium provides a first-order estimate of the change (not necessarily the absolute value) in the mean global temperature due to the addition of minor substances to the air. Variations with latitude (e.g., of sunlight received, local opacity) may be

included in a simple fashion, following North[1,2], by fitting the ground temperature,

$$T_s(x) = T_o + T_2 P_2(x) \quad , \qquad (3.1.2.30)$$

at two points, $x = \sin$ (latitude), where P_2 is the second term in the Legendre series. The two most convenient points to use are $x = 1/\sqrt{3}$, where $T_s = T_o$, and $x = x_s$, which is the location of the ice lines defined by $T_s(x_s) = -10^{\circ}C$. The mean temperature $T_o = \langle T_s \rangle$ for radiative equilibrium of the planet as a whole, is given by Eq. (3.1.2.2).

In the next section we assume that the planet has a change in atmospheric composition (specifically, a doubling of CO_2 for Earth), and that the thermal loss of heat from the atmosphere is everywhere unchanged. This constancy is not so unrealistic as it may seem at first sight. Suppose, for example, that the Earth were uniformly heated from above. A change in composition but not in albedo would require that the Earth re-emit as before, even though the opacity were increased and hence the surface temperature everywhere increased. The effective emitting layer would simply rise to the height corresponding to the original temperature of the emitting layer.

Secondly, we suppose that the increased ground temperature allows an increased water-vapor content by maintaining a constant relative humidity. The local air temperatures are then taken to increase according to the increase in local opacity caused by the water vapor. This final

revised temperature-latitude curve is not constrained to the form of Eq. (3.1.2.30). We shall show that the ΔT feedback, from the additional water burden that the atmosphere can support, is comparable to the ΔT produced directly by an increase in CO_2. A similar result is obtained in Section 3.1.3.

3.1.2.7 The Change in CO_2 Content:

The thermal intensity emitted by the planet may be written

$$\frac{\sigma}{\pi} T_e^4(x) = I_0 + I_2 P_2(x) = \frac{\sigma}{\pi} \frac{T_s^4(x)}{1 + (3\tau_g/4)} = \frac{\sigma}{\pi} \frac{[T_o + T_2 P_2(x)]^4}{1 + (3\tau_g/4)} \qquad (3.1.2.31)$$

which gives the identities

$$I_o = \frac{\sigma}{\pi} \frac{T_o^4}{1 + (3\tau_g/4)} \qquad (3.1.2.32)$$

and

$$I_2 = \frac{4\sigma T_o^3 T_2}{\pi[1 + (3\tau_g/4)]} \qquad (3.1.2.33)$$

Since I_o and I_2 are constant and known from the present run of $T_s(s)$, a specified change in τ_g gives altered values of T_o and T_2. The optical thickness, τ_g, is found from the transparency, Q, which in turn comes from the absorptivities, A, of H_2O, O_3, and CO_2 in a manner explained in Section 3.1.2.3;

$$e^{-1.66\tau_g} = Q = 1 - \left[A(H_2O) + A(CO_2,\ 15\ \mu) + A(CO_2,\ 10\ \mu) + A(O_3)\right]^{1/2} \qquad (3.1.2.34)$$

The numerical values are given in Table 3.1.2.2.

TABLE 3.1.2.2

TEMPERATURE AND ICE LINE* FOR DOUBLED CO_2

CO_2 Ratio (ppm)	333	666
$A(H_2O)$	0424-0.511	0.425-0.517
$A(CO_2,\ 15\ \mu)$	0.214	0.227
$A(CO_2,\ 10\ \mu)$	0.025	0.050
$A(O_2)$	0.020	0.020
τ_g	0.744	0.828
$T_o(^oK)$	288.0	289.94
$T_2(^oC)$	-28.40	-26.76
$P_2(x_s)$	0.873	0.99925
x_s	0.957	0.99975
λ_s	73.1°	88.7°

*The ice line is defined as x_s where $T(x_s) = -10^oC$.

3.1.2.8 H_2O Opacity vs Ground Temperature:

At a specified latitude of x[= sin (latitude)] the overhead water-vapor content in number of molecules/cm^2 column is

$$N(H_2O) = \int_0^\infty N(H_2O;\ x,\ z)dz = \int_0^\infty \frac{p(H_2O;\ x,\ z)}{kT(x,z)}\,dz \quad . \tag{3.1.2.35}$$

We take the vapor pressure to be everywhere equal to half the local saturation pressure. The latter may be approximated in the temperature region of interest by

$$p(H_2O;\ T^*) = \frac{1}{2}\,P_{sat}(H_2O;\ T^*) = \frac{1}{2}\,P_{sat}(H_2O;\ 0)e^{\alpha T^*} \tag{3.1.2.36}$$

where T^* ($\equiv T - 273.2$) is temperature in ^oC. The excellent exponential dependence of p on T^* is illustrated in Fig. 3.1.2.3, which gives α = 0.078 a... $p_{sat}(0)$ = 4.92 mb.

The total vapor in a vertical column is thus

$$N(H_2O) = \frac{P_{sat}(H_2O;\ 0)}{2k}\int_0^\infty \frac{dze^{\alpha T^*(x,z)}}{T(x,z)}$$

$$= \frac{P_{sat}(H_2O;\ 0)}{2Tk} - \int_{-\infty}^{T_s(x)} \frac{e^{\alpha T^*}\,dT^*}{T^* + 273} \quad ,$$

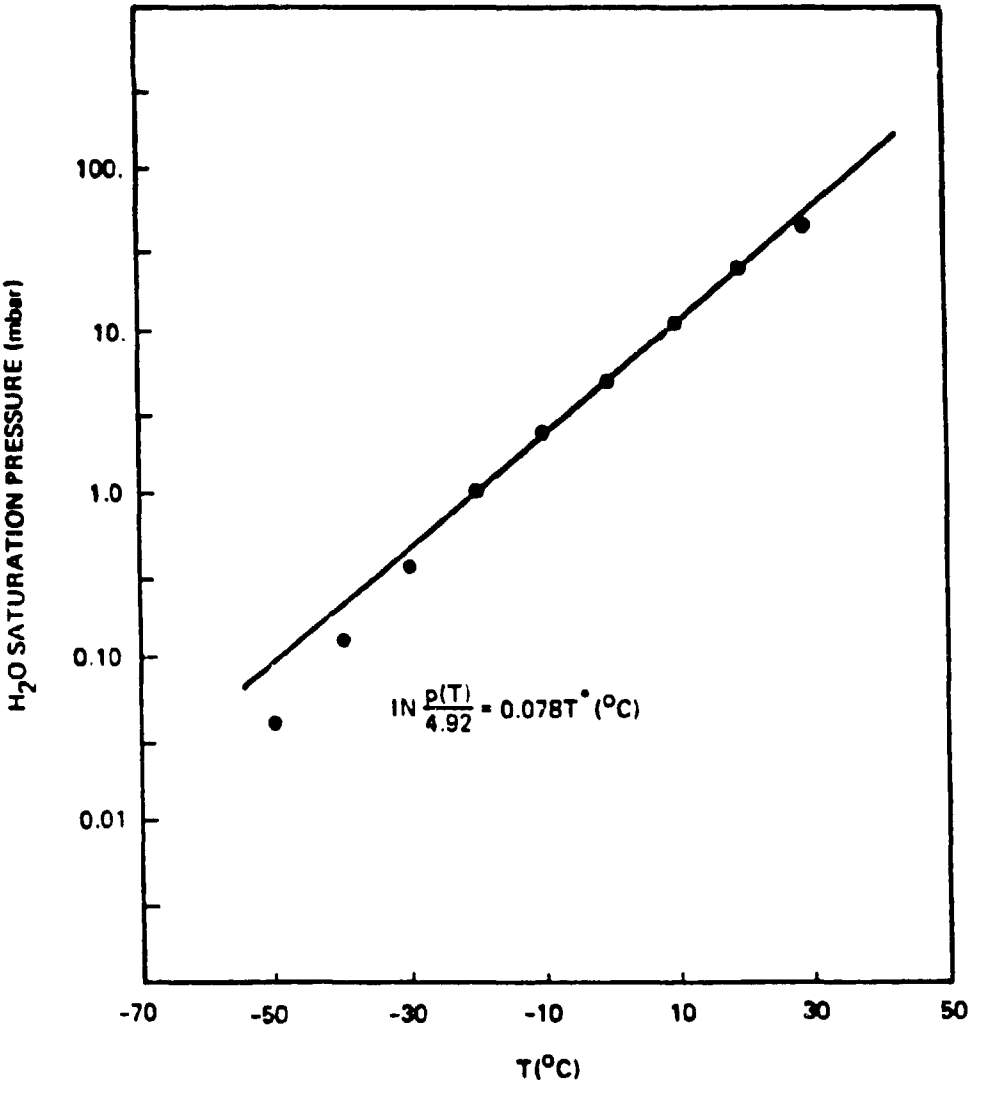

Figure 3.1.2.3 VAPOR SATURATION PRESSURE FOR H_20 VAPOR OVER ICE. THE DOTS REPRESENT MEASURED DATA; THE CURVE IS A STRAIGHT LINE GIVEN BY THE FORMULA.

where we take a linear temperature variation with height (appropriate for a convective atmosphere), $T(z) = T_s - \Gamma z$. (Note that here we equate the ground air temperature with the surface temperature, which is not quite the case in a pure radiative model). This integral may be evaluated with sufficient accuracy by taking T* in the denominator as a constant, 0°C. Then we have

$$N(H_2O) = \frac{p_{sat}(H_2O;\ T^* = 0)\ \exp\ [\approx T^*_s(x)]}{2\Gamma\alpha 273}$$

$$= 1.29 \times 10^{22} \exp[\alpha\Gamma^*_s(x)] \text{mol/cm}^2 \qquad (3.1.2.38)$$

for $\Gamma = 6.5°C/km$ and $\alpha = 0.078/°C$. Expressed in terms of cm of vapor at STP, the numerical coefficient is 479 atm-cm; in gm/cm^2 or cm of precipitable water it is

$$w(H_2O) = 0.39\ e^{0.078T^*_s} \text{gm/cm}^2 \quad . \qquad (3.1.2.39)$$

The absorption due to water vapor varies with w mainly in the 8.5 to 12.5 μm region. Thus

$$A(H_2O) = 0.71 - 0.29\ e^{-0.1w} \qquad (3.1.2.40)$$

and τ_g is found from Eq. (3.1.2.34).

3.1.2.9 Feedback from Change in H_2O Opacity Due to Change in CO_2 Content: Eqs. (3.1.2.39), (3.1.2.40) and (3.1.2.34) give the change in infrared absorption due to a change in the temperature at the surface,

T_s. For the moment, however, let us assume that this surface temperature is responsive only to the CO_2 content of the atmosphere. Figure 3.1.2.4 illustrates the change in surface temperature due to the added CO_2 opacity from Eqs. (3.1.2.34) and (3.1.2.2). If now the H_2O opacity is included in our estimation of T_s , the H_2O cntent is further increased by Eq. (3.1.2.39).

The temperature iteration converges fairly rapidly. The top curve in Fig. 3.1.2.4 gives the increase in temperature due to a doubuling of CO_2, including both the increased greenhouse due to CO_2 itself and the extra water vapor contained by the warmer atmosphere. The results of this analysis are similar to Cess's[15] appraisal of the role of water in zonal climatology. He concluded that cloud amount is not a significant feedback mechanism (clouds are neglected in this study), but water vapor changes induced by temperature changes will double the sensitivity of the global surface temperature to a change in the solar constant.

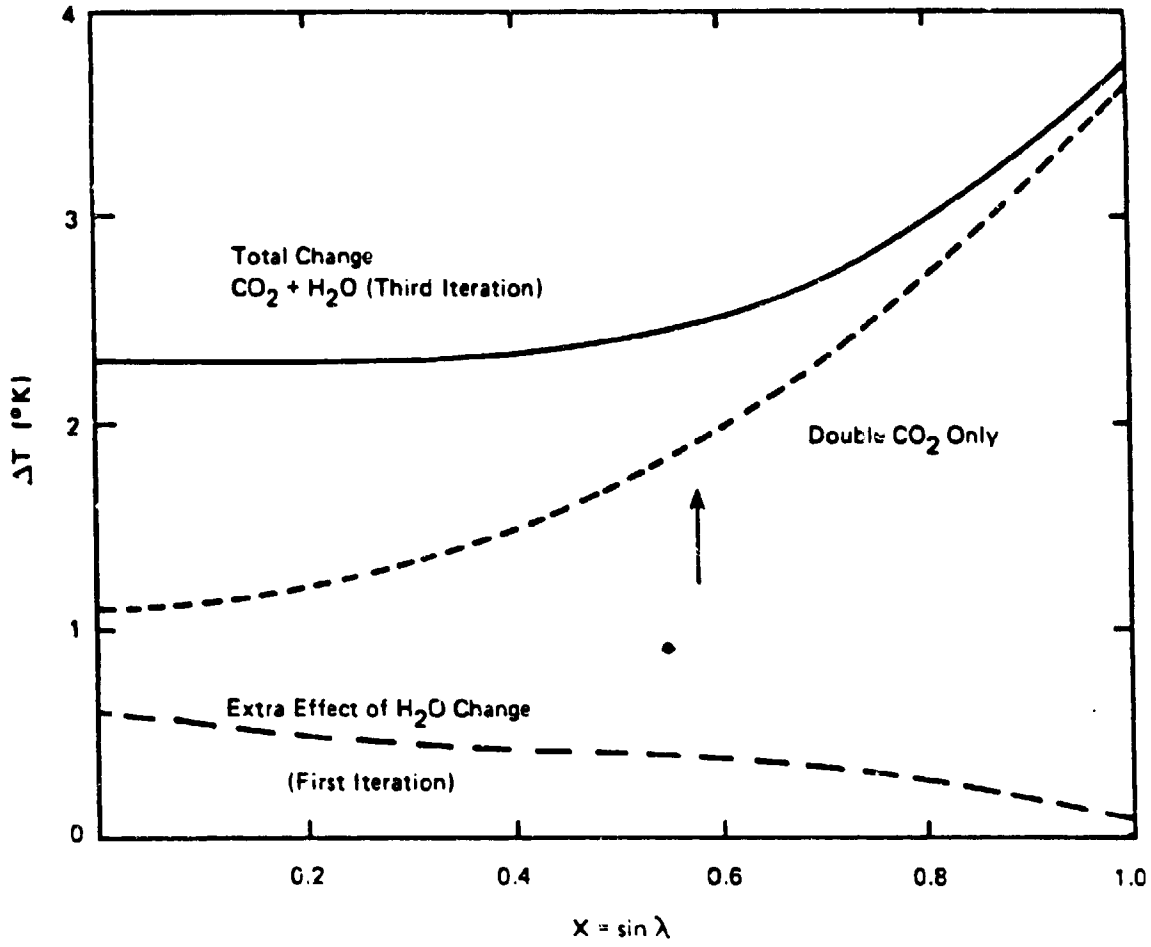

Figure 3.1.2.4 THE INCREASE OF TEMPERATURE AS A FUNCTION OF LATITUDE FOR A "NORTH MODEL" IN WHICH THE ABSORPTION BY H_2O IS DETERMINED BY THE TEMPERATURE. THE MIDDLE CURVE SHOWS THE TEMPERATURE INCREASE DUE TO A DOUBLING OF CO_2 ONLY; THE LOWER CURVE SHOWS THE WATER FEEDBACK IN THE FIRST ITERATION. THE HEAVY UPPERMOST CURVE SHOWS THE NET TEMPERATURE EFFECT FROM BOTH CO_2 AND THE ADDITIONAL WATER IN THE ATMOSPHERE, DUE TO THE GREENHOUSE HEATING BY CO_2 ITSELF AND THE ADDITIONAL H_2O AS WELL. THE ARROW DENOTES $x = \sqrt{1/3}$, WHICH GIVES APPROXIMATELY THE MEAN GLOBAL TEMPERATURE, SINCE $P_2(x) = 0$.

REFERENCES FOR SECTION 3.1.2

1. North, G.R., "Analytic solution to a simple climate model with diffusive heat transport," J. Atmos. Sci., 32, 1301-1307, 1975a.

2. North, G.R., "Theory of energy-balance climate models", J. Atmos. Sci., 32, 2023-2043, 1975b.

3. Budyko, M.I., "The effect of solar radiation variations on the climate of the earth", Tellus, 21, No. 5, 617-619, 1969.

4. Sellers, W.D., "A global climatic model based on the energy balance of the earth-atmosphere system", J. Appl. Meteor., 8, No. 3, 392-400, 1969.

5. Sagan, C. and C. Mullen, "Earth and Mars: evolution of atmospheres and surface temperatures", Science, 177, No. 4043, 52-56, 1972.

6. Henderson-Sellers, A. and A. J. Meadows, "A simplified model for deriving planetary surface temperatures as a function of atmospheric chemical composition", Planet. Space Sci., 27, No. 8, 1095-1099, 1979.

7. Chamberlain, J.W., "Theory of planetary atmospheres; an introduction to their physics and chemistry", Academic Press, New York, 1978.

8. Manabe, S. and R. F. Strickler, "Thermal Equilibrium of the Atmosphere with a Convective Adjustment", J. Atmos. Sci., 21, 361-385, 1964.

9. Kondrat'yev, K. Ya., Radiation in the atmosphere," Academic Press, New York, 1969.

10. Augustsson, T. and V. Ramanathan, "A Radiative-Convective Model Study of the CO_2 Climate Problem", J. Atmos. Sci., 34, 448-451, March, 1977.

11. Schneider, S.H., "On the Carbon Dioxide-Climate Confusion", J. Atmos. Sci., 32, Nov., 2060-2066, 1975.

12. Ramanathan, V., "Greenhouse Effect due to Chlorofluorocarbons: Climatic Implication", Science, 190, 50-51, Oct. 3,1975.

13. Wang, W.C., Y. L. Yung, A. A. Lacis, T. Mo, J. W. Hansen, (1976). "Greenhouse Effects due to Man-Made Perturbations of Trace Gases", Science, 194, 685-690, Nov. 12, 1976.

14. Chamberlain, J.W., "A Mechanism for Inducing Climate Variations through the Stratosphere: Screening of Cosmic Rays by Solar and Terrestrial Magnetic Fields", J. Atmos. Sci., 34, 737-743, May, 1977.

15. Cess, R.D., "Climate Change: An Appraisal of Atmospheric Feedback Mechanisms Employing Zonal Climatology", J. Atmos. Sci., 33, 1831-1842, 1976.

3.1.3 A simple Band Model for Infrared Emission from the Terrestrial Atmosphere

3.1.3.1 Introduction

A proper treatment of infrared emission from the Earth's atmosphere involves a multitude of complex factors, viz. Ramanathan and Coakley[1], Paltridge and Platt[2] or Kondratyev[3]. Our objective here is to attack the atmospheric radiation problem from a direction which is somewhat more complicated than the grey body approach given in Section 3.1.2 above, yet far less complex than the radiative-convective models reviewed by Ramanathan and Coakley. We hope to develop a model simple enough to be tractable yet incorporating enough observational and theoretical knowledge of the atmosphere to be responsive to changes in the atmosphere, such as varying CO_2 and H_2O vapor content.

This model provides an estimate of the infrared flux (F) radiated from a vertical column of the terrestrial atmosphere. The flux estimate F is formulated as a function of the local surface temperature (T_s) and a few other atmospheric parameters such as the CO_2 concentration, relative humidity, lapse rate, etc. By keeping the model relatively simple, we hope to provide new insight into the impact of increasing atmospheric CO_2 on the Earth's climate; for example, by showing the size and relative importance of various feedback mechanisms. The model has two major applications: the first is to provide an estimate of F for use in energy budget climate models such as discussed in Section 3.2.1. The second is to make rough estimates of climatic responses to changes in CO_2

content, etc. by assuming that the Earth is surrounded by a homogeneous atmosphere. In this second application, we note that the present model employs a somewhat different approach and therefore constitutes a somewhat independent estimate of the climatic effects of CO_2 which, as we shall see, lends credence to other modeling efforts such as the quasi-grey model described in Section 3.1.2.

Atmospheric radiation models necessarily include a number of "feedback mechanisms" which either reduce (positive feedback) or enhance (negative feedback) the ability of the Earth to radiate energy into free space. For example, suppose the Earth, with mean surface temperature T_s, normally radiates an energy flux F_o into space, balancing the energy input of the sun. Next, some change, such as an increase in the opacity of the atmosphere, lowers F_o by ΔF_s. For a constant atmospheric pacity, this causes a rise in surface temperature ΔT_s to bring the radiated flux back to F_o and equilibrium with the solar energy input. However, as T_s increases, the atmosphere may change so as to increase its opacity to infrared radiation. If the opacity increases with increasing T_s (thus reducing the Earth's ability to radiate energy away—positive feedback) then ΔT_s must be larger than in the constant opacity case and positive feedback is in effect.

Several positive feedback mechanisms are included in the present model. The most important of these is the increase in water vapor content, and hence opacity, of the atmosphere as surface temperature increases. The molecular absorption characteristics of both CO_2 and H_2O vapor are such

that absorption increases with temperature. This provides another positive feedback mechanism. The tropopause height increases with increasing surface temperature thus providing a small amount of positive feedback in some spectral bands. Among other possible sources of positive or negative feedback are change in the lapse rate, i.e., the strength of convective energy transport, and scale height with temperature and clouds. The limited scope of the present modeling effort did not allow the inclusion of these effects. The most significant omission is cloud effects. However, Cess[26] has argued that cloud amount is not a significant feedback mechanism since the increased opacity due to clouds is balanced by convective adjustment.

The model developed here differs from the grey model presented in Section 3.1.2, as well as the radiative-convective models discussed by Ramanathan and Coakley. Again, our objective here is to provide insight into the climatic effects of the Earth's radiation balance by adopting an alternative view of the problem and not to develop a model which is "more accurate" than other more complex models. In our model, rather than letting radiative transfer determine the temperature structure of the atmosphere, we will assume that the atmospheric structure is known and simply let this assumed structure radiate to space. Our assumed structure is based on the U.S. Standard Atmosphere, 1976. In this sense the model can be seen as a perturbation on this Standard Atmosphere.

Although we compare model results, i.e., values of the infrared (IR) flux radiated to space, with satellite observations and other

empirical data, the model has not been "tuned" to observational data except by the introduction of a normalizing constant for the total infrared flux and the use of empirical values of atmospheric parameters, e.g., lapse rate, scale heights, surface densities, etc. Where possible, these parameters are taken from the U.S. Standard Atmosphere (1976).

We note here that comparisons of terrestrial radiation models with infrared spectral observations from space, e.g., from Nimbus satellites as in Fig. 3.1.3.3, should provide very useful feedback to the climate research community. In spite of the rather obvious nature of this comment, very few comparisons between model predictions and observatons are to be found in the literature. Clearly, some future research effort could be usefully applied to such comparisons.

The average surface temperature increase upon a doubling of atmospheric CO_2 ΔT_s = 2.1°K obtained for the constant absolute humidity case is in substantial agreement with the 2.8°K figure derived from the grey atmosphere above. For constant relative humidity ΔT_s = 3.0°K for the 9-band model. This is interesting because these similar results were obtained by quite significantly different approaches. These results lend credibility to the estimate of about 3°K as the average surface temperature increase in response to a doubling of atmospheric CO_2 content.

The case of constant relative humidity has received considerable attention in the literature. Ramanathan and Coakley review radiative-convective model results for ΔT_s which are appropriate for comparison

with our constant relative humidity result of 3.0°K. They arrive at a representative figure of $\Delta T_s = 2.0°K$. Schneider[4] reviews the impact of increases in atmospheric CO_2 on climate considering a broad range of models. He arrives at $\Delta T_s = 1.5°$ to 3°K as the most probable range of increase in average temperature resulting from a doubling of atmospheric CO_2. Although the result of our 9-band model is some 50% higher than the value of Ramanathan and Coakley[1] and falls at the upper end of the range suggested by Schneider, the agreement between these various models is reassuringly close, especially so in view of the somewhat different and rather simple approach we have taken in our 9-band radiative model. The rough agreement between the results of different approaches supports the view that $\Delta T_s = 3°K$ is a reasonable first approximation to the climatic response of a doubling of atmospheric CO_2. Nevertheless, it is important to remember here that this and other estimates result from imperfect models of nature. Many important factors, such as clouds, have been completely omitted or treated in only an elementary fashion. Further, our models have not been comprehensively compared to observations of nature. Finally, the observed increases in atmospheric CO_2 is not the only factor affecting the Earth's climate. Hence, estimates of climatic change focusing solely on CO_2 and neglecting other, poorly understood factors such as those which cause glacial epochs, are likely to be somewhat incorrect although they are the best estimates one can make using our current understanding of nature.

Returning to results from our 9-band model we note that our estimate for ΔT_s is dependent on the initial value of T_s used. Above we have used $T_s = \langle T_s \rangle = 288°K$ as our base or unperturbed temperature. As

indicated in Fig. 3.1.3.4, ΔT_s would be smaller for base temperatures below 288°K and larger for base temperatures above 288°K. This phenomena arises from the increasingly strong positive feedback of water vapor and absorption band strength as T_s increases.

The model is briefly summarized in terms of three assumptions:

- The atmosphere is locally plane parallel with a temperature profile $T(z)$ given by a piecewise linear curve consistent with the U.S. Standard Atmosphere (1976). For surface temperatures T_s other than 288°K, the lapse rate is held constant and the tropopause temperature held constant at 217°K (See Fig. 3.1.3.1). Structure above the tropopause is also held constant.

- The atmosphere radiates IR emission only in the 8-100 μ (100-1250 cm^{-1}). This spectral range is divided into nine bands chosen so as to reflect salient features of the terrestrial IR spectrum and their changes over different parts of the Earth. The bands correspond to the atmospheric window and the absorption bands of H_2O, CO_2 and O_3 (See Table 3.1.3.1 and Fig. 3.1.3.2).

- The IR Emission of the Earth's surface arises from a black body at the surface temperature (T_s). Emission in the optically thick CO_2 and H_2O absorption bands arises from an atmospheric layer whose temperature is appropriate to an optical depth of 2/3 measured vertically downward from the top of the atmosphere.[7] The O_3 band and optically thin H_2O and CO_2 bands are handled as thin absorbing layers over the surface which radiates as a black body at T_s.

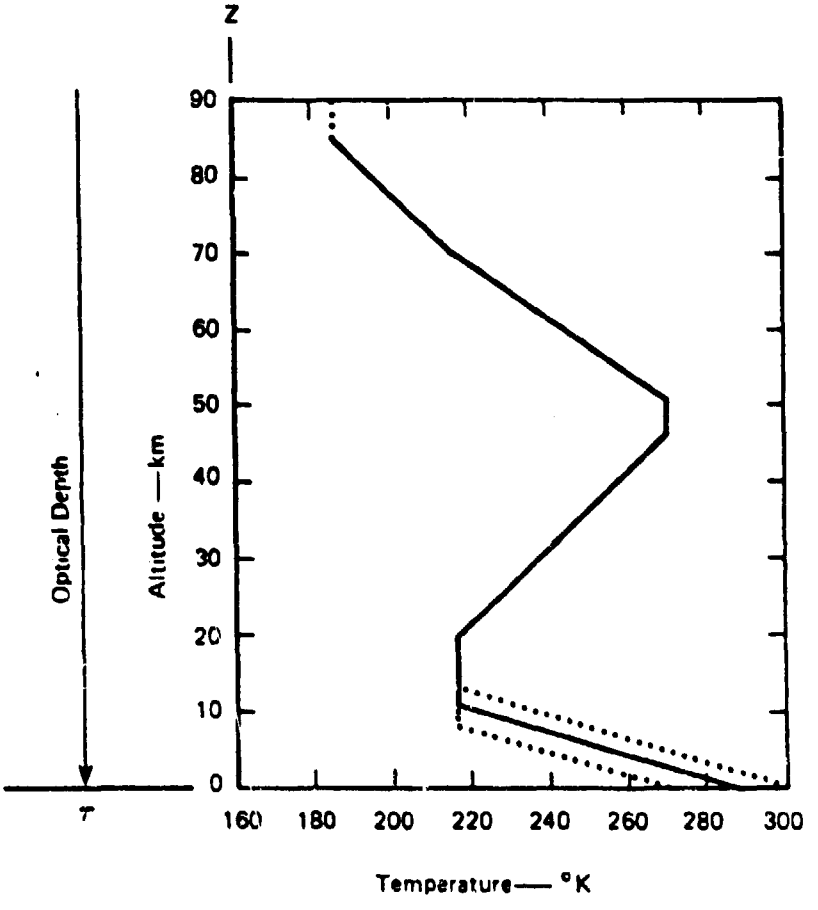

Figure 3.1.3.1 SCHEMATIC DIAGRAM OF TEMPERATURE PROFILE USED IN NINE-BAND IR EMISSION MODEL FOR THE TERRESTRIAL ATMOSPHERE

The ordinates are height (z) or optical depth (τ). Optical depth is measured downward from the top of the atmosphere. The plot of T(z) is taken from the U.S. Standard Atmosphere, 1976. The dotted lines indicate perturbations for surface temperatures above and below 288° K. The effective heights z_i (τ = 2/3 levels) for various bands are given in Table 3.1.3.1.

TABLE 3.1.3.1

BAND CHARACTERISTICS

Band i=	Major Absorber	Spectral Range (cm^{-1})	Band Center $\tilde{\nu}_i$(cm^{-1}), λ(μ)	Bandwidth $\Delta\tilde{\nu}$(cm^{-1})	Spectral Information*	Effective Height** z_i(km)	Effective Temperature** T_i(K)	Power Flux** P_i(Wm^{-2})
1	H_2O	100–400	250, 40.0	300	R_1 = 1002	10.8	218	41.6
2	H_2O	400–550	475, 21.1	150	R_2 = 59.8	3.9	263	48.1
3	H_2O/CO_2	550–600	575, 17.4	50	R_3 = 7.44/12.2	4.3	260	15.4
4	CO_2	600–750	675, 14.8	150	S_4 = 438	18.3	217	19.9
5	H_2O/CO_2	750–800	775, 12.9	50	R_5 = 1.53/8.90	0.4	286	17.9
6	None	800–925	862, 11.6	125	--	0	288	40.9
7	H_2O/CO_2	925–1000	962, 10.4	75	R_7/S_7 = 0.87/0.86	0***	288***	8.1
8	O_3/CO_2	1000–1100	1050, 9.5	100	R_8/S_8 = 1733/1.2	0***	288***	14.1
9	H_2O	1100–1250	1175, 8.5	150	R_9 = 6.2	0	288	25.7

* R_i and S_i were calculated by interpolation from the tables given by Houghton (1977, Appendix 10) with units converted to $cm^{-1}(kgm^{-2})^{-1}$.

** These quantities are obtained by applying the model to the case where T_s = 288K, $v_{CO_2} = 333 \times 10^{-6}$, relative humidity = 50% and a = 1 (see text below).

*** Band treated as transmission through an optically thin layer.

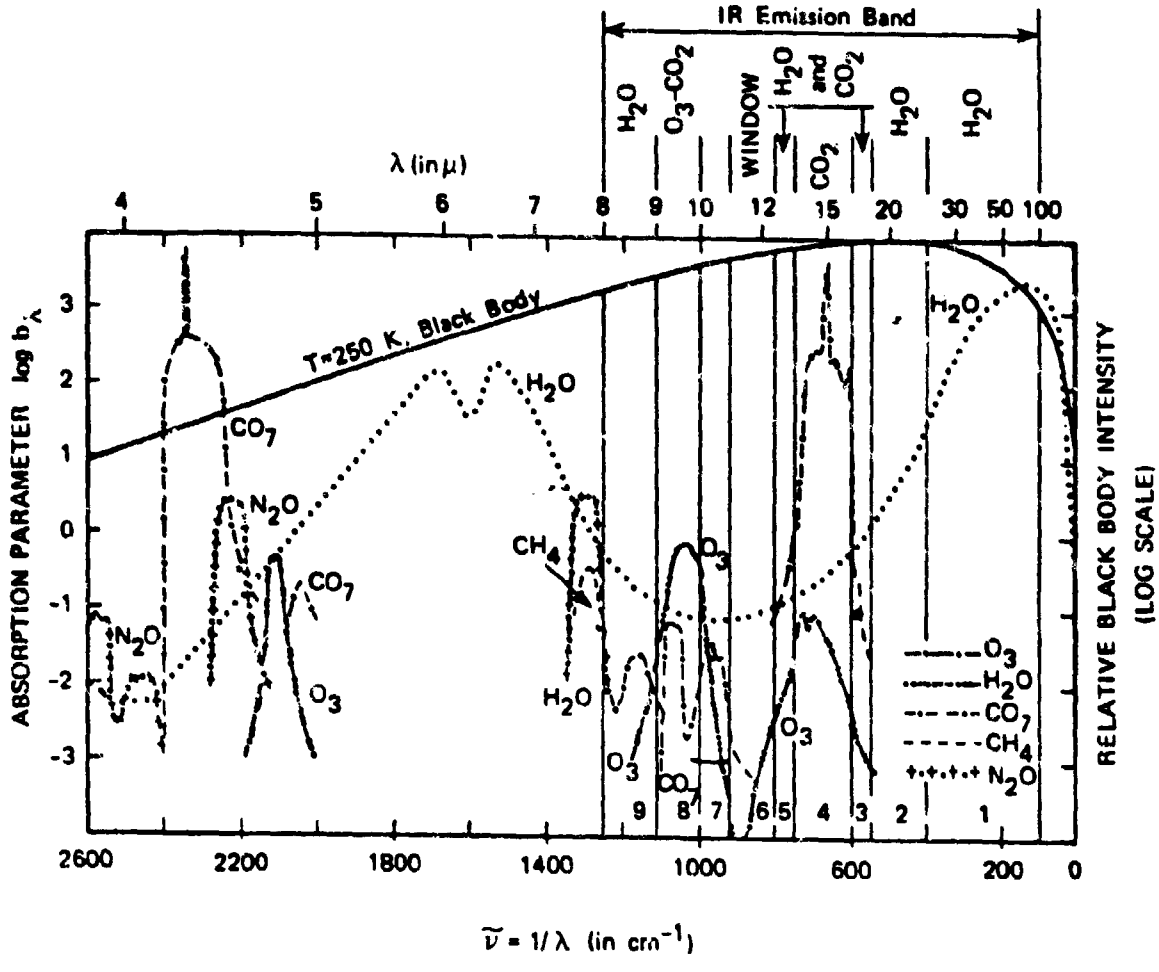

Figure 3.1.3.2 INFRARED BAND ABSORPTION OF ATMOSPHERIC GASES

The IR emission band ($\tilde{\nu}$ = 100-1250 cm^{-1}) in which the model is allowed to radiate is shown as being composed of 9 bands: atmospheric window (6), o_3 (8), CO_2 (3,4,5,7,8) and H_2O (1,2,3,5,9). A black body curve for 250 K is shown normalized to the upper boundary of the graph. The plot is modified from that given by Allen[7] where b_λ is an absorption parameter defined such that $1/b_\lambda$ is the thickness (in the chosen units) required for 50% transmission. The chosen units are the number of atmosphere-cm of each gas normally found in one air mass. In a limited sense b_λ is a kind of "optical thickness" for each gas.

3.1.3.2 Model Description

3.1.3.2.1 Division into Bands

We divide the terrestrial IR radiation spectrum into nine bands as shown in Figure 3.1.3.2. This appears to be about the minimum number one can use and still hope to include the major effects of the absorbing gases. In Table 3.1.3.1 we have summarized the characteristics of these bands. In band 1 we include the strong (50 μ) absorption band of water vapor. Bands 2 and 9 also contain water vapor absorption, but considerably less strong than band 1. The strong CO_2 (ν_2 bending mode) band at 15 μ is accounted for in bands 3, 4 and 5. Water vapor is also included in the wings (bands 3 and 5) of this CO_2 absorption band.

The 8-12 μ atmospheric window is divided into four bands. Band 6 is completely transparent and thus radiates at an effective temperature equal to the surface temperature T_s . One can consider radiation in this band to be from a grey body with emissivity ε . Since $\langle\varepsilon\rangle \sim 0.95$, we shall simply take it as unity in our calculations here. Band 7 presently contains only weak water vapor and CO_2 absorption. We have introduced this band in anticipation of a major rise in atmospheric CO_2 content. As noted in Section 3.1.2, the major effect of increases in CO_2 content, so far as the greenhouse effect is concerned, will probably lie in making currently transparent portions of the atmospheric window more opaque, rather than making the 15 μ CO_2 band even more opaque. Band 8 contains the 9.6 μ ozone and 9.4 μ CO_2 absorption bands. Band 9 contains relatively weak water vapor absorption.

3.1.3.2.2 **Total IR Radiation to Space**

The total IR radiation to space is given by a summation over 9 terms:

$$F = a \sum_{i=1}^{9} \pi B_{\nu}^{\sim}[\tilde{\nu}_i, T_i(T_s, \ldots)]\Delta\tilde{\nu}_i \qquad (3.1.3.1)$$

where the Planck function for $\tilde{\nu}$ in cm^{-1}, T in K is

$$B_{\nu}^{\sim}(\tilde{\nu},T) = c_1\tilde{\nu}^3/[\exp(c_2\tilde{\nu}/T) - 1] \ Wm^{-2}sr^{-1}(cm^{-1})^{-1}$$

$$c_1 = 1.911 \times 10^{-8}$$

$$c_2 = 1.439$$

and

$\tilde{\nu}_i$ = band center wavenumber in cm^{-1} (See Table 3.1.3.1)

$\Delta\tilde{\nu}_i$ = width of the i^{th} band in cm^{-1} (See Table 3.1.3.1)

The factor π arises when converting the radiance or specific intensity $B_{\nu}^{\sim}$ to a flux through a plane parallel atmosphere. The constant a, of order unity, is used as discussed below, to normalize the value of F to some desired value for a specified set of conditions. For example, it could account for IR radiation outside the 100-1250 cm^{-1} band. The effective temperatures T_i are determined for each band as discussed below. Each $T_i(T_s, \ldots)$ is a function of the surface temperature T_s as well as other atmospheric parameters, e.g., CO_2 content, relative humidity, etc.

3.1.3.2.3 Feedback Mechanisms

In the introduction above, several feedback mechanisms were mentioned in connection with the temperature dependencies of atmospheric water vapor concentration, molecular absorption coefficients and tropopause height. These mechanisms will be discussed as they occur in the discussion of effective temperature calculations below.

3.1.3.3 Effective Temperature Calculations

The effective temperatures for optically thick bands are determined by noting the altitude (or equivalent pressure level) at which the mean optical depth measured vertical downward from the top of the atmosphere in band i is 2/3. The temperature T_i at this level is then the effective temperature at which the i^{th} band radiates. The value 2/3 for the optical depth of the effective radiating level is derived by Chamberlain.[7]

Our object is then to find a $T(\tau)$ function where the effect temperature is simply $T_i(\tau_i = 2/3)$. The determination of the $T(\tau)$ function requires a sequence of operations. First τ is function of the total equivalent width (W_i) of the absorption within a given spectral band, which may contain more than one species of absorbing molecule. W_i is in turn a function of the absorption characteristics of the molecular species appropriate to a given band and the column density (kg m^{-2}) of each species encountered as radiation propagates from some atmospheric height z_i upward through the atmosphere and out into the interplanetary space. Thus, in a simplified view we could write

$$T_i \left\{ z_i \left[W_i \left(\tau_i = 2/3 \right) \right] \right\}$$

where the functional relationships at each step require models of the radiative properties of atmospheric constituents, the distribution of constituents with altitude and the distribution of temperature with altitude.

3.1.3.3.1 Equivalent Width to make $\tau = 2/3$

The W_i (τ_i) relation is relatively straight forward. One simply adds up the total equivalent widths of all the important absorption lines of all the important species within the spectral limits of the i^{th} band. However, for altitudes below about 30 Km the lines in the pertinent water vapor bands are not well separated and overlap considerably. In addition to this overlap for a single atmospheric constituent there is overlap involving water vapor bands and absorption bands of other constituents, such as CO_2 and O_3.

Goody[9] has developed a random model to account for this overlap in which the mean transmission $\bar{t}$ in a spectral range $\Delta\bar{\nu}$ is given by

$$\bar{t} = \exp(- W_i/\Delta\bar{\nu}) \qquad (3.1.3.2)$$

where W_i is the total equivalent width of the lines in the range $\Delta\bar{\nu}$. A mean vertical optical depth of 2/3 implies a mean transmission

$\bar{t} = 1 - \exp(-2/3) = 0.487$ above the effective radiating level, z_i. Thus, z_i is defined by making W_i such that

$$W_i/\Delta\tilde{\nu} = -\ln(\bar{t} = 0.487) = 0.72 \qquad (3.1.3.3)$$

3.1.3.3.2 Transparent Atmospheric Window (800-925 cm^{-1}, Band 6)

In this completely transparent portion of the atmospheric window the equivalent width of the atmosphere is zero. However, the Earth's surface is essentially opaque to infrared radiation and the optical depth rises extremely sharply right at the surface. Thus, the effective radiating level is at the surface ($z_i = 0$) and the effective temperature is simply the surface temperature $T_i = T_s$.

3.1.3.3.3 Equivalent Widths for Strong and Weak Lines

Now that the W_i ($t_i = 2/3$) portion of the aforementioned $T(\tau)$ relation has been established, we now need to find the effective height $z_i[W_i]$, i.e., the altitude at which W_i integrated along the path upward from z_i into space attains the value required by Eq. (3.1.3.3). W_i is calculated differently depending on whether or not the lines in the interval $\Delta\nu_i$ are weak (unsaturated) or strong (saturated such that additional absorption can only occur in the wings of a line).[10]

Following Houghton,[10] the equivalent width for weak lines over the i^{th} band is given by

$$W_i = \sum_j W_j = \sum_j \int_{path} s_j c\rho dz = S_i \int_{path} c\rho dz \qquad (3.1.3.4)$$

where W_j is the equivalent width over the i^{th} subinterval inside the interval $\Delta\nu$, c the mass mixing ratio of the absorber and ρ the atmospheric mass density. Here we have assumed s_j constant along the path. The quantity s_j is the line strength for lines in the i^{th} subinterval. $S_i = \sum_j s_j$ in units of $cm^{-1}(kg\ m^{-2})^{-1}$.

For strong lines, the equivalent width is

$$W_i = \sum_j W_j = 2\sum_j \left[\int_{path} (s_j\gamma_j) c\rho dz\right]^{1/2} = 2\sum_j (s_j\gamma_j)^{1/2} \left[\int_{path} c\rho dz\right]^{1/2}$$

where we assume $(s_j\gamma_j)$ is constant along the path.

Taking account of pressure broadening by letting the half width $\gamma_j = p\gamma_{oj}/p_o$ we have

$$W_i = 2\sum_j \left[\int_{path} (S_i\gamma_{oj})(c\rho p/p_o) dz\right]^{1/2} = 2R_i \left[\int_{path} (c\rho p/p_o) dz\right]^{1/2} \qquad (3.1.3.5)$$

where p is the local pressure, p_o the standard pressure (1.013×10^5 Pa), $R_i = \sum_j (s_j\gamma_{oj})^{1/2}$ in units of $cm^{-1}(kg\ m^{-2})^{-1}$, and γ_{oj} is the half width over the i^{th} subinterval at STP. The quantities S and R are conveniently tabulated (cgs, not mks units!) by Houghton[10] for water vapor, carbon dioxide and ozone.

S and R are temperature dependent and especially for weak lines this dependence can be important. To include the temperature variation we have used linear interpolation between the S and R values given for 220, 260 and 300 K by Houghton. This linear interpolation when combined with a simple iterative computational scheme yields values of R and S which are consistent with the effective temperature and summed over bands of interest, are shown in Table 3.1.3.1 for a particular case.

3.1.3.3.4 Water Vapor Bands (1,2,3,5,7,9)

A glance at Fig. 3.1.3.2 shows water vapor to be an important constituent over almost the entire infrared band of the Earth. Hence, we have included water vapor absorption in six of the nine emission bands considered here--the exceptions being the case of the CO_2 15 μ band (5), the transparent atmosphere window (6) and the 9.5 μ O_3 absorption band (8). Referring to Fig. 3.1.3.2 and Table 3.1.3.1, we note that water vapor is the dominant absorber in bands 1, 2 and 9 and is combined with CO_2 in bands 3, 5 and 7.

We now calculate W_i $(z_i, \ldots)$, the equivalent width of water vapor absorption, as a function of the following variables: radiating level z_i, molecular absorption coefficients S_i or R_i for the i^{th} band, surface mass density of water vapor ρ_{wo} (which is in turn dependent on surface temperature and relative humidity) and the scale-heights for water vapor and the atmosphere as a whole. To find W_i we are required to evaluate the integral quantities in Eq. (3.1.3.4) and (3.1.3.5) for both weak and strong lines. In the case of water vapor, we let

$c\rho = \rho_w = \rho_{wo} \exp(-z/H_w)$ with a scale height H_w of 2 km. The surface mass density of water vapor ρ_{wo} is discussed below. For <u>weak lines</u> from Eq. (3.1.3.4) we have

$$W_i = S_i \rho_{wo} \int_{path} e^{-z/H_w} dz = S_i \rho_{wo} \int_{z_i}^{\infty} e^{-z/H_w} dz = S_i \rho_{wo} H_w e^{-z_i/H_w}$$

(3.1.3.6)

where the path is from the effective radiating level z_i vertically upward to infinity.

For strong lines from Eq. (3.1.3.5), letting $c\rho = \rho_w$, as above, and $(p/P_o) = \exp(-z/H)$ where H is the scale height for the atmosphere as a whole, we have

$$W_i = 2R_i \left[\int_{path} \rho_{wo} e^{-z/H_w} e^{-z/H} dz \right]^{1/2} = 2R_i \rho_{wo}^{1/2} \left(\frac{H_w H}{H_w + H} \right)^{1/2} \exp\left[\frac{-z_i (H_w + H)}{2 H_w H} \right]$$

(3.1.3.7)

Using $H_w = 2 \times 10^3$ and $H = 8.5 \times 10^3$m we have $H_w H/(H_w + H) = 1619$ and Eq. (3.1.3.7) becomes

$$W_i = 80.5 \, R_i \rho_{wo}^{1/2} \exp(-z_i/3238) \qquad (3.1.3.8)$$

We must now estimate the surface mass density of water vapor ρ_{wo}. A number of workers have used a constant relative humidity formulation.[11] Following this suggestion we shall calculate ρ_{wo} so as to maintain a constant relative humidity r ($r = 0.5$ for 50% relative humidity). One can fit the saturation vapor pressure of water vapor over pure liquid water (mb) in the range $-10^{o}C < T_s < 40^{o}C$ and over pure ice in the range $-30^{o}C < T_s < -10^{o}C$ rather well by a law of the form $P_{sv}(T_s) = 7.26 \times 10^{-9} \exp(.0745\ T_s)$. The correlation coefficient of the fit on 15 points is 0.994 (See also Fig. 3.1.2.3). The surface mass density then becomes

$$\rho_{wo}(T_s) = r(5.49 \times 10^{-12})\exp(.0745\ T_s) \text{kg m}^{-3} \qquad (3.1.3.9)$$

For 50% relative humidity and $T_s = 288^{o}K$, Eq. (3.1.3.9) gives 5.70×10^{-3} kg m^{-3} which is comparable to the mid-latitude mean water vapor mass density given by the U.S. Standard Atmosphere, 1976.

Using Eqs. (3.1.3.8) and (3.1.3.9), the effective heights z_i and temperatures T_i can be calculated for the water vapor bands 1, 2 and 9. Letting $r = 0.5$ and $T_s = 288^{o}K$ we find, using the data of Table 3.1.3.1, the heights also given in Table 3.1.3.1. In all cases we have assumed strong lines. The heights imply temperatures via an atmospheric temperature-height profile. For $T_s = 288^{o}K$ we go directly to the U.S. Standard Atmosphere. The temperatures T_i corresponding to the heights z_i are shown in Table 3.1.3.1. We will discuss below the temperature profile to be used when $T_s \neq 288^{o}K$.

We note here that positive feedback mechanisms have been introduced by making R_i and S_i functions of the effective temperature and ρ_w a function of surface temperature T_s. To illustrate the positive feedback effects, consider Eq. (3.1.3.8). To find the effective radiating level we simply solve for z_i

$$z_i = 3238 \ln\left(80.5 R_i \rho_{wo}^{1/2} / W_i\right)$$

We know W_i from Eq. (3.1.3.3), ρ_{wo} from Eq. (3.1.3.9) and R_i from the aforementioned table 10 and interpolation. Suppose we find z_i to be 3.9 km (as with band 2 in Table 3.1.3.1) when the Earth is in radiative equilibrium with the solar energy input. Now suppose additional opacity is added in bands 3, 4, 5 and 7 by an increase in atmospheric CO_2. Because the Earth now radiates less power than it takes in, the Earth's temperature increases to reestablish equilibrium. If R_i and ρ_{wo} did not vary with temperature, z_i would remain constant and the required increase in effective temperature T_i at level z_i would be achieved by an increase in T_s (namely, ΔT_s) as shown by the upper dotted line in Fig. 3.1.3.1. However, if R_i and ρ_{wo} are increasing functions of temperature (as they indeed are), then the above equation requires an increase in z_i as T_s increases. So long as z_i remains in the troposphere, z_i must increase as T_s increases. Such an increase in z_i decreases the effective temperature T_i and a further increase in T_s (above ΔT_s) is required to bring about equilibrium. Since z_i is only logarithmically dependent on R_i and ρ_{wo}, this additional increase in T_s is limited, but of considerable significance as we shall see below.

3.1.3.3.5 Carbon Dioxide With and Without Water Vapor Absorption (Bands 3, 4, 5 and 7)

The expression for required equivalent width, Eq. (3.1.3.3) holds equally well for CO_2 as do the expressions for equivalent width, Eqs. (3.1.3.4) and (3.1.3.5), provided z_i is relatively close to the surface, i.e., within about a scale height or two. Since CO_2 is well mixed in the atmosphere up to stratospheric heights, it has the same scale height as the atmosphere as a whole. Thus, for weak lines we have from Eq. (3.1.3.4):

$$W_i = S_i m_{CO_2} \rho_o \int_{z_i}^{\infty} e^{-z/H} dz = 1.86\ \nu_{CO_2} S_i H e^{-z/H} \qquad (3.1.3.10)$$

where $m_{CO_2}(\nu_{CO_2})$ is the mass (volume) mixing ratio of CO_2, ρ_o is the surface mass density of the atmosphere = 1.225 kg m^{-3} and H is the scale height of the atmosphere. For strong lines, Eq. (3.1.3.9) becomes

$$W_i = 2R_i \left[\int_{path} m_{CO_2} \rho_o e^{-2z/H} \right]^{1/2} = 2R_i \left(1.86\ \nu_{CO_2} H/2\right)^{1/2} e^{-z_i/H}$$

$$= 1.93\ R_i \left(\nu_{CO_2} H\right)^{1/2} e^{-z_i/H} \qquad (3.1.3.11)$$

In band 4 where the CO_2 absorption is very strong, Eq. (3.1.3.11) with H = 8,500 m yields an effective radiating level which is on the order of 18

km. At 18 km the scale height is appreciably different from its surface value. Hence, it is appropriate to let $H \to H_0$ where H_0 is a value more appropriate to the expected effective radiating level z_1. Here we choose $H_0 = 7,300$ m which is appropriate to the density change between the surface and about 18 km. In band 4 using $H' = 7,300$ m , $T_s = 288^{\circ}K$, $\nu_{CO_2} = 333$ ppm and R_3 from Table 3.1.3.2, we find that $z_3 = 18.2$ km. Using the 1976 U.S. Standard Atmosphere, this leads to an effective temperature $T = 217^{\circ}K$.

Bands 3 and 5 contain the wings of the strong 15 μ CO_2 absorption band. These two bands have been included as separate bands because it is here rather than in band 4 (which is already very strongly absorbed) that changes in CO_2 concentration will be important so far as radiation balance is concerned.

Water vapor is also important in bands 3, 5 and 7; so in determining W_i for these bands we include contributions from both water vapor and CO_2. Thus for bands 3 and 5 W_i in Eq. (3.1.3.3) simply becomes the sum of the equivalent widths of the two constituents. Water vapor in band 7 is discussed below.

In bands 7 and 8, CO_2 absorption is presently very weak and could well be neglected. However, as discussed in Section 3.1.2 of this report, future increases in atmospheric CO_2 content should make a greater impact in bands 7 and 8 than in band 4. This is because band 7 (at 10.4 μ) is presently a nearly transparent part of the atmospheric window.

TABLE 3.1.3.2

EFFECTIVE HEIGHTS AND TEMPERATURES FOR
THE SURFACE CONDITIONS OF FIG. 3.1.3.3

Band	Major	(a) T_s = 320 K r = 0.5		(b) T_s = 283 K r = 0.5		(c) T_s = 188 K r = 0.5	
i =	Absorber	z_i (km)	T_i (K)	z_i (km)	T_i (K)	z_i (km)	T_i (K)
1	H_2O	14.9	223	10.3	217	0.0	188
2	H_2O	8.1	268	3.4	261	0.0	188
3	CO_2	4.1	293	2.0	270	0.0	188
4	CO_2	18.2	217	18.2	217	19.7	217
5	CO_2	3.9	294	2.1	269	0.0	188
6	None	0.0	320	0.0	283	0.0	188
7	CO_2	0.0*	320*	0.0*	283*	0.0*	188*
8	O_3/CO_2	0.0*	320*	0.0*	283*	0.0*	188*
9	H_2O	1.2	312	0.0	283	0.0	188

* Treated as optically thin

Similarly in band 8, CO_2 absorption near 9.4 μ will add to the ozone absorption present there. In bands 7 and 8 the CO_2 absorption is presently weak hence will grow linearly with increases in atmospheric CO_2 content; whereas in band 4 the CO_2 absorption is strong and will grow only as the square root of the CO_2 concentration. In addition, band 4 is nearly completely opaque already.

In band 7 both water vapor and CO_2 are important (though relatively weak) absorbers (See Fig. 3.1.3.2). For the range of conditions investigated here the water vapor lines are strong while the CO_2 lines are weak. Thus, we use Eq. (3.1.3.8) to find the equivalent width of the strong water vapor lines and Eq. (3.1.3.10) to find the equivalent width of the weak CO_2 lines. Summing these two equivalent widths, we have W_7. Since absorption is rather small in band 7 we treat this band as emission from the surface at temperature T_s with the mean transmission through the atmosphere ($\bar{t}$) given by Eq. (3.1.3.2). Put another way, we calculate the radiative flux to space from band 7 as radiation from a black body at temperature T_s diminished by the factor $\bar{t}$. In Eq. (3.1.3.1), the term for i=7 becomes $\bar{t}_7 \pi B_{\tilde{\nu}} \tilde{\nu}_7$, $T_s \Delta\tilde{\nu}_7$. For the nominal conditions of Table 3.1.3.2, the mean transmission of band 7 is 0.88 and decreases to 0.81 after atmospheric CO_2 has been doubled and radiative equilibrium reestablished.

3.1.3.3.6 Carbon Dioxide with Ozone Absorption Band

The ozone layer near 25 km altitude is a strong absorber at 9.6 μ . Since absorption is relatively weak in band 8 and since ozone is

distributed in a stratospheric layer and the stratosphere is held constant in our model, we treat band 8 as radiation from the surface at temperature T_s with a mean transmission given by

$$\bar{t} = \exp\left(-W_{CO_2} + W_{O_3}\right)/\Delta\bar{\nu}_6 \qquad (3.1.3.12)$$

where W_{CO_2} and W_{O_3} are the equivalent widths of the 9.4 μ CO_2 and 9.6 μ O_3 absorption bands respectively.

Assuming the ozone layer of thickness ℓ to be homogeneous with column density $\langle c\rho\rangle$ $\ell = 3.68 \times 10^{-3}$ kg m^{-2}, $R_{O_3} = 1731.8$ cm^{-3} (kg m^{-2})$^{-1}$, and mean pressure $\langle p\rangle = 25.5$ mb, we have from Eq. (3.1.3.5) for strong lines,

$$W_{O_3} = 2R_{O_3}\left(\langle c\rho\rangle\ell\right)^{1/2}\left(\langle p\rangle/p_o\right)^{1/2} = 33 \text{ cm}^{-1} \quad . \qquad (3.1.3.13)$$

The equivalent width of the weak 9.4 μ CO_2 absorption band is calculated using Eq. (3.1.3.10) and as with band 7, the term for i=8 in Eq. (3.1.3.1) becomes $\bar{t}_8 \pi B_\nu\left[\bar{\nu}_8, T_s\right]\Delta\bar{\nu}_8$. For the nominal conditions of Table 3.1.3.2, $\bar{t}_8 = 0.62$ which reduces to 0.55 after atmospheric CO_2 has been doubled and radiative equilibrium reestablished.

3.1.3.4 Temperature Profile

The temperature profile T(z) is basically that of the U.S. Standard Atmosphere, 1976.[6] For a surface temperature T_s of 288°K the temperature profile is thus the solid line in Fig. 3.1.3.1. For values of T_s

other than 288°K the lapse rate is maintained constant at 6.5 K/km as is the tropopause temperature (217°K). The structure above the tropopause is assumed to remain that of Fig. 3.1.3.1 regardless of surface temperature. Profiles for $T_s \neq 288^{\circ}K$ are illustrated by the dotted lines of Fig. 3.1.3.1.

This scheme of altering the temperature versus height profile in response to changes in surface temperature (T_s) results in an increase in t :popause height at T_s increases. This variation in tropopause height is a well known feature of the terrestrial atmosphere.[12] While this model is clearly not a sophisticated one, it does retain the basic features and the virtue of simplicity.

The alteration of the tropopause height introduces a small negative feedback in that radiation from the region just above the tropopause increases with an increase in surface temperature. If there were no change in tropopause height, the radiation frm the aforementioned region would be constant with increases in T_s. Band 1 of the present model radiates from close to the tropopause (See Table 3.1.3.1) and this feedback mechanism comes into play for certain parameter choices.

3.1.3.5 Comparison with Observations

We now compare the IR fluxes predicted by our model with satellite measurements of the IR radiation emerging from several differ- t geographical areas. One set of such measurements (made by Hanel, et al[13]) from Nimbus 4, is shown in Fig. 3.1.3.3. The thermal emission of the surface

plus atmosphere emitted vertically upward was measured over a 95 km diameter circular area with a spectral resolution of 1.4 cm^{-1}. In each of the three graphs of Fig. 3.1.3.3 the radiances of black bodies at various temperatures are shown for comparison. Also shown are the spectral bands of our model and the radiances predicted for ech band. Model results are shown for relative humidities of 10, 50, and 90% ($r = 0.1$, 0.5 and 0.9). Here we have used $\nu_{CO_2} = 326$ ppm appropriate to 1970 when the observations were made.

For the Sahara desert case of Fig. 3.1.3.1, we let $T_s = 320^oK$ corresponding to the black body temperature in the atmospheric window (band 6). The effective heights z_i and temperatures T_i, determined as above, are shown in Table 3.1.3.2. The 9 band model gives a reasonably good fit to the observational data. The agreement between model and observation is reassuring in that $T_s = 320^oK$ is an extreme case--some 20^oK higher than the highest zonal average shown in Fig. 3.1.3.4.

For the Mediterranean Sea case of Fig. 3.1.3.3 we again estimate the surface temperature from the atmospheric window (band 6) yielding $T_s = 283^oK$. The agreement between model and observation is considerably improved at this more moderate temperature especially in bands 3 and 7. The improvement in model accuracy as the surface temperature approaches the average surface temperature is not surprising since several factors, such as scale heights, have been set constant at values appropriate to $T_s = 288^oK$, the average surface temperature.

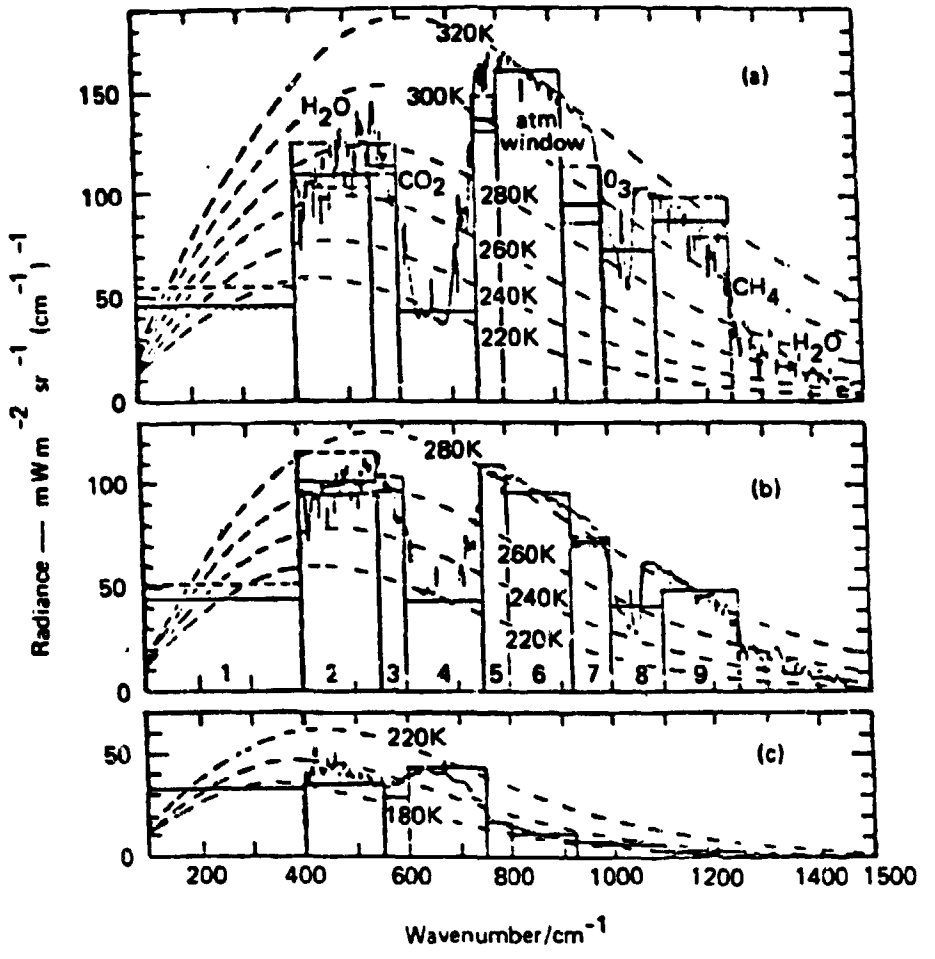

Figure 3.1.3.3 THERMAL EMISSION FROM THE EARTH'S SURFACE AND ATMOSPHERE EMITTED VERTICALLY UPWARDS AND MEASURED BY HANEL ET AL. (1971) USING THE INFRARED INTERFEROMETER SPECTROMETER ON NIMBUS 4(A) OVER SAHARA, (B) OVER MEDITERRANEAN AND (C) OVER ANTARCTIC

The radiances of black bodies at various temperatures are superimposed as dashed lines. Average radiances predicted by the nine band radiation model discussed in the text are given by bar graphs. In each case model radiances are given for three relative humidities. The solid lines correspond to a relative humidity of 50% (r=0.5). The dashed (– – –) and dotted (· · · ·) lines show changes for relative humidities of 10% and 90% respectively. The normalization factor a=1.

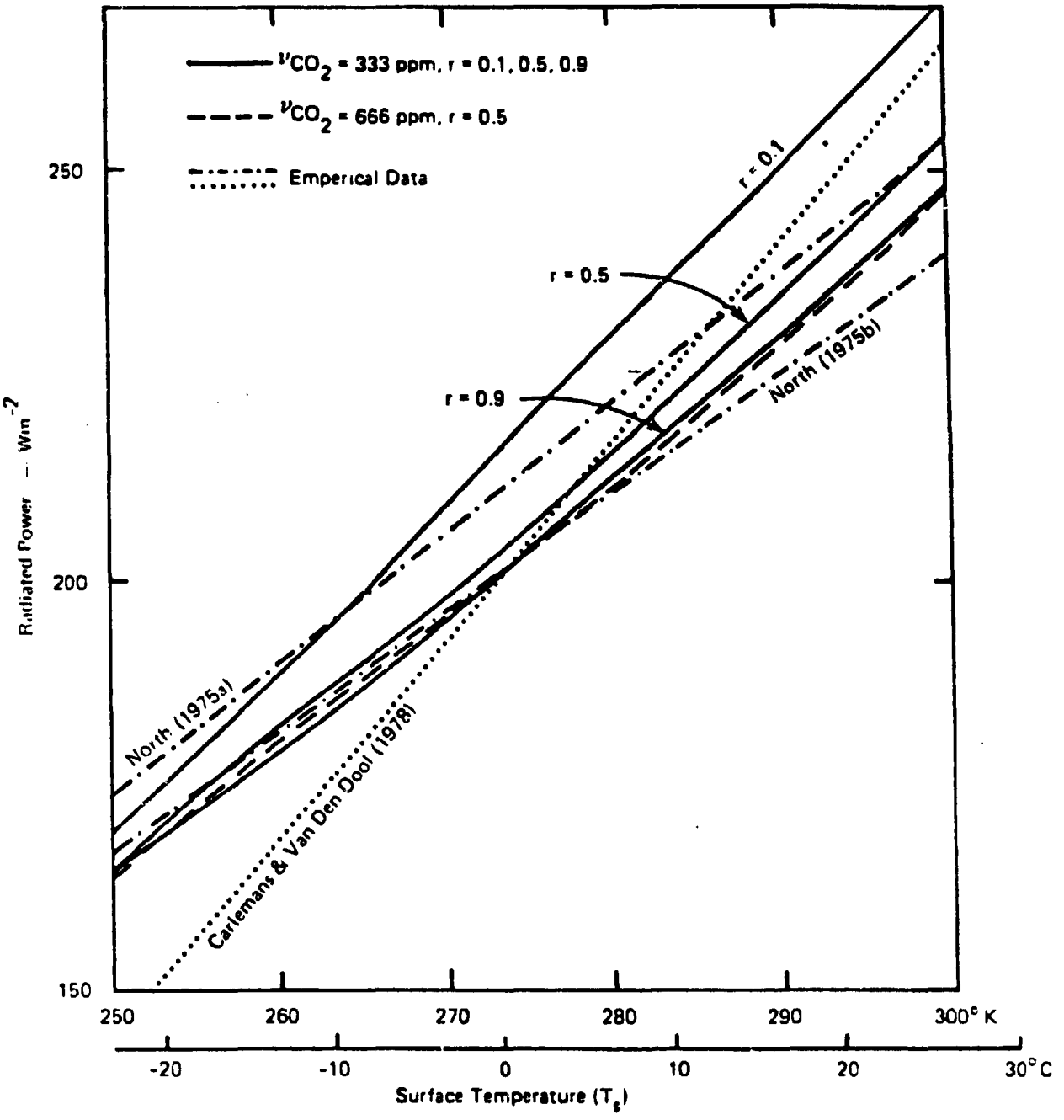

Figure 3.1.3.4 ATMOSPHERIC RADIATION FLUX TO SPACE $F(T_s)$

Curves are given for the 9 band model for ν_{CO_2} = 333 ppm and relative humidities of r = 0.1, 0.5 and 0.9 (solid lines). A model curve is also given for CO_2 doubling to ν_{CO_2} = 666 ppm and r = 0.5. For comparison we include 3 curves (— — — — and ..... lines) which represent straight line fits to observational data. The model curves are normalized to the average of the emperical curves as T_s = 288°K, i.e., a = -.95 in Eq. (3.1.3.1)

In Fig. 3.1.3.3, results are shown for the Antarctic. Here the black body temperature in the atmospheric window indicates $T_s \sim 188^oK$ (-85^oC), very cold indeed. Since our temperature profile model calls for a constant tropopause temperature of 217^oK, this indicates a temperature inversion and we assume a linear gradient of 5K/km from the surface to the 217^oK level. The saturation water vapor pressure is so low at this low temperature that even high values of relative humidity still do not cause significant water vapor absorption. Thus the effective radiating levels in bands 1, 2 and 9 are at the surface. The enhanced radiance in the 15 μ CO_2 band arises because the temperature at the effective height in our model is actually greater than the very low surface temperature, i.e., there is a strong temperature inversion. Again, the comparison shown in Fig. 3.1.3.3 (c) is reassuring in that the agreement between model and observation is reasonably good even in this very extreme case.

Although this comparison between satellite observations and model estimates of the Earth's infrared flux is clearly not definitive, it does illustrate a valuable method for inserting experimental knowledge into models for the Earth's outward radiation flux. To the author's knowledge, comparisons along the lines of Fig. 3.1.3.3 have not been made before. Nimbus satellites, of which Nimbus 7 is the most recent version, can supply pertinent information on the Earth's radiation to space. It seems prudent that model calculations, especially those used by General Circulation Models (GCM's), and satellite observations be compared to provide both the needed feedback for model improvement and confidence in results based on the models. The comparisons of Fig. 3.1.3.3 show that even the rather

simple model investigated here can give reasonably good estimates of the Earth's infrared radiation to space over a rather wide range of surface conditions.

3.1.3.6 Radiated Infrared Flux from the "Average Atmosphere" and its Implications for Climatic Effects of Increased Atmospheric CO_2

As a first approximation, consider the Earth to be covered with a homogeneous average atmosphere. This assumption allows us to extrapolate conclusions about an atmosphere with a single temperature profile, etc. to the Earth as a whole. Clearly, climate models investigated in Section 3.2 and elsewhere will yield more precise results, but this initial approximation is still worth making. For our average atmosphere we take the U.S. Standard Atmosphere, 1976, shown in Fig. 3.1.3.1. Using this profile and setting other parameters as discussed below, Eq. (3.1.3.2) yields the sum of the average radiated flux in each of the 9 spectral bands, i.e., the total estimated radiation flux to space. This total flux F is plotted as a function of surface temperature T_s in Fig. 3.1.3.4.

First, consider the total flux F for the average atmosphere with $T_s = 288^{\circ}K$, $\nu_{CO_2} = 333$ ppm and relative humidity = 50%. The IR flux in each band as well as the effective heights z_i and temperature T_i are shown in Table 3.1.3.2. The total IR flux $F = 242\ Wm^{-2}$ when $a = 1$. This value of F is slightly too high to balance the incoming solar flux $F_0(1-A)/4 = 235\ Wm^{-2}$ calculated when the albedo A has the conventional value of 0.33. However, more recent work indicates A is about 0.29, yielding an incoming flux of $249\ Wm^{-2}$. To make the outgoing flux from our

assumed average atmosphere balance the incoming flux of 249 Wm^2 we must let a = 1.03. Having a > 1 is to some extent justified in that some compensation should be made for IR flux which is not included within the 100-1250 cm^{-1} wave number band of the model, e.g., see the 1250-1500 cm^{-1} portion of Fig. 3.1.3.3. Another way to make the incoming and outgoing fluxes balance is to let a = 1, but raise T_s from 288°K to about 290°K.

Although a is close to unity, it is not clear just what value a should take. From Fig. 3.1.3.4 we note that the data of Oerlemans and Van den Dool[14] indicates F is about 238 Wm^{-2} at T_s = 288°K based on zonally averaged fluxes and temperatures. These data also indicate a difference of about 4 Wm^{-2} between the northern and southern hemispheres. If we take F as 238 Wm^{-2}, a= 0.98.

The key item of interest so far as climate effects are concerned is the alteration of F by changes in the atmospheric constituents such as water vapor and CO_2. Consider the average atmosphere discussed above where ν_{CO_2} = 333 ppm , T_s = 288°K relative humidity = 50%, a = 103 and hence, F = 249 Wm^{-2} balancing the incoming solar flux (insolation). If some factor in our average atmosphere, such as relative humidity or CO_2 content, should change so as to change F ; then, other factors remaining constant, the surface temperature T_s would have to increase or decrease to return F to its equilibrium value of 249 Wm^{-2}. In the real atmosphere other factors will <u>not</u> in general remain constant and further, other factors will changes T_s changes in response to the original perturbation. In the present model we neglect the response of the atmosphere to variations of

CO_2 content per se, but include various feedback mechanisms which respond to changes in T_s (See Section 3.1.3 above).

Using our assumption that the Earth is surrounded by a homogeneous "average" atmosphere, we can calculate this change in average surface temperature ΔT_s required to restore F to its equilibrium value. Below, we consider the surface temperature response ΔT_s of our homogeneous Earth to a doubling of CO_2 concentration from 333 to 666 ppm. ΔT_s is examined under three assumptions regarding water vapor, namely: constant absolute humidity, constant relative humidity and variable relative humidity.

3.1.3.6.1 Doubling of Atmospheric CO_2 with Constant Absolute Humidity

A glance at Fig. 3.1.3.2 should easily convince one that water vapor is the dominant absorber in the Earth's atmosphere and that the climatic effects of doubling atmospheric CO_2 are likely to be strongly dependent on variations in water vapor content induced by the CO_2 increase. As a sort of calibration case we consider this case where the absolute humidity is held constant. Thus, we set the surface mass density of water vapor constant at 5.70×10^{-3} kg m^{-3} (corresponding to $T_s = 288^{\circ}K$ and $r = 0.5$ in Eq. (3.1.3.9) and set the scale height of water vapor constant at 2 km. Under these circumstances a doubling of atmospheric CO_2 lowers F by 5.8 Wm^{-2} to roughly 243 Wm^{-2}. To restore F to equilibrium $\Delta T_s = 2.1^{\circ}K$. This case lets us see the effects of CO_2 doubling in isolation, i.e., without the water vapor feedback discussed in Section 3.1.3.2.3).

We note that the change in outgoing infrared flux induced by a doubling of CO_2 in our model is caused by changes in bands 3, 5, 7 and 8, i.e., the wings of the 15 μ band and the weak 9.4 and 10.4 μ absorption bands of CO_2. Doubling the CO_2 content causes the effective height in band 4, containing the core of the 15 μ CO_2 band, to increase; but since the effective height remains in the tropopause region the effective temperature remains at 217°K and the flux radiated in band 4 remains unchanged.

3.1.3.6.2 Doubling of Atmospheric CO_2 with Constant Relative Humidity

In this case the water vapor content of the atmosphere is allowed to vary with the temperature so as to keep the relative humidity constant. Precisely how this is done is discussed in Section 3.1.3.2.4 above. With $T_s = 288°K$ and relative humidity set at 50% ($r = 0.5$), a doubling of atmospheric CO_2 lowers F by 5.8 Wm^{-2} exactly as in the case of constant absolute humidity. However, $\Delta T_s = 3.°K$ here because the water vapor feedback mechanism is operating, i.e., because the water vapor content of the atmosphere, and hence, atmospheric opacity, have been allowed to increase as T_s increases. Thus water vapor feedback increases ΔT_s for CO_2 doubling by a factor of 1.4 . It is generally agreed that atmospheric models holding relative humidity constant are closer to the truth than those holding absolute humidity constant, e.g., see Manabe and Wetherald[11]. The figure $\Delta T_s = 3.0°K$ is rather insensitive to the exact choice of relative humidity—40% or 60% also yield 3.0°K.

3.1.3.6.3 Doubling of Atmospheric CO_2 with Variable Relative Humidity

Again, consider the aforementioned average atmosphere with $T_s = 188°K$, $r = 0.5$ and $a = 1.03$. In Section 3.1.3.6.2 above, we saw that

doubling atmospheric CO_2 reduced F by 5.8 Wm^{-2} and that a ΔT_s of 3°K was required to reestablish the radiation balance if relative humidity was held constant at 50%. A change in surface temperature could also imply a change in average relative humidity--probably an increase. If we increase the average relative humidity in our model from 50% to 60% in addition to doubling the CO_2 content, the new radiation balance is established at T_s = 291.9°K, an overall 3.9°K increase. If, on the other hand, the relative humidity decreases to 40% in addition to CO_2 doubling, the new radiation balance would occur at T_s = 289.8°K, an overall increase of only 1.8°K. Thus, changes in relative humidity which occur concurrently with changes in CO_2 content can serve to significantly enhance or diminish any CO_2 induced surface temperatures changes[1].

3.1.3.6.4 Comparison of These with Other Model Results

First we consider the constant absolute humidity case in Section 3.1.3.6.1, above. Our result of ΔT_s = 2.1°K is appropriate for comparison with the constant absolute humidity result of 2.8°K obtained from the grey atmosphere model considered in Section 3.1.3 above. Although the two results differ by ~ 25%, they are in reassuringly good agreement considering the relative simplicity of the models employed.

We now come to the case of constant relative humidity discussed in Section 3.1.3.6.2 above. This case has received more attention in the literature. Ramanathan and Coakley[1] reviewed radiative-convective models for infrared radiation from a homogeneous terrestrial

atmosphere including the increase in T_s predicted by such models for a doubling of atmospheric CO_2. They consider a number of results and arrive at $\Delta T_s = 2.0$ in the case of constant relative humidity. The most recent work they consider is that of Augustsson and Ramanathan[15] who arrive at a value of $\Delta T_s = 1.98^{\circ}K$.

Schneider[4] reviews the impact of CO_2 increases on climate considering a broad range of models. He arrives at ΔT_s equals 1.5 to $3^{\circ}K$ as the most probable range of average temperature increase resulting from a doubling of atmospheric CO_2

Although our result for ΔT_s is some 50% higher than Augustsson and Ramanathan's and falls at the upper end of the range suggested by Schneider, the agreement is reassuringly close in view of the somewhat different and rather simple approach we have taken in our 9 band model.

3.1.3.7 Infrared Flux F Radiated to Space as a Function of Surface Temperature T_s for Various Atmospheric Conditions

By summing the radiation flux to space in each of the nine bands according to Eq. (3.1.3.1) we arrive at a total flux F. In Fig. 3.1.3.4 we have plotted F as a function of surface temperature (T_s) for several sets of atmospheric parameters (namely, average relative humidity and carbon dioxide concentration). For comparison we show three empirical curves for $F(T_s)$, which are straight lines fitted to observations. We have normalized the model curves by letting the model curve $F(T_s)$ for

$r = 0.5$ and $\nu_{CO_2} = 333$ ppm pass through the average of the empirical curves $F = 232\ Wm^{-2}$ at $T_s = 288^{\circ}K$, the Earth's average surface temperature, i.e., $a = 0.95$ in Eq. (3.1.3.1).

Perhaps the most striking feature of the model curves themselves is the large effect caused by changes in average relative humidity (r), expecially for $r \gtrsim 0.5$ and $T_s \gtrsim 270^{\circ}K$. This serves to emphasize the importance of water vapor in the atmosphere and points out that changes in average relative humidity, which might occur along with changes in CO_2 content could significantly alter predictions of CO_2 climate effects based on an unchanging relative humidity. The atmospheric radiation model (solid and dashed curves in Fig. 3.1.3.4) includes the effects of water vapor and other feedback mechanisms discussed above.

If the Earth radiated like a black body, we would expect $F(T_s) \propto T_s^4$ and thus, F would double as T_s rises from 250 to $300^{\circ}K$. None of the model or empirical curves rise this fast. In addition, the model curves are much more nearly linear than the T^4 law--the empirical curves are linear fits to observations and hence, are forced to be linear. We thus conclude that linear fits to the $F(T_s)$ function, such as used by North[17,18] and elsewhere in this report, are reasonably close to reality provided the proper constants are used.

We note that for $T_s > 280^{\circ}K$, the three model curves for $F(T_s)$ converge. This occurs because the decreasing temperature decreases the

water vapor content of the atmosphere for a given relative humidity. As temperature decreases, the water vapor absorption becomes less significant in bands 1, 2, 3, 5, 7 and 9 and the model predicts very nearly the same flux regardless of r.

An interesting feature of the model ν curve for $r = 0.5$ and $\nu_{CO_2} = 666$ ppm is that the difference relative to the $r = 0.5$, $\nu_{CO_2} = 333$ ppm curve is most pronounced at higher temperatures. Thus, according to our model, a doubling of atmospheric CO_2 has a greater impact on outgoing radiation $F(T_s)$ at high surface temperature than at low ones. The principal origin of this feature lies in the temperature dependence of the CO_2 absorption strengths $R_i(T)$ and $S_i(T)$. For example, in bands 7 and 8 $S(T)$ more than doubles as T rises from 250 to 300°K. As T_s increases, so does the entire tropospheric temperature profile (See Fig. 3.1.3.1). Since S and R increase with T, and hence with T_s, increases in atmospheric CO_2 cause proportionally larger increases in CO_2 opacity at higher surface temperatures. This feature tends to mitigate CO_2 induced temperature changes at high latitudes.

Comparing the model curves with the observational curves in Fig. 3.1.3.4 we find that our model generally lies between the sets of observation data. In terms of the slope of the model curves, which is really the relevant comparison, the model curves for $r \geq 0.5$ agree best with the Oerlemans and Van der Dool[14] data at $T_s \geq 280$°K and with the North[7] data for lower temperatures. If we consider the empirical curves to represent a range over which $F(T_s)$ varies for the real Earth, then our

model curve for $r = 0.5$ is indeed a realistic approximation. We note, however, that although the work of North, Oerlemans and Van der Dool is quite a good start, more research effort could usefully be applied to defining $F(T_s)$ observationally.

3.1.3.8 Linear Approximation to $F(T_s)$

In connection with energy balance climate models it is convenient and, in view of Fig. 3.1.3.4, reasonable to approximate the atmospheric radiation flux to free space by a linear law of the form:

$$F(T'_s) = A + BT'_s \qquad (3.1.3.4)$$

where T'_s is the surface temperature in degrees centigrade. This law allows analytic solutions to a simple energy balance climate model as discussed in Section 3.2. To provide an input to such models, we have used our 9 band model to calculate A and B for varying CO_2 content with relative humidity held constant at 50% and $a = 0.95$. This value of a is the same as was used for normalization in Fig. 3.1.3.4.

Table 3.1.3.3 gives the values of A and B for CO_2 concentrations ranging from 300 to 1000 ppm. Comparing our values for A and B with those used by other authors, we find $A = 209.9$, 200.0 and 199.3 and $B = 1.57$, 1.45 and 2.40 for North[17,18] and Oerlemans and Van der Dool[14] respectively. Comparing these values for A and B with our 9 band model ($v_{CO_2} = 333$ ppm and $r = 0.5$) we see from Table 3.1.3.3 that our model values fall near the center of the observational values.

TABLE 3.1.3.3

Linear Approximation for $F(T'_s)$ Centered on $0^{\circ}C$,
$F(T'_s \text{ in } {}^{\circ}C) \approx A + BT'_s)$

ν_{CO_2} (ppm)	A (Wm^{-2})	B($Wm^{-2}C^{-1}$)
300	203.0	1.71
333	202.8	1.70
400	202.2	1.69
500	201.4	1.67
600	200.5	1.56
666	199.8	1.53
700	199.4	1.53
800	198.5	1.50
900	197.6	1.48
1000	196.8	1.46

3.1.3.9 Summary and Conclusions

In Section 3.1.3 we have approached the problem of terrestrial infrared radiation to space from a direction significantly different from that of the grey atmosphere model discussed above and from the radiative-convective models reviewed by Ramanathan and Coakley[1]. Our alternative approach thus constitutes a somewhat independent estimate of the climatic effects of increasing atmospheric CO_2. In constructing this 9 band model we hoped to include enough physics of the Earth's atmosphere and of the radiation processes involved to produce a reasonably useful model. The extent to which this goal was achieved is shown graphically in Figures 3.1.3.3 and 3.1.3.4 where we compare model predictions with observational data. From these comparisons we conclude that our 9 band radiation model, while far from complete, should be useful in making at least crude estimates of the impact of increases in atmospheric CO_2 content on future climate, especially when coupled with the energy balance climate model discussed in Section 3.2. Three distinct feedback processes are included in the model by allowing the water vapor content of the atmosphere, the absorption band strengths (R and S) of CO_2 and H_2O vapor and the tropopause height to vary with temperature. The first two of these feedback processes are significant and positive; thus positively reinforcing surface temperature increases induced by increased atmospheric CO_2, while the third is of less significance and is negative.

By assuming the Earth's atmosphere to be homogeneous with an average temperature of $T_s = 288^oK$ we can estimate the change in surface temperature (ΔT_s) induced by a doubling of CO_2 content. Because water

vapor absorption plays such an important role in infrared radiation from the Earth, we have computed ΔT_s for three different assumptions regarding atmospheric water vapor. For constant absolute humidity, i.e., water vapor content held constant at the 50% relative humidity, T_s = 288°K value, regardless of temperature changes, we find ΔT_s = 2.1°K . In this case the water vapor feedback mechanism is suppressed. Next, we assume relative humidity constant at 50% with the result ΔT_s = 3.0°K. Hence, the water vapor feedback has increased ΔT_s by 43%. The ΔT_s = 3.0°K figure is relative insensitivity to the exact choice of relative humidity--40% or 60% also yield ΔT_s = 3.0°K. Finally, we consider varying relative humidity. If relative humidity were to increase by 10% (to 60%) as T_s rises in response to a doubling of atmospheric CO_2, then ΔT_s = 3.9°K is our model result. Conversely, if relative humidity were to drop by 10% (to 40%) then ΔT_s falls to 1.8°K. These results serve to emphasize the importance of water vapor in connection with the CO_2-climate question.

The CO_2 doubling has its impact in the wings of the strong 15 μ CO_2 absorption band (bands 3 and 5 of our model) and in the weak CO_2 absorption bands near 10.4 and 9.4 μ (bands 7 and 8 in our model). In band 4, which contains the core of the strong 15 μ CO_2 absorption, no changes occur for a CO_2 doubling. In this case, although absorption increases drive the effective radiating height upward, this height is in the constant temperature tropopause both before and after doubling; hence, there is no change in radiated flux.

The $\Delta T_s = 2.1^oK$ result for constant humidity is in substantial agreement with the 2.8^oK figure derived frm the grey atmosphere. For constant relative humidity $\Delta T_s = 3.0^oK$ for the 9 band model. This is interesting because these similar results were obtained by quite significantly different approaches. Hence, it lends credibility to the estimate of about 3^oK as the average surface temperature increase in response to a doubling of atmospheric CO_2 content.

The case of constant relative humidity has received considerable attention in the literature. Ramanathan and Coakley[1] review radiative-convective model results for ΔT_s which are appropriate for comparison with our constant relative humidity result of 3.0^oK. They arrive at a representative figure of $\Delta T_s = 2.0^oK$. Schneider[16] reviews the impact of increases in atmospheric CO_2 on climate considering a broad range of models. He arrives at $\Delta T_s = 1.5$ to 3^oK as the most probable range of increase in average temperature resulting from a doubling of atmospheric CO_2. Although the result of our 9 band model is some 50% higher than the value of Ramanathan and Coakley's and falls at the upper end of the range suggested by Schneider, the agreement between these various models is reassuringly close, especially so in view of the somewhat different and rather simple approach we have taken in our 9 band radiation model. The rough agreement between the results of different approaches supports the view that $\Delta T_s = 3^oK$ is a reasonable first approximation to the climatic response of a doubling of atmospheric CO_2. Nevertheless, it is important to remember here that this and other estimates result from imperfect models

of nature. Many potentially important factors, such as clouds, have been completely omitted or treated in only an elementary fashion. Further, our models have not been comprehensively compared to observations of nature. Finally, the observed increase in atmospheric CO_2 is not the only factor affecting the Earth's climate. Hence, estimates of climatic change focusing solely on CO_2 and neglecting other, poorly understood factors, such as those which cause glacial epochs, are not likely to be entirely correct though they are the best estimates one can make using our current understanding of nature. More credable estimates of climatic effects will only come with better understanding of nature.

Returning to results from our 9 band model, we note that our estimate for ΔT_s is dependent on the initial value of T_s used. Above we have used $T_s = \langle T_s \rangle = 288^oK$ as our base or unperturbed temperature. As indicated in Fig. 3.1.3.4, ΔT_s would be smaller for base temperatures below 288^oK. This phenomena arises from the increasingly strong positive feedback of water vapor and absorption band strength as T_s increases.

While our 9 band model is deficient in some respects, e.g., cloud variations are neglected, it does incorporate a modicum of atmospheric physics and agrees rather well with experimental data (Figs. 3.1.3.3 and 3.1.3.4). Hence, it provides some insight into the climatic effects of increased atmospheric CO_2 content. It also provides a radiative loss function dependent on average relative humidity and atmospheric CO_2 content for use in the energy balance climate model discussed in Section 3.2.

REFERENCES FOR SECTION 3.1.3

1. Ramanathan, V. and J. A. Coakley, Jr., "Climate Modeling Through Radiative-Convective Models," Rev. Geophys. and Sp. Phys., 16, 465-490, 1978.

2. Paltridge, G.W. and C.M.R. Platt, Radiative Processes in Meteorology and Climatology: Developments in Atmospheric Scinece, 5, Elsevier, Amsterdam, 1976.

3. Kondratyev, K.Y., Radiation in the Atmosphere: International Geophysics Series, 12, Academic Press, N.Y., 912, 1969.

4. Cess, R.D., (1976), "Climate Change: An Appraisal of Atmospheric Feedback Mechanisms Employing Zonal Climatology," J. Atmos. Sci., 33, 1831-1842, 1979.

5. Schneider, S. H., "On the Carbon Dioxide-Climate Confusion," J. Atmos. Sci., 32, 2060-2066, 1975.

6. NOAA, NASA, USAF, U.S. Standard Atmosphere, U.S. Gov't. Printing Office. Washington, D.C., 1976.

7. Chamberlain, J.W., Theory of Planetary Atmospheres: An Introduction to Their Physics and Chemistry, Academic Press, N.Y., 912, 1978.

8. Allen, C.W., Astrophysical Quantities, 3rd Ed., Univ. of London (Athlone Press), 1976.

9. Goody, R. M., Atmospheric Radiation, I. Theoretical Basis, Oxford Univ. Press, 1964.

10. Houghton, J. T., The Physics of Atmospheres, Cambridge Univ. Press, 1977.

11. Manabe, S. and R. T. Wetherald, "The Effects of Doubling the CO_2 Concentration on the Climate of a General Circulation Model," J. Atmos. Sci., 32, 3-15, 1975.

12. Perry, A. H. and J. M. Walker, The Ocean-Atmosphere System, Longman, London, 1977.

13. Hanel, R. A., B. Schlachman, D. Rodgers, and D. Vanous, Nimbus 4 Michelson Interferometer, Applied Optics, 10, 1376-1382, 1971.

14. Oerlemans, J. and H. M. van den Dool, "Energy Balance Climate Models: Stability Experiments with a Refined Albedo and Updated Coefficients for Infrared Emission," J. Atmos. Sci., 35, 371-381, 1978.

15. Augustsson, T. and V. Ramanathan, "A Radiative-Convective Model Study of the CO_2-Climate Problem," J. Atmos. Sci., 34, 448-451, 1978.

16. North, G.R., "Analytic Solution to a Simple Climate Model with Diffusive Heat Transport," J. Atmos. Sci., 36, 1301-1307, 1975a.

17. North, G.R., "Theory of Energy Balance Climate Models," J. Atmos. Sci., 32, 2033-2043, 1975b.

3.2 JASON Climate Models

3.2.1 Energy Budget Climate Models

We evaluate the effect of increased atmospheric concentrations of CO_2 on the climate by examining simple climate models, the so called energy budget models.

The most elementary energy budget model, which we call zero'th order, simply asserts:

$$\sigma \bar{T}_e^4 = \frac{Q}{4}(1 - \bar{\alpha}) \qquad (3.2.1.1)$$

where

σ = Stefan Boltzmann constant

$\bar{T}_e$ = effective mean radiating temperature

Q = solar constant

$\bar{\alpha}$ = mean albedo of the earth.

From computations made at JASON 1978, we believe the relation between effective and surface temperature is given by

$$\bar{T}_s = (1 + 3\tau/4)^{1/4}\bar{T}_e$$

where τ is a measure of the opacity of the atmosphere whose dependence on CO_2 concentration is described in Section 3.1. For the current atmosphere, τ, computed from first principles, was found to be 0.75. Putting in conventional values of the remaining constants:

$$\sigma = 5.6 \times 10^{-8} \text{ W/m}^2 (^\circ\text{K})^4$$

$$Q = 1360 \text{ W/m}^2$$

$$\bar{\alpha} = 0.29$$

we get the quite acceptable figures $\bar{T}_e = 257^\circ\text{K}$, and $\bar{T}_s = 288^\circ\text{K} = 15^\circ\text{C}$.

As a predictive equation, Eq. (3.2.1.1) suffers from an array of defects. Changing, for example, the solar constant alters $\bar{\alpha}$ in an unknown manner. A change in CO_2 concentrations affects the mean surface temperature, and hence also $\bar{\alpha}$. Its effect on the biosphere, and hence again $\bar{\alpha}$, is unknown and requires further investigation.

A first attempt to overcome these difficulties is present in First Order Models. In these, surface temperature T is permitted to vary with latitude θ, or one may imagine, if one prefers, that T is mean azimuthal temperature at latitude θ. Heat transport is introduced, and the governing equation has the general form

$$D + I = \frac{Q}{4}(1 - \alpha) = q(1 - \alpha)$$

where now

D = transport mechanism

I = outgoing radiative flux as function of T

α = (mean) albedo of earth at latitude θ as function of θ and T.

Various modelings of I, D, and α are possible. The simplest parametrization of $1 - \alpha$ is as follows: (it is convenient to introduce the variable $x = \sin \theta$, in place of θ)

$$1 - \alpha = Z(x) \cdot \begin{cases} 0.7 \text{ if } T > -10^{\circ}C \\ 0.4 \text{ if } T < -10^{\circ}C \end{cases}$$

where $Z(x)$ is a correction for zenith angle, 0.7 is the co-albedo of land-sea, 0.4 that of ice-snow. In this way, ice albedo feedback is incorporated into the model.

The radiative flux I may be modeled by permitting Eq. 3.2.1.1 to hold locally; thus

$$I = \sigma T_e^4 = \frac{\sigma}{1 + .75\tau} T^4$$

where τ can now be adjusted for CO_2 concentration.

It is convenient to modify I by linearizing about zero degrees Celsius to get $I = A + BT$, with T now in degrees Celsius. It appears,

in practice, that A and B are then retrospectively adjusted to better fit current climate data, thus incorporating current cloudiness, for example.

At the same time, there are large, and rather serious discrepancies in the literature concerning the magnitude of B , which significantly affect the sensitivity of the model to changes in the solar constant.

We consider the first order energy budget models to Budyko and Sellers. Subsequent work has been, in the main, variants of the schemes they contrived.

Budyko's choice of D was:

$$D = \gamma(T - \bar{T}) \quad ,$$

T is the mean surface temperature, and γ a phenomenological constant to be adjusted later.

Sellers (and others) used diffusive transport

$$D = -\frac{d}{dx}\left[D\left(1 - x^2\right)\frac{dT}{dx}\right]$$

where D is, according to who you are reading, a constant, a function of x, a function of x and T , or even a function of x , T and $\frac{dT}{dx}$.

Some writers have used a linear mix of Budyko and Sellers type transports.

For present purposes we will take

$$D = -D \frac{d}{dx}\left[(1 - x^2)\frac{dT}{dx}\right] = -D \text{ div grad } T \quad ,$$

where D is a phenomenological constant to be determined later.

The first order energy budget equation becomes

$$-D \frac{d}{dx}\left[(1 - x^2)\frac{dT}{dx}\right] + A + BT = qZ(x) \quad \cdot \quad \begin{cases} 0.7 \text{ if } T > -10^0C \\ 0.4 \text{ if } T < -10^0C \end{cases} \qquad (3.2.1.2)$$

Equation 3.2.1.2 includes Eq. 3.2.1.1 from two points of view, so we may expect Eq. 3.2.1.2 to give reasonable mean surface temperatures. On tne one hand, as D gets large (more energetic diffusion), T gets more nearly constant and Eq. 3.2.1.2 becomes a version of Eq. 3.2.1.1. On the other hand, if Eq. 3.2.1.2 is integrated from -1 to $+1$, the diffusive term vanishes, and what remains is a version of Eq. 3.2.1.1.

Equation 3.2.1.2 is usually solved as follows. Assume T is a decreasing function of x for $0 \leq x \leq 1$, and even. Postulate x_i, $0 \leq x_i \leq 1$, position of the northern ice line where $T(x_i) = -10$. Now the differential equation is an ordinary inhomogeneous one, requiring no

boundary condition which can be solved by variation of parameters, or eigenfunction expansion.

With the solution obtained, Q and D must be adjusted so that $T(x_1) = -10$, and monotonicity and evenness verified.

If one supposes that for current climate, $x_1 = 0.95$, and $q = \frac{Q}{4} = D$ is determined uniquely. With D so determined, and q still fixed at 340, one finds three positions altogether of the ice line meeting the assumed requirements of evenness and monotonicity of $T(x)$, to wit: the normal, a heavily glaciated, and all ice. The heavily glaciated is not stable.

With D fixed by the current climate, one may also investigate the effect of changes in S. A decrease of Q on the order of 2 to 3% is enough to give only an ice covered earth as solution, still on the assumption of evenness and monotonicity of $T(x)$.

There is one consideration of the methodology above which we feel is important to further consideration of such models. It concerns the role of the constant D, which is determined by matching current climate. It would be particularly desirable to give an a priori estimate of D, or at least to present a persuasive argument that D is indeed constant over a reasonable range of the other parameters present.

REFERENCES FOR SECTION 3.2.1

1. P. Chylek and J. A. Coakley, Jr., "Analytical analysis of a Budyko-type climate model; Journ. Atmos. Sci., 32, 1975, No. 675-679.

2. M. Ghil, "Climate stability for a Sellers-type model," Journ. Atm. Sci., 33, 1976, pp 3-20.

3. M. Hantel, "Polar boundary conditions in zonally averaged global climate models," Journ. App. Meteor, 13, 1974, 752-759.

4. I. M. Held and M. J. Suarez, "Simple albedo feedback models of the icecaps," Tellus, 36, 1974, pp 613-629.

5. M. s. Liam and R. D. Cess, "Energy balance climate models--a reappraisal of ice-albedo feedback," Journ. Atm. Sci., 34, 1977, pp 1058-1062.

6. J. Oerleman and H. M. van den Dool, "Energy balance climate models: stability experiments with a refined albedo and updated coefficients for I-R emission," Journ. Atm. Sci., March 1978, pp 371-381.

7. W. D. Sellers, "A new global climate model," Journ. App. Meteor, 8, 1973, pp 241-254.

8. G. North, "Analytical solution to a simple climate model with diffusive heat transport," Journ. Atmos. Sci., 32, 1975, pp 1301-1307.

9. G. North, "Theory of energy balance climate models," Journ. Atmos. Sci., 32, 1975, pp 2033-2093.

10. G. R. North, "Simple Mathematical Models of the Climate," unpublished lecture notes (1978).

11. G. R. North, "Analytical Solution to a Simple Climate Model with Diffusive Heat Transport," J. Atmos. Sci., Vol. 36, pp 1301-1307 (1957a).

12. M. I. Bodyko, "The Effect of Solar Radiation Variations on the Climate of the Earth," Tellus, Vol. 21, pp. 611-619 (1969).

13. G. R. North, "Theory of Energy-Balance Climate Models," J. Atmos. Sci., Vol. 32, pp. 2033-2043 (1975b).

3.2.2 Description of the Time Independent JASON Climate Model

To assess in a quantitative fashion the effects on climate of increasing the CO_2 concentration, we have constructed and analyzed an energy balance climate model of the kind described in the previous section. The ingredients in an energy balance model are specifications of

1) Incoming solar radiation and absorption by land and water: insolation.

2) Outgoing radiation by the earth and by the atmosphere.

3) Transport of energy poleward by the ocean currents, by latent heat and by sensible heat.

More precisely we write

$$C \frac{\partial T}{\partial t} = \text{Insolation} - \text{Outward Radiation} - \text{Transport}$$

where C is some "heat capacity" which sets the time scale for the response of the temperature T to changes in any of the quantities on the right hand side of this equation. In principle, C can be a function of longitude, latitude and even time.

Let us look at the three basic energy quantities listed above:

3.2.2.1 Insolation

The insolation is probably the best established quantity in the First Order Models. The form of insolation is

$$\frac{Q}{4} Z(x)a(x,x_c) \qquad (3.2.2.1)$$

where Q is the solar constant

$$Q = 1380 \text{ watts/m}^2$$

and $Z(x)$ is a zenith angle factor giving the mean annual distribution of insolation over latitude. x is the sine of the latitude and

$$Z(x) = 1 - 0.482P_2(x)$$

$$= 1 - \frac{1}{2} P_2(x) \qquad (3.2.2.2)$$

with $P_2(x) = \frac{1}{2} (3x^2 - 1)$, the second order Legendre polynomial. The factor $a(x,x_c)$ represents the absorption of the solar radiation by land, sea and ice. We will use the idea of Budyko[1] that $a(x,x_c)$ varies with x for $x \leq x_c$ at which latitude the hemisphere is permanently ice covered and $a(x,x_c)$ $x \geq x_c$ is a constant. Actual values for $a(x,x_c)$ are not precisely agreed upon by all workers, but we adopted the following values from North[2]:

$$x_c = 0.95 \quad , \quad \text{Latitude} = 71.8^{\circ} \quad ;$$

for $x > x_c$

$$a(x,x_c) = 0.38 \quad , \quad \text{albedo} = 0.62 \qquad (3.2.2.3)$$

for $x < x_c$

$$a(x,x_c) = 0.697 - 0.0779P_2(x) \qquad (3.2.2.4)$$

which gives an average albedo of ≈ 0.3 including land, water, and ice.

Two comments are in order here: (1) we use zonally averaged quantities so that azimuthal or longitudinal dependence is washed out. This is an important simplification of the real two dimensional geometry of the earth's surface. However, following the orginators of energy balance models we are convinced it is an adequate starting point. (2) The particular values represented in Eqs. 3.2.2.2, 3.2.2.3, and 3.2.2.4 are, of course, important, but variations over small domains are unlikely to significantly affect our discussion or conclusions.

3.2.2.2 Outgoing Radiation

We desire a representation of the infrared radiation escaping the earth at each latitude as a function of the ground temperature. There appears to be agreement among workers that a linearized formula

$$\text{Radiation} = A_R + B_R T(x) \qquad (3.2.2.5)$$

is quite adequate. The coefficients A_R and B_R are, of course, independent of $T(x)$ but may depend on cloudiness and other climatological features. Cess[3] has reviewed the situation and his results derived from

satellite observation are presented in Tables 3.2.2.1 and 3.2.2.2 where A_c is the cloud cover fraction.

Table 3.2.2.1
Summary of Zonal Annual Climatological
Data for the Northern Hemisphere
The Units of F are W/m^{-2}

Latitude (^oN)	T_s (^oC)	A_c	Observed F	Eq. (8)	Error (%)
5	26.3	0.51	250	252	0.8
15	26.3	0.44	257	259	0.8
25	23.2	0.41	259	256	-1.2
35	15.9	0.47	241	239	-0.8
45	8.4	0.57	220	218	-0.9
55	2.2	0.64	204	202	-1.0
65	- 5.5	0.64	191	190	-0.5
75	-12.7	0.61	181	182	0.6
85	-18.0	0.55	179	179	0
Average	15.0	0.51	233	234	0.4

TABLE 3.2.2.2

SUMMARY OF ZONAL ANNUAL CLIMATOLOGICAL DATA FOR THE SOUTHERN HEMISPHERE

The Units of F are W/m^{-2}

Latitude (°S)	T_s (°C)	A_c	F		Error (%)
			Observed	Eq. (8)	
5	26.2	0.50	257	263	2.3
15	24.6	0.47	266	263	-1.1
25	21.4	0.47	262	258	-1.5
35	16.6	0.54	243	245	0.8
45	9.7	0.65	224	225	0.5
55	2.8	0.79	206	202	-1.9
65	-6.0	0.77	188	190	1.1
75	-33.0	0.56	163	164	0.6
85	-43.8	0.47	154	154	0
Average	13.4	0.57	236	237	0.4

Using his values of average cloud cover we find for the Northern Hemisphere A_R = 210.59 watts/m^2 and B_R = 1.57 watts/m^2-°C while for the Southern Hemisphere A_R = 215.83 watts/m^2 and B_R = 1.59 watts/m^2-°C . In our actual calculations we adopted the values of North[4] of A_R = 211.2 watts/m^2 and B_R = 1.55 watts/m^2-°C.

Now as discussed above, the variation of A_R and B_R with CO_2 concentration or the concentration of any atmospheric constituent is given by

$$A_R = \alpha/\left(1 + \frac{3}{4}\tau_g\right) \qquad (3.2.2.6)$$

and

$$B_R = \beta/\left(1 + \frac{3}{4}\tau_g\right) \qquad (3.2.2.7)$$

with τ_g the net opacity at the ground and α and β some constants. By using the relation between ground temperature, T, and the skin temperature T_e needed to radiate back the net insolation

$$T = \left(1 + \frac{3}{4}\tau_g\right)^{1/4} T_e \qquad (3.2.2.8)$$

we determine that $\tau_g = 3/4$ for $T_e = 257^{\circ}K$ and $T = 288^{\circ}K$--the global average temperature.

As the opacity of the atmosphere to the infrared radiation entering in Eq. 3.2.2.5 increases, the radiation coefficients A_R and B_R will decrease and the average global temperature must increase. To get a feeling for this, note that if we are in a steady state and integrate the energy balance equation over the globe it reads

$$\text{Infrared Radiation Out} = \text{Insolation} \quad .$$

As we change CO_2 concentration, say, the net insolation is more or less constant (it is constant in our simple models if the ice line at x_c

doesn't change) so $A_R + B_R \langle T \rangle$ is constant. $\langle T \rangle$ is the global average temperature. Using the rules from Eqs. 3.2.2.9 and 3.2.2.10 we find, on the basis of the radiative transport theory presented before, that doubling the CO_2 concentration from today's value of 332 ppm would result in a change in global average temperature of

$$\left\langle T_{\text{Doubled } CO_2} \right\rangle - \left\langle T_{\text{Today}} \right\rangle = +2.4^{\circ}C \quad . \qquad (3.2.2.9)$$

This is a number consistent with a wide variety of other models, simple and complicated, and emerges because global energy balance really does represent the basic gross structure of our planetary temperature. Precisely how this energy is transported about the globe does not affect in a dramatic fashion these global averages. Details of any climate model, including the one we are discussing here, will differ in how this 2°-$3^{\circ}C$ change is distributed over the globe.

3.2.2.3 Energy Transport

Variations of temperature over space and time are governed by energy transport mechanisms. We restrict ourselves in our models to transport in the latitudinal directions only. The heat flux from the equatorial region toward the pole comes in three main forms: ocean currents, latent heat, and sensible heat. Figure 3.2.2.1 shows these fluxes as recorded by Sellers.[5]

Following the ideas expressed by Stone[6] with somewhat different emphasis we have chosen to view this figure as representing several

varieties of heat transport cells. For example, suppose we consider the net heat flux R_g shown in Figure 3.2.2.1. It vanishes at $x = 0$ and $x = 1$ and peaks around $x \approx 0.6$. We can parametrize this by imagining a net heat flow which is

$$-K \frac{d}{dx}\left[x(1 - x) \frac{dT}{dx}\right] \qquad (3.2.2.10)$$

where K is an "eddy diffusion constant" and the heat flux $-Kx(1 - x)dT/dx$ vanishes at $x = 0$ and $x = 1$ while peaking at $x \approx 0.6$ when dT/dx behaves as $\sim x^{3/4}$. Really this is a representation of the actual heat flow by a lumped diffusion law with one overall constant K which sets the scale of the flow.

If one wanted to make a finer kind of cellular structure, it is easy to imagine constructing several cells corresponding to latent heat alone or ocean currents alone, etc. For example, consider ocean currents. The sea surface temperature, call it T_o, is different from the ground temperature T we have been considering heretofore. The heat flow due to ocean currents in the Northern Hemisphere is poleward from the equator to about $x = 0.94$. One could try a representation of the ocean currents as

$$-K_o \frac{d}{dx}\left[x(0.94 - x) \frac{dT_o}{dx}\right] \qquad (3.2.2.11)$$

with K_o another "eddy diffusion constant" setting the scale for the kind of heat transport being considered—here ocean currents.

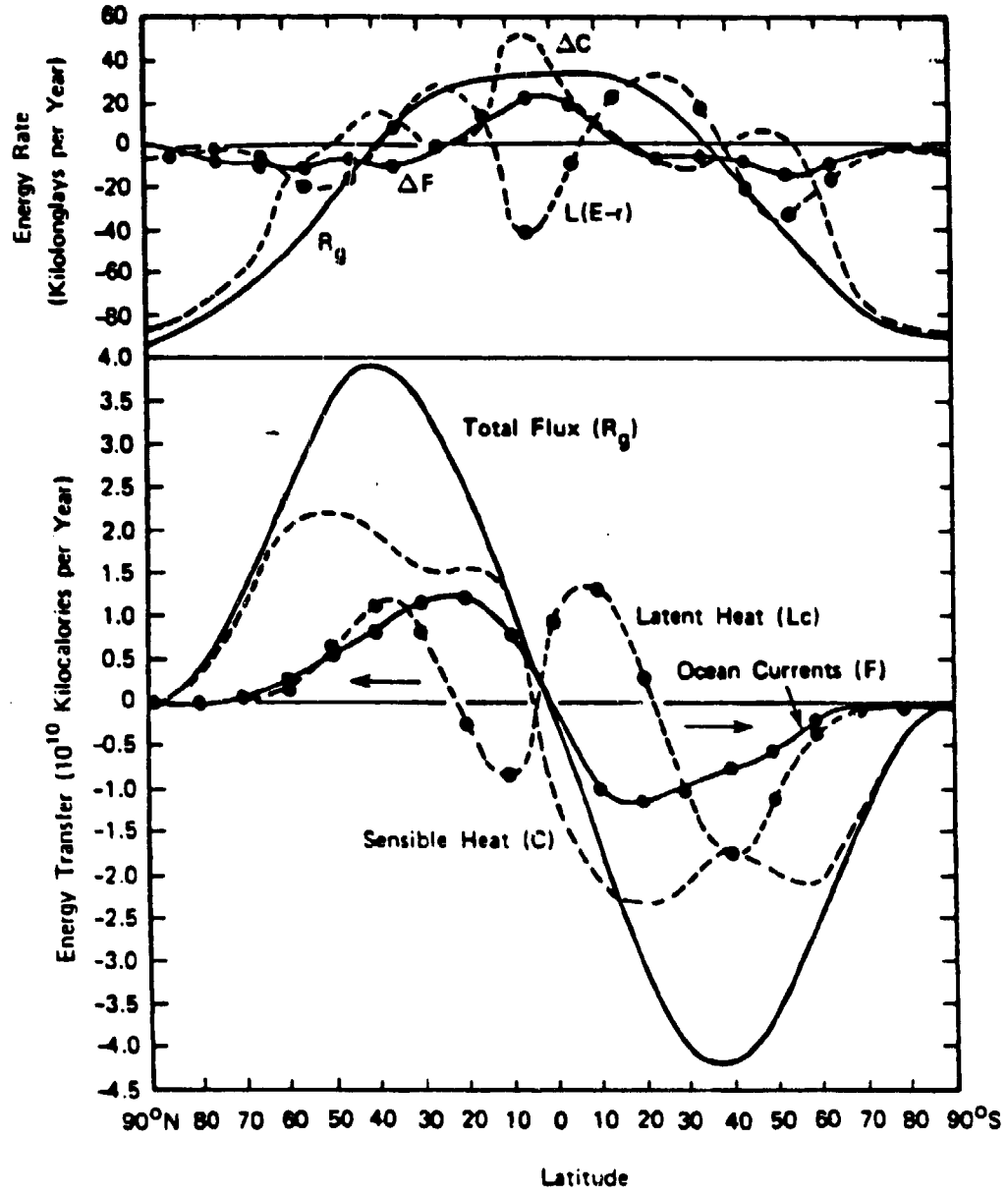

Figure 3.2.2.1 THE AVERAGE ANNUAL LATITUDINAL DISTRIBUTION OF THE COMPONENTS OF THE ENERGY BALANCE OF THE EARTH-ATMOSPHERE SYSTEM IN KLY YEAR^{-1} (top) AND OF THE COMPONENTS OF THE POLEWARD ENERGY FLUX IN 10^{19} KCAL YEAR^{-1} (bottom)

For latent heat in the Northern Hemisphere we would assign an effective temperature $T_L(x)$ to each latitude. Next note that the latent heat flow is negative for $0 \leq x \leq 0.37$ with a peak at $x = 0.17$ and positive for $0.37 \leq x \leq 0.94$ peaking at $x = 0.59$. For this flux we would write

$$-K_{1L} \frac{d}{dx}\left[(0.94 - x)(x - 0.37) \frac{dT_L}{dx}\right] + K_{2L} \frac{d}{dx}\left[x(0.37 - x) \frac{dT_L}{dx}\right] \quad , \tag{3.2.2.12}$$

with the "eddy diffusion constants" $K_{iL} > 0$, $i = 1,2$. A rule relating or coupling T_o, T_L and T would have to be constructed to complete this scheme.

The general zone lying between $\alpha \leq x \leq \beta$ has the flux

$$-K \frac{d}{dx}\left[(\beta - x)(x - \alpha) \frac{dT}{dx}\right] \quad . \tag{3.2.2.13}$$

Here we will take one heat transport cell for each hemisphere and one diffusion constant K for each hemisphere.

The climate model we have arrived at for the Northern Hemisphere, say, is

$$C \frac{\partial T}{\partial t} - K \frac{\partial}{\partial x}\left[x(1 - x)\frac{\partial T}{\partial x}\right] + A_R + B_R T(x,t) = \frac{Q}{4} z(x,t) a(x,x_c,t) \tag{3.2.2.14}$$

We will refer to this and its generalizations as JASON Climate Models (JCM).

Our first concern is with the allowed steady state versions of Eq. 3.2.2.11.

$$-K\frac{d}{dx}\left[x(1-x)\frac{dT}{dx}\right] + A_R + B_R T(x) = \frac{Q}{4}\, z(x)a(x,x_c) \quad . \tag{3.2.2.15}$$

In this set $z = 1 - 2x$ which turns Eq. 3.2.2.15 into

$$\frac{d}{dz}\left[(1-z^2)\frac{dT}{dz}\right] + \sigma(\sigma+1)T(z) = -\frac{1}{K}\left[\frac{Q}{4}\, z(z)a(z,z_c) - A_R\right] = -S(z) \tag{3.2.2.16}$$

with

$$\sigma(\sigma+1) = -B_R/K \tag{3.2.2.17}$$

or

$$\sigma = -\frac{1}{2} + i\sqrt{\frac{B_R}{K} - \frac{1}{4}} \quad . \tag{3.2.2.18}$$

This is the Legendre equation. A heat transport cell with flux given by Eq. 3.2.2.13 becomes Legendre's equation with

$$z = [(\alpha+\beta) - 2x]/(\beta-\alpha)] \quad .$$

The solution to Eq. 3.2.2.16 is

$$T(z) = P_\sigma(z)\int_{-1}^{z} dw Q_\sigma(w)S(w) + Q_\sigma(z)\int_{z}^{1} dw P_\sigma(w)S(w) + \xi P_\sigma(z) + \eta Q_\sigma(z) \qquad (3.2.2.19)$$

where $P_\sigma(z)$ and $Q_\sigma(z)$ are the usual and second kind of Legendre function of index σ . ξ and η are integration constants. The function $Q_\sigma(z)$ is logarithmically singular at $z = \pm 1$ as is $P_\sigma(z)$ at $z = -1$. We must choose ξ and η so the temperature $T(z)$ is finite for all z . Finiteness at $z = 1$ requires $\eta = 0$, while at $z = -1$ it is satisfied only when

$$\xi = -\frac{\pi \cot \sigma\pi}{2}\int_{-1}^{1} dw S(w)P_\sigma(w) \qquad . \qquad (3.2.2.20)$$

To derive these results we need

$$Q_\sigma(z) = \frac{\pi}{2 \sin \sigma\pi}\left[P_\sigma(z) \cos \sigma\pi - P_\sigma(-z)\right] \qquad (3.2.2.21)$$

for z along the real axis between -1 and 1. The result for $T(z)$ is finally

$$T(z) = -\frac{\pi}{2 \sin \pi\sigma}\left\{P_\sigma(z)\int_{-1}^{z} dw S(w)P_\sigma(-w) + P_\sigma(-z)\int_{z}^{1} dw S(w)P_\sigma(w)\right\} \qquad (3.2.2.22)$$

The solution for $T(z)$ inside any heat transport cell has just this form with the $\sigma = -1/2 + i\sqrt{B_R/K_i - 1}$ and K_i the transport coefficient for that cell and $z = (\alpha + \beta - 2x)/(\beta - \alpha)$ in that cell.

It is important to note that we need require no conditions on $T(z)$ or its derivatives except finiteness of $T(z)$ throughout each cell. The "boundary conditions" discussed by North and others are unnecessary.

To determine K, the eddy diffusion coefficient in the JCM, we proceed by setting Q, A_R, B_R and $z_c = 1 - 2x_c$ to their present day values given above. Then K is varied until $T(z_c)$ achieves a definite value, conventionally chosen to be $-10^{\circ}C$. This yields a $K = 1.37$ watts/m^2-$^{\circ}C$. This diffusion coefficient is much larger than the value 0.59 watts/$m^2{}^{\circ}C$ found by North[2,4] when he considered a single heat transport cell running from pole to pole. Our heat flux proportional to $x(1 - x)$ is inhibited in transporting heat near the equator, while North's transport is proportional to $1 - x^2$ which is still sizeable near $x = 0$. It is natural to expect the transport coefficient here to be larger since it is from the equatorial region that heat must be pumped.

Once we have K such that $T(z_c) = -10^{\circ}C$ we may calculate $T(z)$ for today's climate. This is given in Figure 3.2.2.2.

This should be compared to the data recorded in Cess[3] for both the Northern and Southern hemispheres (Figure 3.2.2.3). The JCM gives temperatures too low in midlatitudes, but rather reasonable at high and low latitudes. An effect like this should be expected from our discussion of the structure of heat transport cells in the actual earth-atmosphere-ocean system. Because of the zeroes in latent heat transport and dips in sensible heat transport in midlatitudes, less heat, in fact, is transported

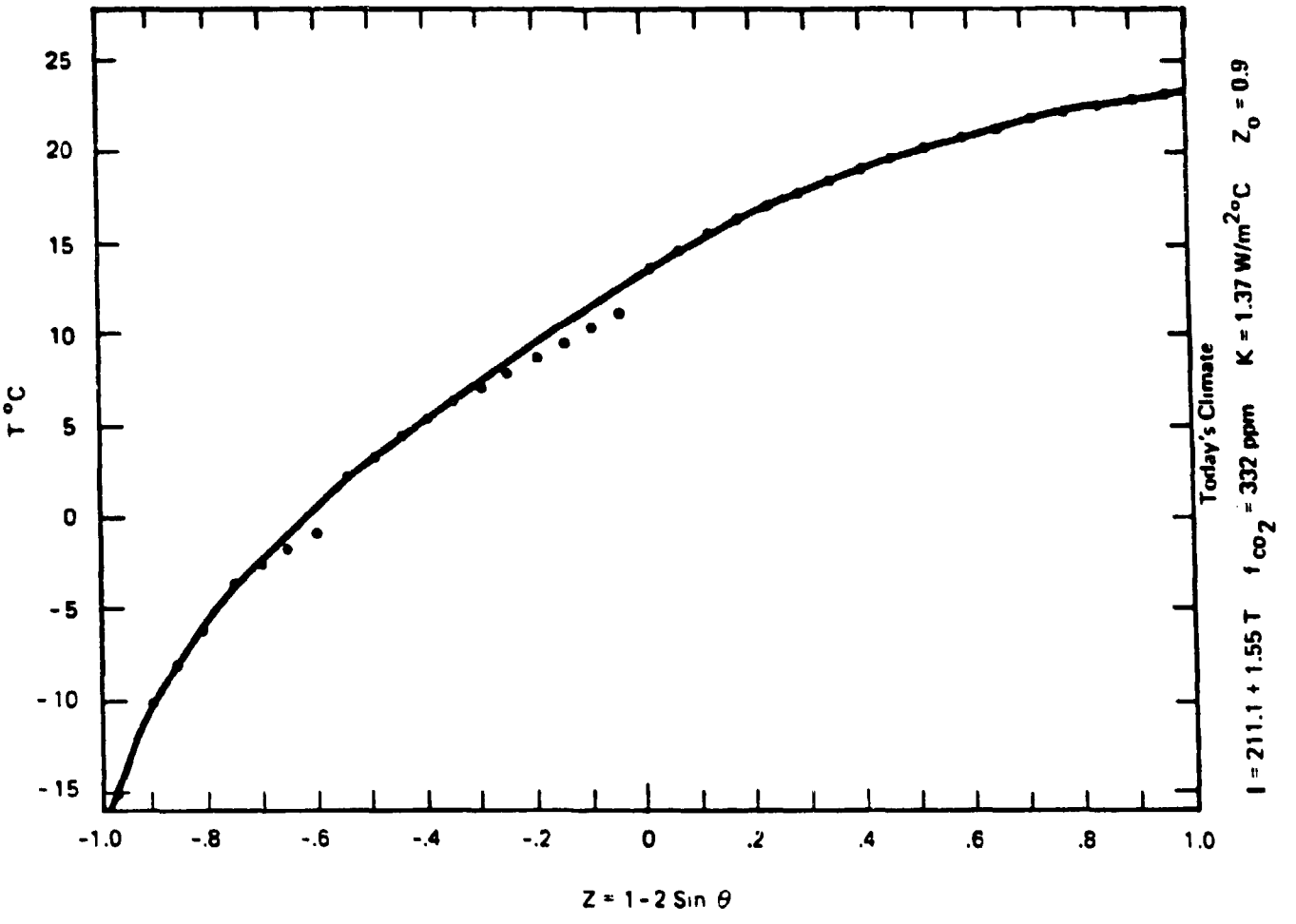

Figure 3.2.2.2 PREDICTION OF THE JASON MODEL FOR VARIANCE IN TEMPERATURE WITH LATITUDE (0) AND A CO_2 CONCENTRATION OF 332 PPM

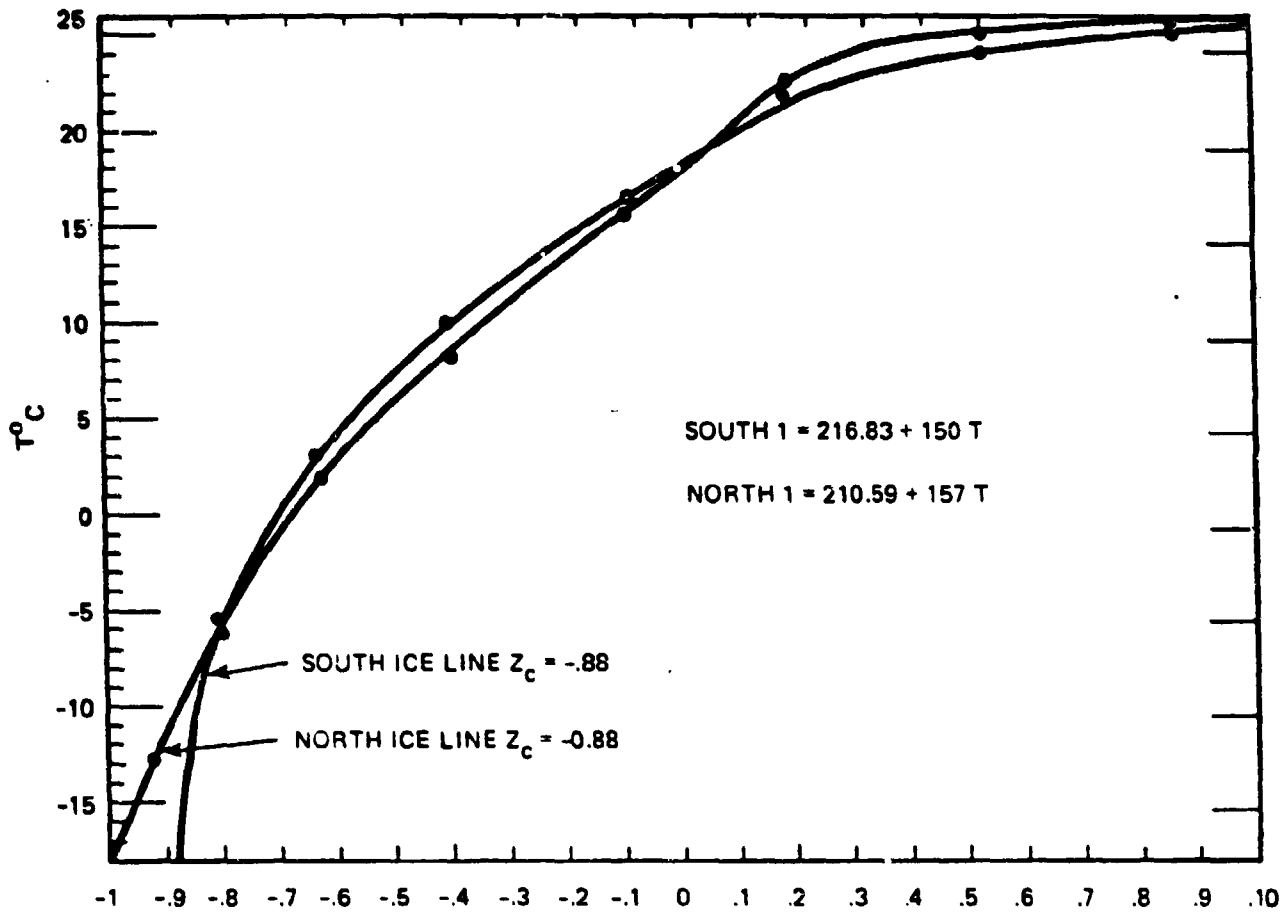

Figure 3.2.2.3 OBSERVATION DATA TAKEN FROM CESS FOR NORTHERN AND SOUTHERN HEMISPHERES (0 is the latitude)

out of those latitudes than the simplest JCM would indicate. So a many celled JCM will push up the midlatitude temperature as desired.

The response of the JCM to changes in CO_2 concentration is examined by changing A_R and B_R according to (9) and (10). Using the results from earlier sections, we find a doubling of CO_2 in the atmosphere to 664 ppm will lead to values of $A_R = 207.7$ watts/m^2 and $B_R = 1.524$ watts/m^2-^oC . Since we have fixed our eddy diffusion parameter K , we adjust z_c so $T(z_c) = 10^oC$. We find that $z_c = -1$ for this A_R and B_R , which means the ice line has retreated to the pole. So a doubling of CO_2 concentration according to the one heat transport cell/hemisphere JCM is likely to cause the ice caps to melt.

The rate of increase of CO_2 concentration has been 4.3%/yr of the industrial contribution. Taking 285 ppm as the preindustrial level we see that the fraction of CO_2 in ppm increases as

$$f_{CO_2} = 285 \text{ ppm} + (1.043)^N \cdot 47 \text{ ppm} \quad ; \qquad 3.2.2.23$$

N is in years from today. So a doubling of CO_2 to 664 ppm should occur as soon as 50 years hence. If the ice line instantaneously follows the $T = 10^oC$ line as is assumed in energy-balance models, the ice line should retreat and disappear as CO_2 doubles.

Comparing Figures 3.2.2.2 and 3.2.2.4 we see that the average rise in T is slightly more than the 2.4^oC evaluated from the conservation of

$A_R + B_R T$. This is clearly because of the retreat of the ice line, and this is emphasized by the large rise in T in the polar region.

These results are the essence of our analysis of the JCM. We have not explored to any extent questions such as the variation of the ice line as the solar constant varies or the sensitivity to the values of A_R , B_R , albedo, x_c , or the assumption that $T(x_c) = -10^{\circ}C$. These are interesting issues and important for one's confidence in the general scheme represented by the JCM. We feel it is rather clear that our heat transport cell description of heat flow in the earth-ocean-atmosphere system promises a realistic version of the actual complicated processes involved yet within the attractive simplicity of the energy balance models.

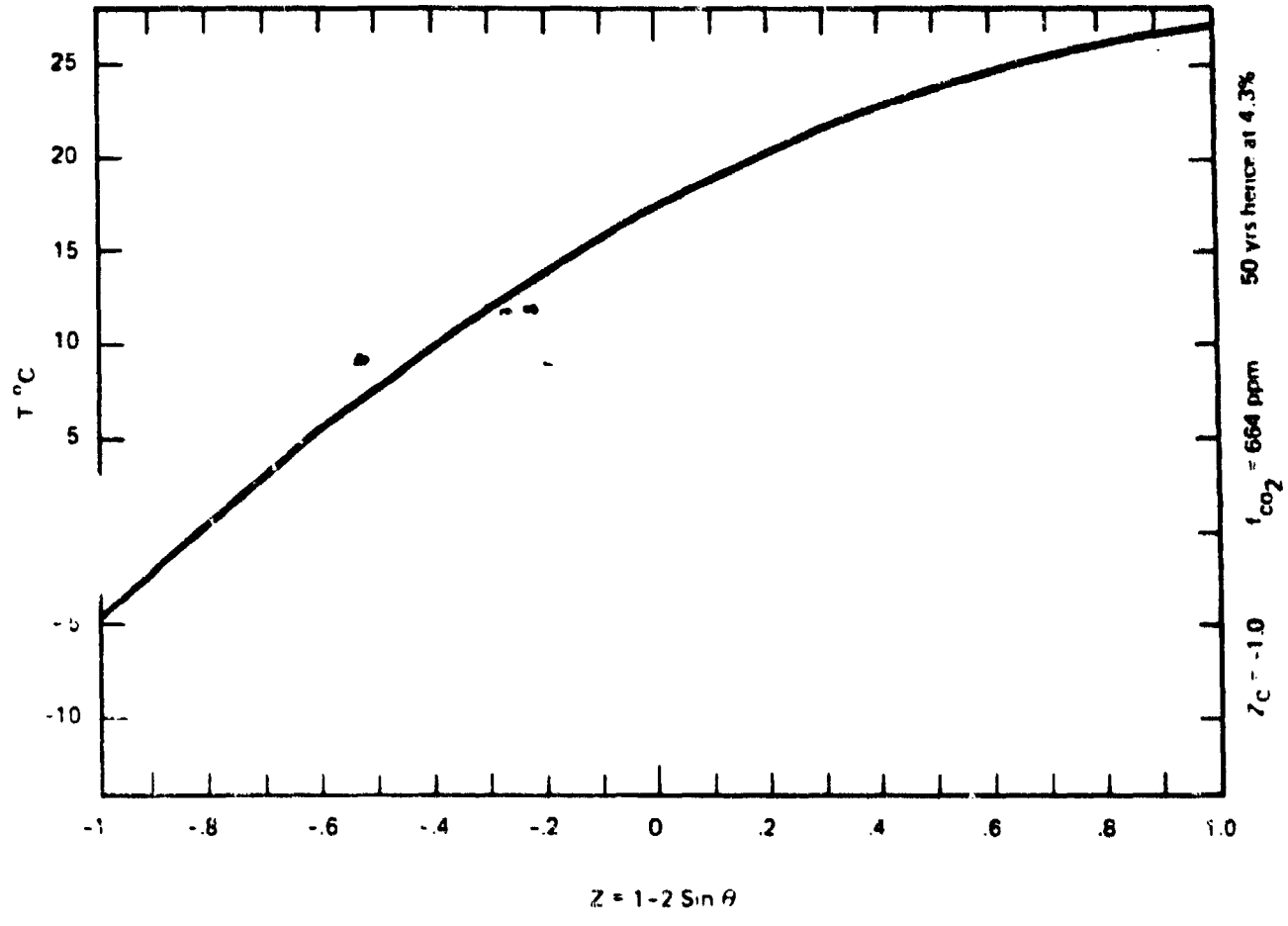

Figure 3.2.2.4 PREDICTION OF THE JASON MODEL FOR VARIANCE IN TEMPERATURE WITH LATITUDE (0), AND ASSUMING A DOUBLING OF THE CO_2 CONCENTRATION FOR PRESENT LEVELS

REFERENCES FOR SECTION 3.2.2

1. P. Chylek and J. A. Coakley, Jr., "Analytical analysis of a Budyko-type climate model; Journ. Atmos. Sci., 32, 1975, No. 675-679.

2. M. Ghil, "Climate stability for a Sellers-type model," Journ. Atm. Sci., 33, 1976, pp 3-20.

3. M. Hantel, "Polar boundary conditions in zonally averaged global climate models," Journ. App. Meteor, 13, 1974, 752-759.

4. M. Held and M. J. Suarez, "Simple albedo feedback models of the icecaps," Tellus, 36, 1974, pp 613-629.

5. M. S. Liam and R. D. Cess, "Energy balance climate models--a reppraisal of ice-albedo feedback," Journ. Atm. Sci, 34, 1977, pp 1058-1062.

6. J. Oerleman and H. M. van den Dool, "Energy balance climate models: stability experiments with a refined albedo and updated coefficients for I-R emission," Journ. Atm. Sci., March 1978, pp 371-381.

7. W. D. Sellers, "A new global climate model," Journ. App. Meteor, 8, 1973, pp 241-254.

8. G. North, "Analytical solution to a simple climate model with diffusive heat transport," Journ. Atmos. Sci., 32, 1975, pp 1301-1307.

9. G. North, "Theory of energy balance climate models," Journ. Atmos. Sci., 32, 1975, pp 2033-2093.

10. G. R. North, "Simple Mathematical Models of the Climate," unpublished lecture notes (1978).

11. G. R. North, "Analytical Solution to a Simple Climate Model with Diffusive Heat Transport," J. Atmos. Sci., Vol. 36, pp. 1301-1307 (1957a).

12. M. I. Bodyko, "The Effect of Solar Radiation Variations on the Climate of the Earth," Tellus, Vol. 21, pp. 611-619 (1969).

13. R. North, "Theory of Energy-Balance Climate Models," J. Atmos. Sci., Vol. 32, pp. 2033-2043 (1975b).

14. W. D. Sellers, Physical Climatology University of Chicago Press, 4th Edition, 1974) (1965).

15. H. Stone, "The Effect of Large-Scale Eddies on Climatic Change," J. Atmos. Sci., Vol. 30, pp. 521-529 (1973).

16. R. D. Cess, J. Atmos. Sci., 33, 1831 (1976).

3.2.3 Discussion of Energy-Budget Climate Models

The energy-budget climate models described in 3.2.1 and 3.2.2 focused on equilibrium states only. We considered the generic model

$$c\,\frac{\partial T}{\partial t}\,(\vec{x},t) + \text{Diffusion} + \text{IR radiation} = \text{Insolation}$$

for the case where T is time independent. These equilibrium states were expected to describe the present climate first of all and then the final state to which the earth would settle when the IR term is suddenly altered by changes in the atmospheric CO_2 concentration. In these simple models the key feedback effect among those from our long list given in 3.0 is the ice albedo feedback which is lurking in the insolation term. The equilibrium calculations indicated that when the CO_2 concentration is doubled, the ice line, originally at 72.2° latitude would retreat to the pole. Since the coefficients A and B in the IR radiation $= A + BT$ formula changed only by $\sim 1.5\%$, this is a measure of the severe sensitivity of the model. Nonetheless, the temperature rise as a function of latitude given by the model was much the same as more complicated General Circulation Model calculations. This point has been critically reviewed by Watts[1] and we find ourselves in general agreement with his arguments.

The real time scale for the retreat of <u>all</u> the ice on the earth is likely to be so long, as much as 10^3 to 10^5 years,[2] that predictions for the period 2030 to 2050 would not seem to be much affected by such possible future events. What is much more likely is that the permanent ice sheets of Greenland and the Antarctic will survive the few degrees centigrade

change induced by doubling CO_2 concentrations. However, the seasonal snow cover which blankets 38 million $(km)^2$ (7.4% of the earth's surface) and the sea ice covering 35 million $(km)^2$ (6.8% of the earth) are much more fragile. In the Antarctic 85% of the sea ice disappears each season, while the snow cover on the land masses in the Northern Hemisphere almost totally retreats on the same time scale. So a much more plausible scenario than "real" equilibrium is to assume that the seasonal snow cover and the sea ice will both disappear on the time scale of 50-75 years in which we are interested. Certainly the time scale for sea ice is on the order of 1-10 years, so it is plausible that it too will be absent when CO_2 doubles.

We have thus taken our equilibrium models and considered them to be yearly average models and recomputed the effect of doubling atmospheric CO_2 when the ice line is varied to correspond to our scenario of no sea ice or snow cover. We represent this in the model by moving the effective ice line (that is, the latitude where the albedo changes from earth-water to "ice") poleward in each hemisphere. In the Northern Hemisphere we move the ice line from 72.2° N to 83° N, while in the Southern Hemisphere we move the ice line from 66.9° S to 70° S.

In Figure 3.2.3.1 we show the change in temperature in °C in the Northern Hemisphere for the following conditions: (1) we fix the CO_2 concentration at today's value and remove the ice completely; (2) we double the CO_2 concentration but leave the ice line fixed at 72.2° N, and (3) we double the CO_2 and remove the ice--this is the calculation reported

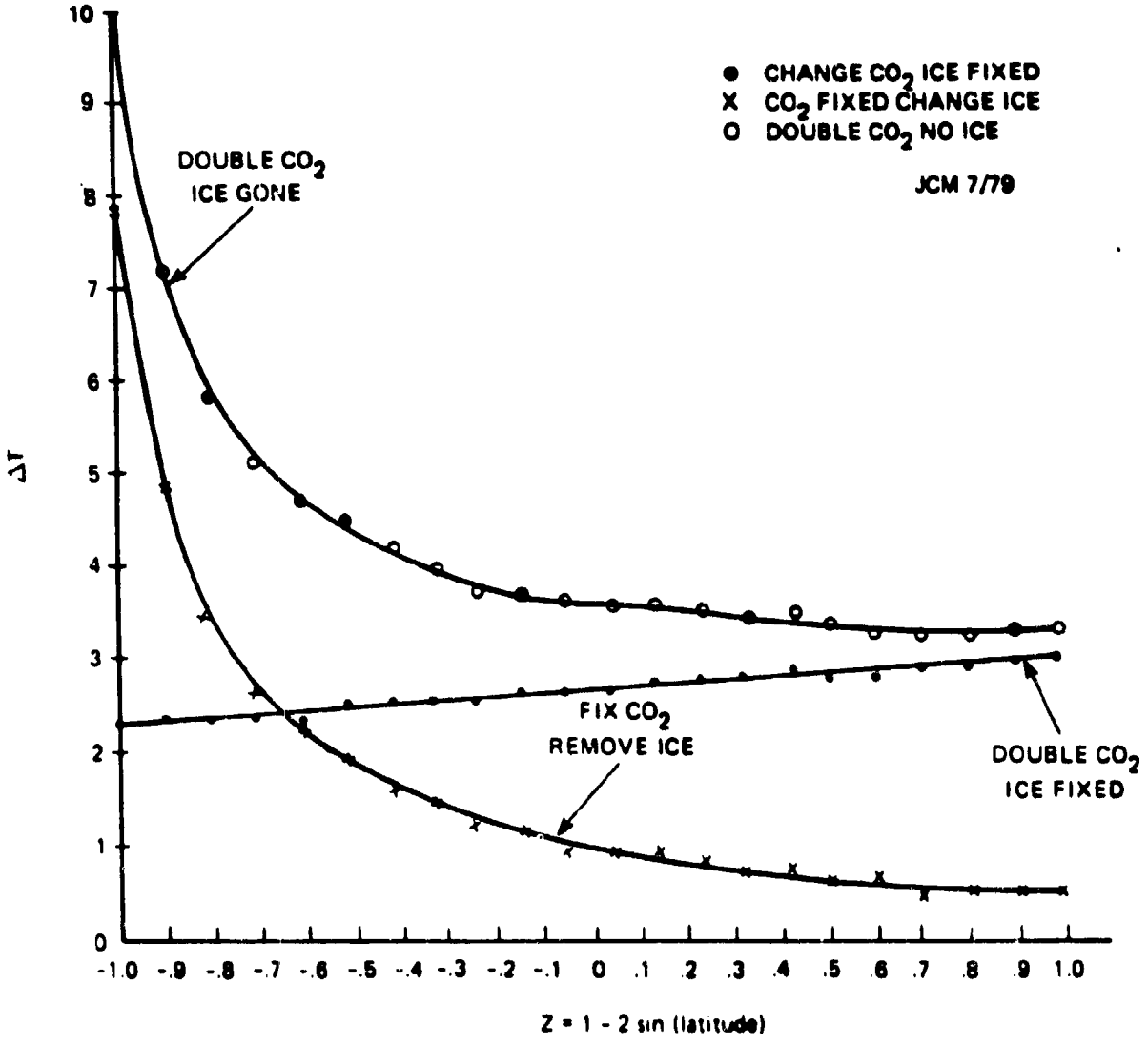

Figure 3.2.3.1 TEMPERATURE CHANGES IN THE NORTHERN HEMISPHERE FOR (a) FIXING THE CO_2 CONCENTRATION AND REMOVING THE ENTIRE ICE CAP (indicated by x) (b) DOUBLING THE CO_2 BUT FIXING THE ICE CAP (indicated by) (c) DOUBLING THE CO_2 AND REMOVING THE ICE (indicated by o).

earlier. The sensitivity to the removal of the ice cover is apparent especially in the polar latitudes. [The horizontal variable is $z = 1 - 2$ sin (latitude).]

In Figure 3.2.3.2 we investigate both what occurs as we increase the CO_2 concentration and keep the ice line fixed and the amount the temperature rises when the CO_2 concentration is double the present value and the sea ice is absent. There are three lessons here: (1) the onset time of significant temperature change is about 40 years. At that time the CO_2 concentration will be ≈ 500 ppm if it continues to rise at the rate observed over the past 20 years. After that initial important increase, temperature rises are significant on time scales of 5-10 years; (2) by comparing the top two curves we see the effect of removing only the sea ice after the CO_2 concentration has been doubled; (3) by comparing the top curve with the top curve in Figure 3.2.3.1 we see how removing only the sea ice and not all the ice has significantly modified the remarkable temperature increase in the polar regions which is the "real" equilibrium state. Figure 3.2.3.3 repeats this same calculation for the Southern Hemisphere. The general behavior is the same as the Nothern Hemisphere. There is much less ice removed in the South but it is also much more effective than the Northern ice in changing the net insolation because it was and remains further equatorward than Northern ice and the zenith angle effect therefore is larger. Nonetheless, the whole effect on ΔT is about 10% less in the South than in the North.

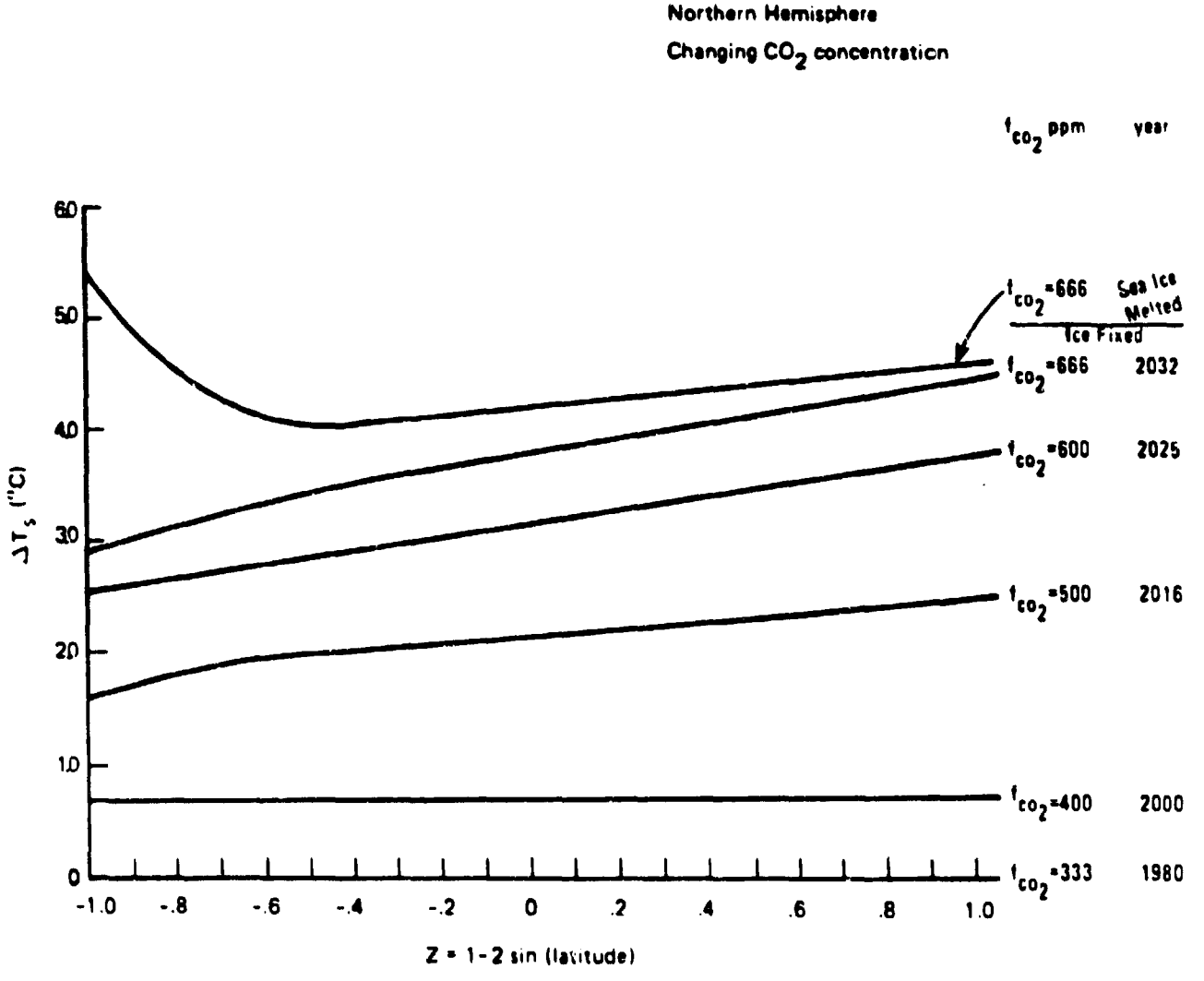

Figure 3.2.3.2 Temperature changes in the Northern Hemisphere resulting from changing the CO_2 concentration to 400, 500, 600, and 666 ppm. The year is calculated from CO_2 concentration = 285 ppm + 47 ppm x $(1.043)^N$ with N = years from 1979. The top curve is for double present CO_2 concentration (so f = 666 ppm) and sea ice removed.

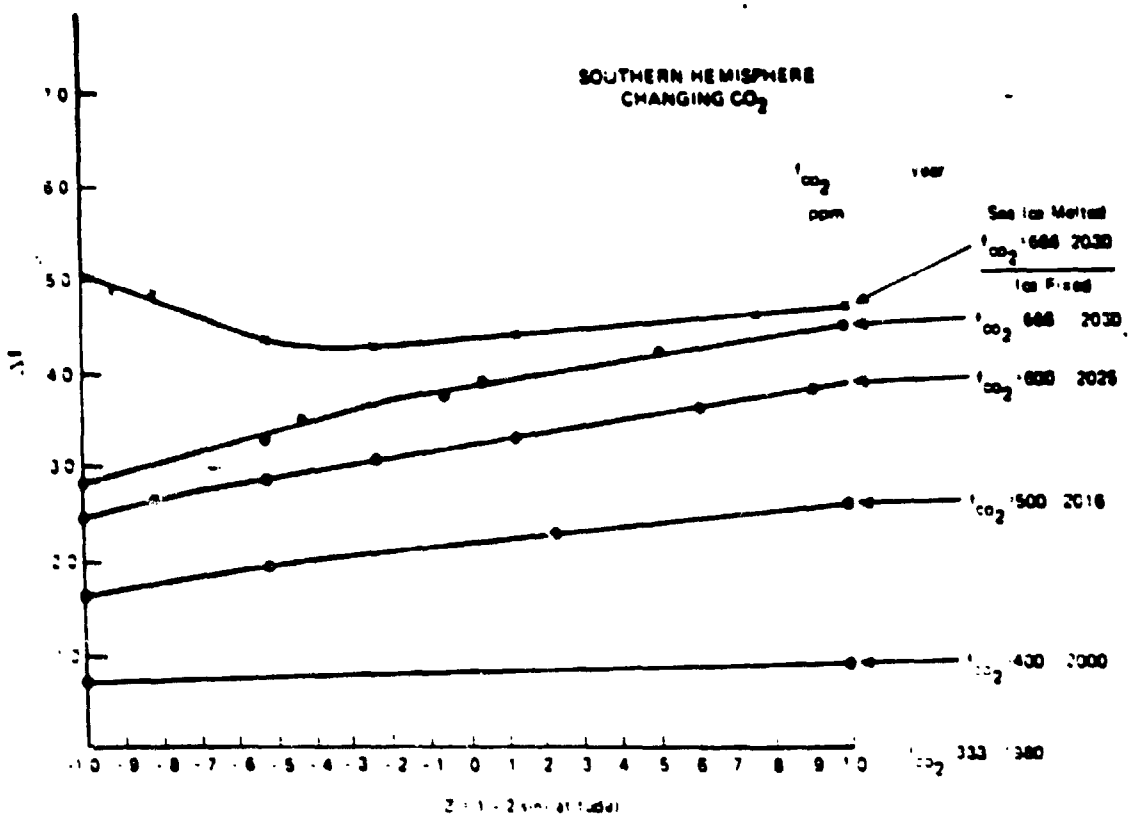

Figure 3233

TEMPERATURE CHANGES IN THE SOUTHERN HEMISPHERE RESULTING FROM CHANGING THE CO_2 CONCENTRATION TO 400, 500, 600 AND 666 PPM. THE YEAR IS CALCULATED FROM CO_2 CONCENTRATION = 285 PPM + 47 PPM $\times (1.043)^N$ WITH N = YEARS FROM 1979. THE TOP CURVE IS FOR DOUBLE THE PRESENT CO_2 CONCENTRATION (so f = 666 ppm) AND SEA ICE MOVED

These little calculations demonstrate the real power of the energy-budget models. One is able to answer a series of interesting questions about the behavior of a climate, albeit characterized by a single variable T(z), in an easy and rapid fashion. Each of the curves in these figures represents about 2.5 min of time on a Prime 500 system to compute and print. We will make further remarks on the reliability of energy-budget models a bit later; nevertheless it is fair to note at this point that both the sign and general magnitude of these results is likely to be accurate.

REFERENCES FOR SECTION 3.2.3

1. Watts, R.G., "Climate Models and the Prediction of CO_2-Induced Climatic Change," Oak Ridge Preprint ORAU/IEA-78-24(m), 1978.

2. Barry, R.G., "Cryospheric Responses to a Global Temperature Increase," CO_2 and Climate, ed. J. Williams, 169-180, 1978.

3.2.4 Time Dependent Energy-Budget Models--Seasonal Variations in Climate

We have investigated the time dependent JASON Climate Model to see how seasonal variation affects our expectations on the doubling of CO_2. With seasonal variations in the albedo and zenith angle factors entering the insolation driving term of the climate model

Insolation = (Solar Constant/4) * (Zenith Angle) x (1 - Albedo),

we expect that in the summer when the sun is "high" longer and the snow cover and sea ice are substantially removed from polar regions the temperatures predicted by our seasonal model will be quite a bit higher than the averages given by the seasonally averaged version above. Similarly, winter temperatures will be quite a bit lower. Furthermore, cross terms in the time dependence of albedo and zenith angle factors which do not average to zero upon averaging over the year will also lead to the average temperature of the seasonal model to be higher than the prediction of the averaged model. The seasonal model clearly has more real physics built into it. A proper use of the model would be to take the albedo, zenith angle and IR radiation terms as given functions of time and adjust the parameters (one here) of the diffusive transport term in the energy balance until it produced T(x,t) which nicely matched the present climate. Doubling of CO_2 concentration or other time dependent effects could be investigated.

We have adopted the view that the diffusion constant calculated in our equilibrium considerations is accurate enough and used it with the

Legendre series presentation of albedo and zenith angle given by North and Coakely[1] to evaluate T as a function of $z = 1 - 2 \sin$ (latitude) and time.

Our calculations were performed taking the time scale setting heat capacity C in $C \frac{\partial T}{\partial t}$ to be that of land, $\frac{C}{B}$ = two months. We began our calculations with two different initial temperature distributions: (1) $T(z,t = 0) = 10^{o}C + 20^{o}C \times z$ and (2) $T(z,t = 0) = 10^{o}C$. In each case a plot of $T(z,t + 1 \text{ year}) - T(z,t)$ shows this quantity became zero (i.e., less than $0.1^{o}C$) after eight "months" of computer time (actually about 10 minutes). In each case the same periodic solution was reached. Figure 3.2.4.1 shows the temperature as a function of time (after the periodic solution was reached) for the latitude $I = 5.74^{o}N$, which is that of Panama, and for the latitude $I = 64.2^{o}N$, which is that of Reykjavik, Iceland. The temperatures averaged over the year are, indeed, a bit higher than those generated by the "average" models. One could tune the transport parameter to fix this.

As one can see the model now contains quite interesting phase lags betwen parts of the hemisphere. Indeed, it is altogether sensible, for example, that the hottest part of the year should come later in Panama than in Iceland. Further, it is sensible indeed that variations in temperature near the equator should be much smaller than near the pole. (The time variation of zenith angle gives zero insolation during polar night.)

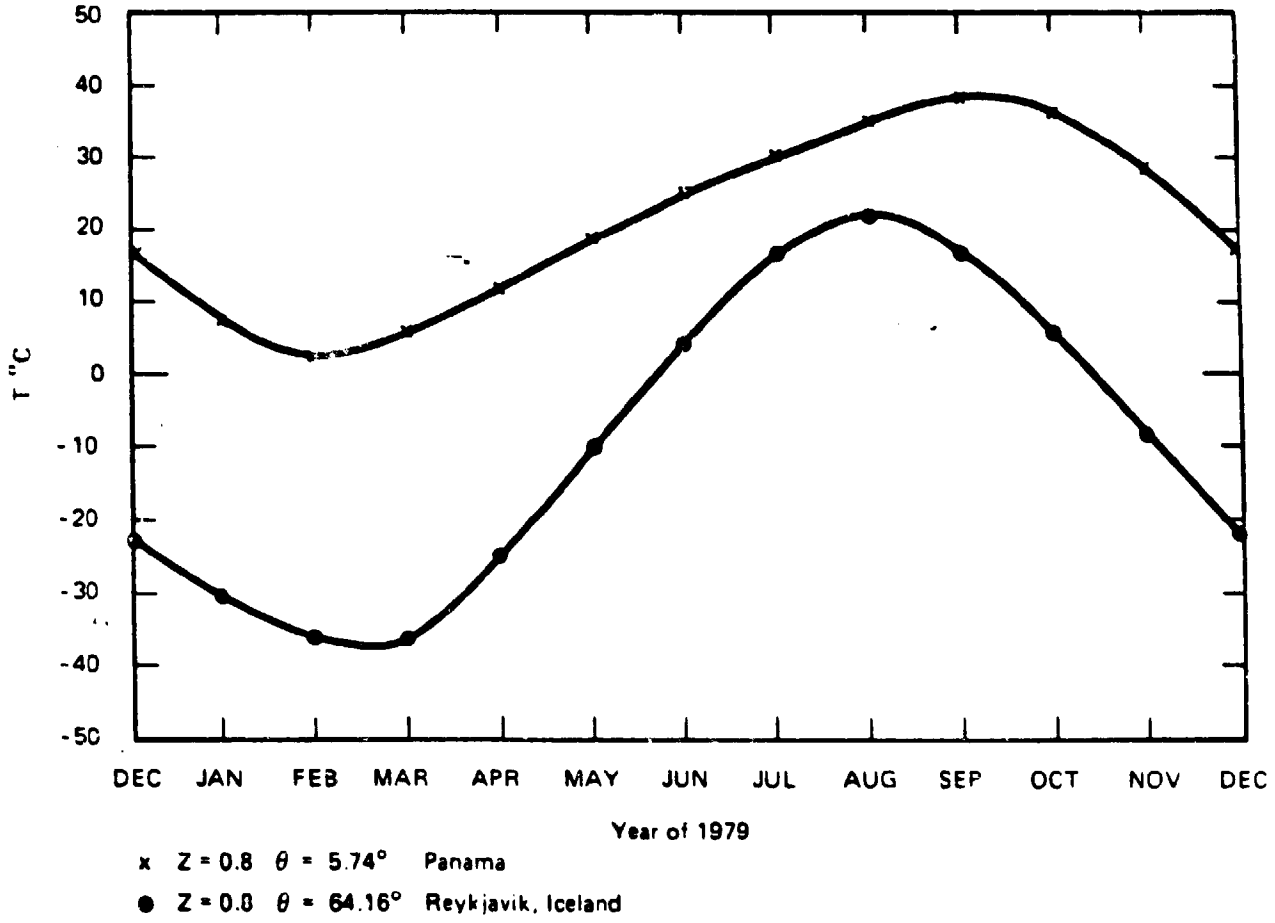

Figure 3.2.4.1 THE PREDICTION OF THE SEASONAL VARIATION OF TODAY'S CLIMATE AT TWO SELECTED NORTHERN HEMISPHERE LATITUDES
θ = 6° N for Panama; θ = 64° N for Iceland.

We have presented and carried out calculations only for the Northern Hemisphere. Since the JASON Climate Model is a hemisphere model, we could easily perform the same investigations for the Southern Hemisphere. In our calculations, we have also left out the observed seasonal variation of the parameters A and B which enter the IR radiation part of the energy balance. These variations are small compared to the main effect (~ 1% of the mean value yearly) and show a significant latitude variation as seen in comparing Mauna Loa and Point Barrow data. The full latitude dependence of the variation is not known.

One can also display T(z,t) for various months as a function of latitude. No particularly notable features arise except perhaps that pole to equator temperature differences are most marked in winter ($\Delta T \approx 45^0C$) and quite a bit less ($\Delta T \approx 25^0C$) in summer.

The effect of doubling the CO_2 is carried out as in the scenario above. First the IR formula is altered by lowering the values of A and B by the ~ 1.5% calculated before. Next, sea ice and snow cover are removed up to a permanent ice line taken to be about = 83° N. Equatorward of 83° N the albedo is unchanged at $I < 72.2^o$ and smoothly matched between these latitudes. Several "smooth" matchings were tried and no essential difference in T(z,t) was produced.

From these calculations we have made graphs of the change in seasonal temperature expected at various latitudes after the doubling of CO_2 and the retreat of sea ice. In Figures 3.2.4.2, 3.2.4.3, and 3.2.4.4

we present these ΔT values for the latitude of La Jolla, California; Washington,D.C.; and Moscow, U.S.S.R.

Our model, as noted above, lacks any hydrologic cycle, so implications of ΔT alone are not useful in drawing much in the way of even qualitative conclusions about the effect of all this on the important issues of soil moisture or precipitation which strongly influence crucial human activities such as agriculture.

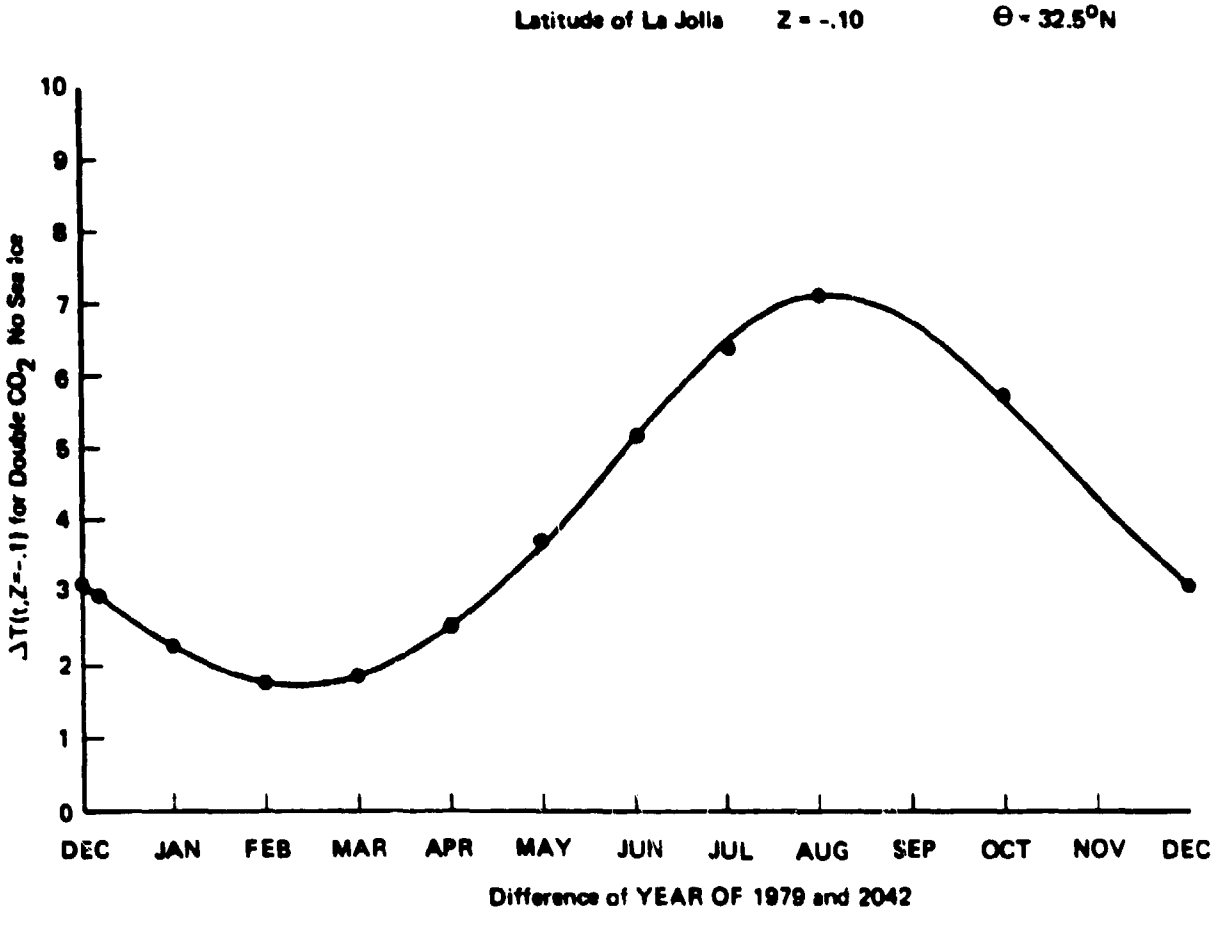

Figure 3.2.4.2 THE SEASONAL VARIATION OF THE TEMPERATURE CHANGE AT THE LATITUDE OF LA JOLLA, CALIFORNIA, AS A RESULT OF DOUBLING THE CO_2 AND REMOVING THE SEA ICE.

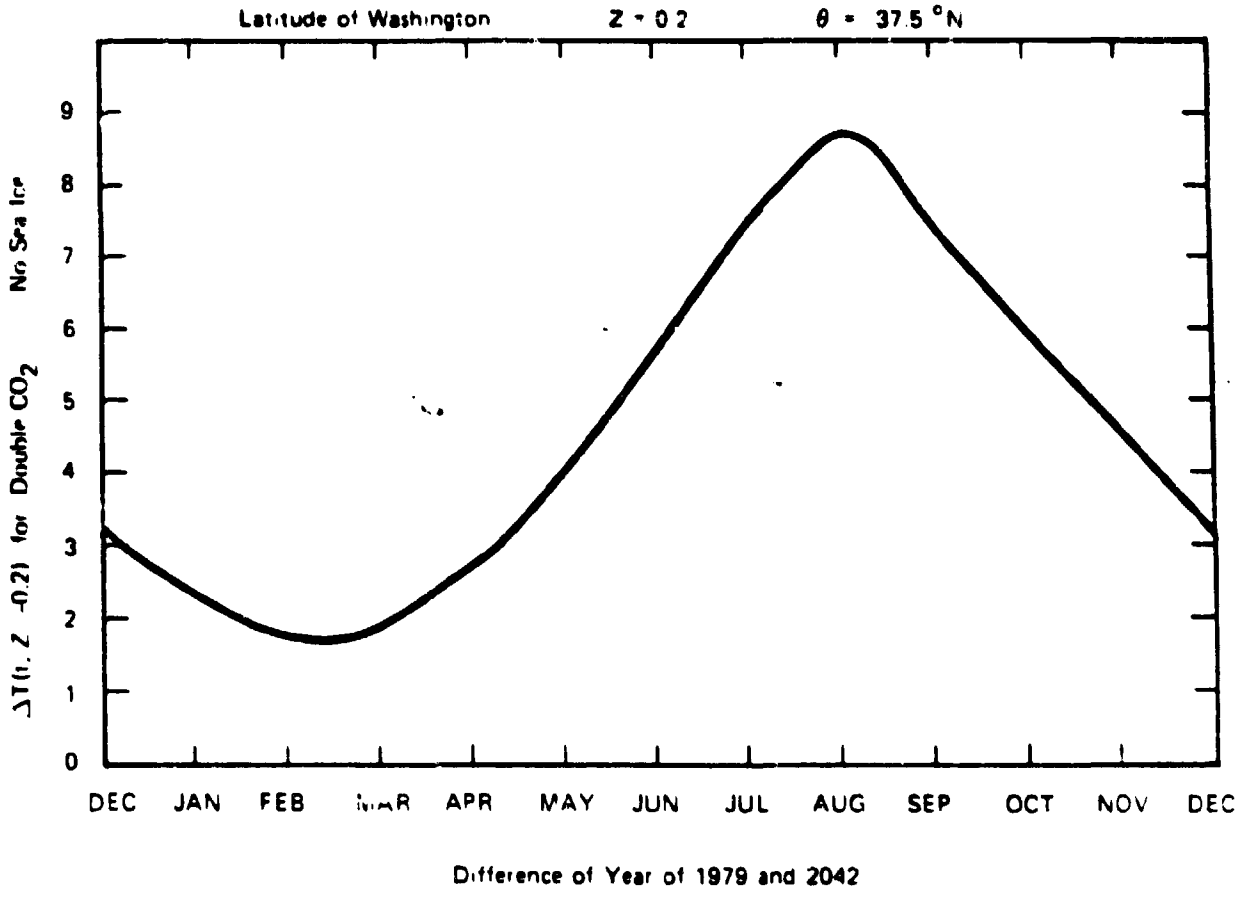

Figure 3.2.4.3 THE SEASONAL VARIATION OF THE TEMPERATURE CHANGE AT THE LATITUDE OF WASHINGTON, D.C., AS A RESULT OF DOUBLING THE CO_2 AND REMOVING THE SEA ICE

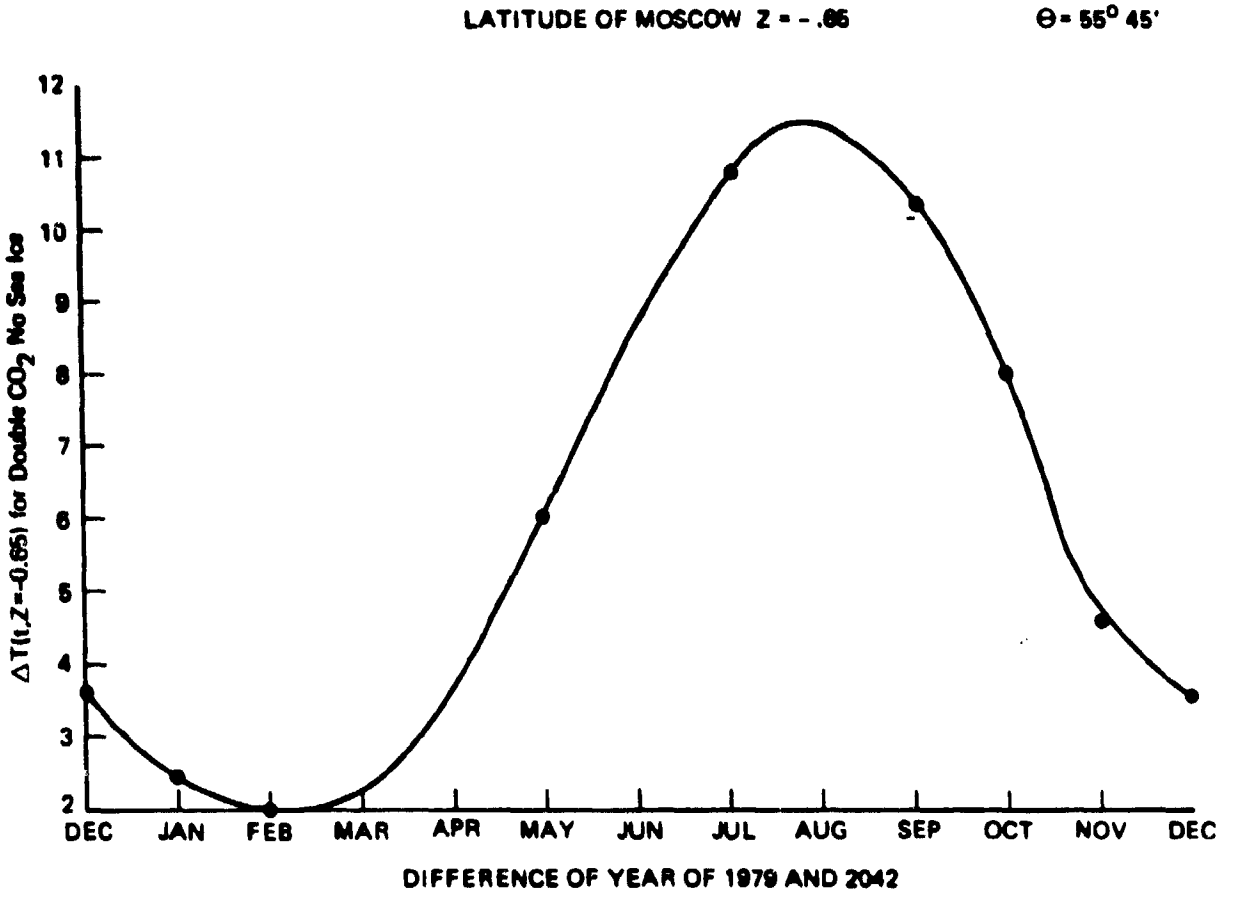

Figure 3.2.4.4 THE SEASONAL VARIATION OF THE TEMPERATURE CHANGE AT THE LATITUDE OF MOSCOW, U.S.S.R., AS A RESULT OF DOUBLING THE CO_2 AND REMOVING THE SEA ICE.

REFERENCES FOR SECTION 3.2.4

1. North, G.R. and J. A. Coakley, Jr., "Differences between Seasonal and Man Annual Energy Balance Model Calculations of Climate and Climate Sensitivity", J. Atmos. Sci., 36, July, 1979.

3.3 Comments on Various Approaches to Modeling the Earth's Climate

The work reported on the JASON Climate Model is one of many attractive and fruitful approaches to the study of climate. Earlier in this report we have given a kind of hierarchy in terms of the number of dimensions of space explored by the models. Here we make some comments on several kinds of climate models: (I) General Circulation Models--three dimensional computer codes which attempt to predict in detail the temperature, pressure, wind, cloud cover, precipitation, etc.; (II) Energy Conservation Models (ECM)--one or two dimensional models, such as the JCM, which express energy balance in terms of temperature alone; (III) Stochastic Climate Models (JCM)--zero dimensional models which treat climate as a Brownian motion of long time scales buffeted about by weather--a short time scale phenomenon.

(i) General Circulation Models (GCM) are the most ambitious attempt to compute the behavior of fundamental climate variables: pressure, temperature, wind, precipitation, etc., from the basic equations of motion and state. They have reached a point of impressive sophistication including an ocean with heat capacity for the mixed layer, snow and rainfall, cloud formation, and other such complicated phenomena. There is no doubt that these models represent the most interesting a priori attempt to evaluate the important set of climate variables. GCMs, however, suffer from several drawbacks. Among them are these: (1) in order to actually carry out the numerical computations required, it is necessary to make a grid (typically 500 to 1000 km on a side for the largest grids) within which all climatological phenomena are represented by spatially averaged

physical parameters. This grid size is large compared to important atmospheric phenomena, so many details are wiped out from the start. Also, numerical instabilities arising from the method of solution of the different equations on the lattice of grid sites limits the credence of the output. (2) The climate system is an impressive non-linear mathematical problem. Recent studies of non-linear classical systems have revealed that when the number of degrees of freedom is large (three is often large enough) the detailed motion of any degree of freedom is extremely chaotic.[1,2] Even though the system is deterministic it can be described as effectively stochastic or random. Clearly the climate system can be expected to exhibit this "intrinsic stochasticity" with a vengeance. If the fluctuations intrinsic to the equations of evolution of the climate system are indeed severe, one should contemplate averaging the dynamics over both space and time to reduce the severity of the problem. Such a reduction is inherent in the energy conservation models and the stochastic models below. (They are perhaps over averaged.) Some intermediate model between the GCMs and those over-simplified models are perhaps what is called for. (3) The amount of input data ($\sim 10^6$ pieces of information), the amount of coding, and the length of time to run one realization of a GCM make it a very difficult tool for probing variation of climatological parameters such as CO_2 concentrated extent of ice lines, insolation, etc. Each variation results in a lengthy and expensive calculation. The general variation of pressure, temperature, etc., are hard to predict because of the complicated dynamics involved. Finally, after the calculation is done, the intrinsic stochasticity and numerical problems with the calculation leave the user of the results with an uneasy uncertainty about what is provided.[3,4,5,6]

(ii) Energy Conservation Models (ECM) study the highly parametrized distribution of energy through the climate system by expressing each complicated phenomenon (IR radiation and atmosphere, transport, insolation and albedo changes, transport of energy by ocean currents, wind, and latent heat,...) in terms of one or a few basic functions of space and time. In most models this function is the temperature; this is certainly the case with the JCM treated in detail in Section 3.2.

These ECMs treat the density of energy which is the only quantity thought to be singled out in non-integrable classical systems. This is a virtue and puts some believability in the results. The ECMs, however, generally suffer from an absence of a fundamental understanding of the parameters entering them. In the diffusive transport models like the JCM, for example, the use of a simple diffusive term scaled by an overall constant is believed by no one to be an accurate representation of ocean currents, latent heat fluxes, etc. What this warning means is that one should forbear from asking these parametrized ECMs to give more than a 30% to 50% correct answer for, say, the temperature in Chicago in October. Absent are local effects (e.g., Lake Michigan), a good hydrological cycle, a real treatment of cloud, and other serious matters. Nonetheless, one may believe the sign and magnitude of effects predicted by such models. There will be significantly larger ΔT in Moscow than in La Jolla when the CO_2 is doubled. Perhaps ΔT in Moscow in August will only be 5-7°C, rather than the 11°C indicated by the JCM calculations presented here. However, the trend and general size of the effects are likely to be cor..e

A real virtue of the ECMs--one which tends to blind the practitioners to its faults--is the simplicity of the equations formulating the models. With such simplicity, one is able to easily change parameters and rapidly probe the answers to numerous interesting questions--many of significant social import. Infrequently, after enough idealization, one can do these probes analytically, but the ease and speed with which one can extract numerical results makes analytic results an amusing sideline.

To repeat: one should use these ECM results as an indicator of directions and magnitudes of responses of a climate system to alterations in its input. Using ECM results in conjunction with the more comprehensive GCM calculations will improve the quality and utility of both.

(iii) Stochastic Climate Models (SCM) are based on an idea of Hasselmann.[7] One treats the climate as the motion of the climate system (earth-atmosphere-cryosphere-ocean-biosphere) on long time scales while shorter time scales, called weather, are treated as a random driving of the slow motions. The analogy with Brownian motion is direct and made quite explicit in the papers.[8] With weather considered gaussian noise, the formalism becomes identical to that used in the study of the Langevin equation for Brownian motion. Since climate is driven by a stochastic force, it is stochastic itself. In computing correlation functions of climate variables (for example, autocorrelations of sea surface temperatures) one has three input parameters: (1) the time scale on which the weather acts--this is taken to be zero, relative to climate time scales; (2) the strength of the weather driving force; (3) the decay time of the

climate system after being "bumped" by the weather. With this much freedom some data on sea surface temperature autocorrelations has been impressively fit.[9,10]

It seems to us that the real use of SCMs is to give an indication how much of climate variability arises from the inevitable averaging process used in extracting the "climate" from the "weather" and how much is really intrinsic to climate dynamics. This will allow climatologists to focus on the dynamical aspects of climate motions rather than try to re-explain weather.

SCMs are likely to be deducible by suitable space and time averaging from GCMs. Their connection with GCMs deduced by this kind of averaging will be useful in giving some footing to the value of the parameters they deduce from their limited data. The connection of SCMs with ECMs is ad hoc as far as we can see.

REFERENCES FOR SECTION 3.3

1. Ford, J., "Picture Book of Stochasticity," Topics in Non-Linear Dynamics, (S. Jorna, ed.; Am. Institute of Physics, 1978).

2. Lorenz, E. N., "The predictability of a flow which possesses many scales of motion," Tellus, 21, No. 3, 289-307, 1969.

   Wetherald, R. T., and S. Manabe, "Response of the Joint Ocean-Atmosphere Model to the Seasonal Variation of the Solar Radiation." Mon. Wea. Rev. 100, 42-59 (1972).

3. Leith, C. E., "Predictability of Climate," Nature, 276, 352-355, (1978).

4. Manabe, S., and R.T. Wetherald, "The Effects of Doubling the CO_2 Concentration on the Climate of a General Circulation Model," J. Atmos. Sci., 32, 3-15, (1975).

5. Schutts, G. J., and J.S.A. Green, "Mechanisms and Models of Climate Change," Nature, 276, 339-342, (1978).

6. Gilchrist, A., "Numerical Simulation of climate and climatic change," Nature, 276, 342-345, (1978).

7. Hasselmann, K., "Stochastic Climate Models, Part I, Theory," Tellus, 28, [illegible]85, (1976).
   Hasselmann, K., and C. Frankignoul, "Application to sea-surface temperature anomalies and the monocline variability, Part II," Tellus, 29, 289-305, (1977).

8. Paltridge, G.W., "Global dynamics and climate--a system of minimum entropy exchange," Quart. J. R. Met. Soc., 101, 475-484, (1975).

9. Gates, W.L., and K. Hasselmann, "The Influence of the Ocean on Climate," WMO Publication #472, WMO-Geneva, (1977).

10. Reynolds, R. W., "Sea Surface Temperature Anomalies in the North Pacific Ocean," Tellus, 30, 97-103, (1978).

(This page left blank intentionally)

4.0 SOME CONSEQUENCES OF MAN'S CHANGING THE COMPOSITION OF THE ATMOSPHERE

An increased carbon dioxide concentration in the atmosphere is equated by many scientists and policy makers with the "greenhouse effect," that is, a warmer planet. As we emphasized, climate is much too complicated to be described solely by average surface temperature or changes in temperature at various latitudes. Changes in climate will alter the biosphere, both terrestrial and marine, by changing temperature, precipitation, length of the growing season, etc. Further changes in concentration of carbon dioxide can alter the biosphere as has been discussed in Sections 2.2 and 2.5.

In this section we briefly comment on several consequences of man's activities that change atmospheric composition. The use of models to predict climate is discussed in Section 4.1. The changing temperature and the latitude dependence of these changes affects the distribution of sea ice and as a result a component of the oceans' circulation with major implications for the marine biosphere. These questions are taken up in Section 4.2. As the earth warms with the warming accentuated at high latitudes, melting and disintegration of the "permanent" ice sheets can be expected. In Section 4.3, we consider the impact of the warming on the most vulnerable part of the Antarctic ice mass, the West Antarctic ice sheet which is grounded below sea level. Both the change in climate and the change in the carbon dioxide content of the atmosphere will affect the

biosphere. Section 4.4 briefly notes the anticipated effects which, we emphasize, are poorly understood.

4.1 CO_2 Atmospheric Modeling and Climate Prediction

4.1.1 Introduction

The situation with respect to atmospheric models and predictions on this question is essentially as follows. There exist a number (~10) of more or less independent model calculations of some aspect of the CO_2-Climate question, with differing results. While all agree on the sign of the temperature response and on its general magnitude, there is considerable disagreement on other climate features, and indeed on what are the dominating factors. Only two or three incorporate even crudely the actual dynamics of the atmosphere acting in response to physical laws; the others simulate the effects of dynamics by gross simplifications, e.g., global circulation simulated by heat diffusion. In the simplest models conservation of energy and certain optical atmospheric properties are included, but not much else.

From the cruder models we can expect to extract only very simple properties of the climate, such as average global temperature increase $\overline{\Delta T_s}$. $\overline{\Delta T_s}$ is the space and time average of $\Delta T_s(x,t)$. For this not much more than energy conservation and some assumptions about average albedo and IR emission is needed. With increasing complexity in the model more detailed atmospheric properties can be predicted. The level of required inputs for various outputs can be tabulated.

Output	Minimum Requirements
(i) $\Delta\bar{T}_s$	Energy input, average albedo and IR emission
(ii) $\Delta T_s(x,t)$seasonal, $\Delta\bar{T}_s$ latitude	Seasonal solar input, albedo vs latitude and IR vs latitude (actually temperature), the latter gotten empirically or by analysis of a radiation model.
(iii) Changes in precipitation, humidity, wind patterns, etc.	Global circulation, correct thermodynamics, radiation theory and ocean coupling

The degree of arbitrariness still allowable in the parameterizing even among one dimension models is large. Typically each such model has been selected to emphasize one or more sensitive "feedback" mechanisms to the neglect of others.

The more elaborate GCM models contain their own special assumptions, as with respect to changes in cloud height, stability and lapse rate, optical properties of clouds and ice, etc., which may make for quite different climate predictions with increased CO_2 concentration. In assessing the elaborate models and in trying to understand their different predictions, it is important to learn the sensitivity of the predictions to

these assumptions or assigned properties. Here the one dimensional models may be helpful, as in some cases the sensitivity to particular model features can be tested directly. Thus for any climate feature $K[\text{conc.}, T_s(x), \text{etc.}]$ we can define a sensitivity α_k such that $\Delta K = \alpha_k \frac{\Delta [CO_2]}{[CO_2]}$. By examining the value of α_k for a series of models some idea of the relative importance of a special feature (e.g., cloud height variation) can be gained.

One reason for the necessity for such indirect methods to analyze the structure of an elaborate GMC output is the inability, so far, to develop perturbation methods to treat small effects in all but the most primitive models. (The use of differential notation in the formula above for ΔK does not imply that we can construct the implied derivatives.) Thus for the "doubled CO_2" investigation the complete calculation is performed twice, for the two different $[CO_2]$ values. (It is not clear that intermediate values are given by linear interpolation.) Evidently the strong interaction between the various feedback mechanisms makes it difficult to construct a perturbation procedure.

4.1.2 Atmospheric Feedback Sensitivities

We examine the sensitivity of climate properties, particularly $\Delta \bar{T}_s$, for a given input $[CO_2]$ to the following feedback mechanisms:

A. Base Case--no feedback

B. H_2O vapor density

C. Amount of cloud cover

D. Ice Cap albedo variation

E. Cloud height

We imagine here that the CO_2 concentrations are given; not included are such effects as the additional plant absorption of CO_2 with photosynthesis increasing with the concentration of CO_2, or the additional emission of CO_2 from soils or methane hydrates in a warmer climate.

Additional "feedbacks" on climate are:

F. The effect of the breakup of icebergs into smaller floating units over a large area, nearer the equator, in increasing the net ice albedo. The possible magnitudes and time scales are unknown.

G. The effect of the loss of sea ice in reducing the sea currents from polar regions to the ocean deeps, allowing the oceans to warm and drive out CO_2. The time scale is probably long.

As we have emphasized throughout this report, $\Delta\bar{T}_s$ is a poor description of world-wide climate change, certainly of the effects of most consequence for human life; it represents, however, a relative measure of CO_2 effects between models. For the cruder models it is the only result with much credibility.

Actually there have been more detailed studies of the sensitivity to small increases in solar radiation than of changes in CO_2. In a series

of papers, Cess[1,5,7] has studied these questions in detail, and we will be guided by his analysis. We will argue that the effect of increased solar input, which primarily warms the ground, and increased CO_2 density, whose absorption and emission increases the insulating effect of the atmosphere, are governed by the secondary feedback effects--cloud cover, etc., —in much the same way, at least sufficiently to enable us to judge the relative importance of different feedbacks. Clearly there will be some real differences between these two cases; CO_2 increase has cooling effects in the stratosphere, which will affect the IR emission and conceivably affect global transport--no such effect is produced by an increase in insulation.

As a matter of fact, a certain degree of "calibration" of these two effects can be attempted. The Manabe and Wetherald[2] one dimensional model (1967) and their (1975)[3] three dimensional model both yielded results for $\Delta\bar{T}_s = \alpha\frac{\Delta[CO_2]}{[CO_2]}$ and $\Delta\bar{T}_s = \alpha\frac{\Delta S}{S}$. The ratios in each case were such that a 1.6% increase in insulation is equivalent to a doubling of CO_2. The JASON model (see Section 3.2) is in agreement with this ratio. Actually, we will use this parallelism only to indicate the relative importance of the various feedbacks in the CO_2 problem.

A. Base Case--no feedback. The average IR flux is represented by $F = \varepsilon\sigma T_s^4$ and the average solar input by $\frac{S}{4}(1-a)$, where $S = 1360\ w/m^2$ and a is average albedo. If ε and a are independent of T_s then from energy conservation we have for the sensitivity $\lambda = \frac{\partial T_s}{\partial S} S = T_s/4 = 70^\circ$ or 0.7° increase for a 1% change in S . All other results can be compared with this "base."

B. Variable H_2O Vapor. If we fix humidity at 50%, allow no change in cloud cover or height or in total ice reflection, this corresponds to the Manabe-Wetherald[2] 1D model, from which $\beta = 130^0$. We note that the Budyko[4] "empirical" formula for IR flux $F = A + BT_s$ presumably contains several physical effects, but for fixed cloud and ice cover it may correspond to these same conditions. It gives a value $\beta = 160^0$.

C. Variable Cloud Cover. This provides two feedback mechanisms of opposite sign, (i) the "greenhouse" effect of added cloud cover, and (ii) the reduced solar flux onto the ground. Cess[5] has examined these effects in detail, each of which turns out to be quite large. According to Cess, however, the effects almost cancel on an average global basis. He gets an overall sensitivity of 145^o, about the same as in (8). In this investigation, two other effects of interest were explored. To assess the feedback the connection between amount of cloud A_c and surface temperature T_s must be found. In spite of the "intuitive" guess of most people that dA_c/dT_s is positive, from a careful study of satellite data Cess found $dA_c/dT_s \tilde{=} -0.02$. This required a rather indirect argument in which the important variation of cloud albedo with zenith angle must be sorted out first. He also finds, not surprisingly, that at high latitude the IR greenhouse effect, on an annual average, considerably dominates over the weak albedo effect of solar input. Thus there is a

considerable positive effect of cloud variation in polar regions. We note here, to be dis-cussed in Section 4.1.4, that much of the heat input to polar regions, annually, comes from the atmospheric and oceanic flow olewards from regions of high solar radiation. (Near summer solstice, of course, the direct solar input greatly exceeds this convectional flow of heat.)

D. Ice Cap Albedo. In the early model calculations this has evidently been regarded as the single most important feedback mechanism which governs the global temperature response to changes in solar radiation. In the early Budyko[4] and Sellers[6] models it is the only explicit feed-back included. Subsequent calculations, of course, include several of the feedback factors discussed here, especially the elaborate Manabe and Wetherald[3] analysis of the effect of solar radiation increase. One way to examine the relative importance of ice albedo is to find the increase in $\alpha = S\frac{dT_s}{dS}$ due to the inclusion of this factor over the value of β from the same model without such inclusion (Cess). The Budyko result, based on empirical modeling of the temperature dependence of cloud albedo and IR flux yielded an increase factor in α of 158%. This was criticized by Cess, however, for not taking into account the strong cloud albedo dependence on sun zenith angle in the empirical modeling, which gives a large false apparent temperature dependence from the albedo-latitude data. Correction for this effect

from modern satellite data, according to Cess, brings the ice albedo increase in α down to 25%. This then agrees with the value of 27% increase from the Manabe-Wetherald[3] model referred to above. On the other hand, the Sellers model, which employs a step function increase in albedo at the "ice line" latitude gives an ice albedo increase in α of 117%. Evidently the use of a step function ice albedo gives a very much larger effect than do other quite plausible calculations. (See Section 4.1.4.)

E. Cloud Height. The effect of this potentially important feedback mechanism has not yet been analyzed very fully. In the GCM type calculation of Manabe and Wetherald[2] the cloud altitude distribution was kept fixed. For an increase in solar radiation this means the cloud tops are warmed as the general atmosphere is warmed, and thus they radiate more strongly. Many clouds are essentially opaque black bodies; if the atmosphere above them is quite transparent the IR radiation to outer space is then governed by the cloud top temperature. In fact, the assumption of fixed cloud height in Manabe-Wetherald[2] resulted in a small <u>negative</u> feedback factor (0.85), according to the analysis of their work by Cess[5,7]. With increasing surface temperatures one may expect that the enhanced humidity will extend the (moist) adiabatic lapse region to higher altitudes, with a resulting equilibration of clouds at higher altitudes. In one limiting model the cloud top temperature remains constant, with a

marked resulting positive feedback. According to Cess, the assumption of constant cloud temperature in the MW model would give a feedback factor of 1.6, which would then give an overall sensitivity $\alpha = 185^0 \frac{1.6}{0.85} = 340^0$. This is not very conclusive; it appears that only a calculation that incorporates a dynamical theory of cloud formation can be expected to clarify this important question.

Summary of Sensitivities

There seems to be agreement among the models that, in the absence of ice-snow albedo variation, and with fixed relative humidity, cloud amount and altitudes, a 1% increase in insolation will produce a global temperature rise of about 1.5^o. This is true of the semi-empirical models (Budyko) as well as the elaborate GCM models. Including the ice albedo and its feedback by melting results in greater divergence among models; the Budyko model (uncorrected) gives a very large effect, most of the others giving a modest 25% additional positive feedback. (The "corrected" Budyko, see above, is in fair agreement with other calculations.) The sensitivity to varying cloud cover is not well established. There may indeed be a near cancellation of albedo and greenhouse effects here, but not in polar regions (see Section 4.1.4). Cloud height is a potentially important factor, but very likely only a theory that shows what the clouds do will clarify the situation.

Depending on this last factor the predicted rise in temperature for a 1% increase in insolation is in the range 1.8^o to 3.4^o, the upper value probably rather extreme.

There are other important factors that influence climate which are even less well understood than those discussed here, among them the effect of seasonal oscillation and the complex subject of the role of convection and stability at various latitudes and in different climate conditions. These questions will be of importance in the problem of high latitudes and the polar regions, and we will discuss them, as best we may, at that point.

4.1.3 CO_2 Model Predictions

There have been about a dozen "modern" model-calculations of the effect of doubling CO_2, running through the spectrum of models from one dimensional energy balance estimates to recent attempts at full three dimensional calculations which include atmospheric dynamics. In the latter, quantities such as ice and snow, humidity, cloud formation and altitudes are not input parameters but are <u>calculated</u> outputs. While the very simple models, guided by observed input data are useful for estimates of a few variables such as global temperature rise, probably only the latter more complete theory can be expected to yield reliable statements on the variation of CO_2 effects with latitude and season, not to mention precipitation and other climate effects. There have been excellent reviews of this subject by Schneider[8] and Watts[9] on which we will draw freely. Note that the actual temperature rise ΔT_s is related to the "sensitivity" index $\alpha = \frac{dT_s}{d[CO_2]}[CO_2]$ by $\Delta T_s = \alpha \log 2$.

Here we will describe these models briefly, and give the predicted global temperature rise for CO_2 doubling from each of them. This is equivalent to the sensitivity parameter $\alpha = \frac{dT_s[CO_2]}{d[CO_2]}$ in each case.

A. Energy Balance Models. The prototype is the Budyko[4] calculation of the effect of changing insolation. (The JASON climate model is of this type.) There is one space dimension--latitude, and the atmosphere is parameterized by IR and albedo functions which are usually written as linear functions of temperature. Cloud cover and ice extent are input quantities, which may be taken to be functions of temperature. The IR flux and cloud albedo are empirical, following Budyko and the later improved values of Cess[5], in agreement with satellite observa-tions. Horizontal circulation is simulated by heat diffusion type expressions, with diffusion constants adjusted to describe present conditions. For the CO_2 problem these empirical functions must be adjusted to new values for the doubled CO_2 density. Subtleties such as the stratospheric cooling by CO_2 can hardly be incorpo-rated in these models. (For these latter reasons these models are probably better suited to describing changes in insolation than in composition of the atmosphere.) (i) JASON (1978) Climate Model. Here the CO_2 effect in IR emission and absorption is obtained by calculating the change in "overall optical path length" from CO_2 doubling, treating the atmosphere as a uniform "grey" absorber. To relate this absorption to the ground temperature the lapse rate is taken to be that of pure radiative equilibrium (no convection). The other properties, albedo, heat flow, are taken empirically. This model also

gives latitude variation of ΔT_s , and with the correct solar radiation input can yield seasonal changes, described in Section 3.2. The global temper-ature rise, for CO_2 doubling is $\bar{\Delta T}_s = 2.4^0$. (ii) Ramanathan,[11] from such an energy balance model, has obtained, with fixed cloud altitude $\bar{\Delta T}_s = 2.2^0$ but with fixed cloud top temperature $\bar{\Delta T}_s = 6.3^0$. (iii) It is also reported[9] that Cess, from a Budyko type model but with new radiation-temperature relation, has obtained $\bar{\Delta T}_s = 3.3^0$.

B. One Dimension Radiation-Convection Models. At an "average" location the atmospheric radiation processes are treated in some detail. Various assump-tions are made as to cloud cover and height and humidity. Care is presumably taken to use the correct lapse rate, radiative or convective, at each altitude. We note that the stratospheric cooling by CO_2 seems to have a pronounced effect on infrared feedback, and its inclusion gives a marked increase in $\bar{\Delta T}_s$. (i) Rasool and Schneider[10] assumed a fixed humidity, cloud structure, and lapse rate, and omitted strato-spheric cooling, hence obtain a small $\bar{\Delta T}_s = 0.8$. (ii) Manabe and Wetherald.[2] A careful treatment of radiation-convection relations, includes stratospheric cooling but assumes fixed humidity and cloud distribution obtain $\bar{\Delta T}_s = 2.4^0$. (iii) Ramanathan[13] fixed humidity and clouds, different IR radiation assumptions from Manabe-Wetherald (above) $\bar{\Delta T}_s = 1.5^0$. (iv) Augustsson and Ramanathan.[12] Similar

to above, but including the weaker CO_2 bands $\bar{\Delta T}_s = 1.98^0$ but if cloud <u>temperature</u> is constant, then $\bar{\Delta T}_s = 3.2^0$.

C. Three Dimensional GMC Models. These calculations, in principle, attempt to construct a description of climate, starting from such basic input data as insulation, atmospheric composition, land and water geography, IR radiation theory, optical properties of air and clouds and surfaces. An approximation to the real equations of motion and thermodynamics is integrated to a (presumably) unique steady state. This integration is accomplished on a grid with simulated geography. Of order ten vertical levels are employed. Actually in the results published to date, some of the climate features as humidity or cloud distribution are, in fact, inserted as inputs. The only completely pub-lished and analyzed CO_2 calculation to date is that of (i) Manabe and Wetherald.[3] Cloud amount and cloud height distributions are prescribed and are held fixed in this calculation. Evaporation and humidity are calcu-lated from the insolation and wind flow, as are snowfall and rainfall. A region of permanent icecap is defined by an isotherm which varies as CO_2 increases. The ocean serves as a source of water vapor only and has no heat capacity. No transport of heat by ocean currents is allowed for. This latter is probably the most serious defect of this and the other GCM models employed to date. The resulting temperature rise is $\bar{\Delta T}_s = 2.93^0$. Other results of this model will be dis-cussed later. We

note here that an average (steady) insolation function is employed, so no seasonal effects are present. (ii) Hansen GISS Model.[13] Besides a more detailed land and water geographical input this differs from Manabe and Wetherald[3] as follows:

(a) Cloud formation in convective rising and cooling is calculated, so amount and height distribution is not an input.

(b) Condensation and optical properties of clouds are also calculated (assuming 10m drop size).

(c) The oceans are given the 70m depth heat capacity of the mixing layer.

(d) Daily and seasonal solar variation is employed. The CO_2 doubling sensitivity of global temperature is $\Delta\bar{T}_s = 4.5^0$. The reason for this high value is not fully understood but it may very well be the relaxation of the cloud height restriction to allow ascent to cooler regions. In this model the clouds may more nearly approx-imate to constant temperature. We recall that in Section 4.1.2 it was seen that between constant height and constant temperature there was a factor of some seventy percent. Compared with Manabe and Wetherald, the Hansen value is within this range.

4.1.4 CO_2 Effects in Latitude, Seasons, and Polar Regions

Predictions of climate change will be determined, in the first place, by the variation of temperature with latitude and with seasons.

Unless we can predict these driving forces in a satisfactory way, we can hardly expect to make reliable statements about precipitation, arctic ice melts, regional shifts in aridity, etc.

Annual average latitude variation $\overline{\Delta T}_s(x)$ from CO_2 doubling from the Manabe-Wetherald[3] and the recent Budyko[11] results is shown in Figure 1. (The latter is an application of the old Budyko model[4] to the CO_2 problem.) The rise in $\overline{\Delta T}_s$ at high latitudes is marked in both cases, amounting to as much as 10^o, in comparison with the average value of about 3^o. On the face of it, this rise seems to be a direct result, as a feedback, of the loss of ice albedo by melting. (A similar latitude effect was found in the Budyko's 1969 evaluation of the effect of increased insolation.) This picture has changed somewhat as a result of analysis of the recent GCM results, Manabe and Wetherald[3,5], and re-appraisal of the Budyko parameterization by Lian and Cess[15] and Watts[9] as follows:

A. The re-evaluation of cloud albedo by Cess,[5] in particular the realization of the importance of zenith angle on cloud albedo led Lian and Cess[15] to re-evaluate the ice albedo function of Budyko. As was discussed in Section 4.1.2, this led to a reduction in the global temperature sensitivity to ice albedo to a modest 25%. Watts[9] has applied this new albedo function to the Budyko model, and finds that the rise in ΔT_s at high latitudes is reduced to about 1^o.

B. The GCM results do not make use of empirical albedo inputs, thus the predicted rise of ΔT_s is not subject to this same criticism. In the opinion of the authors the ice albedo effect makes only a modest contribution to the Manabe-Wetherald predicted rise in ΔT_s with lati-tude. They point out that the occurence of "radiation stabilized" atmospheres at high latitudes is a more important factor. Such a stabilized atmosphere (no convection) conducts heat from the surface more poorly than does a convecting atmosphere. This enhanced green-house effect is found in colder and dryer regions. In addition, the sharp rise in temperature near the surface in the stabilized profile even gives a somewhat spurious effect, as the large ΔT_s values are surface tempera-tures, and not representative of the whole troposphere. The introduction of convection mixes the troposphere, not only transporting heat thereby, but also reducing the thermal gradiant in the troposphere. Watts[9] has shown that a vertical average of temperature shows only a mild increase with latitude.

C. In the polar regions there are special problems. Most of the model calculations published so far do not include sea-sonal variation of insolation. While this may not be a serious defect in tropical or temperate latitudes, the huge seasonal variation in polar regions will emphasize non-linearities in the dynamical response and will intro-duce "beats" between solar and albedo oscillations. An elementary example is the

fact that in polar regions when ice albedo is a maximum there is no sun, but 24 hour sun when it is a minimum. A treatment based on "annual aver-age" insolation is not very meaningful. It is also the case that most of the annual heat input into the arctic circle is not solar but comes from heat flow from more equatorial regions. Ice albedo plays no role in this energy flow, nor does cloud albedo, so the quoted near cancellation of it with cloud greenhouse effect, Section 4.1.2, does not apply to this heat flow in polar re-gions. Thus cloud cover variations could be an added feedback effect. With respect to the question of the melting and possible disappearance of the polar ice, the annual average treatments essentially calculate a mean temperature at the pole from energy balance; if it is above some assigned ice melting temperature (0° or -10°) this is interpreted as the disappearance of the ice cap. Only by carrying the system through annual cycles, with latent heat included, can this question be answered. There is the further elementary fact that the melting ice, either in the Arctic Ocean or as glaciers in An arctica, acts as a thermal ballast and ensures that the summer surface temperature stays at $0^{\circ}C$ as long as the ice lasts. The one GCM model which includes seasons and latent heat--Hansen-GISS[13]--does show this effect. The ice does not all melt for doubled CO_2, and summer temperature stays at $0^{\circ}C$.

D. For a climate prediction, the effect throughout the year of a CO_2 increase should be known, in particular the answer to "Is ΔT_s greater in summer or in winter?" The Budyko and JASON models yield the ready answer that in summer the melting ice increases the amount of absorbed solar radiation whose CO_2 greenhouse effect maximizes ΔT_s in summer. In GCM models, as we have seen, ice albedo seems to play a lesser role, and it is less clear when the maximum ΔT_s takes place. The radiation stabilization effect may dominate, and it is stronger and more widespread in winter than in summer. The Hansen-GISS model shows a greater ΔT_s in winter. It will be inter-esting to see whether independent GCM models verify this rather surprising result.

4.1.5 Climate Prediction

The foregoing discussion leaves one with a sense of caution about predictions of the general climate effects of CO_2. A few features are fairly clear: there is doubtless an overall greenhouse effect as CO_2 increases, which will lead to an average temperature rise, probably of order 3°-4°. There is a strong case that this temperature increase will be discernably larger at high latitudes. What actually happens at the poles, including whether a CO_2 doubling makes the ice caps vanish, seems to be quite open at present. We believe that this question can only be resolved by analyses that carry the atmosphere and oceans through the annual cycle. Since an important part of climate description is the seasonal cycle, it would seem that computational effort should be placed in that direction.

In the Manabe-Wetherald three dimensional model[3] one result to which they point, and which stands out clearly, is the substantial increase in the "hydrological cycle"; precipitation increases by about 10% in a band polewards of 40° latitude, with a corresponding increase in evaporation below this latitude. The Manabe and Wetherald 3D evaluation of insolation increase shows the same effect. More important, the recent Hansen[13] GCM model shows very much the same effect. Perhaps we are nearly in a position to make as definite a statement about this poleward shift of rain belt as we can make now about the temperature rises.

We note that the stratosphere warming is a specific CO_2 effect, not found with insolation increases. This will de-stabilize the stratosphere somewhat, perhaps shift the tropopause upward. This, and the effect that stratospheric warming may have on high altitude currents such as the poleward flow of ozone, has not been examined.

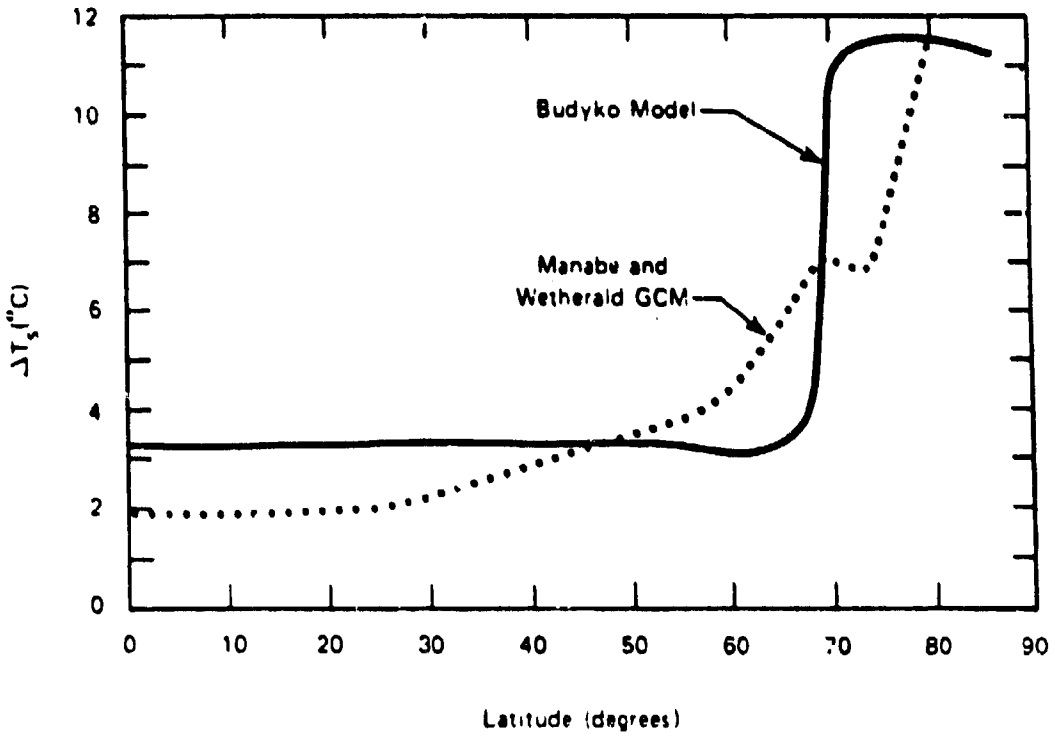

Figure 4.1 ZONALLY AVERAGED ΔT_s FOR A CO_2 DOUBLING MANABE AND WETHERALD AND BUDYKO MODEL[10]

REFERENCES FOR SECTION 4.0 AND 4.1

1. Cess, R. D., "Radiative Transfer due to Atmospheric Water Vapor: Global Considerations of the Earth's Energy Balance," J. Quant. Spec. Rad. Trans., 14, 861, 1974.

2. Manabe, S., and R. Wetherald, "Thermal Equilibrium of the Atmosphere with a Given Distribution of Humidity," J. At. Sci., 24, 251, 1967.

3. Manabe, S., and R. Wetherald, "The Effect of Doubling the CO_2 Concentration with Climate of a General Circulation Model," J. At. Sci., 32, 345, 1975.

4. Budyko, M., "The Effect of Solar Radiation Variations on the Climate of the Earth," Tellus, 21, 611, 1969.

5. Cess, R. D., "Climate Change: An Appraisal of Atmospheric Feedback Mechanisms Employing Zonal Climatology," J. At. Sci., 33, 1831, 1976.

6. Sellers, W., "A Global Climatic Model Based upon the Energy Balance of the Earth-Atmosphere System," J. Appl. Met., 8, 392, 1969.

7. Cess, R. D., "Global Climate Change: An Investigation of Atmospheric Feedback Mechanisms," Tellus, 27, 193, 1975.

8. Schneider, S. H., "On the Carbon Dioxide-Climate Confusion," J. At. Sci., 32, 2060, 1975.

9. Watts, R. G., "Climate Models and the Radiation of CO_2 induced Climatic Changes," Oak Ridge Pub., ARAU/IEA, 78-24, 1978.

10. Rasool, S., and S. Schneider, "Effects of Large Increases in Atmospheric CO_2 and Aerosols on the Global Climate," Science, 173, 138, 1971.

11. Ramanathan, V., "Interaction Between Ice Albedo, Lapes Rate, and Cloud Top Feedbacks: An Analysis of the Non-linear Response of a GCM Model," J. At. Science, 34, 1885, 1977.

12. Augustsson & Ramanathan, "A Radiative-Convective Model Study of the CO_2 Climate Problem," J. At. Sci., 34, 448, 1977.

13. Hansen, J., "Proposal for Research in Global Carbon Dioxide Sink/Budget and Climate Effects," GISS, (1979) to be published.

14. Budyko, M., "The Heat Balance of the Earth," Chapter V in Climate Change, Camb. Univ. Press, 1978.

15. Lian, M., and R. J. Cess, "Energy Balance Climate Models: A Reappraisal of Ice-Albedo Feedback," J. At. Sci., 34, 1058, 1977.

4.2 Deep Ocean Currents and Polar Warming

4.2.1 Deep Ocean Flows

The transfer of water between the surface and deep layers of the oceans has important consequences for earth surface temperatures, and for the capacity of the oceans to absorb CO_2 from the atmosphere. The atmosphere, in turn, affects the oceanic surface layers and thus ultimately the flow of water in all parts of the ocean. We focus here on possible effects on the flow patterns arising from CO_2-induced atmospheric warming, and on some of the consequences of altered flow.

In attempting to analyze the current state of flow one has to face the fact that our fundamental understanding and knowledge of the facts is limited and that the motions are complicated. A very rough sketch of major ocean flows in a vertical plane of the Atlantic is shown in Fig. 4.2.1. The important vertical motions are the following:

1. A downflow to the [illegible] Arctic region, mainly in the Norwegian and Labrador Seas. Estimates of the magnitude of this flow range from 3×10^6 m^3/sec to 30×10^6 m^3/sec.
2. A downflow originating in the Weddell Sea area of the Antartic, with rate, known only very roughly, of about 20×10^6 m^3/sec.
3. A general upwelling though the oceans, with upward velocity of about 4 m/year, balancing the 25 - 50 m^3sec downflow.
4. A southward-moving flow of deep North Atlantic water which penetrates the upper layers of the Weddell Sea in Antartica.

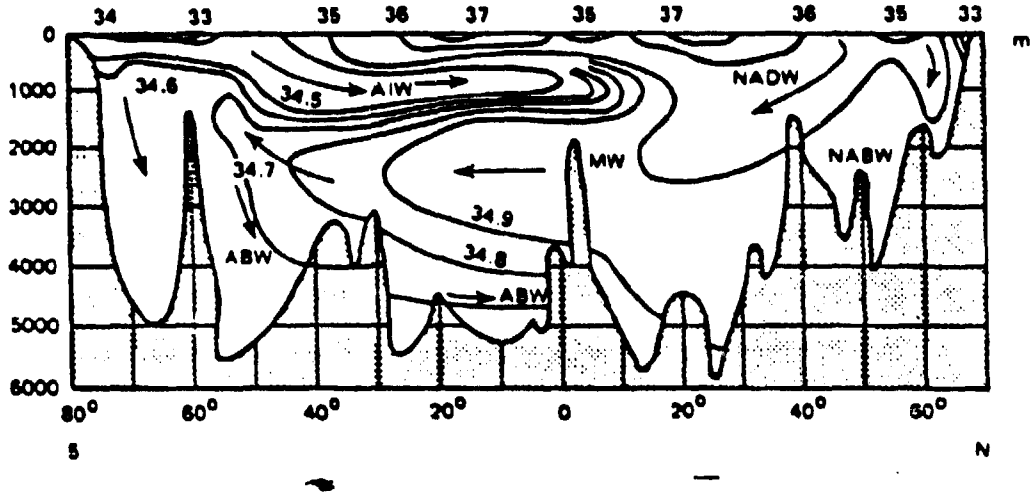

Figure 4.2.1 VERTICAL SECTION OF THE ATLANTIC OCEAN (near 30° W) FROM THE WEDDELL SEA IN ANTARCTICA TO GREENLAND. THE NUMBERS ARE SALINITIES IN MG SALT PER G OF WATER. NADW = NORTH ATLANTIC DEEP WATER, NABW = NORTH ATLANTIC BOTTOM WATER, MW = MEDITERRANEAN WATER, ABW = ANTARCTIC BOTTOM WATER, AND AIW = ANTARCTIC INTERMEDIATE WATER. (From Lamb, Vol I).

4.2.2 Formation of Dense Surface Waters

The chief mechanism (pump) that drives this circulation probably involves the continual creation of polar surface water which is considerably denser than the waters of the underlying layers and which therefore flows the way to the bottom. Density is determined by temperature and salinity, changes in these quantities being related by

$$\frac{\Delta\zeta}{\zeta} = -0.12 \times 10^{-3}\,\Delta T + 0.8 \times 10^{-3}\,\Delta S \quad , \qquad (4.2.1)$$

where T is the temperature in ^{o}C and S the salinity, mg of salt per g of water (0/00). For most of the bottom waters of the oceans T T $\lesssim 1^{o}C$ and S ≈ 34.7 0/00 (see Table 4.2.1).[2] Surface waters obviously cannot be made much colder than this without being transformed into floating ice. (The melting temperature for sea ice is $T_m = -1.8^{o}C$.) But there is scope for increasing the salinity of surface water. This increased salinity seems to be achieved, by district mechanisms, in the South and North Polar seas.

Much of the North Atlantic surface waters are maintained at relatively high salinity by evaporation and by a small influx of the very salty water which flows out of the Mediterranean Sea. Typical parameters for North Atlantic upper layers (upper km) correspond to S ≈ 35.4 (Table 4.2.1). This salinity is larger than that of the South Atlantic and other ocean surface layers and larger than that of bottom waters generally. Owing to its high salinity, the North Atlantic surface water becomes dense enough to sink wherever the temperature is sufficiently small ($T \lesssim 4^{o}C$). The cooling needed to accomplish this seems to be achieved in the Artic seas, so that water moving into this polar region and then back into the Norwegian Sea then drops to the ocean bottom (see Fig. 4.2.2). As said, surface waters in the southern oceans and in the North Pacific are less salty than for the North Atlantic. For the former surface waters S ~ 34.7, about the same as for bottom water; and near Antarctica, in particular, the surface salinity is typically even smaller. In this region, however, two circumstances combine to produce bodies of cold and salty water, dense enough to flow to the bottom even after entrainment of

Table 4.2.1

Some Ocean Water Temperatures and Salinity[2]

Deep Water	T(°C)	S(°/oo)
Atlantic Artic Bottom	0.0	34.7
Labrador Sea Bottom	3.3	34.9
Antarctic Deep Circumpolar (3 km)	1.5	34.74 (max)
Antarctic Bottom (5 km)	0.6	34.7
Surface (upper km)		
North Atlantic	12.0	35.4
South Atlantic	8.0	34.7
North Pacific	10.0	34.4
South Pacific	10.0	34.7
Mediterranean Efflux	12.0	38.5

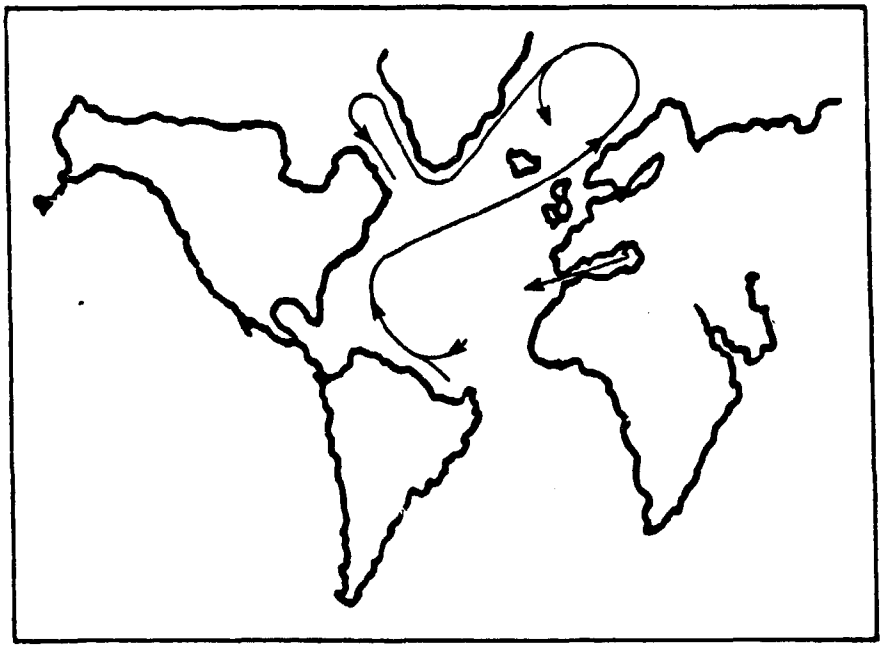

Figure 4.2.2 MAIN SURFACE CURRENTS OF THE NORTH ATLANTIC

less saline, ambient water. For one thing, a large amount of sea ice is formed each winter and melted each summer around the Antarctic continent (cf. Figs. 4.2.3 and 4.2.4). Eighty-five percent of the Antarctic ice pack melts and is refrozen each year. The new ice covers an area of $\sim 15 \times 10^6$ cm^2, with an average thickness of ~ 1.5 m. Since ice contains very little salt, the residual water is very briny, hence dense, that it can drop to the bottom. A salinity equal to that of bottom water is achieved when the brine is mixed with a volume V of ambient, near-surface water, with nominal salinity $S = 34.0$, such that

$$V = \frac{1.5\text{m} \times 15 \times 10^{12}\text{m}^2}{34.7 - 34.0} \times 34.0 \sim 1 \times 10^{15}\ \text{m}^3 \quad .$$

If all of this cold surface water were to flow to the ocean bottom it would contribute an abyssal flow of 30×10^6 m^3/sec. (Dilution of this flow with less saline water on the way down would bring in water less saline than that at the bottom so that the abyssal salinity could not be maintained.)

The above mechanism for production of dense, sinking water in the Antarctic region probably cannot work without special oceanographic and geographic features. Although the formation of sea ice surely leaves behind residual salt, the brine must not mix with too much ambient water, since the final salinity must not drop significantly below that of bottom water if the diluted brine is to reach the ocean floor. The above estimate would restrict the mixing to less than about 100 m of subsurface water and it is hard to see why the mixing would be so limited for waters so far above the ocean floor. There is wide support, instead, for assigning the

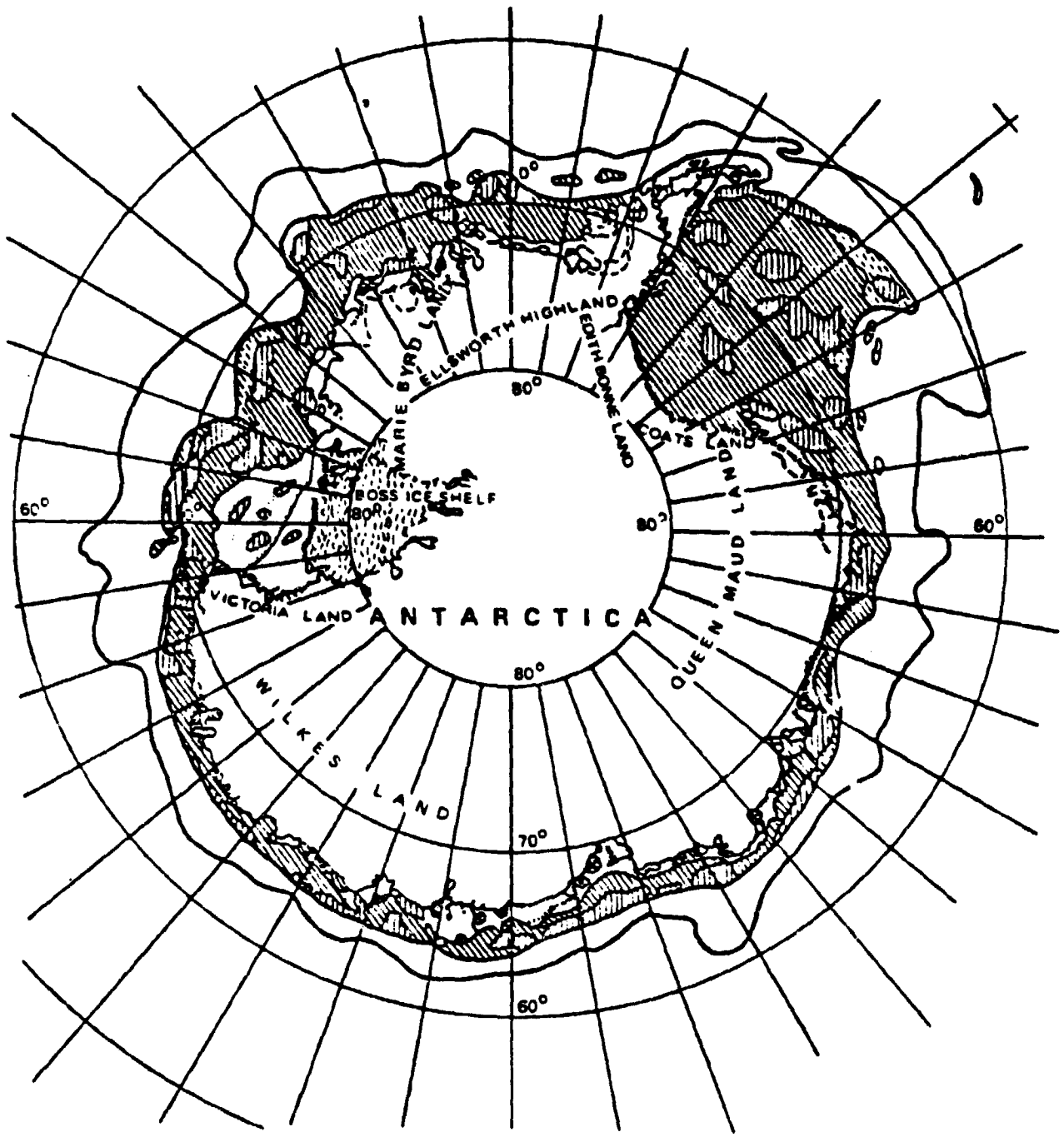

Figure 4.2.3 ANTARCTIC SEA ICE IN FEBRURAY. (POLAR REGIONS ATLAS)

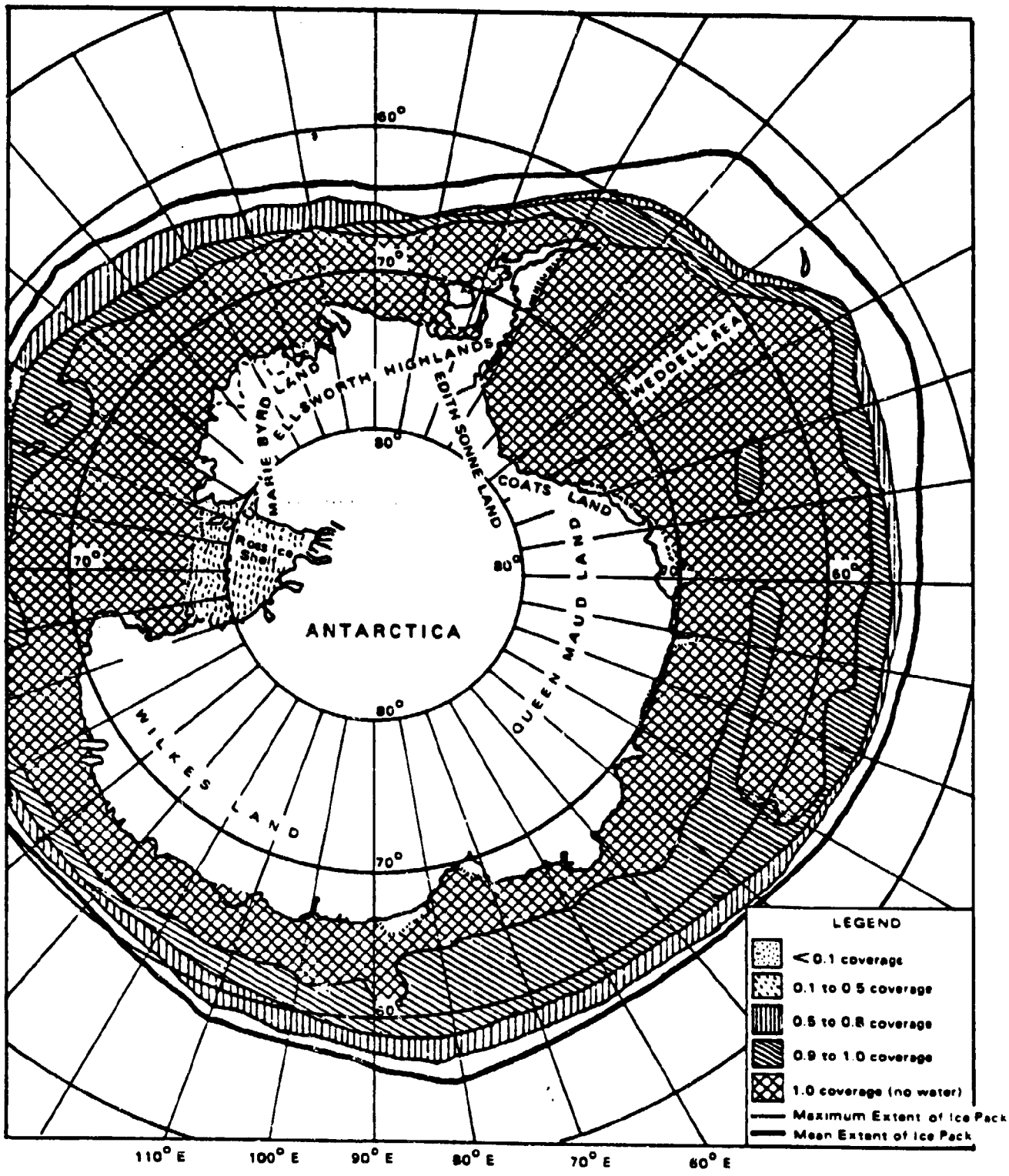

Figure 4.2.4 ANTARCTIC SEA ICE IN OCTOBER (POLAR REGIONS ATLAS)

manufacture of downflowing salt water to a more restricted region: the continental shelf area of the Weddell Sea. The area of the shelf there is about 10^6 km^2, and the depth below sea level is typically a few hundred meters. This region of ocean is reached by a rising layer of deep, North Atlantic water, with salinity $S_o = 34.25$ which is higher than that of most of the surrounding Antarctic water. In winter the Weddell Sea shelf water is near the freezing temperature $T_m = -1.8^oC$. When a thickness t of new ice is formed at the surface, a volume $V = Ah$ of mixed brine is formed on the shelf, where A is the area of the Weddell Sea shelf, and H = few hundred meters is the depth of the shelf. The salinity of the mixed brine is

$$S_1 = S_o + \frac{t}{h} \times 34 \quad . \qquad (4.2.2)$$

A not inplausible picture which would describe the flow of new bottom water of appropriate salinity is then as follows: With $t = 1.5$ m, $h = 130$ m, a volume of $V \sim 1.3 \times 10^{14}$ m^3 of mixed salty shelf water is formed, with salinity $S_1 = 34.63$. If this water on the way down then entrains 2.7 times its own volume of ambient Antarctic circumpolar water ($S = 34.74$, $T = +1.5^oC$), figures appropriate for ocean bottom water in the Antarctic region. On this picture the annual production of briny shelf water is 1.3×10^{14} m^3/year $\approx 5 \times 10^6$ m^3/sec; and adding the entrained circumpolar waters, the net production of new bottom water comes to 18×10^6 m^3/sec, which compares well with the conventionally assumed rate.

4.2.3 Environmental Consequences of the Vertical Flows

The operation of the polar pumps, which drive cold, saline surface waters by the ocean bottom has several important implications:

1. It is probably the major driving mechanism that produces the general upwelling (velocity ~ 4 m/year).
2. It ventilates the mixed surface layer of the ocean, on a time scale of 10 - 20 years, and the deep ocean on a time scale of 500 - 1000 years. Thus, for example, an increase of atmospheric CO_2 can be shared with the entire ocean in less than 1000 years.
3. It is a major pump driving the horizontal poleward flow of upper ocean waters and thus a mechanism for transfer of heat from equatorial to polar regions of the earth. Presently, about one-third of the equatorial to polar heat transfer is accomplished by such currents, which thus constitute a significant determinant of the latitude dependence of earth surface temperature. In energy budget climate models, this heat transfer is represented by a diffusion constant K. Typical temperature changes that would result from varying changes in the diffusion constant are shown in Fig. 4.2.5.
4. It keeps the deep oceans cold. A more stagnant ocean, on the average, would be significantly warmer. This in turn would result in the release of dissolved CO_2 into the atmosphere as the new equilibrium between the atmosphere and the oceans is achieved. The decrease in the concentration of dissolved CO_2 with increasing temperature is shown in Fig. 4.2.6. We may note that the burying of $0^{\circ}C$ polar surface water can remove almost twice as much dissolved CO_2 as is contained in an equal mass of $20^{\circ}C$ water. An increase of the average ocean

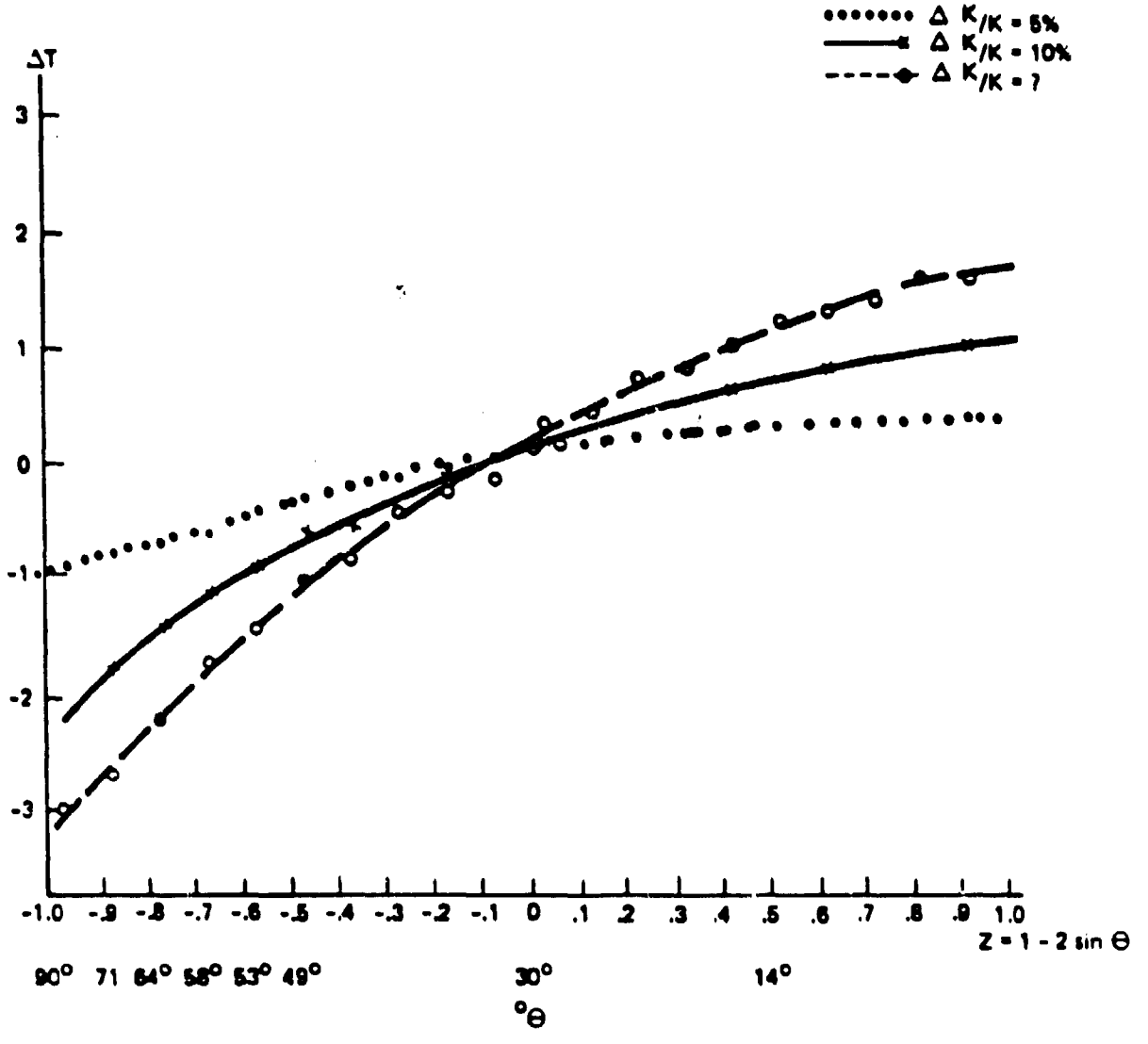

Figure 4.2.5 EFFECT ON TEMPERATURE OF CHANGING HEAT TRANSPORT DIFFUSION CONSTANT K IN THE MODEL OF SEC. (3.2)

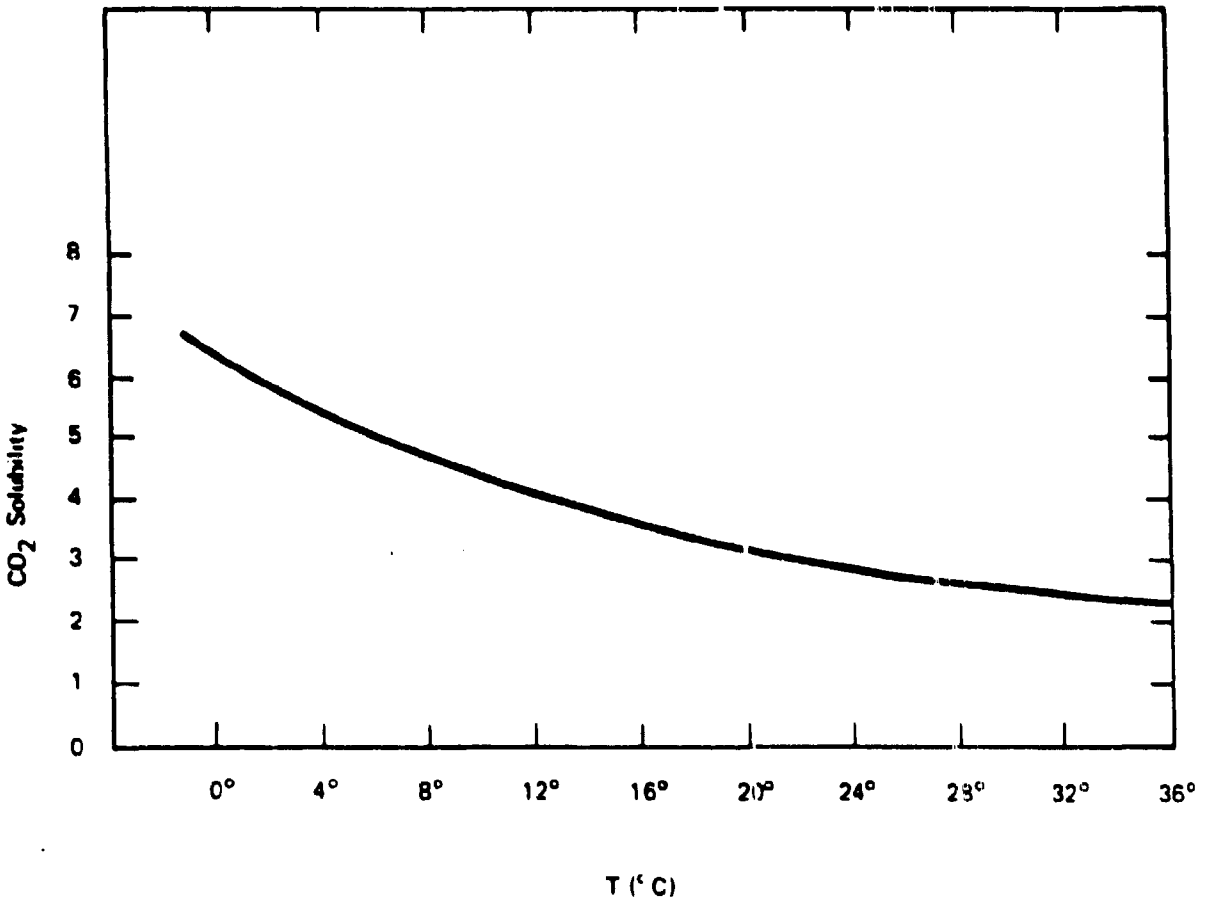

Figure 4.2.6 WITH NO SEA ICE CO_2 IN SEA WATER (S = 34 0/00) VS. TEMPERATURE

temperature by 4°C would ultimately release about 1/7th of the presently dissolved CO_2, content of the atmosphere. If such a release were accomplished over a period of 10^3 years (this is roughly the time scale for turnover of the deep waters) the CO_2 release rate would come to 6×10^{15} gm of C/year-more than the amount contributed by present fossil fuel burning (and more than twice the rate of the present increase of atmospheric carbon).

4.2.4 Vulnerability of the Deep Water Pumps to Polar Warming.

The question here is whether the operation of the pumps that drive abyssal circulation is vulnerable to CO_2-induced climate warming. Expecially relevant may be the greatly increased warming in the polar regions predicted by some climate models (Fig. 4.2.7). Qualitatively, one would expect the Weddell Sea pump to weaken insofar as climate warming reduces the production of winter sea ice or insofar as the ice survives for too short a time each year to allow the saline water to move off the shelf before the melting season, which injects new fresh water. As for the Norwegian Sea pump this would weaken if there were less cooling of the saline water recirculated in that sea. In addition, both solar pumps defend (but in different ways) on a supply of the fairly saline North Atlantic waters--as discussed above. How sensitive the pumps in fact are to polar climate warming is hard to assess and we can only recommend here that the question deserves further investigation. The Weddell Sea mechanism seems to defend mainly on the total amount of new sea ice frozen there each year. We believe that this may not in fact be too sensitive to modest CO_2-induced temperature increase, for two reasons:

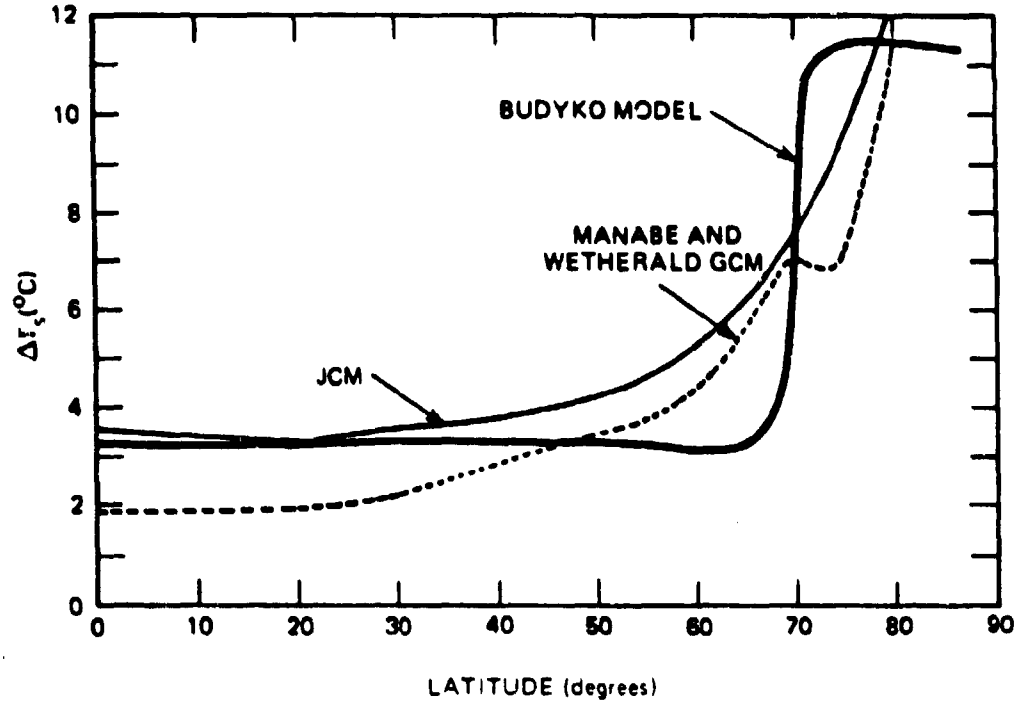

Figure 4.2.7 ZONALLY AVERAGED ΔT_s FOR A CO_2 DOUBLING MANABE AND WETHERALD BUDYKO MODEL, AND JASON CLIMATE MODEL.

1. The predicted rise in <u>winter</u> polar temperatures is less than the predicted rise in seasonally average temperature of Fig. (4.2.7). At least this is so in many climate models. Namely, the reduction in albedo caused by smaller sea ice covers is very effective in increasing surface light absorption in the summer but it makes much less difference in winter, when the solar input to the polar region is anyhow small. But what is critical for the pump is not so much the rate of summer melting as the amount of new ice produced in the winter season.

2. The amount of new sea ice produced around the Weddell Sea continental shelf may not be particularly sensitive to just low the winter surface temperature is in that region, so long as the temperature is well below freezing. Present mean winter temperatures (T_s) there lie in the range (depending on location) $-16^{\circ}C$ to $-32^{\circ}C$, well enough below the temperature $T_m = -2^{\circ}C$ needed to freeze sea ice. If one maintains a fixed temperature difference $T_s - T_m$ across a growing thickness of sea ice, and if one neglects the heat capacity of the ice, then the thickness of new ice formed over a time t (the winter season time) is

$$d = \frac{2}{4} \, t \left| T_s - T_m \right| \qquad (4.2.3)$$

where $= 5 \times 10^{-3}$ cal/$^{\circ}$C sec is the heat conductivity of ice, and $H = 80$ cal/gm is the latest heat. (The ratio of heat flow from local cooling to that from latent heat is

$$\tfrac{1}{2} C_v \left| T_s - T_m \right| / H \sim 8 \times 10^{-2} \ll 1 \quad ;$$

so the neglect of heat capacity is reasonable). For

$$T_s + \overline{T}_s \sim -24^{\circ}C, \quad T_m \approx 2^{\circ}C \ ,$$

and $t = 4$ months , $d \approx 1.7$ m.

An increase $\Delta d \sim d \, \Delta\overline{T}_s / \overline{T}_s$ so long as $\left| \overline{T}_s \right| \gg 2^{\circ}C$. Thus, for example, an increase $\Delta\overline{T}_s \sim + 5^{\circ}C$ reduces the amount of brine production by only $\sim 10\%$. This suggests that the Weddell Sea pump is not too sensitive to any but very subtantial increases in Antartic temperature. As for the Norwegian Sea pump, which involves the winter cooling of already saline waters, this is indeed sensitive to increasing surface and upper layer temperatures. But, although the freezing and melting of sea ice is not itself the main pump mechanism here, sea ice <u>does</u> serve to insulate the water below rising atmospheric temperatures, by reducing the production of sea ice in the Artic region could actually increase the water cooling effects in relevant regions--an effect that would tend to stabilize the pump in a warming north polar climate. But warming means less sea ice, hence less brine, an effect that destabilizes the pump. The situation, in short, is complicated.

Finally, we observe that even if the polar pumps were to diminish in a warming polar climate, the response in the deeper ocean layers would lag in time. It takes of order 10^2 years for newly formed dense surface waters to descent to the bottom.

REFERENCES FOR SECTION 4.2

1. Lamb, H. H., "Climate, Present, Past, and Future," I, Methven, London, 1977.

2. Flatté, S., ed. "Sound Transmission Through a Fluctuating Ocean," Cambridge Univ. Press, London, 1979.

3. Central Intelligence Agency, Polar Regions Atlas, (1978).

4.3 Effect of Climatic Warming on West Antarctic Ice Sheet

4.3.1 Introduction

In this section we discuss the possibility that CO_2 climatic warming could cause a major reduction in the Antarctic ice sheet and a dramatic rise in ocean level within the next 100-300 years. Although direct melting of the ice sheet would require much longer time periods, mechanical disintegration of the West Antarctic part of the ice sheet might take place rapidly because that part of the sheet is based on land below sea level. A review of the basic physics of ice flow and creep is given in the Appendix to this section (4.3A).

We also briefly consider possible effects on climate if the West Antarctic ice sheet were to disintegrate into icebergs causing an increase in albedo.

In the study of ice sheets, we have developed two simple models of the creep and flow of ice sheets to highlight the basic physics involved. These simple models yield predictions that agree reasonably well with those of more sophisticated models with important exceptions as noted in the following sections. Based on our reading of the literature and on our own analysis, we have come to the following conclusions:

1) The West Antarctic ice sheet could in principle be set afloat within a 500 year time span or less after triggering by a 5 to 10° C warming. This possibility should be taken seriousy and warrants further investigation.

2) Not enough is yet known about:

   (a) the dynamics of large ice movements in general,

   (b) the actual movement of Antarctic ice, or

   (c) the topographical features below marine-based antarctic ice to make accurate predictions of ice movements in West Antarctica.

3) Further investigation should emphasize intensified study of movements and basal topography of West Antarctic ice streams and ice shelves. We mention specifically the Thwartes and Pine Island outlet glaciers as possibly critical areas to monitor over the next decades.

4.3.2 The Antarctic Ice Cover

The Antarctic ice sheet is generally 1 to 4 kilometers thick and covers a land area of about 16 million km^2. A map of the continent is shown in Fig. 4.3.1. The total volume of ice, if set afloat, is sufficient to raise the worldwide ocean level by about 100 meters. The portion of the ice sheet in the eastern hemisphere is based on continental land that is above sea level, whereas the portion in the western hemisphere is based on continental land mainly below sea level. If only this marine-based portion were to disintegrate, the worldwide ocean level would rise about 6 meters.

Floating parts of the ice sheet called ice shelves fringe the continent. These shelves are typically 1-2 km thick at their junction with the land-based ice sheet. Some are enormous, such as the Ross and Filchner-Ronne ice shelves in West Antarctica, which cover about 0.5 million km^2.

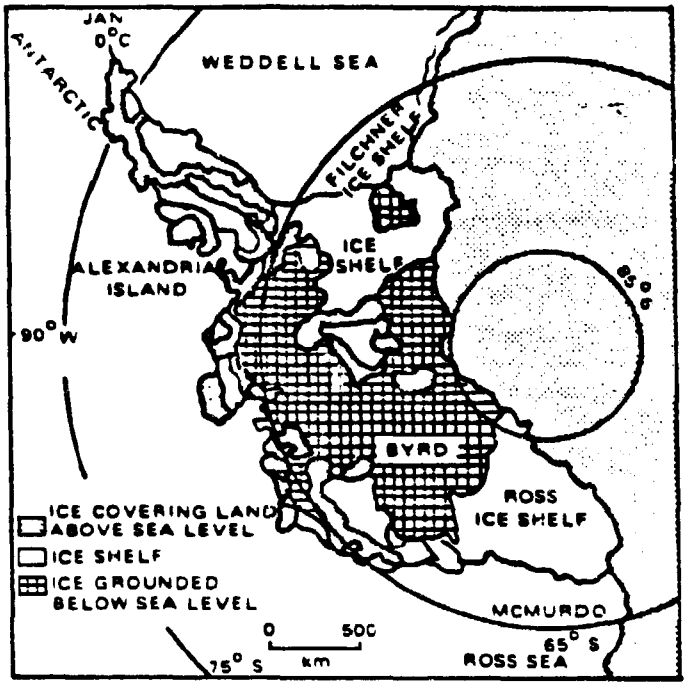

Figure 4.3.1 WEST ANTARCTICA, SHOWING ICE SHELVES, ICE GROUNDED BELOW SEA LEVEL, ICE COVERING LAND ABOVE SEA LEVEL, AND POSITION OF THE 0° C JANUARY ISOTHERM IN THE ANTARCTIC PENINSULA (BASED ON INFORMATION UP TO THE YEAR 1962).
(1) PRINCE GUSTAV CHANNEL; (2) WORDIE ICE SHELF; (3) GEORGE VI SOUND; (4) WILKINS SOUND; (5) ARGENTINE ISLAND.

Fast flowing currents of ice, called ice streams, drain the ice sheets into the fringing shelves. These streams are also called outlet glaciers if they flow in fjords through coastal mountains. Ice stream velocities of 0.5 km/yr are typical though the velocities can be highly variable.

Ice is added to the continent by snowfall, flows in ice streams from the ice sheets to the fringing ice shelves, and is lost mainly by calving into icebergs at the outer edges of the ice shelves. The ice shelves are probably close to a steady-state in which they lose as much ice by calving as they pick up from entering ice streams and snowfall. Melting underneath is not well understood. The total snow accumulation over the continent is very roughly estimated to be 2000 km^3/yr. This yearly exchange of mass is less than 1/10,000 the total mass of the Antarctic ice sheet.

The ice shelves are usually pinned at their sides and on seabed shoals so that they buttress the edges of the ice sheet by restraining the outflow of the ice streams. If key ice shelves were removed by a major climatic change, unrestricted flow, or "surging" of ice streams might well destroy a major part of the West Antarctic ice sheet. We will examine this possibility as it has been discussed in recent literature, and by our own highly simplified models of ice stream and ice shelf movements.

4.3.3 Recent Literature on this Subject

Vulnerability of the West Antarctic ice sheet to climatic warming has been widely discussed by a number of authors[1,2,3]. Currently, much of

the drainage of the ice sheet is into the Ross and Ronne ice shelves, which are grounded on shoals that produce ice rises. The ice shelves serve to buttress and stabilize the ice sheet. Warmer temperatures could weaken the shelves, through increased thinning due to melting and by enhancing lines of weakness such as rifts and bottom crevices. This would tend to increase rates of calving at the seaward edge of the shelves and eventually to disappearance of the ice rises. Once this happens there is the possibility of rapid deglaciation of the whole West Antarctic ice sheet: once the shelves have lifted from the shoals they are expected to go everywhere into longitudinal tension, a condition that should lead to rapid rates of calving.

Thomas, Rose and Sanderson[3] have recently attempted a quantitative estimate of the time scale for these events, according to what they viewed as a worst case treatment. In particular, they begin with a situation in which warming has somehow already removed portions of the ice shelf seaward of the shoals. The time scale for this first step is not treated in detail, though the authors record their expectation that it may be of order of several centuries even for a warming rate of 5° C per century. The detailed treatment focuses on the subsequent developments, leading to destruction of the ice rises and then more rapid deglaciation of the ice sheet. The time scale for substantial collapse of the ice sheet is on the order of several centuries, following initial destruction of portions of the shelves seaward of the ice rises. In this whole treatment the chief sensitivity to climate warming is associated with destruction of the outer shelf--the triggering event. It is conceivable that the West Antarctic ice sheet is inherently unstable and that it's disintegration could be

triggered by mechanisms unconnected with climate, as discussed for example by Hughes[1]. Indeed, Hughes adduces several lines of evidence suggesting that disintegration effects were inaugurated already several millenia ago. On the other hand Mercer[2] argues for stability against all mechanisms except for climate warming beyond a critical level that would rarely occur in the natural course of events (the last such occasion during the interglacial era $\sim$ 1000,000 years ago), but one which rising levels of CO_2 might produce within a short time.

4.3.4 Creep Models of Ice Stream Flow

In this section we will discuss a simple model of a parallel-sided ice stream as shown in Fig. 4.3.2. Our aim is to calculate the possible rate of retreat of the grounding line, where the ice sheet part of the stream turns into a floating ice shelf.

It is helpful, for a qualitative understanding, to recall that ice behaves approximately as an ideal plastic solid. Such a solid does not deform up to a critical yield stress σ_o (which we may take for ice as 1 bar), beyond which it deforms without limit. Thus the slope angle α of the upper surface of the ice sheet is usully held well below the val which the basal shear stress $\rho_I g h \sin \alpha$ exceeds σ_o. In Antarctica, the observed values of α satisfy approximately the relation:

$$\rho_I \; g \; h \sin \alpha = \sigma_o/4 \qquad (4.3.1)$$

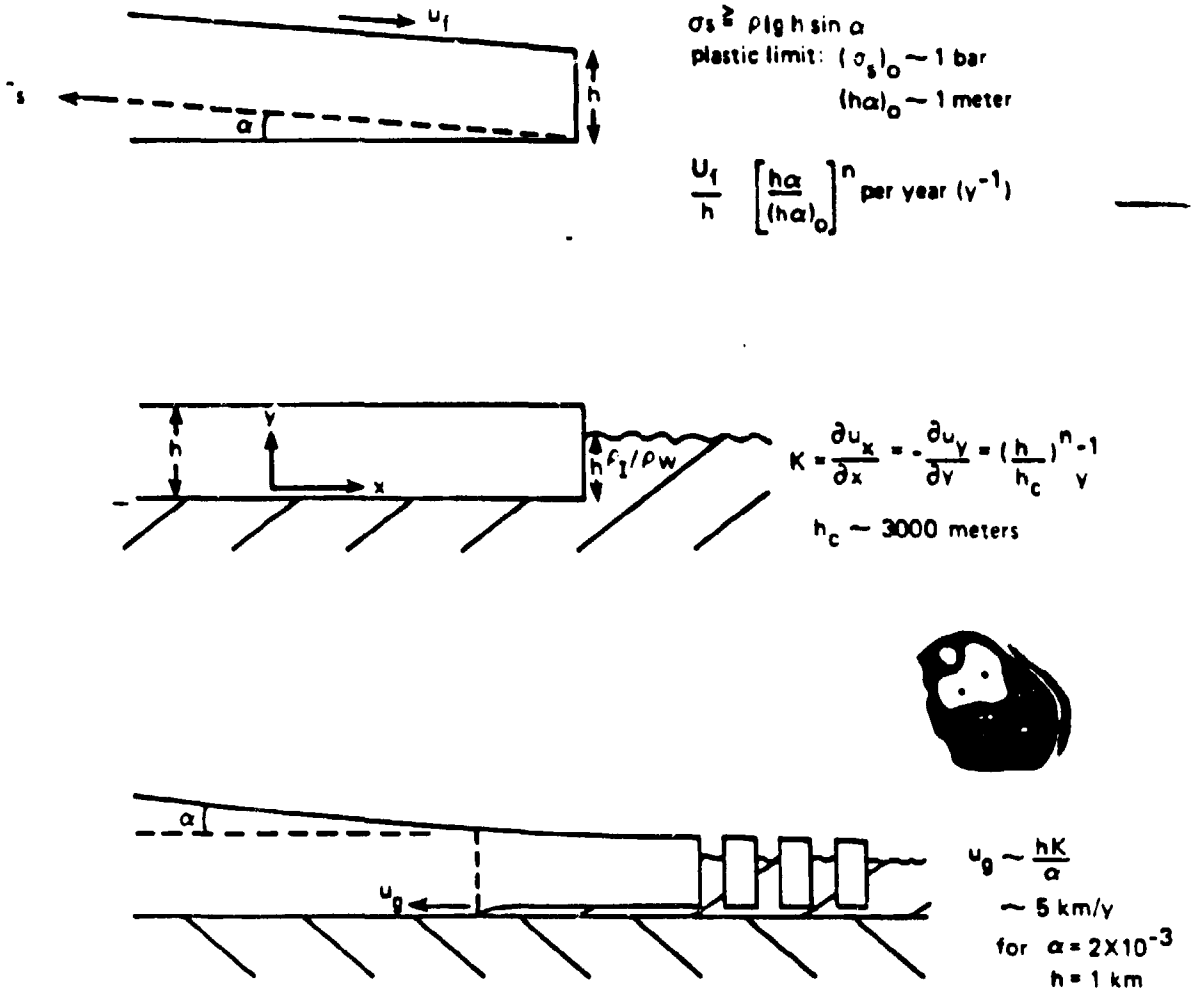

Figure 4.3.2 CREEP MODEL OF ICE SHEET

More precise formulations of ice creep and flow[4] predict that the ice stream velocity varies as $(\rho_I\ g\ h \sin\alpha\ /\sigma_o)^n$, where $n \approx 4$; thus the ice stream tends to adjust its flow to hold a steady value of $h \sin\alpha$.

The weight of the ice stream causes it to thin by creeping. The analysis of creep-thinning is particularly simple for an ice shelf of great length compared to its thickness. The thickness is found to be reduced by creep at a fractional rate K given by[5]:

$$K = \frac{1}{h}\frac{dh}{dt} = A\left(\frac{\Delta\rho\ g\ h}{4\ \sigma_o}\right)^n \qquad (4.3.2)$$

where $\Delta\rho = \rho_w - \rho_I$ and A is a constant whose value depends on the temperature and density profile of the shelf. Experiments on ice creep indicate $A \approx 2 \times 10^{-3}$ (year)$^{-1}$ for temperatures found in Antarctic ice shelves. The creep rate in the ice shelf remains close to this value up to the grounding line, and then falls off rapidly in the ice sheet inside the grounding line due to the sheer stress at the bottom. As an approximation, we take Eq. (4.3.2) to apply at the grounding line.

The creep thinning at the grounding line will set that part of the ice sheet afloat and cause the grounding line to retreat inland. The stream flow will maintain the angle α consistent with Eq. (4.3.1). Thus the grounding line should retreat at a rate:

$$U_g = \frac{Kh}{\alpha} \qquad (4.3.3)$$

Taking $h = 1000$ meters and $\Delta\rho = \frac{\rho_I}{10}$, we find: $\alpha = 2.5 \times 10^{-3}$, $K = 10^{-2}$, and $U_g = 4000$ meters/year. Since the distance from the grounding line of West Antarctic ice streams to the center of the West Antarctic ice sheet is tyically about 500 km, we see that in this model, the ice sheet might be set completely afloat within about 100 years.

4.3.5 Mass-Conservation Model of Ice-Sheet Disintegration

In this section we obtain a time scale for ice sheet disintegration using mass conservation and observed rates of creep of ice streams.

Consider a flat-bottomed ocean with bottom at depth D below sea level (see Fig. 4.3.3). At the grounding point P the ice thickness is $7/6\ D = h$. At the center C of the ice sheet the ice thickness is H. Let the distance PC be L and suppose that the contour of the ice-sheet is maintained under plastic flow so that H varies with L^{β}. We calculate the rate of retreat u_g of the grounding point,

$$u_g = \frac{dL}{dt}, \tag{4.4.4}$$

assuming that the flow is plane-parallel. Circular geometry would make only trivial changes.

Consider the plastic flow of the ice in the region just inland from P. Because of the discontinuity in the bottom boundary of the ice at P, there are unbalanced shear stresses of magnitude.

$$S = k\rho g h \ ,$$

where k is a numerical coefficient depending only on the local topography. The rate of flow of mass past a fixed point on the bottom is then

$$F = Whv\rho \qquad (4.3.5)$$

where W is the width of the flow. But the total mass inland of the grounding point is roughly

$$M = W\rho LH\left(\frac{1}{1+\beta}\right) . \qquad (4.3.6)$$

The law of conservation of mass says that

$$\frac{dM}{dt} = \frac{d}{dt}\,(W\rho Lh) - F . \qquad (4.3.7)$$

Since h is constant, while H varies with L^{β}, this equation gives

$$F = W\rho vh = W\rho\left(\frac{dL}{dt}\right)(h - H) = W\rho u_g(H-h) .$$

Hence finally

$$u_g = \frac{vh}{H-h} . \qquad (4.3.8)$$

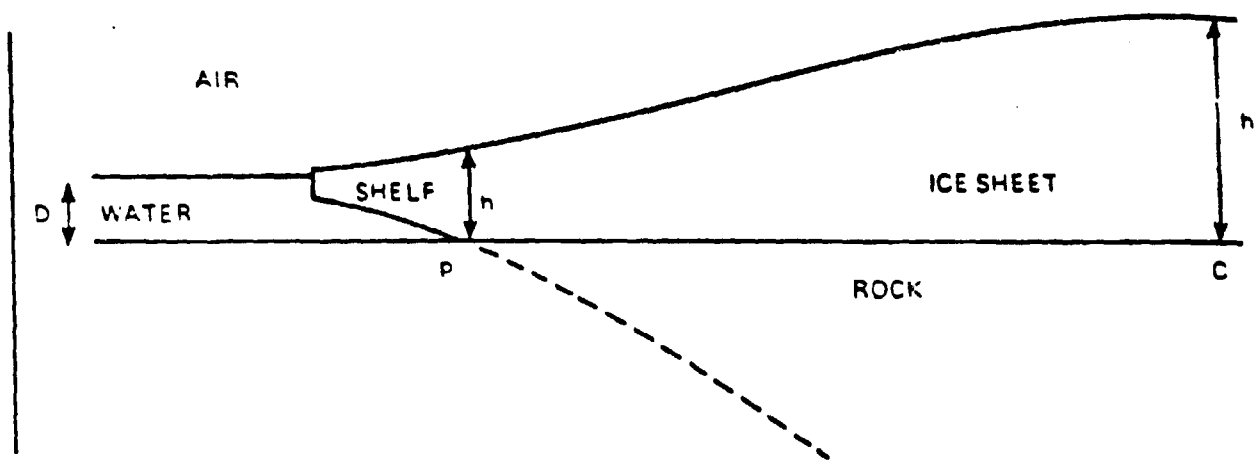

Figure 4.3.3 SIMPLE MODEL OF AN ICE SHEET

Since we have roughly $H \cong 2h$, the rate of retreat is

$$u_g = v \qquad (4.3.9)$$

within a factor of two.

Thus, Equation (4.3.3) yields an estimate of the rate of movement of the grounding of 4 km/year while Equation 4.3.9 yields an estimate of 1 km/year. The corresponding times for disintegration of the ice sheet are one and four centuries respectively.

4.3.6 Additional Consideration in Ice Sheet Flow

A number of processes have been ignored in the simple models discussed above. The most important are: melting or freezing underneath the ice shelf, snowfall accretion at the grounding line, advection of thicker ice at the grounding line by the flow from upstream, and the restraining effect on the ice shelf of any shoals underneath it and of shear stress at its sides.

All of these factors have been included in the calculation carried out recently by Thomas, et al.[3] and applied to two ice streams draining into the Ross ice shelf. A figure from this publication is reproduced in our Fig. 4.3.4, and shows their results for the retreat of the grounding line for each stream. Our simple models approximate the grounding retreat they find for each stream when the ice shelf is not held by shoals or

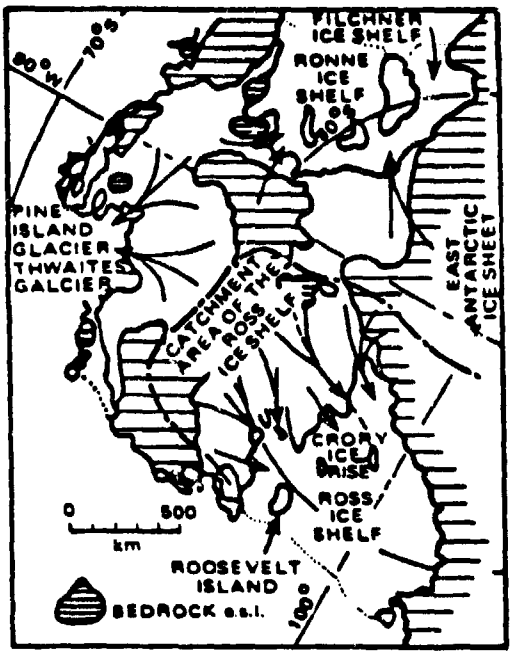

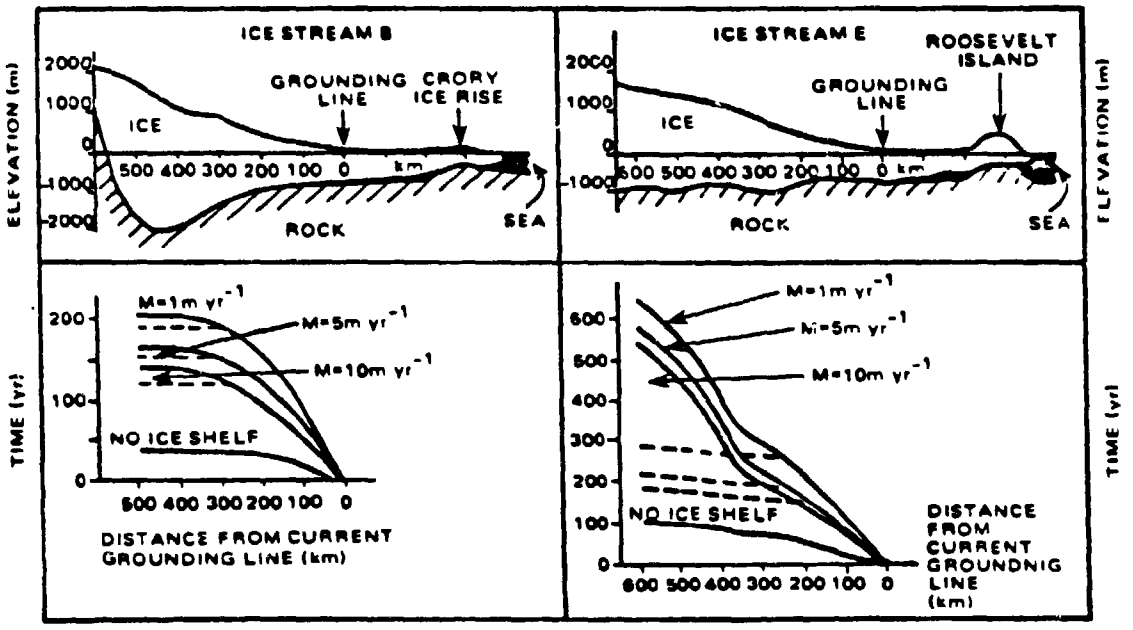

Figure 4.3.4 THE LONGITUDINAL PROFILES OF ICE STREAMS B AND E AS THEY ARE TODAY, AND PLOTS OF GROUNDING-LINE POSITION VERSUS TIME FOR THESE ICE STREAMS DURING RETREAT. RETREAT IS MOST RAPID IF THE ICE SHELF IS COMPLETELY REMOVED, AND LEAST RAPID FOR LOW VALUES OF ICE-SHELF MELT RATE, M . ONCE THE GROUNDING LINE REACHES THE DEEP BASIN BENEATH ICE STREAM B RETREAT IS EXTREMELY RAPID. IN CONTRAST, ICE STREAM E FLOWS OVER A COMPARATIVELY HORIZONTAL BED AND RETREAT RATES ARE ULTIMATELY DETERMINED BY THE RATE OF COLLAPSE OF THE ICE-SHELF MARGINS. THE BROKEN LINES SHOW RETREAT FOLLOWING COMPLETE BREAKUP OF THE ICE SHELF AS THE ICE RISES COLLAPSE.

islands. Our creep-thinning model actually reproduces these results in several respects. Note for example the rapid increase in grounding-line retreat for ice stream B when it reaches the deep basin. This increase comes from the critical dependence in Eq. (4.3.2) of the creep rate on thickness h. At least in this one case, creep-thinning seems to provide the dominant mechanism for ice stream behavior when the shelf is not buttressed.

4.3.7 Possible Consequences of a Warming in West Antarctica

We have seen in the previous section that both our simple models, and the more complete treatment of Thomas, et al predicts a retreat of the grounding line of at least certain West Antarctica ice streams once the buttressing of ice shelves is removed. A major question then is whether a 5 or 10° C warming near the pole could cause ice shelves to retreat by increased calving rates to the point at which they no longer hold in the ice streams. Hughes[1] argues that the calving line at the edge of the Ross ice sheet, for example, would quickly move to the shore of the ice sheet in response to a "minor" warming. Although this may be a possibility, others believe that the Ross shelf in particular would not begin to shrink until the ocean warmed up, which they believe would take hundreds of years. Only then would the process of ice stream retreat discussed in the previous section actually begin. That process then might take anywhere from 100 to 500 additional years before major de-glaciation was complete.

In our view calving and bottom melting are not as yet well enough understood to permit a clear prediction of what will happen to large ice

shelves after warming. This indeed is one of the big uncertainties, and will probably remain so for some time even if active research in this field continues or accelerates.

This uncertainty may not apply to some ice streams which terminate in small ice shelves. In fact, the major drainage from the north coast of the West Antarctic ice sheet is through the Thwaites and Pine Island glaciers, terminating in small ice shelves that probably do not provide much buttressing of the ice streams. As Thomas, et al[3] points out, if the depth of the grounding lines of these streams is in a critical range of 400 to 500 meters, then a small warming might push the grounding line back where the depth is greater, causing accelerated creep as shown in Eq.(4.3.2) , which could begin the rapid retreat outlined in the last section.

If any one ice stream were to surge, it is not clear what would happen to the rest of West Antarctica. However, it seems probable that the stream would begin to expand into substantial portions of other drainage areas, and would begin to drain out much of the marine-based ice sheet. Thomas et al,[3] and Hughes[1] agree on this point, although we have not examined the topography of West Antarctica to reach an independent conclusion.

4.3.8 Recent Instabilities of Antarctic Ice

Concerning instabilities on a somewhat lesser scale of affected area and of time, it is sobering to contemplate the evidence gathered by

H. H. Lamb.[6] From reports of early voyagers, in the period between Cook (1773) and Biscoe (1831) he infers that the limits of the southern ice pack at the end of the melting season had retreated 1°-2° farther south of the normal limit. A deterioration then followed, the ice increasing on the whole until about 1900, with some recession after 1907. There were extraordinary years, with large numbers of great icebergs--in extreme cases reaching to the River Plate and near to the Cape of Good Hope. The area and height reported for many of the icebergs was remarkable. All of this suggests to Lamb the breaking adrift of one or more ice shelves, the great bights in the Pacific section of the Antarctic coast, or the Ross or Weddell Seas, seeming the likeliest sources. It may be significant that the Billingshausen Seas around 70°s , 70°-90°w, was found abnormally clear of ice in 1893, in one of the periods when great bergs were unusually abundant on the oceans in temperate zones. The evidence suggests the break up, in several stages during the 19th century, of an area of order 100,000 km^2. The causes of such phenomena are unlikely to be meterological in any direct sense but may be due to ice surges possibly initiated by volcanic activity.

4.3.9 Effect of Disintegration of West Antarctica on Climate

It is difficult enough to reliably predict the fate of the West Antarctic ice sheet even under natural developments, but it does seem reasonable that substantial climate warming must inevitably trigger its destruction via instabilities, perhaps within a few centuries as a result of the warming associated with rising levels of CO_2. Destruction of the ice sheet would in turn trigger other events, apart from the 5 meter rise

in sea level. The pictured destruction takes the form of accelerated calving of icebergs at the margins of the ice shelves. If the main collapse occurs on a short enough time scale, before substantial loss of the icebergs through drift, melting, and destruction, then the initial effect of deglatiation would be to distribute the enormous volume of the ice sheet as floating ice. If we take the thickness to be ~ 200meters, that of the current ice shelves at their margins, this corresponds to a huge area of floating ice, of order $10^7 km^2$, comparable to the current area of the whole Antarctic ice sheet. Insofar as the floating ice survives in the warmer era that triggered its production, the effect is to increase the albedo in the southern polar region. This in turn entails a local cooling in that region--a negative feedback effect. As described, this feedback does not restore the West Antarctic ice sheet but it does serve to delay the destruction of the floating ice itself. The details depend on timing--on the CO_2-induced temperature rise that prevails when the ice sheet collapses, an event which then lowers the temperature because of increased albedo. For illustration, consider the era corresponding to doubled CO_2 levels. Here, in the absence of ice sheet collapse, the usual thin ice pack will have largely disappeared and the seasonally averaged temperature change (relative to today) is as shown by the solid line in Figure 4.3.5 (this is based on the energy budget climate model described in Section 3.2). The corresponding distribution, with floating ice contributed by collapses of the West Antarctic ice sheet, is indicated by the dashed curve.

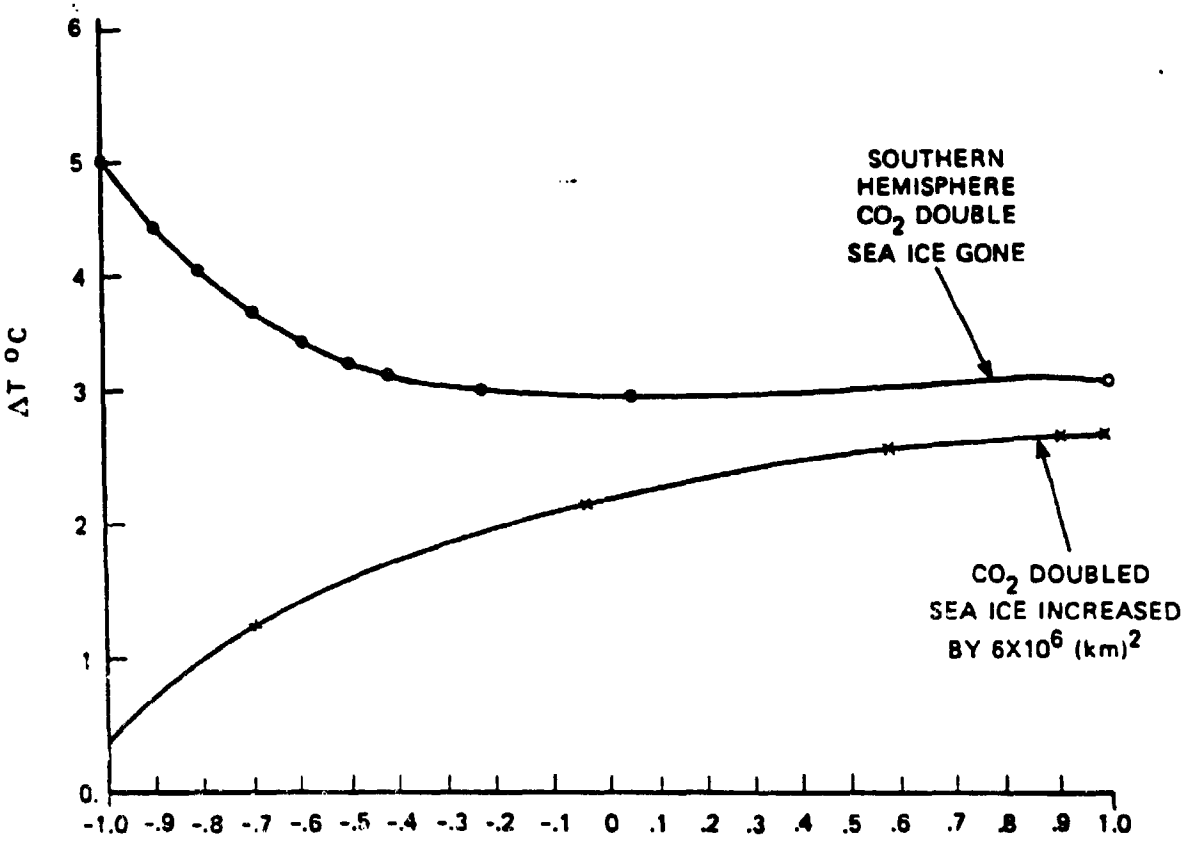

Figure 4.3.5 TEMPERATURE DISTRIBUTION AS CALCULATED FROM JASON CLIMATE MODEL

4.3.10 Conclusions

The West Antarctic ice sheet probably disappeared during the last inter-glacial period, and may do so again. On the basis of very simple mechanical considerations, the creep thinning of marine-based ice streams could be fast enough to draw down the ice sheet in as little as 100 years. The marine-based portion of the Lavientide ice sheet covering Hudson Bay apparently disintegrated within about 200 years at the end of the last ice age. The question of whether a polar warming due to CO_2 doubling could remove ice shelves sufficiently to initiate such mechanical disintegration at the moment has no clear answer. However, some important ice streams do not drain into large ice shelves, and may be in a more precarious state.

REFERENCES FOR SECTION 4.3

1. Hughes, T., "West Antarctic Ice Streams," Rev. Geophys. Space Phys., 15, No. 1, 1-46, 1977.
"The West Antarctic Ice Sheet: Instability, Disintegration and Initiation of Ice Ages," 13, No. 4., 502-526, 1977.

2. Mercer, J. H., "West Antarctic Ice Sheet and CO_2 Greenhouse Effect: A Threat of Disaster," Nature, 271, 21, 1978.

3. Thomas, R. H., T.J.O. Sanderson, K. E. Rose, "Effect of Warming on the West Antarctic Ice Sheet," Nature, 277, 355, 1979. (Further literature can be traced from Refs. 1, 2, and 3.)

4. Paterson, W.S.B., The Physics of Glaciers, Oxford Pergamon Press, 1969.

5. Weertman, J., "On the Sliding of Glaciers," J. Glaciol., 3, No. 21, 33-38, 1957.

6. Lamb, H. H., Climate: Present, Past and Future, 1, (Meutheu, London), 1972.

APPENDIX 4.3A

4.3A.1 Creep and Flow of Ice:

Here we write down the basic equations governing the creep and flow of ice, and then solve them for the simple example of a floating ice shelf.

4.3A.1.1 Basic Equation:

When a solid is in equilibrium, the stress components σ_{ij} satisfy the equations:

$$\sum_i \frac{\partial \sigma_{ij}}{\partial x_i} = f_j \qquad (4.3A\text{-}1)$$

where the f_j are external forces (per unit volume) acting within the ice. In glaciers, f is the gravitational force ρg .

Ice under stress will creep; that is, the strain will change gradually under the action of a constant stress. It is convenient to introduce a strain-rate $\dot{\varepsilon}_{ij}$ defined by:

$$\dot{\varepsilon}_{ij} \equiv 1/2 \left(\frac{\partial u_j}{\partial x_j} + \frac{\partial u_i}{\partial x_i} \right) \qquad (4.3A\text{-}2)$$

where u_i is a velocity component. Nye's[1] relation of steady-state creep may then be written:

$$\dot{\varepsilon}_{ij} \equiv C \, \sigma^{n-1} \, \sigma'_{ij} \qquad (4.3A\text{-}3)$$

where $\sigma^2 = \sum_{ij} 1/2\ (\sigma'_{ij})^2$ and σ'_{ij} gives the stress deviation from the hydrostatic pressure

$$\sigma'_{ij} \equiv \sigma_{ij} - 1/3\ \delta_{ij} \underset{R}{} \sigma_{kR}$$

The constant C which depends on the temperature, and the exponent n each have been measured in the laboratory. According to Glen,[2] n = 4.2 and $C = 1/2\ \sqrt{3n+1}\ B \exp.\left(\frac{Q}{kT_m} - \frac{Q}{kT}\right)$ where $B = 0.017$ bars^{-n} (year)$^{-1}$, Q = 32,000 cal./mole, R is the gas constant, and T_m is the ice melting temperature.

4.3A.1.2 Example - A Floating Ice Shelf:

As a simple illustration of the basic laws of plastic flow, and also to provide results used in main text, we will find the creep-thinning rate of a floating ice shelf. Referring to Fig. 2 in the section on ice stream models, we consider a shelf of height h and length much greater than h that is free to creep horizontally in one direction, which we cal' the X axis. (The creep-thinning rate when the shelf is free to expand horizontally in two dimensions turns out to be onlyu 10% greater than the simple case we take here.0 We orient the Y axis vertically and set y = 0 at the bottom of the shelf.

Far from the edges of the shelf, the stresses are independent of x and z. There is no shear stress at the top or bottom, and $\sigma_{yy} = 0$ at the top. Thus, Eq. (4.3A-1) is reduced to:

$$\frac{d\sigma_{yy}}{dy} = -\rho_I g \qquad \sigma_{ij} = 0 \quad i \neq j \tag{4.3A-4}$$

Integrating yields $\sigma_{yy} = \rho_I g(y-h)$. Since $\dot{e}_{zz} = 0$, we have

$$\sigma'_{zz} = 0 \quad \text{or} \quad \sigma_{zz} \; 1/2 \; (\sigma_{xx} + \sigma_{yy}) \quad .$$

Thus, Eq. (4.3A-3) becomes

$$\dot{\varepsilon}_{xx} = -\dot{\varepsilon}_{yy} = (1/2)^n C |\sigma_{xx} - \sigma_{yy}|^{n-1} \; (\sigma_{xx} - \sigma_{yy})$$

$$\dot{\varepsilon}_{ij} = 0 \quad i \neq j \tag{4.3A-5}$$

These equations (and 4.3A-2) are mutually consistent if $\dot{\varepsilon}_{xx}$ and $\dot{\varepsilon}_{yy}$ do not depend upon y . This is the only solution that satisfies all conditions. Combining Eq. (4.3A-4) and 4.3A-5), we have:

$$\sigma_{xx} = 2\left(\frac{K}{C}\right)^{1/n} + \rho_I g(y-h) \tag{4.3A-6}$$

where $K \equiv \dot{\varepsilon}_{xx}$ and turns out to be positive. Because the shelf is floating in water of density $\rho_w = \rho_I + \Delta\rho$ we may require:

$$\int_0^h \sigma_{xx} dy = -\int_0^{h\rho_I/\rho_w} \rho_w g(h\rho_I/\rho_w - 1) dy$$

which yields:

$$K^{1/n} = \rho_I g h^2 \Delta\rho \Big/ \left[4\rho_w \int_0^h C^{-1/n} dy \right]$$

Normally, T will depend upon the depth, so that C will depend upon y. To get an approximate answer, we take C as independent of y, in which case:

$$K = C\left(\rho_I g h \Delta\rho / 4\rho_w\right)^n \qquad (4.3A\text{-}7)$$

In the text we set $C = A\left(\rho_I / \sigma_o \rho_w\right)^n$ . .

REFERENCES FOR SECTION 4.3A

1. Nye, J., "The mechanics of glacier flow", J. Glaciology, 2, 82-93, 1952, Proc. Roy. Soc. A219, 477, 1953.

2. Glen, J. W., "The creep of polycrystalline ice", Proc. Roy. Soc. 228, Series A, 519-538, 1955.

3. Weertman, J., "Deformation of floating ice shelves", J. Glaciology, 3, No. 21, 38-42, 1957.

4.4 Impact of Increased Carbon Dioxide on the Biosphere

An increased carbon dioxide content of the atmosphere will affect the terrestrial biosphere in two more ways; by increasing the carbon that is available for fixation by photosynthesis and by changing the climatic conditions and thus altering net primary productivity. In addition, increasing the acidity of rainfall and surface and subsurface waters will alter rates of weathering and affect the transport of nutrients. None of these impacts are well understood, and the latter is of such complexity that we will not treat it here even though it may be of great significance to the biosphere. The situation with respect to the marine biosphere may be simpler. In almost all parts of the ocean, carbon is not the limiting nutrient, so that increased carbon content of the surface waters should not alter net primary productivity. However, the pH of the oceans will change, and altered weathering conditions on land changes the terrestrial flux of nutrients to the oceans. The net impact of these perturbations is completely unknown.

4.4.1 Non-climatic effects of CO_2 on the Biosphere

4.4.1.1 Fertilization of Crop-Plants

Elementary biological considerations suggest that if a plant system is at a proper temperature and has sufficient water, nutrients, and and sunlight, then an increase in carbon dioxide content of the atmosphere should result in an increase in the amount of carbon dioxide that is fixed by the plant system. Indeed, vegetable farmers in northern climates have added CO_2 to their closed greenhouses to increase marketable yield of

lettuce, tomatoes, cucumbers, etc. Lemon[1] illustrates that conventional biology may be misleading in predicting change in net primary productivity as a result of changes in CO_2 concentrations. The Dutch use CO_2 in greenhouses to give an earlier and bigger crop of fresh lettuce. Yet the CO_2 fertilized lettuces fix the same amount of carbon as does the unfertilized lettuce. The Dutch housewife is paying for more water packaged in the green leaves.

A field of plants utilizing full vertical sunlight for photosynthesis with 1% efficiency would use up all the CO_2 in the air within 1 meter of the ground in about 15 minutes. Under field conditions the CO_2 near the ground will be replenished by convection and breezes in a time shorter than 15 minutes. Nevertheless it is possible that local depletion of CO_2 may be a factor limiting the growth of crop-plants.

A few CO_2 fertilization studies under tents in the field have been carried out.[2] For healthy sugar beet plants under sunshine, Thomas and Hill found that doubling the CO_2 content of air increased the photosynthetic response by 30 to 40%. Lemon[1] states that this result is representative of plants having a C_3 photosynthetic system. For corn, a C_4 plant, measured under a clear plastic tent in the field, the photosynthetic response was 50% for a doubling of the carbon dioxide content.[1]

In addition to the field observations, many experiments have been done in growth-chambers (for example, Hofstra and Hesketh with soybeans,[3] Krenzer and Moss with wheat[4]) to measure the effect on various crop-plants

of varying the concentration of CO_2 in the air. The results are generally consistent and show that when growth is not limited by other factors there is a strong positive correlation of growth-rate with CO_2 concentration. The growth-rate, measured by dry weight or seed weight, increases by a substantial fraction (typically on the order of 50%) when the CO_2 concentration is doubled. The increase in growth-rate saturates at about two times the natural CO_2 concentration for corn and three times for wheat and soybeans.

The results of both the field tent and growth-chamber experiments do not give any reliable answer to the crucial question: what is the effect of increasing atmospheric CO_2 upon crop-plant growth in the open? In many parts of the world, crops are well supplied with water and with nitrogen and phosphorus fertilizer, so that a positive response to CO_2 increase may be expected. But the factors influencing agricultural yields are so multifarious that the magnitude of any response to CO_2 cannot be deduced from data currently available.

4.4.1.2 Saving Water Lost in Transpiration

Plants must open the stomata of their leaves in order to allow CO_2 to diffuse from the air into their tissues. The air in the stomata in summer-time contains about 100 water molecules for every molecule of CO_2. The plant therefore loses by diffusion about 100 times as much water as it gains CO_2. When the CO_2 concentration in the air is increased, the plant may partially close its stomata and maintain the same intake of CO_2 while reducing its transpiration of water. Alternatively, it may leave the

stomata open and increase CO_2 intake while keeping transpiration constant. In other words, CO_2 can act as a substitute for water when water is scarce. And the plant's growth-rate may respond positively to CO_2 increase even when growth is water-limited.

Leaf-chamber experiments of Regehr et al[5] with intact leaves of cotton-wood trees show dramatically the water-economizing effect of CO_2. When CO_2 concentration was doubled, photosynthesis increased by 40% and at the same time water-transpiration decreased by 25%. In addition to its possible direct effect as a fertilizer, the CO_2 produced by fossil-fuel burning may also be helping to increase agricultural yields by reducing the water-demand of crop-plants in dry areas.

4.4.1.3 Effects on Natural Plant Communities

If the magnitude of growth-response to CO_2 increase in agricultural crops well supplied with artificial fertilizers is unknown, the magnitude of the response in natural plant communities is even more uncertain.

Numerous growth experiments reviewed by Lemon[1] indicate short-term (one year or so) increases in growth rate (40 to 80%) in response to 3 to 5 times atmospheric CO_2 concentration in species such as the ponderosa pine, blue spruce, scotch pine, etc. How far these studies can be extrapolated to the real world is not known. Seedlings, studied in growth chamber experiments are not representative of other states of maturity. The impact of increased CO_2 over the entire growth cycle of a tree has not been

measured nor has the impact of CO_2 on a plant community. In a natural forest, there is no reason to believe that the overall rate of fixation of carbon is CO_2-limited. Nobody knows whether or not the total biomass in natural forests has increased in response to the 7% increase in atmospheric CO_2 since 1958.

From an ecological point of view, the total biomass is not the most important parameter in assessing the environmental effects of CO_2. A more important question is whether the increase of CO_2 is producing shifts in the balance of species in natural plant communities If some species are better adapted than others to increased CO_2, we should expect major disturbances of the natural equilibrium to occur over time of the order of decades. Unfortunately, it is difficult to separate such disturbances produced by CO_2 from similar disturbances produced by other industrial pollutants.

4.4.2 Impact on the Biosphere of Climatic Shifts

Available models of climate do not provide predictions of regional shifts in such biospherically important parameters as the length of growing season or seasonal fluctuation in precipitation resulting from increased atmospheric carbon dioxide concentrations; though a poleward shift of the temperature precipitation belt has shown up in a number of models (see Section). The rapidity of climate change and the variability of the new climate are particularly important, since the composition and productivity of plant communities as well as geographical extent are strongly determined by the occasional severe event. These features of climate

clearly cannot be predicted. Because of this, one can only speculate as to the impact of climatic changes on the biosphere.

The principal anticipated change is a world-wide increase in temperature accentuated at higher latitudes. In general, an increase in mean temperature decreases photosynthesis provided the availability of sunlight, nutrients, and water remains unchanged.[6] However, for the anticipated changes in temperature of a few degrees resulting from a doubling of the CO_2 content, the temperature effects on world biomass are probably small compared to the direct effect of CO_2 fertilization.

The impact of temperature change on agriculture will depend on the crops, water availability and soils (nutrient availability). The complexity of the situation is illustrated by considering North American agriculture. In most of the United States, the corn and soy bean belt summer temperatures (hence evaporation) are too high for optimal production; yields improve in cooler years. Optimum temperatures for corn and soy beans, given enough moisture, lie in the range of 32-35°C. Growth of these two crops ceases for temperatures above 45°C. If these crops were grown in areas currently under cultivation in the United States, then an increase in average temperature would reduce annual yields. In the northern part of the Canadian prairies, wheat yields are cut by colder summers and the occurrence of early frost. A warmer temperature could be expected to increase wheat yields in that part of North America. However, the optimum temperature for the growth of wheat is about 25°C so that the wheat belt in southern regions of the United States would be expected to

have lower yields if temperatures increased. The net effect on wheat produciton in areas where it is currently under cultivation is uncertain.

The impact of climate change on agricultural productivity is further complicated because the longer term average yield depends on the standard deviation as well as the mean of the parameters determining climate. Years of low productivity usully occur when the temperature, precipitation, etc., vary greatly from average conditions. The models of climate discussed in Section 4.1 do not provide any indications to whether weather shows a greater or lesser year to year variation under warmer planetary atmospheric condition.

In general, one might expect agriculture to adjust to climatic change provided land areas are available with appropriate soil characteristics. For example, if a given corn producing area becomes warner and drier, then sorghum might be a replacement crop. One crop that may be adversely affected by temperature change is wheat. An increase in temperature in the northern latitudes would move the optimal growing season north into the nutrient-poor soils of northern Canada and the Soviet Union. With current uncertainties in what regional climatic changes will be, it is impossible, at present, to predict changes, if any, in wheat or other crops productivity.

4.4.3 Summary

The non-climatic effects of CO_2 as a nutrient of agricultural and natural plants may be at least as important as the climatic effects.

Unfortunately the attention of the government and of the public has been focused almost exclusively upon the climatic effects. The non-climatic effects of the 7% rise in CO_2 since 1958 may already be significant in human terms. Compared with climatic effects, the non-climatic effects may be

i. more immediate,

ii. easier to observe and measure,

iii. more crucial to the economic and ecological problems of human survival.

We urge that the existing programs of research into the effects of atmospheric CO_2 be broadened so as to give appropriate weight to the study of non-climatic effects.

REFERENCES FOR SECTION 4.4

1. Lemon, E., The Lands Response to More Carbon Dioxide, Paper presented at U.S. Office of Naval Research Conference on "The Fate of Fossil Fuel CO_2", Honolulu, January, 1976.

2. Hofstra, G. and J. D. Hesketh, "The Effects of Temperature and CO_2 Enrichment on Photosynthesis in Soybean", Environmental and Biological Control of Photosynthesis, R. Marcelle Ed., The Hague, 71-80, 1975.

3. Krenzer, E. G. and D. N. Moss, "Carbon Dioxide Enrichment Effects Upon Yield and Yield Components in Wheat", Crop Sci., 15, 71-74, 1975.

4. Regehr, D. L., F. A. Bazzaz, and W. R. Boggess, Photosynthesis, Transpiration and Leaf Conductance of Populus Deltoides in Relation to Flooding and Drought, Photosynthetica, 9, 52-61, 1975.

6. Ehlringer, J. and O. Bjorkman, "Quantum Yields for CO_2 Uptake in C_3 and C_4 Plants, Plants Physiology, 59, 86-90, 1977.

5.0 RESEARCH NEEDS

5.1 Introduction

A central theme of this report is that the future increase of atmospheric carbon dioxide levels raise questions which include important considerations other than climate. Most recent surveys discuss only climate[1]. Changes in climate can have a profound effect on agriculture and many other of man's activities but altering the carbon dioxide levels of the atmosphere can directly influence agricultural productivity as well as that of the natural biosphere. The research efforts in the United States and in other countries mirror the view that changes in climate and their direct impact are all important. In our view, future research should also examine those impacts of carbon dioxide change that are not climate-related, as well as changes in climate and the consequences of these changes.

The prediction of future levels of carbon dioxide in the atmosphere requires an understanding of the world's future energy needs, the nature of the atmospheric-oceanic-biospheric interaction and the response of nature's large reservoirs of carbon to changing surface temperature. Forecasting the world's future energy requirements and the mix of fuels that would be used to meet those requirements would require a model of the future world economy. It is unlikely that definitive models would be developed given our present limited understanding of the interaction between energy demand and economic growth.[2] Probably the best approach at

present is to examine models with different rates of energy consumption and different fuel mixes (see Section 2.5). However, the main uncertainty seems to lie in just when a given CO_2 level will be reached rather than whether it will.

5.2 Role of the Biosphere in the Carbon Cycle

Determination of the size and magnitude of the biospheric carbon contribution to the atmosphere is clearly a high priority research need. As we discussed in Sections 2.3 and 2.4, one approach is to monitor the oxygen content of the atmosphere to a precision of about one part in a million and in the oceans to a part in a thousand over a period of years. For the atmosphere, the present stations used to determine the carbon dioxide levels of the atmosphere should be adequate. It would appear that Raman scattering observations (see Section 2.4A) may achieve the required precision and that mass spectrometric techniques may also be applicable. Determination of changes in oxygen levels in the oceans presents a more difficult sampling problem. Certainly the oxygen chemistry is simpler than carbon chemistry but local oxygen concentration will depend on the ambient level of biological activity. Determination of trends in the ocean's oxygen concentration will require repeated observations at various stations away from coasts and from regions of nutrient-rich upwellings.

Further observations at a number of localities are needed to determine the magnitude of the Riley-Williams pump in which carbon dioxide is taken from the atmosphere to the deep oceans (see Section 2.2.4). The required observation involves determining the rain of particulate carbon

from euphotic layer to the deeper part of the ocean. As in the case of determining the oxygen content, the determination of the total ocean rain of particulate carbon will require observations at a number of localities over several years. In particular it would be of interest to determine whether or not the seasonal variations in primary productivity show up as fluctuations in the rain of carbon.

The response to temperature changes of the large reservoirs of carbon, soils and methane hydrates, are poorly understood (see Section 2.5.3). The world's soils differ greatly in their chemical and physical properties. The rates of oxidation of carbon and of the upward diffusion of carbon dioxide are not known but could be large enough to be of consequence in considering future atmospheric carbon dioxide levels. The recognition that large quantities of carbon in the form of methane are trapped in the permafrost regions of the world is relatively recent. The response of the methane hydrates to an increase in temperature can only be crudely approximated.

Extensive literature exists on the response of plants to increases in atmospheric carbon dioxide; for example, see Strain.[3] Most of the data are derived from growth chamber experiments, though lack of documentation on temperature, moisture and nutrients reduce the value of much of this experimentation. A few field experiments have been carried out under plastic tents. The relevance of these data is uncertain since most of the world's biomass is in the form of trees. The direct observation of enhanced carbon dioxide levels on the growth of a tree over its lifetime

poses a substantial challenge. Progress in this area is almost certain to come from a better theoretical understanding and/or from a measurement of the oxygen cycle in nature than from direct observation. Substantial uncertainties still exist as to the magnitude of the standing biomass and the world's net primary productivity and these will have to be resolved before reliable estimates of the impact of higher carbon dioxide level on the biosphere can be made.

The impact of climate change on net primary productivity remains uncertain. General ecological considerations lead us to expect that the productivity of natural systems may respond to changes in climate in the manner illustrated in Figure 5.2.1 (provided that changes in climate take place on a time scale short compared with genetic adaption, migration of species, etc.) A mature ecosystem will adjust to prevailing climatic conditions with an average productivity. For small deviations in weather from the mean, some species will have increased productivity, others less but the total will in general initially be lower than the productivity for the mean conditions. For large deviations from the mean, the productivity may depart from a Gaussian-like dependence. (Note that in Figure 5.2.1, this possibility is not shown).

For monocultures, agriculture, the drop off of productivity with changes in climate should be much sharper than for a natural ecosystem as illustrated in Figure 5.2.1. A particular optimal variety is usually developed for prevailing climatic conditions in a given geographical locality.

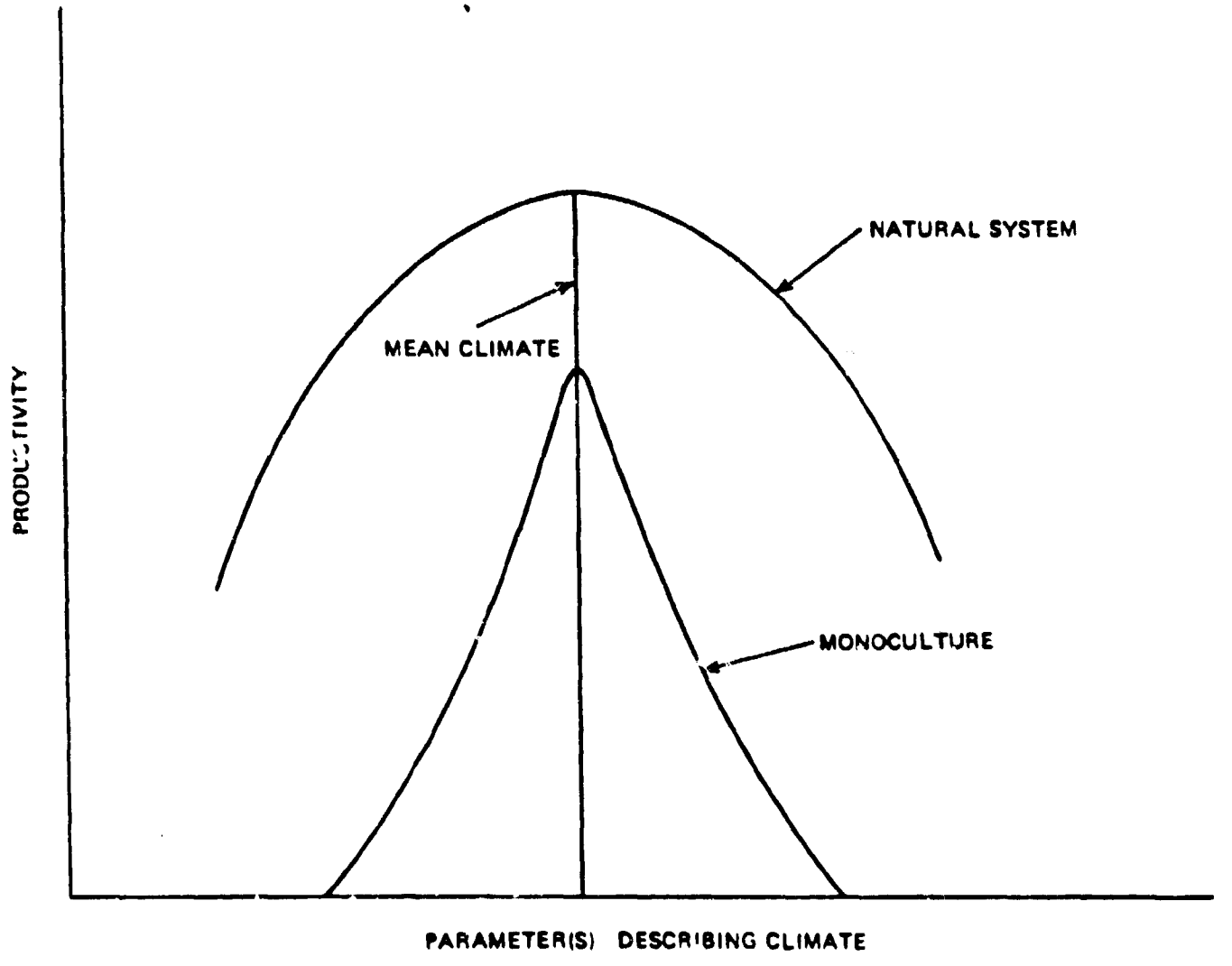

Figure 5.2.1 SCHEMATIC VARIATION OF PRODUCTIVITY WITH CHANGES IN PARAMETERS DESCRIBING CLIMATE

The above hypothesis is an oversimplification in that climate is not characterized by a single parameter. While a decrease in temperature may yield a lower monoculture productivity, a dcrease in temperature accompanied by an increase in precipitation may result in higher yield than for mean climatic conditions. While some work has been done on productivity responses to changes in climate for both natural systems and monocultures,[4] more detailed statistical analyses using observed climatic change is required before the impact of climate change on the biosphere can be predicted. For example, it is conceivable that increased carbon dioxide may reduce variability and so ameliorate conditions in most of the places which now suffer from extreme conditions.

5.3 Role of Large Carbon Reservoirs

The rate at which the carbon dioxide concentration of the oceans' upper layers responds to a change in temperature is relatively well understood. The response and even the magnitude of the giant reservoirs of carbon stored in the soil and in the hydrates of methane are not. The amount of carbon stored in the various soil types needs to be determined. The temperature dependence of the rate of oxidation of both organic and inorganic carbon in various soil types should be investigated as well as the rate of diffusion of carbon dioxide in the soils. While the existence of large methane hydrate deposits has been known for decades the magnitude of carbon stored in the permafrost region of the world is probably uncertain by a factor of ten. The temperature dependent properties of methane hydrates are poorly known. With respect to the methane hydrates it is of special interest to determine whether the large seasonal fluctuation

in carbon dioxide observed at Point Barrow is in any way associated with a seasonal outgassing of methane.

5.4 Modeling of Climate Change

In Section 4.1 we consider certain of the problems associated with current climate models. Ever more sophisticated General Circulation Models are under construction. We are concerned that the complexity of the models may be so great as to hide the underlying physics and that the numerical approximations employed may distort the longterm interactions. Heat budget models such as the JASON Climate Model cannot provide the details on the parameters determining climate which are essential in assessing the long term impacts on activities such as agriculture. Research into models intermediate in complexity between heat budget models and the Global Circulation Models may provide useful insights into the climate prediction problem.

Satellites such as the Nimbus series, provide a wealth of empirical information on the temperature distribution in the atmosphere as well as the infra-red absorption. These data over extreme climatic regions, oceans, icecaps, deserts, could provide guidance in the construction of climate models of the earth.

In addressing the impact of climate changes on man's activities three key questions arise:

- Does the rise in mean temperature produced by carbon dioxide occur mainly in summer or in the winter?

- o Does the rise in temperature occur mainly by day or by night?
- o Does the rise in temperature increase or diminish the magnitue of damaging local extremes?

If it should turn out that temperature increases occur mainly in winter and/or at night or mainly in places which are uncomfortably cold, then the climatic impact of carbon dioxide could be favorable. Similarly, if there are fewer extreme variations in a warmer climate the impact could be favorable.

The seasonal variations have been examined in both heat budget models and in numerical models of global circulation (see Section 4.1). General physical considerations suggest that the warming should be greater in summer since the winter-time solar radiation is less and there should be less of an effect on the reradiated infrared. The heat budget models do, indeed, show heightened summer-time maximum temperature (see Section 3.2.4), but at least one global circulation model shows the opposite effect.[5] Until this difference is settled, the seasonal response should be considered uncertain. We do not know of any models that attempt to deal with the day/night cycle. Since the atmospheric circulation is sensitive to small scale details which no existing model can fully represent, the impact of carbon dioxide on day/night variations will probably require an approach quantitatively different from existing models.

The problem of modeling changes in the statistical properties of the climate are formidable. The heat budget models depend on very few

parameters. Because of the sensitivity of the models to small changes in the parameters, the running heat budget models with random changes in the parameters may be uninformative but should be tried. General circulation models which simulate tens of thousands of atmospheric variables have, in theory, the potential to provide simulations of climatic fluctuations. But these models have serious disadvantages (see Section 4.1) and further, the amount of computer time required to obtain representative climate statistics is prohibitive at present. Models of intermediate complexity, for example; ten parameters or statistically parameterized models, may provide useful insights into climatic fluctuations.[6]

5.5 Trace Compounds in the Atmosphere

Carbon dioxide is not the only compound resulting from man's activities that alter the atmospheric energy balance. As noted in Section 3.1.2.5, oxides of nitrogen, freon, methane, ozone and a variety of hydrocarbons can enhance the "greenhouse effect" dominantly carbon dioxide and water vapor. Routine observations of ozone and its variation are currently carried out but the determination of the concentration of other minor constituents has been sporadic. A continued effort in monitoring these trace constituents should be an important element in any international research program on climate.

5.6 Determining Trends in Climate

The determination of climatic trends is made difficult both by the great year to year variations in weather and the number and geographical distribution of sampling sites. Two principal methods of determining

trends in temperature change have been employed. Surface temperatures, as measured by thermometers at the surface, are averaged over a given time interval, usually a year, and the time averages are then averaged over the whole earth or over a belt of latitudes. The placing of weather stations poses a sampling problem since the northern hemisphere and the continents are heavily favored. Alternatively, the height of a constant pressure level, 500 millibars for example, can be measured and the average temperature for the column of air under the pressure level determined from the equation of state. However, heights of constant pressure levels are measured at far fewer sites than those at which temperature is measured and a similar land/northern hemisphere bias exists.

Measurements of the earth's infrared radiation from space provides an alternative means of obtaining spatially averaged atmospheric temperatures at various levels (see Section 3.1.3). Monitoring of satellite derived surface or near surface temperatures over a period of years may provide a more reliable estimate of temperature changes than the alternative methods. The forecast of future levels of atmospheric carbon dioxide (see Section 2.5) and the results of climate models (section 3.2) suggest that the warming due to carbon dioxide will be at most a few tenths of a degree Celsius in the 1980's. The very difficult task of detecting a secular trend of this small in magnitude against the noise background will require the use of a variety of sensors as well as modern statistical analysis. However, such observations and analysis are essential if the postulated temperature increase due to carbon dioxide is to be empirically observed.

5.7 International Nature of the Carbon Dioxide Question

By its intrinsic nature climate is global; changes in climate and in the composition of the atmosphere should be a global concern. To measure, understand and to be able to respond to changes in atmospheric composition and the consequences of these changes, international cooperation is essential. Special attention should be given by the United States and other countries to securing international cooperation in collecting and disseminating data relevant to the carbon dioxide question, in undertaking the necessary research and assessing the overall impacts of changing the composition of the atmosphere brought about by man's activities.

REFERENCES FOR SECTION 5.0

1. National Research Council, Carbon Dioxide and Climate: A Scientific Assessment, National Academy of Sciences, Washington, D. C. 1979.

2. Landsberg, Hans., Ed., et al, Energy: The Next Twenty Years, Ballinger, Cambridge, Mass., 1979.

3. Strain, B., Report of the Workshop on Anticipated Plant Responses to Global Carbon Dioxide Enrichment, Duke University, Durham, N.C., 1978.

4. National Foreign Assessment Center, Relating Climate Change to its Effects, GC78-10154, Library of Congress, Washington, D. C., 1978.

5. Hansen, J., Private Communication. Paper in preparation for submission to J. Atmos. Sci. Information available from Goddard Institute of Space Studies, 2880 Broadway, New York, N. Y., 10025, 1979.

6. Wright, P., "A Simple Model for Simulating Regional Short-Term Climatic Changes", Mon. Weather Review, 107, No. 12, 1567-1580, 1979.

DISTRIBUTION LIST

ORGANIZATION	NO. OF COPIES
Dr. Henry D.I. Abarbanel 1217 Campus Drive Berkeley, CA 94708	1
Dr. Wallace Broecker Lamont Doherty Observatory Palisades, NY 10964	1
Dr. Robert D. Cess Laboratory for Planetary Atmospheric Research State University of NY Stonybrook, NY 11794	1
Dr. Joseph W. Chamberlain 18622 Carriage Court Houston, Texas 77058	1
Dr. Robert Chervin NCAR P.O. Box 3000 Boulder, CO 80307	1
Dr. Charles Cooper San Diego State University San Diego, CA 92182	1
R. Dahlman Office of CO_2 Effects Research & Assessment Office of Asst. Secy. for Environment Department of Energy Washington, D.C. 20545	1
Dr. Robert E. Dickenson National Center for Atmospheric Research P.O. Box 3000 Boulder, CO 80307	1
Dr. Freeman J. Dyson Institute for Advanced Study Princeton, NJ 08540	1
Dr. William Elliott ARL, NOAA U. S. Dept. of Commerce 8060 13th St. Silver Spring, MD 20910	1
Dr. Henry M. Foley Department of Physics Columbia University New York, NY 10027	1
Dr. Norval Fortson Department of Physics (FM15) University of Washington Seattle, WA 98195	1
Dr. Robert Fossum, Director DARPA 1400 Wilson Boulevard Arlington, VA 22209	2
Dr. Robert M. Friedman Office of Technology Assess. U.S. Congress Washington, D.C. 20510	1
Dr. Edward A. Frieman Director, Office of Energy Research, U.S.DOE M.S. 6E084 Washington, D.C. 20585	1
Dr. William Happer 560 Riverside Drive New York, NY 10027	1
Mr. John Kaufman Department of Energy OER, ER-30, MS6E084 Germantown Washington, D.C. 20584	1
Dr. Gordon MacDonald Apartment 1017 4300 Old Dominion Drive Arlington, VA 22207	2

ORGANIZATION	NO. OF COPIES
L. Machta NOAA U.S. Department of Commerce 8060 13th Street Silver Spring, MD 20910	1
Dr. Syukuro Manabe Geophysical Fluids Dynamics Lab NOAA/Princeton University P.O. BOX 398 Princeton, NJ 08540	1
Dr. Walter H. Munk 9530 La Jolla Shores Drive La Jolla, CA 92037	1
Dr. Gerald Namias Scripps Institution of Oceanography University of California La Jolla, CA 92093	1
Professor William Nierenberg Scripps Institution of Oceanography University of California La Jolla, CA 92093	1
The Honorable William Perry Under Secretary of Defense (R&E) Office of the Secretary of Defense Room 3E1006, The Pentagon Washington, D.C. 20301	1
The Honorable Frank Press Director, OSTP Room 360, Old Executive Office Bldg. Washington, D.C. 20500	1
Dr. V. Ramanathan National Center for Atmospheric Research P.O. Box 3000 Boulder, CO 80307	1
Dr. Roger Revelle Scripps Institution of Oceanography University of Cal, S.D. La Jolla, CA 92093	1
Dr. Oscar Rothaus 106 Devon Road Ithaca, New York 14850	1
Dr. Ralph Rotty Institute for Energy Analysis Oak Ridge Associated Universities P.O. Box 117 Oak Ridge, TN 37830	1
Dr. Malvin A. Ruderman 29 Washington Square West New York, New York 10011	1
Dr. William Schlesinger Department of Biological Sciences University of Cal/Santa Barbara Santa Barbara, CA 930167	1
Dr. Stephen H. Schneider NCAR P.O. Box 3000 Boulder, CO 80307	1
Dr. Don G. Scroggin Council on Environmental Quality 722 Jackson Place Washington, D.C. 20006	1
Dr. David Slade Director Office of CO_2 Effects Research & Assessment Office of Asst. Secy for Environment U.S. DOE Washington, D.C. 20545	1
Dr. Joel A. Snow Senior Technical Advisor Office of Energy Research, U.S. DOE, M.S. E084 Washington, D.C. 20585	1
Dr. Peter Tans Lawrence Berkeley Lab 1 Cyclotron Road Berkeley, CA 94720	1

ORGANIZATION	NO. OF COPIES	ORGANIZATION	NO. OF COPIES
Dr. Sam Treiman 60 McCosh Circle Princeton, NJ 08540	1		
Dr. John F. Vesecky Center for Radar Astronomy Stanford University Stanford, CA 94305	1		
Dr. George M. Woodwell Marine Biological Lab Woods Hole, MA 02543	1		
Dr. Fredrik Zachariasen (452-48) California Institute of Technology Pasadena, CA 91125	1		